Integration of well data into dynamic reservoir interpretation using multiple seismic surveys

Yi Huang

Submitted for the Degree of Doctor of Philosophy
Heriot-Watt Institute of Petroleum Engineering
Heriot-Watt University,

December, 2011

Abstract

This thesis develops and tests a new technique which integrates information from well production and 4D seismic data directly in the data domain. This method is of value when seismic data are acquired by multiple surveys over the same area of a hydrocarbon reservoir. Sequences of 4D seismic changes can then be extracted over different time intervals from multiply repeated seismic surveys and these are cross correlated with identical time sequences of cumulative fluid volumes produced or injected from wells. The technique is applied to frequently repeated seismic surveys from three North Sea fields, including two compartmentalised reservoirs: the Schiehallion and Norne field, and a compacting reservoir: the Valhall field. Maps of well to seismic cross-correlations are proven to produce a strong, localised and stable signal in the connected neighbourhood of individual wells.

The correlation signatures from the Schiehallion and Norne application investigated in this thesis are the consequence of pressure performance due to reservoir compartmentalisation. In the Schiehallion study, the mapped results help identify the production signal related only to individual wells, thus leading to a better delineation of reservoir compartments. In the Norne study in particular, an extra reservoir volume connected to the original segment is highlighted by the technique. The reservoir simulation model is subsequently updated and a better match between the observed and simulated data can be achieved. The application to the compacting Valhall field involves using data from the Life of Field Seismic project, for which the 4D signature is dominated by compaction-assisted pressure depletion. For these data, both AI and time-shift attributes are found to have a remarkably consistent correlation with the well activity for selected groups of wells. Further, maps of these results possess sufficient fine scale detail to resolve and disentangle interfering seismic responses generated by closely spaced wells and localised zones of gas breakout along long horizontal producers. These case studies indicate our proposed methodology of uniting well data and 4D seismic and confirm that this does indeed provide an insightful product for dynamic interpretation of the producing reservoir.

Acknowledgements

In my PhD, I have had the experiences that a PhD student would typically have - full of many pieces of different memories: nights suffering from insomnia thinking about the project, the joy after a paper was accepted, etc. My PhD not only gives me knowledge about reservoir geophysics but also the unique attitude of cautiousness and spirit of exploration characteristic of academics.

Firstly, I wish to express my warm and sincere thanks to my supervisor Professor Colin MacBeth for giving me the opportunity to be part of the Edinburgh Time Lapse Project (ETLP). His understanding, encouragement and personal guidance have provided a good basis for the present thesis. Thanks also to Olav Barkved and Jan-Paul Van Gestel from BP-Norway. Olav gave me access to the Valhall data and the chance to visit BP Norge in Stavanger. Also, he devoted plenty of time and involved a few other people in BP and Hess to the further development of the technique, including developing a GUI integrating the method into BP's daily life workflow, and recruiting a summer intern from NTNU to optimize the codes. I am also grateful for his support by actively promoting the technique in several conference and workshops. I am also grateful to Svend Øsmo and Ole Petter Dybvik for kindly offering me the internship in the Statoil Research Centre in Trondheim, Norway where I spent a very productive winter. During my internship, I received the most sincere help and support from the colleagues in both Trondheim Research Centre and the asset team of the Norne field in Harstad Norway. I would like to mention their names here: Trine Alsos, Bård Osdal, Nan Cheng, Ola-Petter Normann Munkvold, Sindre Lillehaug, Lill-Tove Wetjen Sigernes, Mark Thomson.

This thesis could not be accomplished without the financial support of the sponsors of the Edinburgh Time-Lapse Seismic Project (ETLP), Phase III and IV: BG Group, BP, Chevron, ConocoPhillips, ENI, EnCana, ExxonMobil, Hess, Hydro, Ikon, Landmark, Maersk, Marathon Oil Corporation, Norsar, Petrobras, RSI, Shell, Statoil, Total and Woodside.

I have great memories of my time at Heriot-Watt in Edinburgh. I was very lucky to have the opportunity to meet and share great moments with really nice and smart people during that time. Alejandro, Hamed, Reza, Fabian, Valeriy, Yesser, Sean are great friends of mine and have been a source of encouragement!

I also wish to thank my Mom and Dad for giving me a lot of encouragement and so much support financially and mentally. I wish Dad can get through all the troubles he is having right now and return to home to reunite with us as soon as possible. Thanks to God for giving me abundant life: health, happiness and pain, relaxation and struggling, and most importantly the new life with my wife – Huan Tong.

Publications

Part of this work is presented in the following publications:

- Huang, Y. and MacBeth, C. (2009) 'Direct correlation of 4D seismic and well activity for dynamic reservoir interpretation', In SEG International Exposition and Annual Meeting, Houston, USA.

- Huang, Y., MacBeth, C., Van Gestel, J.-P. and Barkved, O. (2010) 'Correlation of well activity to time-lapsed signatures in the Valhall field for enhanced dynamic interpretation: application to Valhall field', EAGE/EUROPEC Conference and Technical Exhibition, Barcelona, Spain.

- Huang, Y., MacBeth, C., Barkved, O. and Gestel, J-P. "Enhancing dynamic interpretation at the Valhall Field by correlating well activity to 4D seismic signatures", First Break, 29 iss.3, March 2011.

- Huang, Y. and MacBeth, C. "Direct correlation of 4D seismic with well activity for a clarified dynamic reservoir interpretation", Accepted for publication in Geophysical Prospecting, 2011.

- Huang, Y., MacBeth, C., Barkved, O., Van Gestel, J-P., Dybvik, O-P. "Direct correlation of 4D seismic with well activity for a clarified dynamic reservoir interpretation", Accepted for publication in The Leading Edge, September 2011.

Software used in this thesis

The well-to-seismic correlation as described above along with the threshold selection process is implemented with well2seis code written in Matlab. The improved version of this code incorporating the Graphic User Interface (GUI) is written by BP and Hess using Matlab and Java language. The code is now in-house Edinburgh Time-lapse Project (ETLP).

For any work related to fluid flow simulation, the author used the Schlumberger numerical simulation software – ECLIPSE. For visulisation of horizons, structural maps, attribute maps and seismic volumes, the Schlumberger seismic to simulation software platform PETREL is used for the Schiehallion and Valhall study, and ROXAR RMS is used for the Norne study.

Content

List of figures

List of Tables

Chapter1 Introduction

This chapter provides an introduction to the importance of time-lapse seismic as a reservoir management tool. The wide range of static and dynamic information about the reservoir that can be derived from 4D seismic is discussed. Over the last decade, the quality of 4D seismic data has improved significantly due to technical advances in 4D seismic acquisition. Two technological trends have been noted and will be discussed in this chapter: first, increased adoption of permanent systems in the oil industry; second, acquisition of 4D seismic surveys at increasingly frequent intervals in general. These two trends have opened up new opportunities for the dynamic interpretation of 4D seismic data, whilst bringing new challenges. This chapter also discusses several major challenges that reservoir geophysicists in an asset team might face for 4D interpretation in the practical environment based on the data available in this PhD study. Finally, the main challenges and contributions of this thesis in particular are discussed.

1.1 Information from the 4D signature

The 4D seismic change is the consequence of reservoir property changes imaged by the acoustic wave induced in seismic surveys. The reservoir property changes are, in turn, caused by temperature, pore pressure and saturation changes due to one type of fluid replacing another. 4D seismic is the first technique that can provide information about these three kinds of dynamic reservoir processes in a reservoir spatially in 3D. For different fields, we usually focus on various 4D seismic interpretation issues depending on the main uncertainties (usually controlled by geology) of a particular reservoir. For instance, the major task of 4D seismic interpretation could be to detect vertical fluid contact movement in a reservoir composed of thick layers where the production might be significantly affected by water coning (e.g. the Norne field, Osdal et al. 2006). However, such vertical OWC interpretation may not be possible for a thin reservoir (e.g. 10-50m) where aquifer support may not be sufficiently active (e.g. the Valhall field, Barkved et al. 2003). Industrial and research 4D projects around the world published in open literature provide an insightful view of what information 4D seismic data may possibly provide to the reservoir engineer as part of an asset team.

1.1.1 Static reservoir information

Static reservoir information refers to the reservoir parameters that are considered to be almost[1] invariant throughout the time of hydrocarbon production, such as permeability and the fluid flow behaviour of a fault. There are several static parameters that can be better described by 4D seismic signatures. These will be discussed within this section with examples from publications in the literature.

Firstly, 4D seismic can dramatically reduce the uncertainty related to unknown reservoir compartmentalization or flow barriers over that of using the baseline seismic survey alone.

[1] Clearly in a compacting reservoir in particular, this definition breaks down as permeability and fault transmissibility may vary significantly with changing stress.

The causes of reservoir compartmentalisation can be classified into two types: structural and stratigraphic, the same as those forming the traps of the reservoir. Faults with considerable throw may be visible in 3D seismic section; however, their dynamic behavior to fluid flow cannot be determined simply by quantifying throw. In addition, a large proportion of faults that are important to fluid flow are sub-seismic owing to their minor displacement and the limit of vertical seismic resolution. Well testing may give some indications to the presence of these faults but their exact location remains unknown. Inter-well lithological barriers such as cemented sands can play a similar role to that of faults in fluid flow in the reservoir, but have no chance of being detected by conventional seismic technology. Therefore, flow barriers revealed by observed 4D signals may be unexpectedly different from those predicted using baseline seismic. For example, Figure 1.1a shows an area of a North Sea field where the reservoir sands are imaged by an amplitude-based seismic attribute derived from 3D seismic data acquired by the baseline seismic survey. A rough interpretation of reservoir connectivity based on the discontinuities in this attribute may infer possible flow barriers and thus be used as a guideline for placing new wells. However, the 4D signature as shown in Figure 1.1b displays a noticable red, triangular-shaped signal caused by an unexpected pressure increase caused by water injection. In this regard, 4D seismic is the key to understanding of the exact location of the flow barriers between the wells, and has played an important role in placing in-fill drilling wells in many fields (e.g. the Magnus field, Watts et al., 1996; Schiehallion field; Dijksman et al., 2007).

Secondly, permeability is a reservoir parameter that has a first order of impact on simulation model predictions, and is important for optimising the simulation model predictions (Villegas et al. 2009). However, the 3D spatial distribution of permeability in the reservoir model is usually estimated by extrapolating the measured values at well locations using geo-statistical approaches. There are some attempts published in literature to extract 2D horizontal permeability from 4D seismic attribute map. In this case, 4D seismic data can either be used as a constraint in an objective-function-based iterative history matching process to invert for permeability (Villegas et al., 2006) or be directly transformed into an averaged permeability map through several proposed procedures published in the literature (Vasco et al., 2004; Al-Maskeri and MacBeth, 2006; Johann et al., 2009). Using the simulation model with updated permeability derived from the 4D seismic (e.g. Figure 1.2), the predictions of dynamic reservoir performance appear to be improved as shown in several studies (e.g. Villegas et al. 2009).

Moreover, a quantification of fault sealing capacity defined as fault transmissibility multipliers (Manzocchi et al., 1999) is also possible using 4D seismic data. Fault transmissibility is a key parameter that controls the seal behaviour of a fault. The traditional approach to investigate fault transmissibility is based on well measurement, in particular, log data (e.g. Gamma Ray). This is because fault seal properties are considered to be related to rock properties thus linked to the properties of fault gauge. Nevertheless, the traditional well-log based analysis carry large uncertainties as sufficient well data may not be possible for analysis due to limited well coverage (Benguigui and MacBeth, 2008). Thus, in the area of poor well coverage, the fault transmissibility derived from 4D seismic data along with estimated uncertainties can be incorporated into the reservoir simulation model to optimise field development through the established seismic history matching approach. One such example is given by Benguigui and MacBeth (2009) (see Figure 1.3). Figure 1.3a shows an area of Heidrun field, the faults (red) interpreted using baseline seismic data, which has been superimposed on the observed 2001-1995 4D signatures (green). Figure 1.3b and c indicate that a better match is obtained between the observed 4D signature and water saturation change predicted by the reservoir simulation model with updated fault multipliers from the 4D seismic.

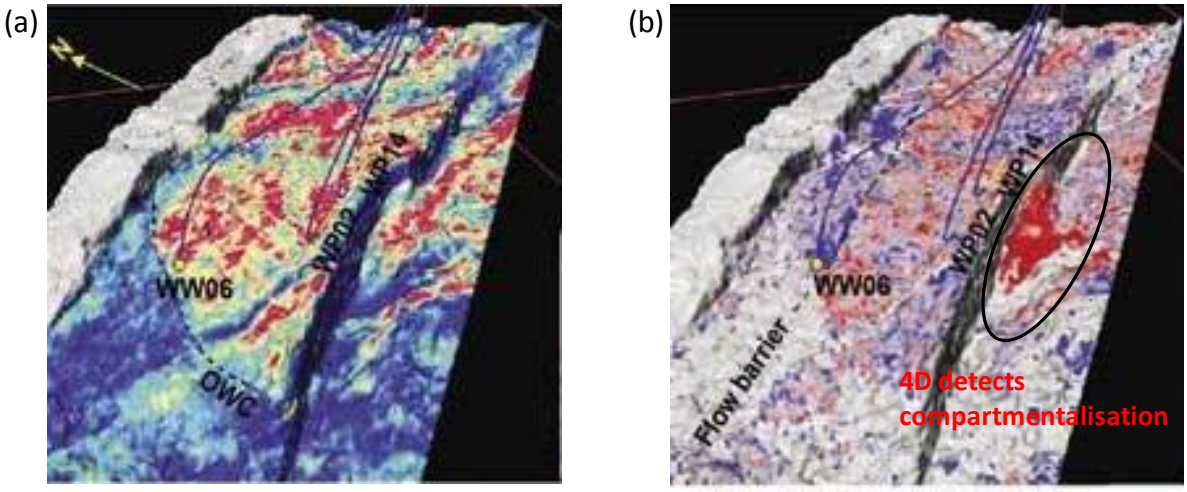

Figure 1.1 (a) Amplitude map taken from the baseline survey in 1996 over the Schiehallion field. Brightening indicates the distribution of reservoir channel sands and amplitude discontinuities may imply possible flow barriers. (b) Observed 4D signal (2004-1996) after production highlights an area of significant pressure build-up, revealing the exact location of the flow barriers in this area of interest (after Dijksman et al., 2007).

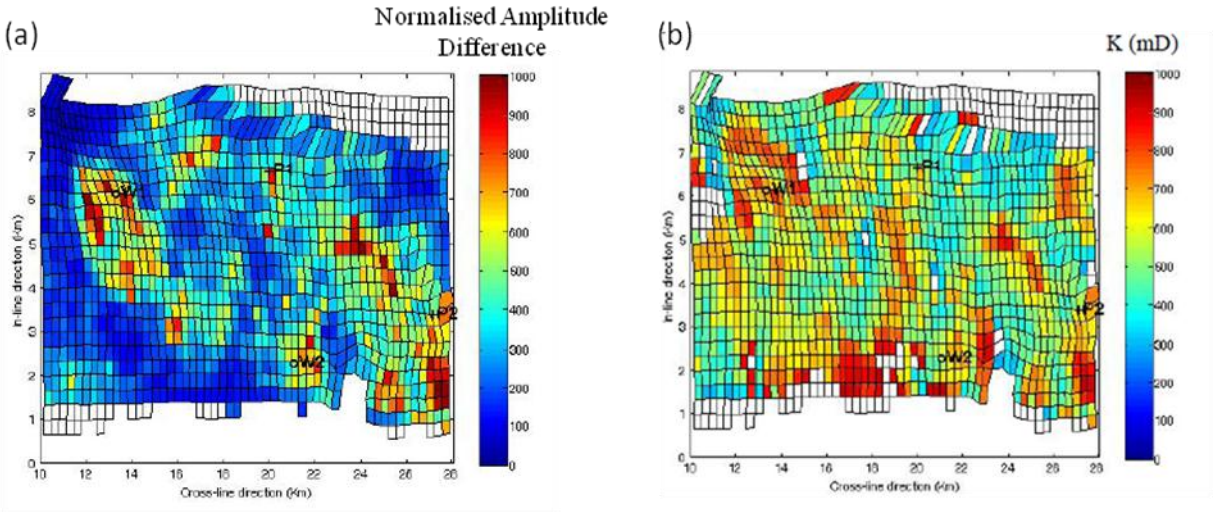

Figure 1.2 (a) 4D amplitude difference for a segment of the Schiehallion field drawn on the simulation grid. (b) Average 2D permeability distribution (K) directly derived from (a) **(**after Villegas et al., 2009).

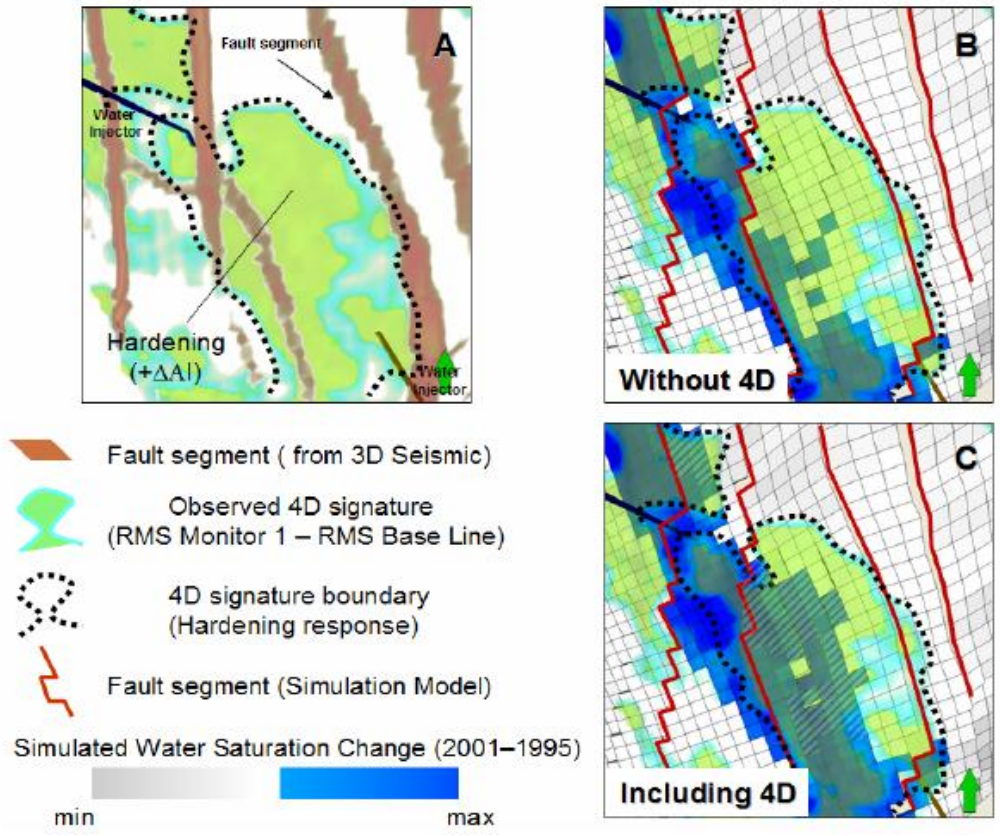

Figure 1.3 (a) Observed 4D signature (2001-1995) superimposed on faults (red) derived from the baseline seismic data using attribute analysis. (b) Comparison between observed 4D signature and water saturation change predicted by the simulation model without 4D seismic derived 4D fault multipliers, and (c) including 4D-derived fault multipliers.

1.1.2 **Dynamic reservoir information**

Producing hydrocarbon from the reservoir involves extracting or injecting fluid into the connected pore network in the reservoir rock. This has a variety of effects on the elastic properties of the reservoir rock and existing fluid. Here, I will only investigate the 4D response due to the following production effects.

Firstly, during production, reservoir fluid will flow due to the established pressure field which may result in one type of fluid replacing another. Fluid substitution can take place in both horizontal (e.g. water sweeping) or vertical direction (e.g. OWC movement). The changed composition of fluid in the pore space will result in a corresponding compressibility change of the fluid mix which will lead to the 4D seismic change. 4D seismic has been applied most widely on fields with aquifer drive (e.g. the Norne fields; Osdal et al. 2006) and water injection (Draugen; Koster et al. 2000). Increasing gas saturation in the reservoir pore space due to gas injection (e.g. Chirag field; Foster et al. 2008) or solution gas breakout due to pressure drop below bubble point (Foinaven field; O'Donovan et al. 2000) will significantly reduce the compressibility of the saturated reservoir rock, thus yield strong 4D seismic signal. This can not only be applied to a methane injection project (Cere-la-Ronde et al., 1998) but also CO_2 injection projects (e.g. Sleipner field; Chadwick et al., 2004) despite the more complex physical processes expected at the contact between CO_2 and brine. For instance, Figure 1.4 shows an area of the Heidrun field where the 4D attribute map around the top reservoir reflector displays the effect of both gas cap expansion and water saturation change as a result of gas injection and water injection carried out up and down the flank of the field.

Secondly, the pore pressure changes during the process of field development as a result of extraction or injection of fluid from and into the reservoir. This effect may cause the stress to re-distribute in the reservoir rock and also pressure to equilibrate in the fluid, thus changing the compressibility of the saturated reservoir rock. In turn this leads to changes of the density and velocity of the rock. Strong 4D signals are often present around poorly communicating water injectors due to the pressure build-up process (e.g. Figure 1.5) and the subsequent pressure ‘relaxation’ process when well rate is reduced (for example, Schiehallion, Gainski et al., 2010). However, pressure depletion below the initial bubble point is not equally detectable due to different petro-elastic responses of the saturated rock to these two kinds of scenario. Pressure depletion can be easily recognised in 4D seismic though due to its

associated effects, i.e. reservoir compaction and solution gas breakout (e.g. Schiehallion field; Dijksman et al. 2007).

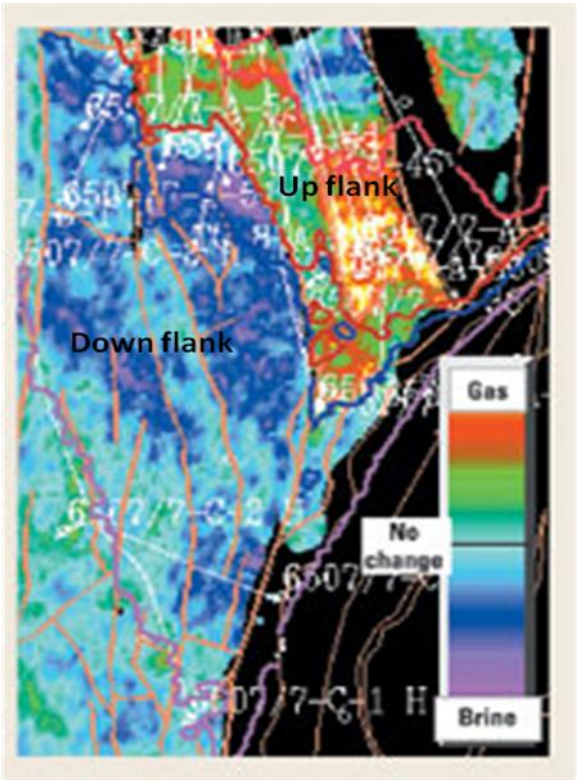

Figure 1.4 Amplitude difference map between 2001 and baseline survey showing gas cap expansion (red and green) due to up flank gas injection, and OWC movement due to down flank water injection (blue and purple), Heidrun field (after Eiken, 2003).

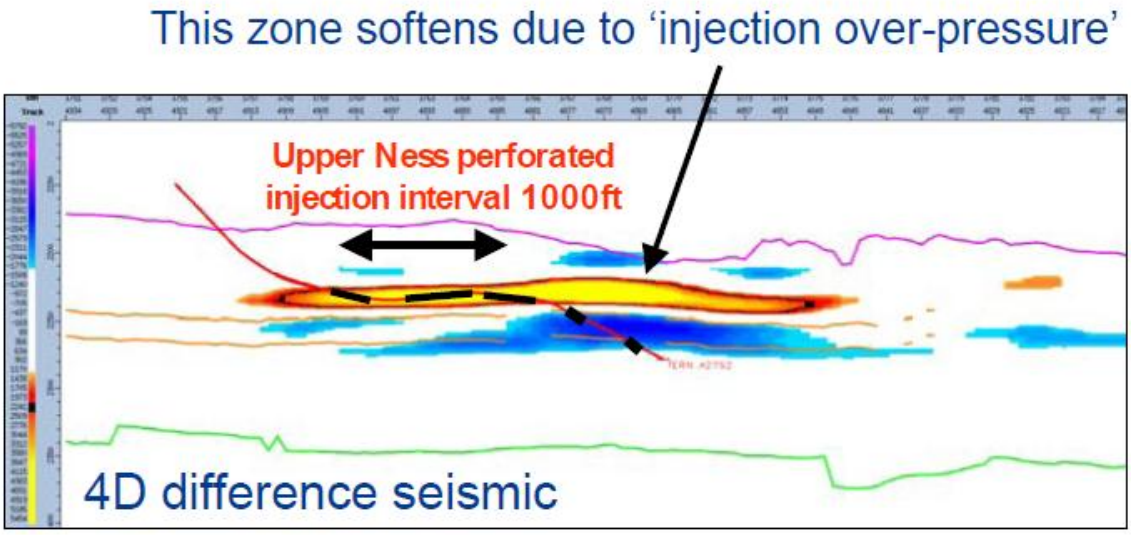

Figure 1.5 Strong 4D signal interpreted to be caused by overpressure due to injection into confined fault block (after Stammeijer and Staples, 2003).

Thirdly, depletion of the reservoir may cause the compaction of the reservoir rock which has important consequences inside and outside the reservoir, e.g. reduction in porosity, redistribution of the overburden stress and sea floor subsidence. Strong 4D seismic signatures from compaction can be observed in many well-known North Sea chalk reservoirs, including: Valhall (Barkved et al. 2003), Ekofisk (Johnson et al., 1988), Dan (Ovens et al., 1997), Tyra (Nykjaer, 1994), and Gorm (Nederveen and Damm, 1993). The compaction effect is usually very strong and easy to recognise on various seismic attributes, e.g. time-shift and amplitude change (see Figure 1.6).

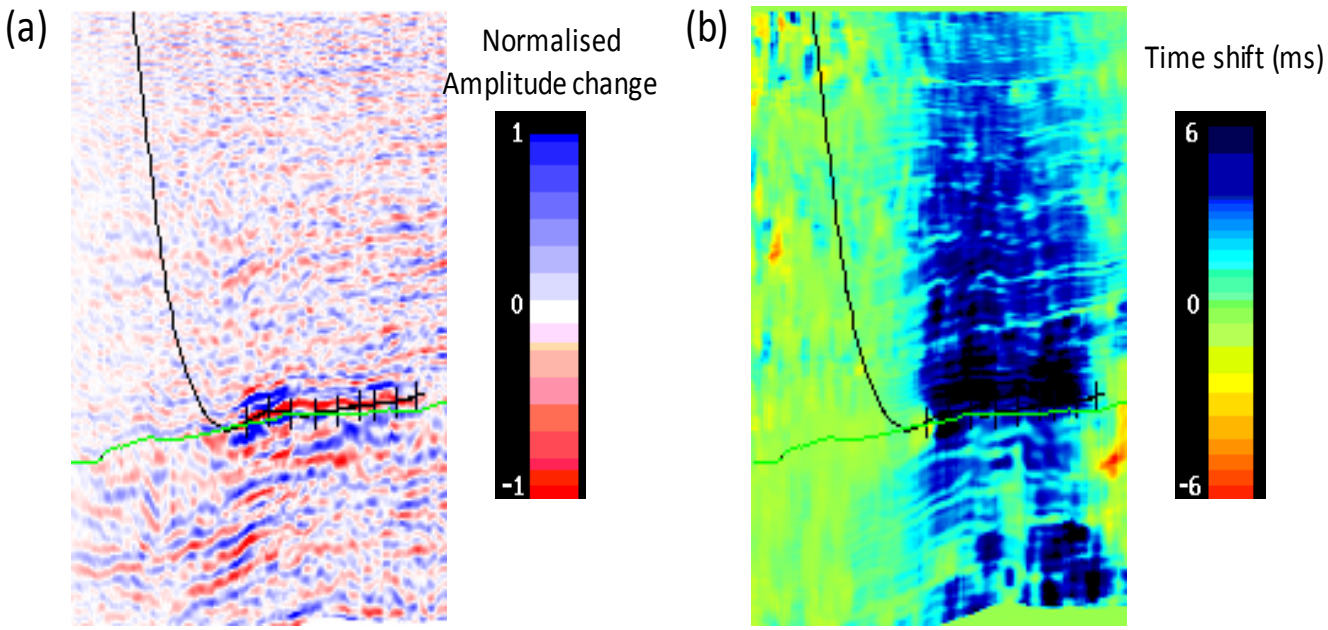

Figure 1.6 (a) A section intersecting a well in the Valhall field through two seismic attributes volumes: (a) amplitude difference and (b) time shift.

On one hand, compaction itself provides additional drive energy for production (amounting up to 50%-80% of the total energy); on the other hand, the effects of compaction occurring inside and outside the reservoir are important causes for well failures Settari (2002) claims that, in some cases, this may affect 20-30% of wells injected. Therefore, a better understanding of reservoir deformation is the key to optimise field development in a compacting reservoir and 4D seismic has already made a great impact on this topic of research.

1.2 Trends in the development of 4D acquisition

The development of new concepts and technologies for 4D seismic application has grown exponentially over the past two decades. Nowadays, most of the current 4D seismic applications around the world rely on data acquired by towed-streamer method. However, new 4D acquisition techniques, e.g. permanently installed Ocean Bottom Cable system are slowly gaining acceptance with their technical advantages of delivering high quality data and frequent surveys with relatively low cost. Another clear trend is the acquisition of multiple seismic surveys at increasingly frequent intervals. In general, the monitor surveys for most of the early 4D applications were typically shot at the minimum intervals of a few years (e.g. Draugen field, where the pre-production survey was shot in 1990 and the monitor survey shot after 8 years, Mikkelsen and Guderian, 2008). Those for recent projects can be at as short as several months (e.g. average 3 months for the Valhall field, Barkved et al., 2003). This reflects the fact that 4D seismic has become a proven in-depth reservoir management tool after two decades development. In addition, this is also driven by a larger ambition: to monitor the reservoir using continually acquired seismic through its entire life cycle - 'Seismic on Demand', proposed by Watts et al. (2006). In this section, I will discuss the current status of 4D acquisition techniques and the impact of frequently acquired 4D seismic on reservoir management and decision-making process.

1.2.1 From towed-streamer to permanent OBC

It has been more than 25 years since the concept of 4D seismic was first proposed, but the technology was not fully embraced by oil and gas companies until 1990's. Traditionally, the North Sea and Gulf of Mexico (GoM) regions have been the core areas of 4D seismic application but rapidly increasing interest is being registered elsewhere in the world in the recent years (Figure 1.7). Most of these 4D applications utilises data acquired by the towed-streamer method since it is a cheaper option per km^2 and more familiar to the subsurface team. Over the last decade, the towed-streamer technology has also been improved significantly. For example, Q-Marine system which features a range of technological improvements such as steerable streamers, calibrated positioning and source signature now can delivers highly

repeatable 4D seismic data (Musser et al., 2006).There has undoubtedly been a significant success of streamer 4D data for reservoir management over the last decades, especially on the UK and Norwegian Continental Shelf (e.g. Schiehallion, Dijksman et al., 2007; Heidrun, Furre et al., 2006). However, there is a limitation to the improvement of 4D data quality with towed-streamer method. Published studies in the literature (e.g. Watts, 2005) indicated that the best fully processed streamer results could not be as repeatable as single-fold OBC data. With continuous drive to improve 4D data quality, increasing attention is being paid to other recently developed techniques, e.g. re-locatable OBS node, sparse, and in particular, permanently installed OBC system (Calvert, 2005). This is because these new technologies can optimally repeat positions of the sources and receivers which can be hardly achieved between towed streamer surveys due to changes in environmental conditions (e.g. feathering, tidal level and wind). For instance, Figure 1.8 is a schematic illustration of the possible effect of the environmental conditions on the positioning of streamers. Figure 1.9 is a schematic diagram of permanent ocean bottom system, using ocean bottom cable and down-hole sensors.

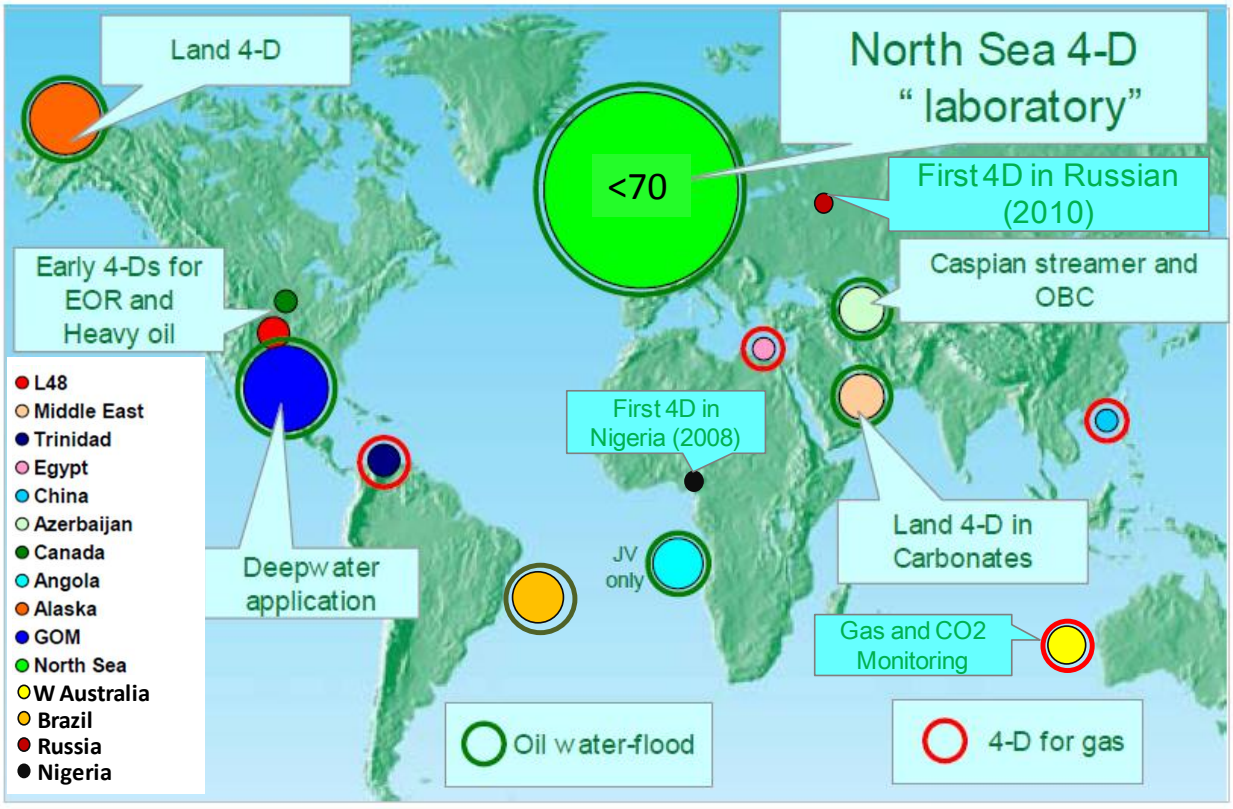

Figure 1.7 4D surveys by region as of 2011 (adapted from Foster, 2008)

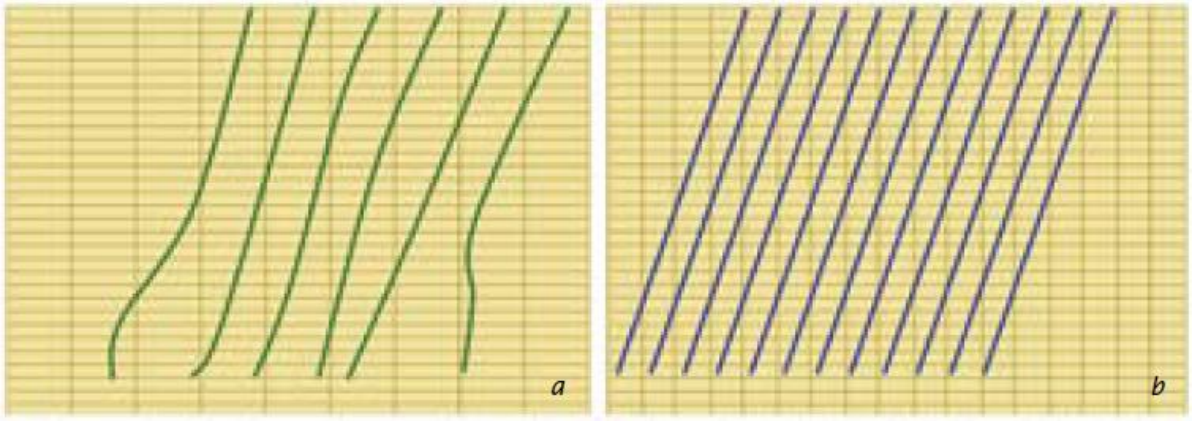

Figure 1.8 (a) Schematic illustration of streamers affected by current change, wind and tide, (b) planned streamer locations.

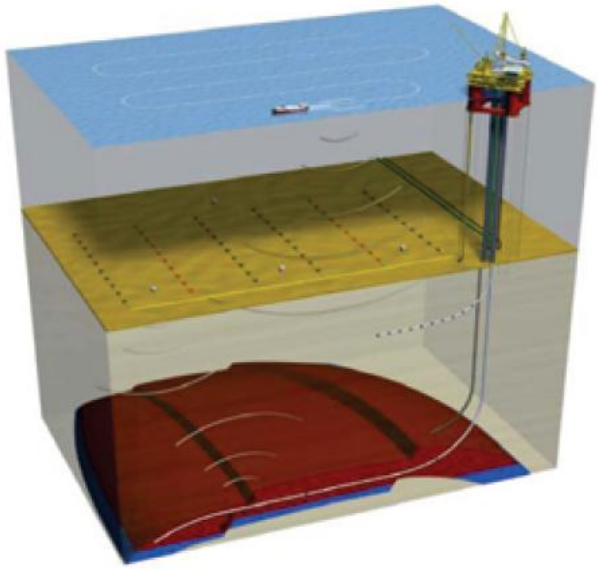

Figure 1.9 A schematic example of an Ocean Bottom Cable system (after Smit et al., 2006)

For an OBC system, receiver arrays are fixed on the sea floor, thereby maximising the repeatability on the receiver side. Without the need to tow and position the steamers from a few hundred to thousand meters, the mission of the seismic vessel concentrates on entering the planned positions for a single source array, normally achieved with high level of precision (+/- 5 meters with the help of GPS, Smit et al., 2006). With the perfect repetition of the acquisition geometry, the OBC system offers a chance to focus on evaluating and minimising

errors related to other non-geometric parameters such as source signature and to streamline the acquisition and processing flow. With better repeatability, 4D surveys acquired by permanently installed seismic system can reveal smaller production-related changes and provide earlier, more detailed, and better understanding about reservoir performance than the streamer 4D method (Smit et al., 2006). The system can also record passive seismic events induced by production activity and background noise, suggesting a prospect for better synthesis and integration with data from other measurements (Kristiansen et al., 2000). A generic comparison between the OBC and streamer method with regard to a range of practical acquisition factors is shown in Table 1.1. The first pilot OBC project in 2003 over the Valhall field achieved great success (Barkved, 2004); and its application in parts of the world started to gather pace. For example, similar projects have been initiated on the Clair Field (Foster et al., 2008), the Snorre Field (Morton et al., 2009), and the Ekofisk Field (Haugvaldstad et al., 2010).

	Streamer	*Permanent OBC*
Baseline costs	+	
Repeat costs		+
Turnaround time	–	–
Vessel availability		+
Weather sensitivity		+
Surface obstructions		+
Subsea obstructions	+	
4-D repeatability		+
4-D confidence		+
S/N		+
S-wave imaging		+
Subsurface imaging		+
Vertical resolution	+	

Table 1.1 Comparison between streamer and OBC method, '+' indicate preferable option (after Smit, 2006)

1.2.2 **Increasingly frequent 4D acquisitions**

For production engineers, it is a common practice to measure parameters such as flow rate, and pressure in wells continuously. For seismic, monitoring is only achieved at discrete time snapshots. In most of the early 4D applications, most commonly, only one monitor survey is shot and at least a few years after the baseline is acquired, owing to the high initial cost and limited acceptance of 4D seismic. Nowadays, 4D surveys are shot at unprecedentedly short intervals and there is evidence (e.g. Ricketts & Barkved, 2011; Johnston, 2011) that the frequency for 4D acquisitions will see further increase.

Infrequent 4D surveys are satisfactory for infill drilling and updating the reservoir model but frequent surveys are required for reservoir management and to influence the well intervention program. Firstly, drilling in deep water (over 300 meters of water) environment is a very expensive activity. A typical deepwater well costs upwards of US$ 35 million and the drilling expense routinely accounts for a large proportion of the development cost (Adrian and Macfarian, 2008). Thus, deepwater developments tend to have a lower economic tolerance to dry wells; however, the task of well positioning can be extremely difficult for a deepwater project due to the large geological uncertainty related to a low level of well control and data constraint. Consequently, 4D seismic is the only tool to provide the spatial information about the reservoir, therefore can become extremely important for well planning and production management. This is particularly true if an aggressive drilling schedule is planned at certain points in the field development, with the cost for repeated 3D monitoring with a towed-streamer survey in the approximate range of US$ 4-6 million.

Secondly, the acquisition of multi-vintage data at frequent intervals is part of the prospect of ‘Digital field’ - involving optimal management of the reservoir through frequent reservoir monitoring and quick reservoir model updating (Watts, 2005; Foster et al., 2008). As time elapses, dynamic reservoir changes caused by well production or injection develop from the near well bore regions to other regions of the reservoir. The resulting water front movement or pressure changes in the reservoir are controlled by the heterogeneous geology, and thus will reveal details of the reservoir heterogeneity in the 4D signature, see for example the Sleipner field (Figure 1.10). A close monitoring of such dynamic changes occurring in the reservoir provides a reality check for the simulation results – leading to better simulation predictions. The need to acquire frequent surveys is driven by a decrease in the net value of

the existing information (information entropy increase) upon which the future reservoir status is predicted as shown in Figure 1.11 (Calvert, 2005).

Furthermore, to acquire multiple seismic surveys at frequent intervals has become economically viable due to the reduced cost. For conventional towed-streamer 4D surveys, it can be attributed to the increasingly mature and rapidly expanding 4D acquisition market which has significantly driven down the price to acquire each individual monitor survey (Sandø et al., 2009). For example, many fields such as Norne (Osdal and Alsos, 2010) and Schiehallion (Floricich et al. 2008) have been repeatedly shot with seven or eight towed streamer surveys at intervals of 12 to 24 months apart. For the OBC solution, it is shown that monitor surveys shot at frequent intervals of less than a year can be acquired at relatively low cost in spite of a high initial cost (Foster et al., 2008). A range of field examples can be found in publication, e.g. Valhall field (Barkved et al. 2006), Clair field (Foster et al. 2008), the Snorre field (Morton et al. 2009), and the Ekofisk field (Haugvaldstad et al. 2010).

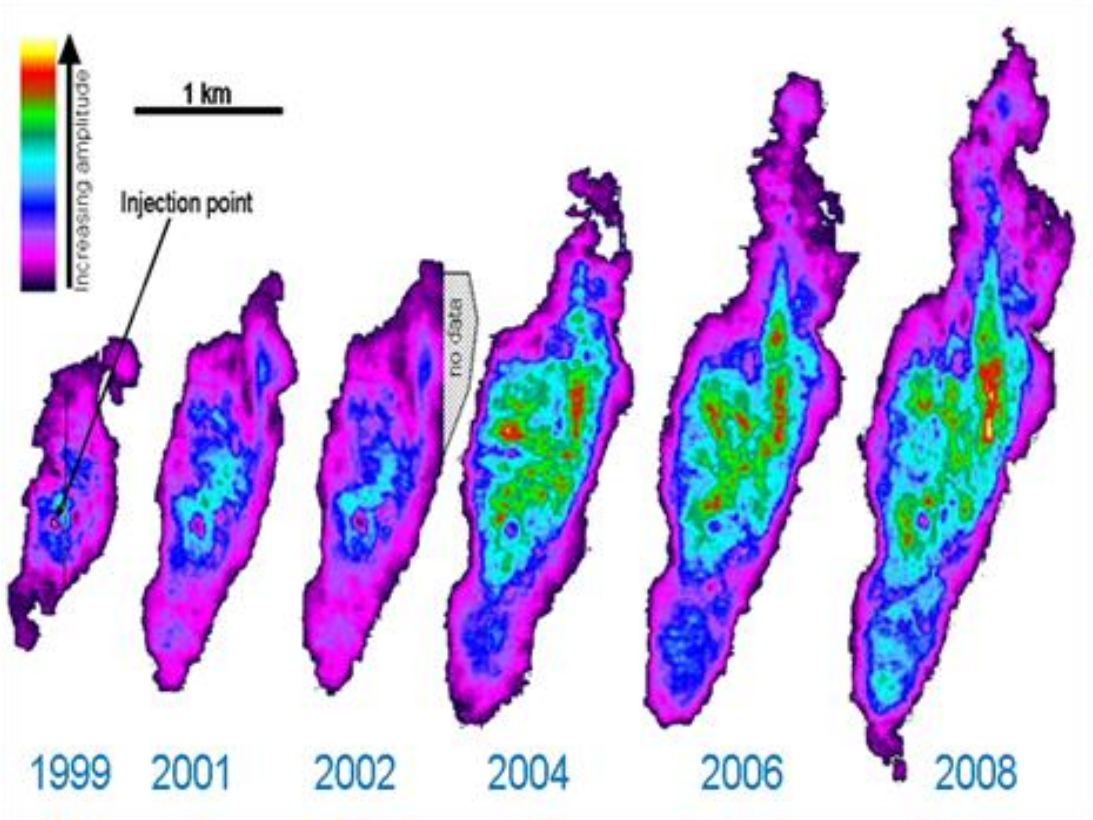

Figure 1.10 Frequently acquired 4D data illustrate the development of a CO2 plume over 10 years since first injection (after Sandø et al., 2009).

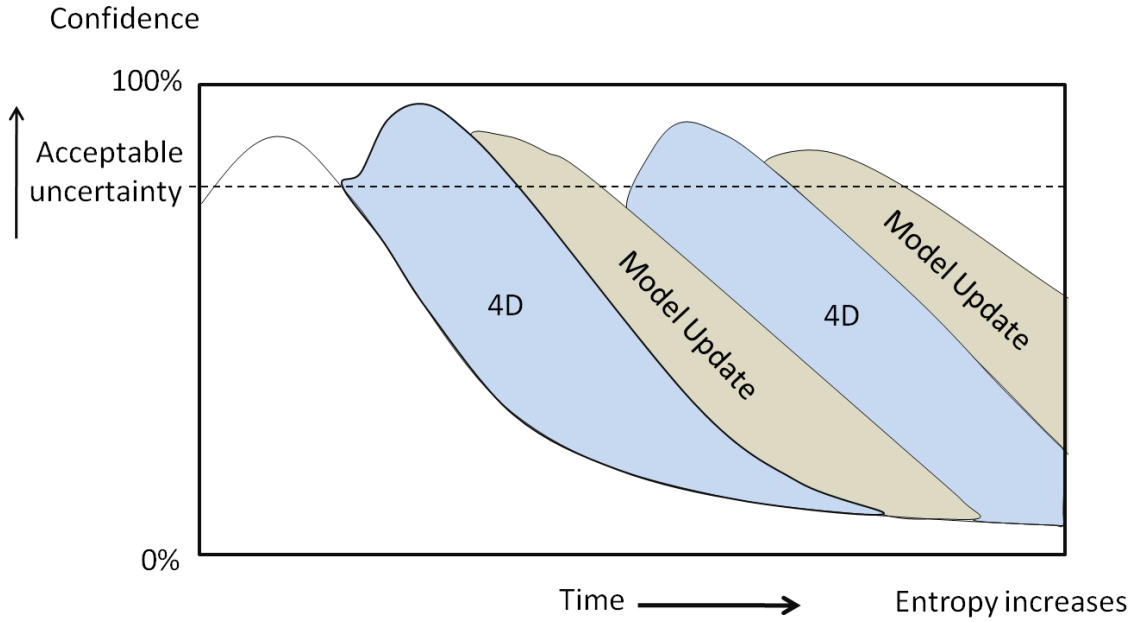

Figure 1.11 Schematic illustration of increased uncertainty on simulation predictions following 4D surveys (adapted from Calvert, 2005).

1.3 Practical challenges in 4D interpretation

At the asset team level, a 4D study focuses on planning the location of in-fill wells by identifying un-drained areas, thus is mostly carried out on the seismic products where 4D signals have been optimally enhanced through one or multiple processing workflows conducted by a service company. However, some practical issues related to inherent problems of 4D seismic may still complicate the simple underlying concept of 4D seismic, even for 4D data that have gone through most sophisticated workflows.

1.3.1 Non-repeatability noise

In principle, the 4D seismic signal is expected to only image the production-related reservoir changes if seismic vintages are acquired by an unchanged observation system, under the same environment conditions and passed through an identical processing workflow. Under these ideal conditions, the ray path for each shot is perfectly repeated, allowing the image of

unchanged geology and noise in different seismic vintages to cancel out each other. However, such perfect repetition of a baseline survey is impossible to achieve in reality. In practice, the non-repeatability issue may be rather noticeable if the seismic vintages used for 4D interpretation were acquired without any 4D application in mind. This is usually the case for early 4D applications when the technique had just entered the attention of the asset team. However, the level of repeatability can be significantly improved if all the possible factors varying between the seismic surveys are treated meticulously (e.g. dedicated 4D surveys). The residual differences between repeated seismic data, independent of production-related reservoir changes, are often referred to as '*non-repeatability noise*'. *Appendix 1* will give an overview of the most commonly observed non-repeatable factors between 4D seismic surveys, which if not properly repeated, will have major impact on the quality of 4D data. Such type of noise is usually measured by a value of Normalised RMS (*NRMS*) computed for the difference data within a defined window above the reservoir interval (see Appendix 2). An example for the Nelson field is presented by Brain (2007) as shown in Figure 1.12. Poor repetition of baseline source-and-receiver positions due to congestion of the production facility (high *NRMS* values in the red color of Figure 1.12a) results in a stripe-shaped undershooting area where noise levels are clearly higher as shown in the 4D amplitude difference map (Figure 1.12 b). This type of noise, interferes with the real production-related signals, and can lead to ambiguities when an attempt is made to understand the observed signals in a 4D attribute map. This is particularly true because *NRMS* mapped from a time window above the reservoir is the 4D noise in the attribute difference map generated for the reservoir interval – a high noise level may also be present where a low *NRMS* is indicated. Such erroneous information may impose uncertainty to understanding the true production-affected area, increasing risk for the planning of new wells.

(a)

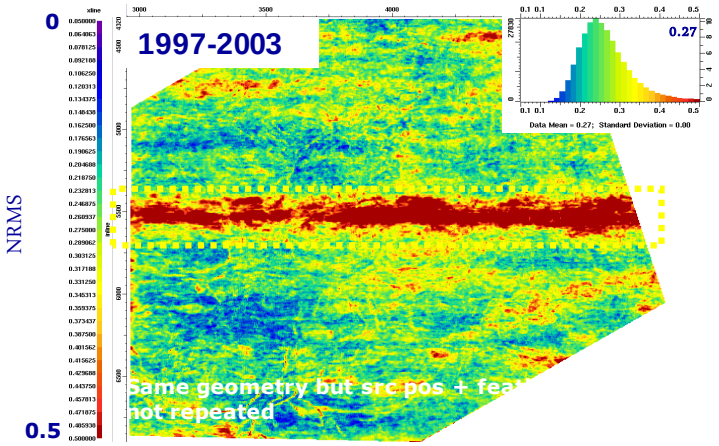

(b)

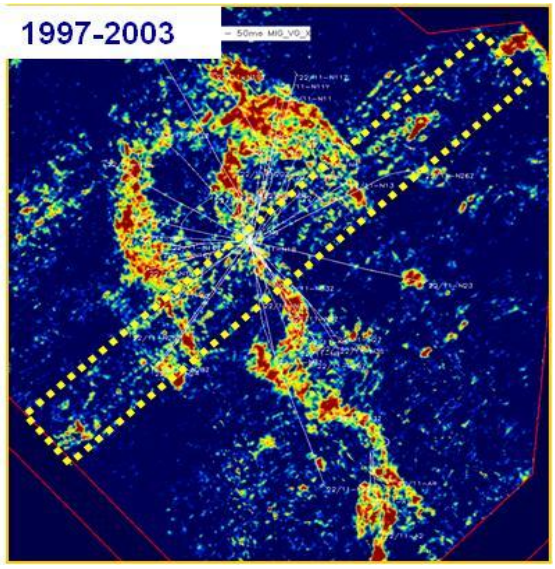

Figure 1.12 (a) *NRMS* map calculated for a defined time window above the reservoir interval of the Nelson field, and (b) Corresponding 4D amplitude difference between 1997 and 2003 extracted from a time window surrounding the picked reservoir top (Brain, 2007).

1.3.2 Overlapping of pressure and saturation effects

Production activity from a hydrocarbon reservoir is known to induce more than one type of change in the reservoir, among which changes in oil/water saturation and pore pressure are the focus of most 4D projects. To interpret 4D signals dominated by each individual type of change is usually straightforward, and many successful examples for 4D applications relied on the simplicity in the 4D signals afforded by special reservoir conditions. For instance, in a

highly permeable and connected reservoir, localised pressure changes around a production well can rapidly dissipate into aquifer or are balanced by the pressure effect of neighbouring injector wells. Under such condition, reservoir pressure may remain at an almost constant level across the field during production which is ideal for monitoring water sweep (e.g. Daugen field as shown in Figure 1.13). In many cases, changes in both pressure and fluid saturation are expected for most of the production scenarios (e.g. water injection). These two effects may overlap and result in a weakening or enhancement of the 4D response of each individual effect depending on the production scenarios (Figure 1.14). No matter which case it is, the interpretation of the 4D signal will almost certainly become complicated when multiple simultaneously acting effects contribute to the seismic.

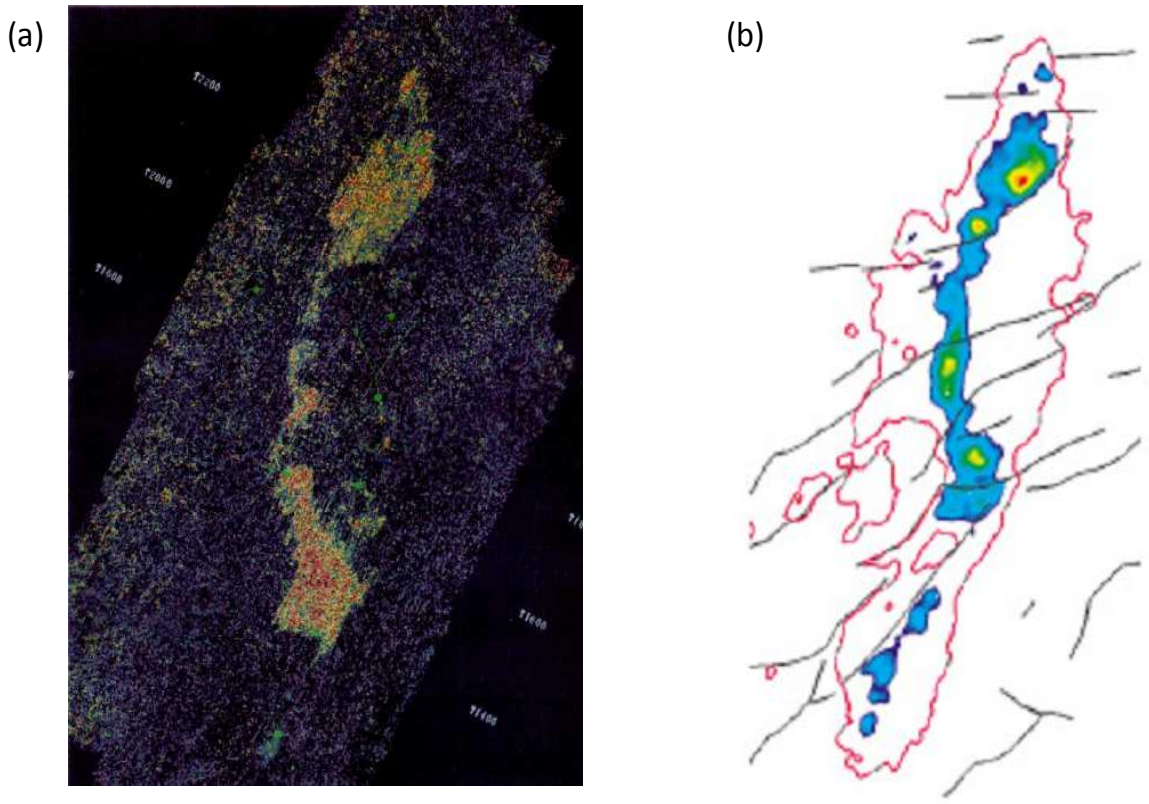

Figure 1.13 (a) Observed saturation-driven 4D signal between monitor and baseline survey over the Draugen field, (b) manual interpretation of the 4D difference map in (a) indicates the clear effect of water saturation changes. Fault locations across the field are highlighted by black lines and OWC by red line (after Koster et al., 2000).

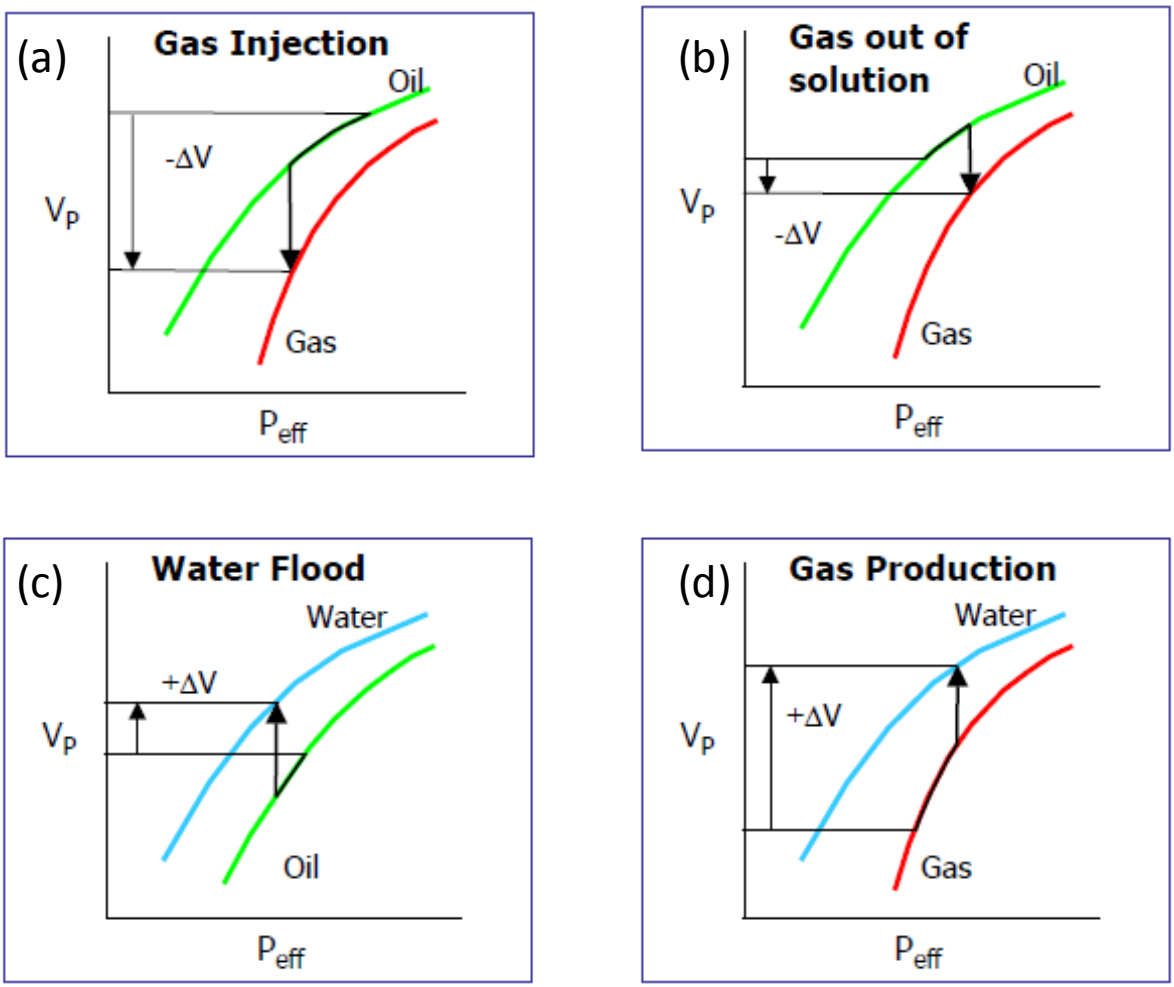

Figure 1.14 Generalised plots of P-wave velocity change in the following production scenarios, (a) gas injection; (b) gas out of solution; (c) water flood and (d) gas production (after Marsh, 2004).

For instance, increased gas saturation during the gas injection operation (gas is highly compressible fluid) increases the overall compressibility of the rock, reducing the velocity at which seismic wave travels in the rock. On the other hand, the injected gas volume may cause pressure escalation within an area from the well, which reduces the effective stress (defined as the difference between the confining pressure and the pore pressure) on the reservoir rock frame – which will also reduce the velocity as shown in Figure 1.14a. In this case, 4D signals related to increased gas saturation may be masked by the pressure build-up as both effects are associated with the same polarity. On the other hand, interpretation of the 4D signal as result of pressure and saturation change with contradictory effects on seismic velocity is considered to be an even more challenging situation. Such situation is associated with a variety of

production scenarios, such as water injection and gas coming out of solution due to reservoir pressure below bubble point (see Figure 1.14b and 1.14c). For instance, seismic velocity of the reservoir rock is reduced by increased pressure, but increased by increased water saturation within an area from injectors, which results in the weakening of the 4D response associated with either production effect. Moreover, it has been noticed that dominance of the pressure or saturation effects in the 4D signature might vary according to rock type, facies distribution and their relative strength of them in different regions – possibly leading to rather complex patterns in the 4D signature. Figure 1.15 shows such an example, where an injection well is placed in a closed compartment. The 4D signature (Figure 1.15a) shows that a 'hardening' signal related to a water saturation increase can be observed in a region around the injection well; and beyond that, pressure change is the main drive for the 4D seismic changes. Furthermore, many methods can be found in the literature to decipher the 4D seismic signal into changes in saturation and pressure, e.g. Bervik (1999), Landrø (1999, 2001, 2002 and 2003), Tura and Lumley (1999), Ribeiro and MacBeth (2004 and 2005), He et al. (2005), Hansen et al. (2005), Floricich et al. (2005), etc. These methods commonly utilise multiple independent attributes, and rock physics relationships established either by empirical or experimental methods. Nevertheless, with considerable uncertainty in the inverted results for pressure and saturation changes, interpretation of the 4D signal related to multiple dynamic reservoir changes still represents a major challenge for 4D studies.

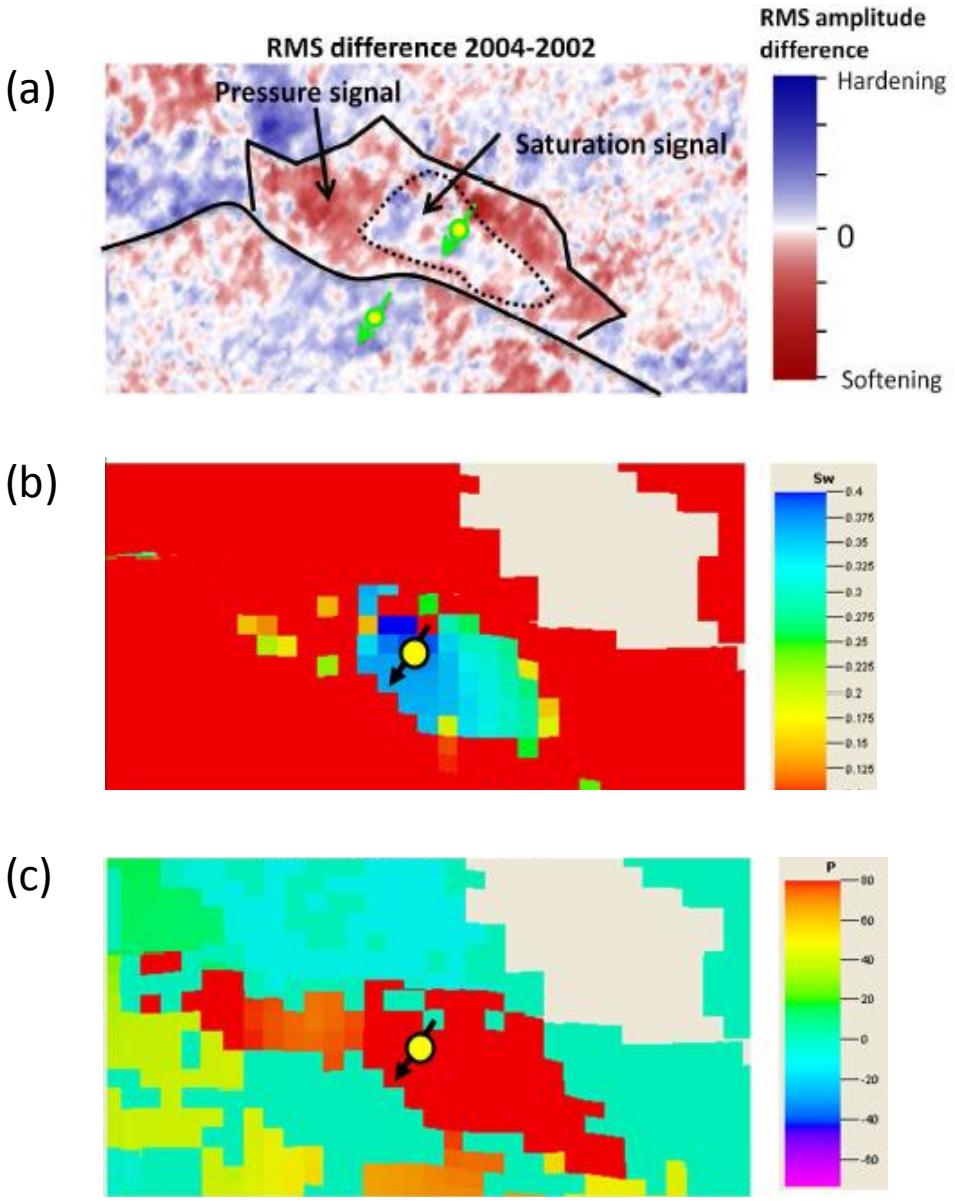

Figure 1.15 (a) Mapped 4D changes over the Schiehallion field reveal a reservoir compartment (highlighted by the black line) in which only one injection well is positioned. Within an area from the injector, the 4D change is saturation driven, beyond which, pressure effects become dominant; (b) and (c) show the predicted changes in water saturation and pressure from the simulator.

1.3.3 The interfering response of densely positioned wells

To develop a hydrocarbon reservoir, it is a common strategy to drill a considerable number of wells as each individual well can only effectively recover the hydrocarbon volumes within a limited surface area from the well bore due to reservoir heterogeneity (see Figure 1.16). Conventionally, the density of the wells is further intensified during the secondary recovery stage in which new in-fill production wells and water injectors are drilled to provide an opportunity for enhanced oil recovery.

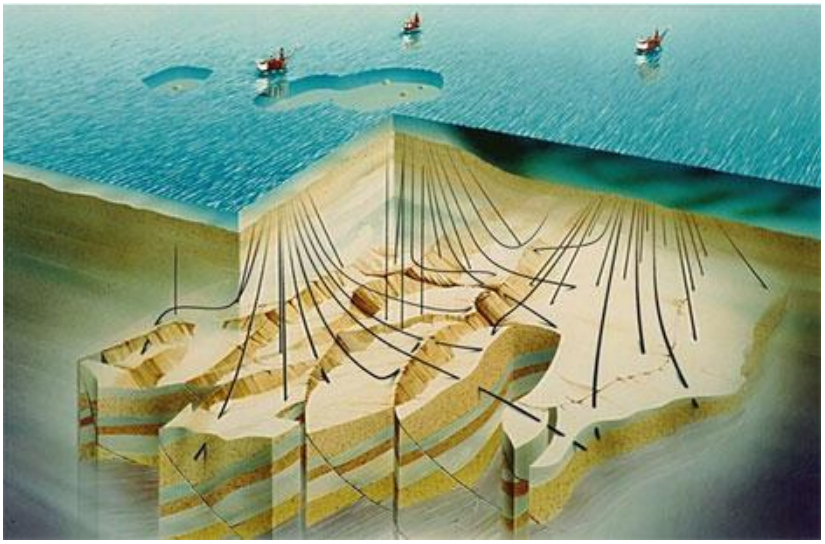

Figure 1.16 Densely positioned wells in a reservoir for enhanced oil recovery (Courtesy of Statoil)

Understanding the reservoir fluid movement between water injection and production wells, and the pressure evolution between production wells, represents the main challenges to optimise the oil recovery in a North Sea reservoir. For instance, the knowledge of water movement in-between the wells is the key to reservoir management that delays water breakthrough in production wells. 4D seismic data have been widely accepted as a key information source for dynamic reservoir changes, particularly, those occurring in the inter-well space. However, the ability to recover full value from such data is usually made difficult by the fact that wells are densely positioned in the reservoir. The precise resolution of the 4D response of each individual well cannot be recovered, which leads to non-uniqueness in the 4D interpretation under certain conditions. Van Gestel et al. (2010) shows such an example from the Valhall field (see Figure 1.17) where a horizontal water injection well (WiB) is located amid a number of production wells, and the distance between the neighboring wells

ranges from 100 to 500 meters. Water saturation increase is expected in a localised area around the water injection well (see simulated water saturation change in Figure 1.17b), and pressure depletion around the producers. Both effects are dominant in the 4D signature and result in 'hardening' of the reservoir rock, yielding positive changes in seismic amplitude which represents a challenge to interpretation of the exact location of water front related to this injector. With such 4D signature, an analysis on drainage or injection efficiency of each individual well is not possible despite excellent data quality due to good repetition of survey conditions. In addition, the grey lines superimposed on Figure 1.17 indicate fault locations, and interpretation of reservoir connectivity across these faults is mainly dependent on understanding the 4D seismic signals. This is not possible since determination of pressure and saturation response is difficult using the 4D attribute map due to the proximity of these wells.

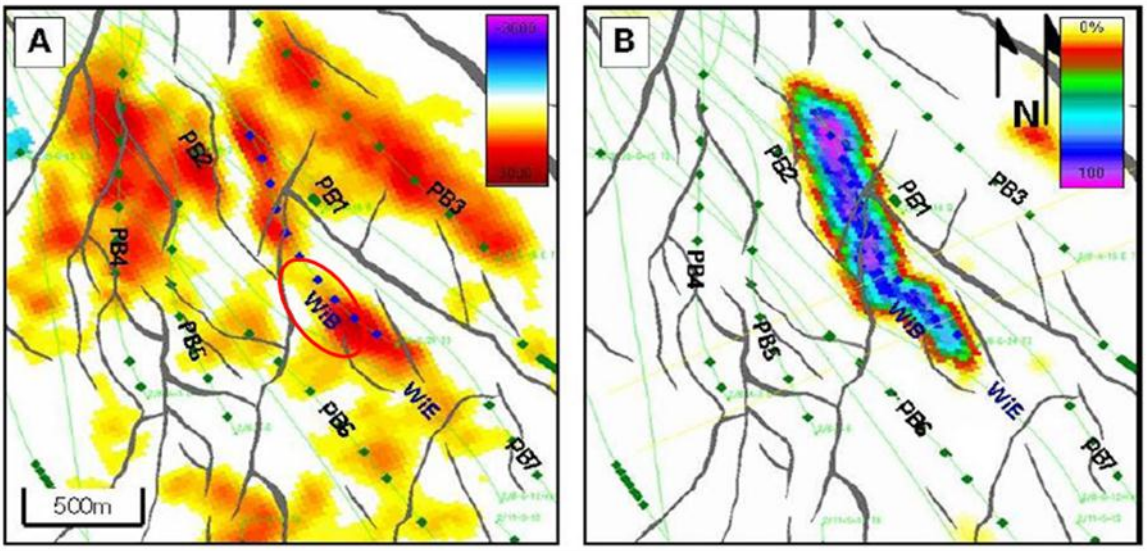

Figure 1.17 (a) Observed amplitude difference between the 10th monitor survey and the baseline, (b) Modelled changes in water saturation over the corresponding period. The green lines are wells, and green diamonds are perforations, grey lines are mapped faults (after Van Gestel et al., 2010).

1.3.4 Inconsistencies between the 4D seismic and engineering domains

Due to the non-uniqueness in the 4D seismic data, the best way to minimise the uncertainty in the 4D interpretation is to cross-validate 4D information with engineering (Figure 1.18).

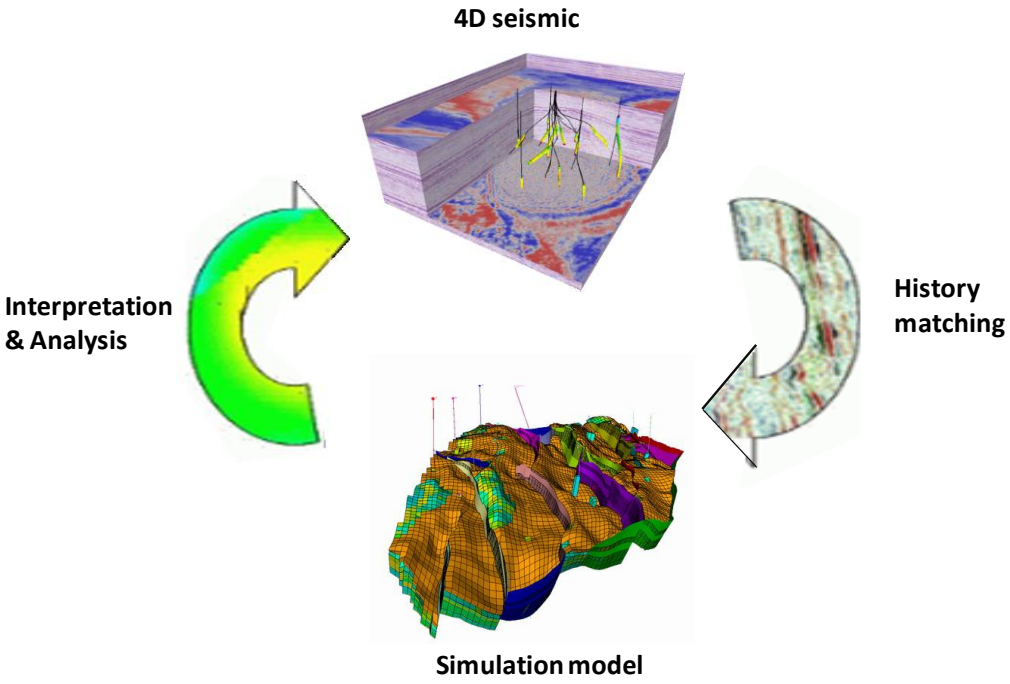

Figure 1.18 4D seismic interpretation & analysis rely on information from simulation model, whilst 4D seismic data provide an extra constraint to simulation model.

A reservoir simulation model, built to honour all available data apart from 4D seismic (e.g. production, well log, geology and 3D seismic, etc.), represents our best understanding about the reservoir (Floricich, 2006 and Hatchell, 2010). In the qualitative approach, the comparison is often performed directly between predicted pressure and saturation changes (engineering domain) and the 4D signal (seismic domain). This can be very effective particularly when the 4D response is associated with the changes in a single dynamic reservoir property. Meanwhile, a quantitative comparison is done in an identical domain with the assistance of *forward seismic modeling* or *seismic inversion*. No matter which method is used, a certain level of similarity in the pattern is expected between simulator-based results and 4D response so that the physical processes created by fluid flow modeling can be related to the observed 4D signals.

When 4D data quality is excellent, such consistency can be easily explained (e.g. mis-positioning of flow barriers in simulation model) subsequently leading to modification of model properties, manually or using automated *Seismic History Matching* (SHM) techniques (see Huang et al., 1997; Stephen et al., 2006; Gosselin et al., 2003). Helgerud et al. (2009)

presented an example from the Marshall field where the location and transmissibility of faults in the simulation model are modified in order to match the clear 4D responses observed.

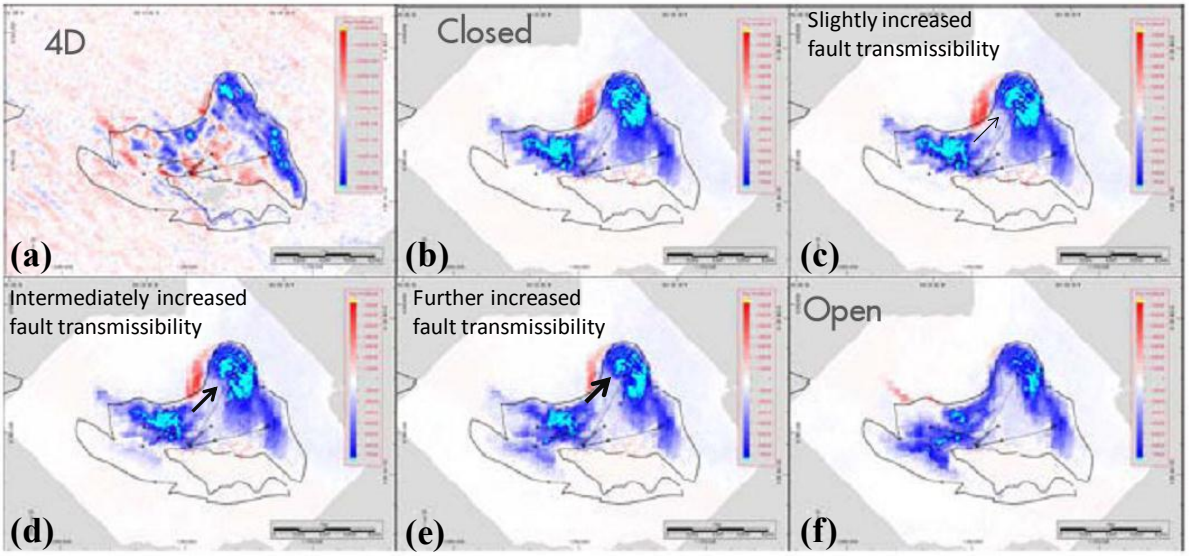

Figure 1.19 (a) Observed 4D signal and calculated synthetic 4D response from the simulation model with fault transmissibility varied from closed to open (b), (c), (d), (e) and (f).

However, when 4D data quality is poor and uncertainty associated with 4D signals is large, a support from engineering domain becomes extremely important to the understanding of the 4D signal. In this case, if there is a large discrepancy between simulated and observed 4D results, it may be difficult to determine whether the disparity should be attributed to the noise in 4D seismic or errors in the simulation model. For instance, Figure 1.20 shows the observed (a) and synthetic (b) seismic change between 2006 and 2004 over the same area in the Schiehallion field. The highlighted area illustrates a discrepancy between observed and synthetic 4D signal. The synthetic is calculated using the *sim2seis* code developed in ETLP which converts the simulated changes in pressure, gas and oil saturation to the 4D response. Between the time of these two surveys, production well P1, and water injection wells I1, I2 are active. The signal in blue around I1, indicating a 'hardening' effect, can be related to the *pressure relaxation* after the injector I1 is switched off. According to the simulation, this pressure-relaxation signal is extensive and stretches into the highlighted area in Figure 1.20 (b). In contrast, a red signal indicating 'softening' of the reservoir is observed in the same area in the mapped attribute changes taken from the observed data as shown in Figure 1.20a.

A possible explanation of this 'softening' signal is gas breakout due to pressure depletion related to production from P1. As the Schiehallion field is very complex in terms of structure and intra-reservoir hydraulic connection, the simulated result may contain large uncertainty whilst 4D data cannot be unambiguously interpreted due to low signal-to-noise ratio in some local areas. Therefore, there is a risk to simply modify the simulation model to create a similar response without understanding the meaning of the unexpected 'softening' signal (it may simply be noise, e.g. a shadowing effect related to production in the upper layers or 4D multiples). Such noise has been reported previously by other researchers in other areas of the Schiehallion field (e.g. Floricich et al., 2007).

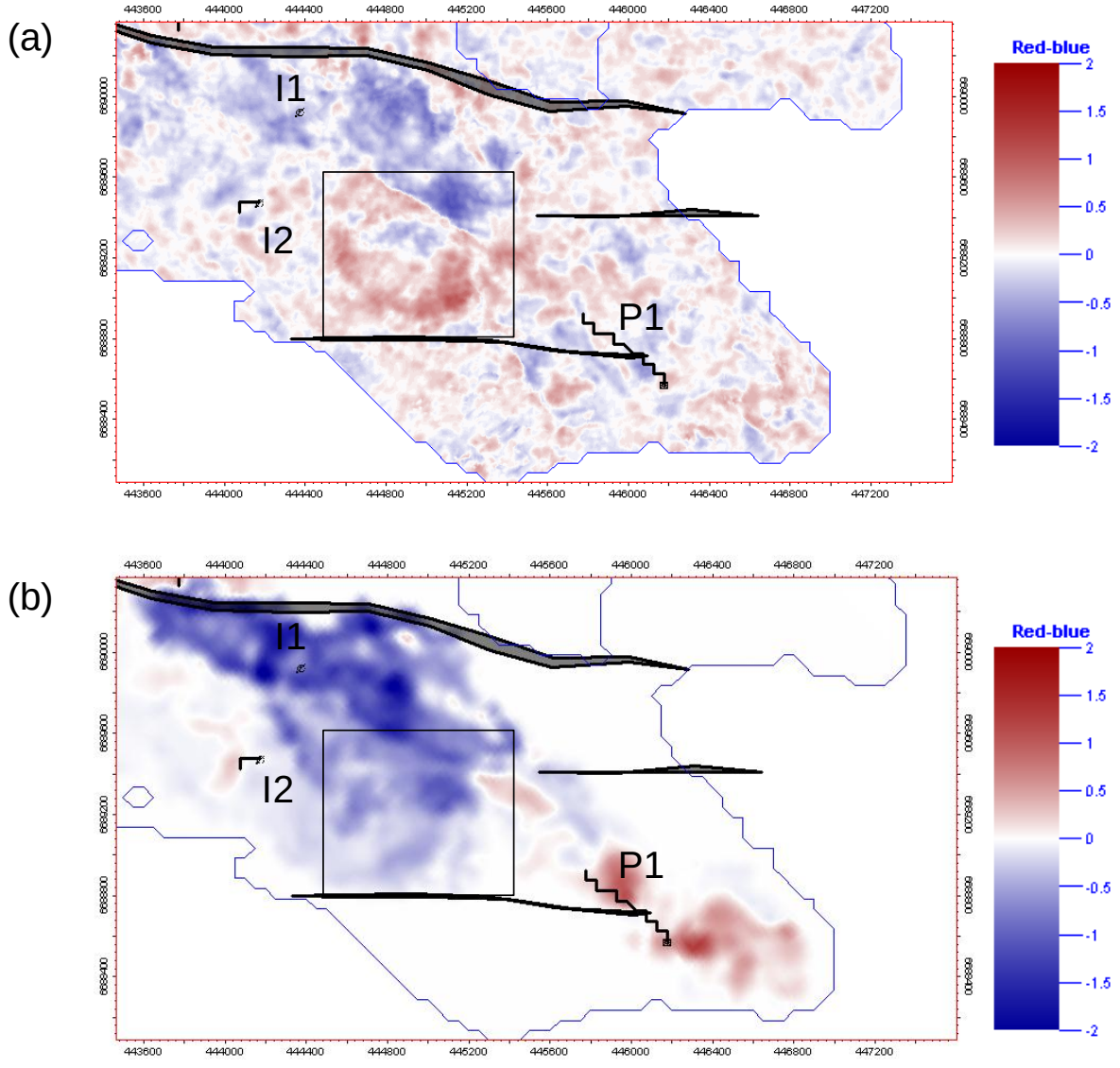

Figure 1.20 Distinct differences between the observed (a) and synthetic (b) 4D signals lead to considerable interpretation uncertainty.

1.4 Main challenges of this thesis

Despite the geoscientific community possessing significantly improved 4D data quality compared to early studies, a number of practical challenges in 4D interpretation are still facing asset team in everyday life, and these challenges have been discussed in this chapter. These problems are thought to be not only related to the residual non-repeatability but also inherent limitations of the 4D seismic product (e.g. 4D signal sensitive to saturation and pressure changes simultaneously). Thus the major challenge of this thesis is the development of a technique to address these problems with 4D interpretation. Moreover, two industrial trends for the development of 4D seismic have been discussed: first, the market share of towed-streamer surveys is slowly evolving to incorporate more sophisticated acquisition techniques (e.g. retrievable node, high density OBC, and permanent OBC); second, acquisition of multi-vintage data at frequent intervals. These developments have provided additional dynamic reservoir information to the field operators – it is believed that the information can be included in conventional engineering workflows (e.g. history matching). Another challenge of this thesis is to explore ways to utilise the largely redundant information from multiple seismic surveys – a temporal behavior of the 4D signature should be taken into account in the 4D interpretation.

In principle, well production and injection induce changes in the dynamic status of the reservoir, and in turn manifests as 4D seismic changes – thus causality should exist between 4D seismic and well activity as shown in Figure 1.21. Therefore, it is also my understanding that there is more information content in the 4D signatures than initial inspection suggests and this may be explored by a closer integration of 4D seismic and well activity. Huang et al. (1997) have shown that such integration, if performed directly in the data domain, has many advantages over the modeling domain. I believe that this idea can be further developed using multi-vintage data. Thus another challenge of the thesis is to explore methods which provide a better integration between 4D seismic data as 3D volume or 2D maps with well production data (1D time sequences).

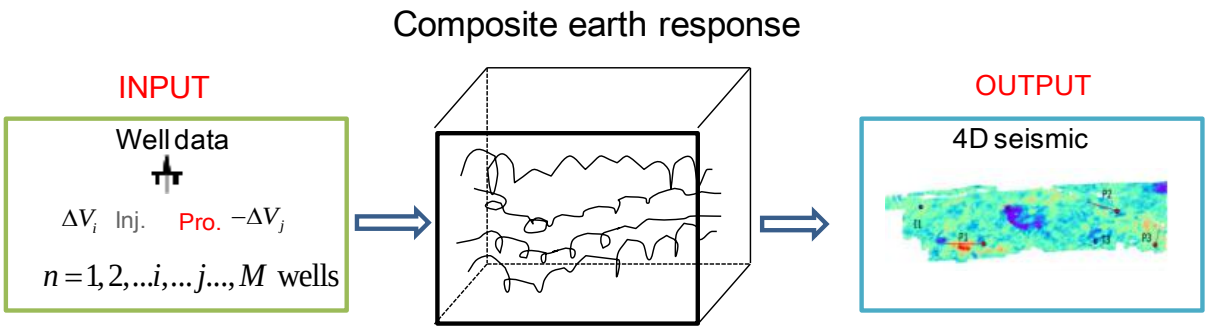

Figure 1.21 Causality between well activity and 4D seismic signatures via a system linking them defined as '*composite earth response*'.

1.5 Thesis outline

The remainder of this thesis is divided into six chapters:

Chapter 2 discusses the nature of 4D signals as result of well production and injection – highlighting the importance in establishing the link to production data in the context of 4D interpretation. This chapter provides an overview of the techniques in the literature used for such integration. These methods are compared in terms of their advantages and disadvantages, indicating a need to explore new techniques for direct integration of the two data types.

Chapter 3 introduces a new correlation technique to directly connect production data (expressed as cumulative fluid volumes) to 4D seismic responses over corresponding survey periods, where sequences of seismic changes are calculated at each location in the reservoir. These are correlated to an identical sequence of cumulative volumes derived from well activity of each particular well, generating a map of *Normalised Correlation Coefficients* (NCC). The potential application of this technique is explored using model-controlled data for an idealized compartmentalised reservoir. An overview of the field datasets used for testing the new technique is also given in this chapter.

Chapter 4 presents the application of this newly developed methodology to a *UKCS* field - Schiehallion. The results highlight connected regions to each particular well of interest and reduce ambiguities in dynamic reservoir interpretation. Correlation signatures (NCC) from the technique are validated by the latest simulation model and are useful to simulation model updating.

Chapter 5 applies the technique to frequently acquired surveys from the *Life of Field Seismic* (LoFS) system installed in the Valhall field in the *Norwegian Sector* of the North Sea. The Valhall field is featured by low permeability compacting chalk yielding very different 4D signals in character from the Schiehallion. The results are encouraging as it shows potential to solve some of the previously identified problems with interpretation of 4D signals, e.g. the location of gas breakout is masked by strong compaction.

Chapter 6 discusses another field study carried out on the datasets from the Norne field. Similar to Schiehallion, the Norne field consists of a number of segments and the technique is tested on the G-segment aiming to solve uncertainty in the interpretation of reservoir connectivity. This field application raises a number of interesting questions related to reservoir characterisation and 4D interpretation, which requires an explanation. This involves using the *NCC* map to identify uncertain flow pathways to the G-segment and the previously mis-interpreted water flooded region. A study of 4D noise with regard to the routinely used non-repeatability measure (e.g. *NRMS*) has been carried out and will also be shown in this chapter.

Chapter 7 presents a summary and conclusions for this work. In addition, recommendations are suggested for future development of the techniques shown in this thesis.

Chapter2

Integrating well production data with 4D seismic interpretation: an overview

This chapter is devoted to discussing the nature of the 4D signal as consequence of the well activity. In practice, to identify such a causal link is important to understanding the underlying physical processes that a particular 4D signal represents. For instance, the 'hardening' of the 4D signal is interpreted as a water saturation increase when it is associated with a water injection well, but as pressure depletion if it is situated around a production well. On the contrary, if a 'softening' signal surrounding a water injector is observed, localised pressure 'build-up' is inferred; but if the anomaly surrounds a producer, gas breakout is thought to be the cause. Clearly, true physical meanings for the 4D signal cannot be un-ambiguously understood without being put into the context of the well activity. In this chapter, existing methods used to establish such a well-to-seismic link are classified into two categories: direct and indirect methods. In the first category two methods are discussed: the first is based on *visual correlation* and the second which was proposed by Huang et al. (2007) is based on the linear relationship established between injected gas volume and 4D amplitude changes from empirical observation. The indirect approach utilizes a range of modelling techniques (*fluid flow simulation*, *petro-elastic modeling* and *forward seismic modelling*) aimed to transfer information in the engineering domain (predicted changes in dynamic reservoir properties) to the seismic domain (synthetic 4D) so that it can be compared to the observed 4D data. The

uncertainties in this model-based method are reviewed in this chapter – promoting a need to explore alternative methods.

2.1 Causality between well activity and the 4D seismic response

Historical production data are usually organised in the format of a spread sheet which contains instantaneous flow (daily or monthly) rates of different types of fluid produced or injected at wells under the surface condition. For instance, the production data of a typical producer in a North Sea reservoir is plotted and shown in Figure 2.1 (water rate shown in red and oil rate shown in blue). Generally, instantaneous (time-averaged) flow rates, containing temporally high-resolution information, reflect the real-time status of a producing reservoir, e.g. *water cut* indicative of sweeping efficiency. As a result, they are usually used in production history matching to the improve accuracy of simulator predictions. For interpretation of 4D surveys, such daily (or monthly) averaged flow rates are not considered to be suitable since seismic surveys are currently shot at intervals of several months to years apart. Between the times of the two surveys, it is understood that the 4D difference must be related to the total cumulative volumes produced or injected (under the reservoir conditions). Cumulative volume for each type of fluid is calculated using *equation* 2.1, and formation volume factor is employed to convert the fluid volume measured under the surface condition to that in the reservoir.

$$\Delta V = B_f \int_{t1}^{t2} q_f(t)dt \tag{2.1}$$

Where B_f is the *formation volume factor* for a given fluid (i.e. B_o for oil and B_w for water); q_f the flow rate; t_1 and t_2 the times at which the baseline and monitor survey are shot. Thus the total fluid volume (green line in Figure 2.1) produced by the production well of which fluid rates are plotted in Figure 2.1 can be written as *equation* 2.1, given that only oil and water phases are produced.

$$\Delta V = B_w \int_{t1}^{t2} q_w(t)dt + B_o \int_{t1}^{t2} q_o(t)dt \qquad (2.2)$$

Where, $q_w(t)$ and $q_o(t)$ are production rates of oil and water, respectively. Thus, at any particular location in the reservoir, the 4D signature is a direct function of the nearby well activity (Figure 2.2). By modifying the proposed pressure-saturation equation of MacBeth et al. (2005) to involve only well activity, the 4D signature ΔA at location (x_i , y_i) and between a fixed time period ΔT can be written as the summation of a number of functions $f(\Delta V_j)$ of the cumulative injected or produced volumes ΔT_j from each of the N wells (j=1, N) in the field (see *equation 2.3*).

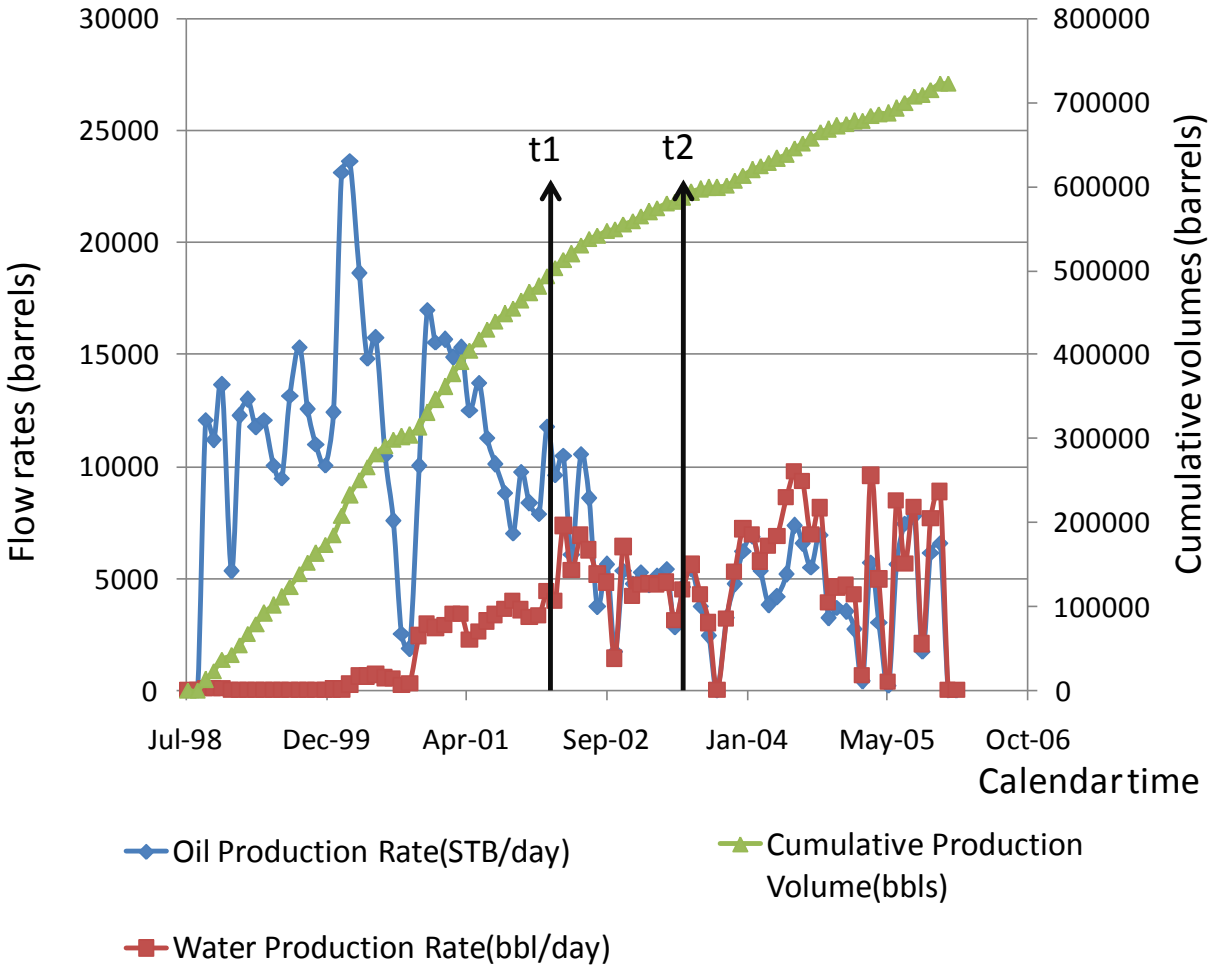

Figure 2.1 The production data from a typical production well, with oil and water production rate indicated by blue line (with diamonds) and red line (with squares) respectively. From oil and water

production, the cumulative fluid volume (oil + water) at reservoir condition can be calculated, shown by green line with rectangles.

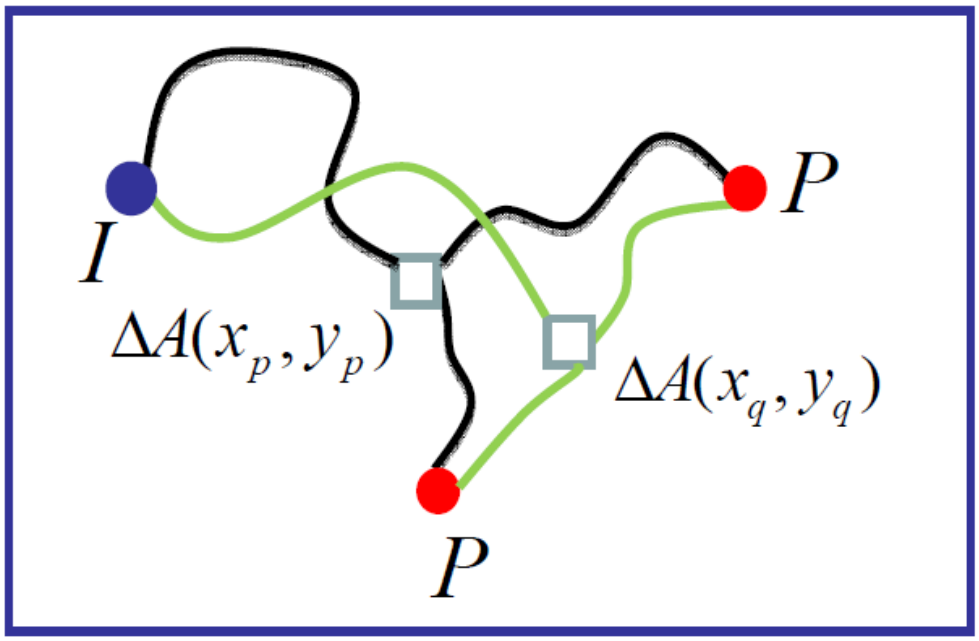

Figure 2.2 The 4D signature and connectivity for two generalised locations (xp,yp) and (xq,yq) are given by differently weighted sums of the cumulative volumes from the producing (-ΔV) and injecting (+ΔV) wells.

$$\Delta A(x_i, y_i) = \sum_{j=1,N} [\psi_p(x_i, y_i) f_p(\Delta V_j, G_{ij}) + \psi_s(x_i, y_i) f_s(\Delta V_j, G_{ij})] \qquad (2.3)$$

The coefficients $\psi_p(x_i, y_i)$ and $\psi_s(x_i, y_i)$ determine the strength of the response to local pressure and saturation change respectively, and are related to local geological conditions (the petroelastic model). These two coefficients are considered to be unchanged throughout the time of production. The functions $f_p(\Delta V_j, G_{ij})$ and $f_s(\Delta V_j, G_{ij})$ convert the cumulative fluid volumes injected or produced into vertically-averaged changes in pressure and saturation at location (x_i , y_i). These two functions are controlled by G_{ij} which lumps together the connectivity between the well and location (x_i , y_i), the boundary conditions and initial state of the reservoir. Given the complexities for fluid flow in a heterogeneous reservoir, it is usually not possible to determine the explicit forms for $f_p(\Delta V_j, G_{ij})$

and $f_s(\Delta V_j, G_{ij})$. According to *equation 2.3*, it may not be straightforward to relate the 4D response ΔA at location (x_i , y_i) and well activity ΔV injected or produced at a particular well over a survey period ΔT. For instance, consider the 4D signature is driven by pressure change, the amount of pressure change caused by a given well (e.g. water injection well) may be balanced by pressure effect of the neighbouring wells (negative ΔV for producer and positive ΔV for injector), resulting in no significant pressure change in the region. This may explain why there could be no 4D changes observed around a well that has been actively producing or injecting. However, most 4D studies are based on understanding the 4D signals which are solely controlled by a production effect related to a single well. Under this condition, *equation 2.3* can be simplified. For instance, consider an area influenced by a single well and the seismic change driven by pressure change, the *equation 2.3* can be written into the following format:

$$\Delta A(x_i, y_i) = \psi_p(x_i, y_i) f_p(\Delta V_j, G_{ij}), \tag{2.4}$$

Where, $f_p(\Delta V_j, G_{ij})$ represents the function linking the pressure changes to the fluid volume injected or produced at the well over the survey period. Thus it should reflect two different pressure regimes - the transient and stable state - established after a well is activated. As explained in Appendix C, the function $f_p(\Delta V_j, G_{ij})$ can be as simple as a linear relationship in a closed compartment once a stable state is established, where the *equation 2.3* can be further simplified as below:

$$f_p(\Delta V_j) = \frac{\Delta V_k}{c_t V} \tag{2.5}$$

This gives

$$\Delta A_k(x, y, \Delta T_k) = \frac{\psi_p(x_i, y_i)}{c_t V} \Delta V_k. \tag{2.6}$$

Where c_t is the total compressibility of the reservoir rock and V is the total volume of the compartment studied. This relationship is shown to be valid for pressure changes of up to

±8MPa (Floricich, 2006). Interpretation of the 4D signals in the Schiehallion and Norne field (Chapter 4 and 6) are based on this linear relationship.

2.2 Direct approach for well and 4D seismic integration

2.2.1 Visual correlation

As discussed above, to establish the connection between the 4D signature and nearby well activity is in the centre of 4D interpretation. Most of the value from 4D is derived through *visual correlation*. In practice, the 4D signature can either be directly compared to well activity or maps of predicted pressure and saturation from the simulation model (Hatchell, 2010). To directly compare 4D with wells, historical production data are usually plotted as pie charts (sectors with different colours indicate fluid volumes injected or produced over a fixed period between two vintage surveys) which are overlain on a 4D seismic map to facilitate *visual correlation* (e.g. Figure 2.3). Subsequently, information inferred from 4D is directly used to determine drilling prospects and helps in production optimisation. Alternatively, 4D anomalies are usually compared with simulator predictions (adapted well information). Such an example is shown in Figure 2.4 for comparison between 2002 and 1999 surveys on Girassol to saturation change predictions from the simulator. There is a generally good match between them except that the observed 4D seismic indicates gas liberation in the southern part of the surveyed area due to insufficient pressure support from the nearby water injectors. As a result, the 4D information leads to increase in water injection from the two injectors in the southern area, and systematic comparison between the 4D seismic and simulation result has also been used to update simulation model. 4D interpretation using *visual comparison* has achieved great success in many studies where a fusion of information from production and 4D seismic data takes place through logical analysis. This interpretation method could be very subjective and may result in ambiguous interpretations. Furthermore, the outcome of *visual correlation* is fully qualitative in contrast to the prediction of reservoir performance made using a highly-quantitative tool - numerical fluid flow simulation. As a result, there is a need for quantitative information from the 4D seismic.

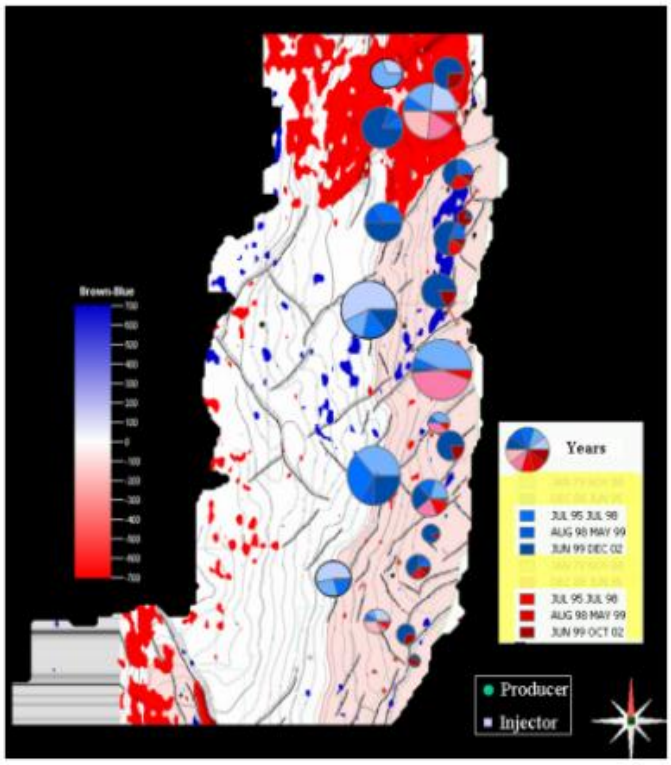

Figure 2.3 Comparison of 4D anomalies to historical production data.

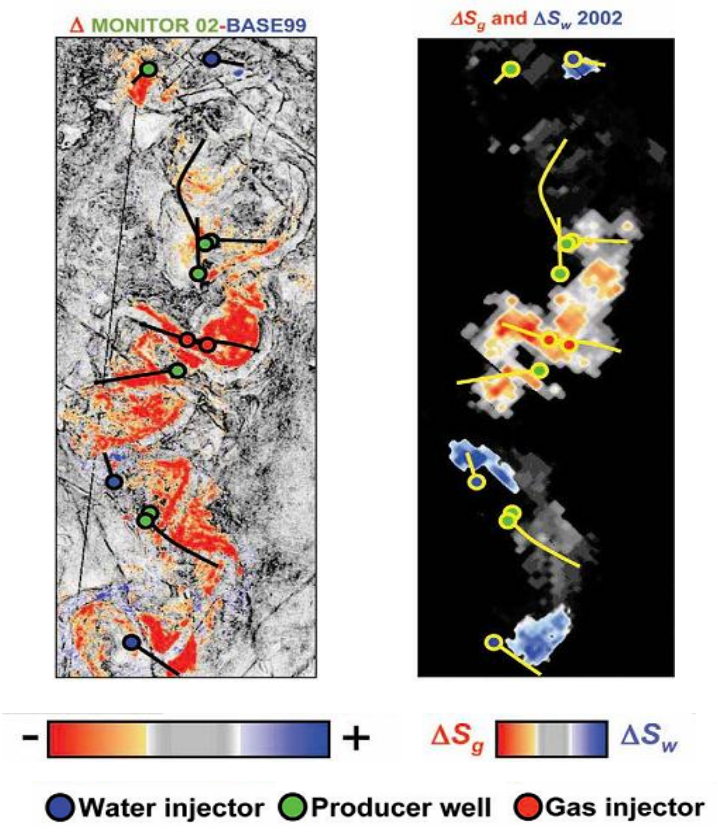

Figure 2.4 Comparison of 4D anomalies (2004-1999) on the Girassol field with simulation water saturation change predictions.

2.2.2 **A material balance-based approach**

An integration of the 4D and production data directly in the data domain can also help in reducing uncertainty in both domains. Huang (1997) presented such a study where a workflow was designed to identify 4D anomalies using a threshold derived from produced gas volumes from a gas field in the *Gulf of Mexico* (GOM). His method is based on the principle of material balance in which produced gas volume Q_P should be consistent with the quantity estimated from 4D seismic.

$$G_{pr} = B_g Q_P , \tag{2.7}$$

Where G_{pr} is cumulative production over the period between t_2 and t_1, calculated from the surface volume with the gas *formation volume factor* B_g.The seismic difference (see Figure 2.5a) is caused by water displacing gas between surveys, and is proportional to the gas volume produced. The volumetric estimation of cumulative gas production, from 4D seismic G_{gs}, is implemented using the following equation:

$$G_{gs} = h * A * \Phi * S_g , \tag{2.8}$$

where h is reservoir thickness input from geological map; A is the area of swept region indicated by 4D; Φ is average porosity (assumed to be 30%); S_g is an average gas saturation change (assigned to be 32%). As a result, area A of the swept zone can be determined which corresponds to a seismic amplitude threshold applied to define the exact boundary of the swept zone (see Figure 2.5b).

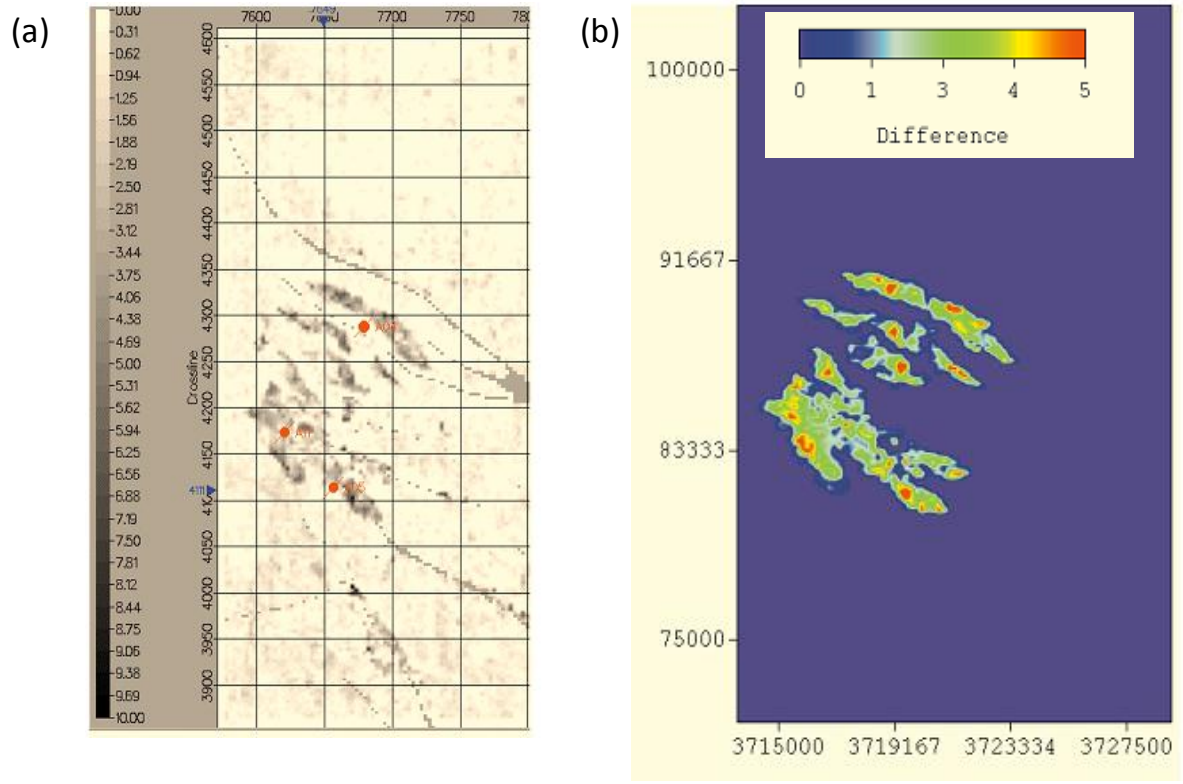

Figure 2.5 (a) Conventional 4D amplitude difference; (b) 4D anomaly after reconciling with production data through material balance (after Huang et al., 1997)

The 4D signature, after matching with production data, aided in solving the ambiguity with regard to the estimation of remaining gas reserves in P/Z analysis:

$$\frac{P_1 G}{Z_1} = \frac{P_2(G_r + G_{pr})}{Z_2} \tag{2.9}$$

Where, P_1 , Z_1 , P_2 , Z_2 are the average reservoir pressure and gas compressibility factor respectively at the time of baseline (t_1) and the time of monitor survey (t_2). G and G_r represent initial and remaining gas reserves at t_1 and t_2, which are unknown parameters and cannot be uniquely solved using production data alone. If properly thresholded, the amplitude maps at t_1 and t_2 yields a set of G and G_r, thereby *equation 2.9* will be eventually satisfied by adjusting the amplitude threshold. The resulting G and G_r are the best estimates of initial and remaining reserves as they are consistent with engineering. This study represents an early effort in the literature to integrate well and 4D seismic through data fusion.

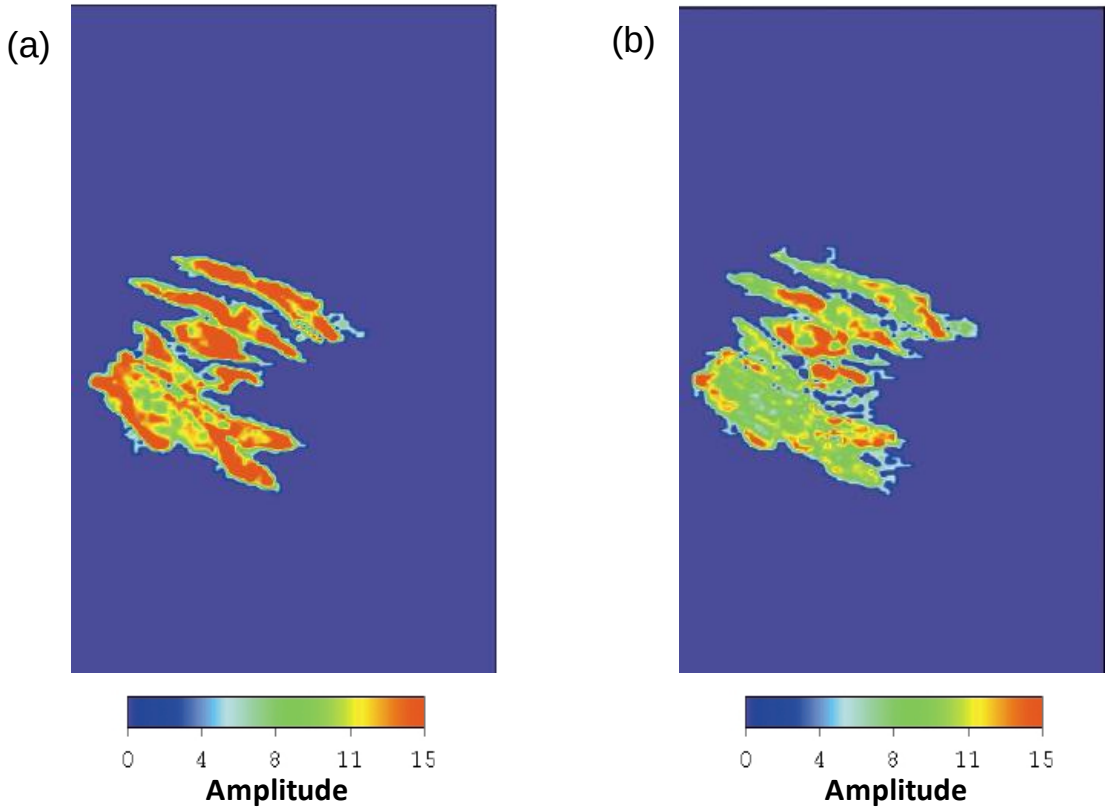

Figure 2.6 Threshold-limited 4D anomalies representing the distribution of gas reserves at the time of (a) the baseline survey, and (b) monitor survey.

2.3 A fully quantitative method and its uncertainties

2.3.1 Connecting production data using synthetic 4D seismic

The biggest hurdle to the integration of well and 4D seismic data in a full quantitative sense is the different dimensions of these two data types. Historical production data is essentially one dimensional whilst 4D seismic information is three-dimensional although the seismic difference volume can be mapped at a reservoir horizon. To make these two data types compatible, fluid flow simulation method is employed to transfer the one-dimensional information in the production data to spatial information in simulator prediction domain. Subsequently, *4D inversion* for pressure and saturation is used to transfer information in the seismic to the engineering domain, or the other way around via *simulator-to-seismic modeling* so that the information in 4D seismic and well production data can be compared in

the same way. In practice, the modeling route is mostly used because of the notorious difficulty in the separation of pressure and saturation changes from the 4D seismic (Gosselin et al., 2003).

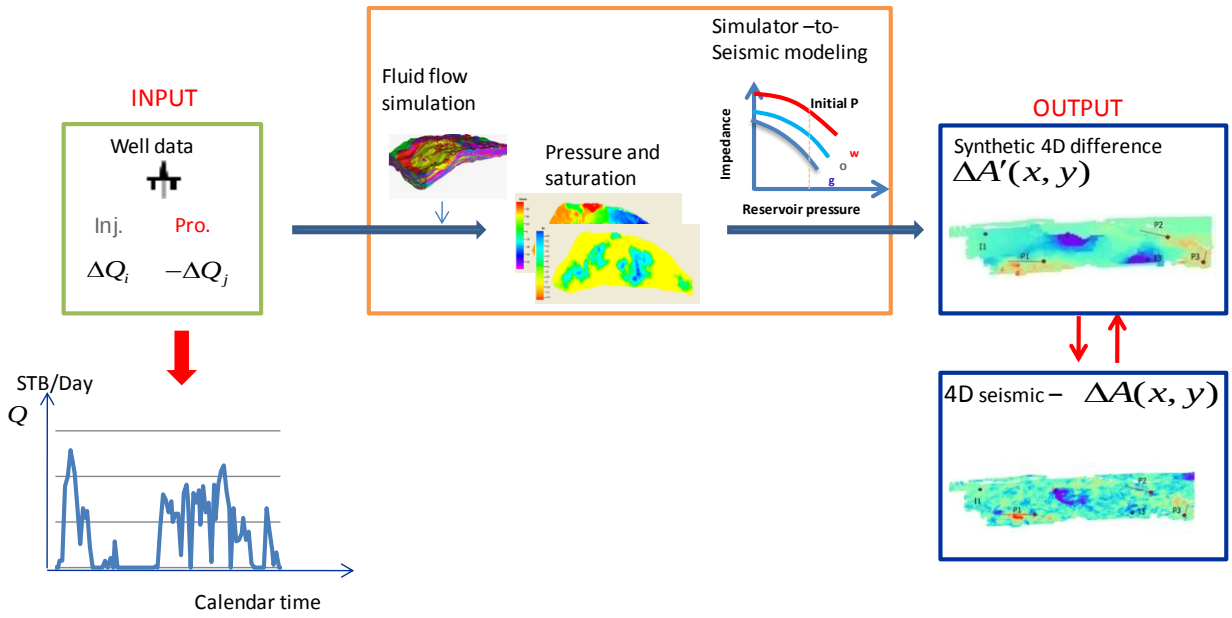

Figure 2.7 Quantitative workflow for integration of production and the 4D seismic data, which consists of two modelling techniques: fluid flow modelling and simulator-to-seismic modelling.

In practice, this method is implemented as an iterative procedure aimed to the update simulation model, which involves generating a large number of equal-probabilistic realizations (models), and selecting those models to yield the best match to the observed 4D signature. In terms of integrating production data for enhanced understanding of the 4D signals, this method is inefficient in the sense that a considerable amount of 'soft' (non-unique) information is used – suggesting that the synthetic 4D product might be associated with a high level of uncertainty. Potential problems with this workflow are reviewed in the remaining part of this chapter.

2.3.2 An assessment of the quantitative method

Uncertainty in fluid flow simulation

Fluid flow simulation is a major source of error in the synthetic 4D seismic products. Firstly, a reservoir simulation model is built on information from many types of measurements

(Figure 2.8), e.g. well tests, 3D seismic, well logs, and core measurements. However, each individual measurement has its own uncertainty and intrinsic limitation. For instance, the seismic method is restricted by its vertical and areal resolution, and the features such as sub-seismic faults which are important objects to fluid flow, might be overseen in the seismic data (Sheriff, 1991). As a result, the overall information provided by the data available is very limited compared to the level of details in the process of multi-phase fluid flow in porous system of a real producing reservoir. In addition, each data type has an 'intrinsic

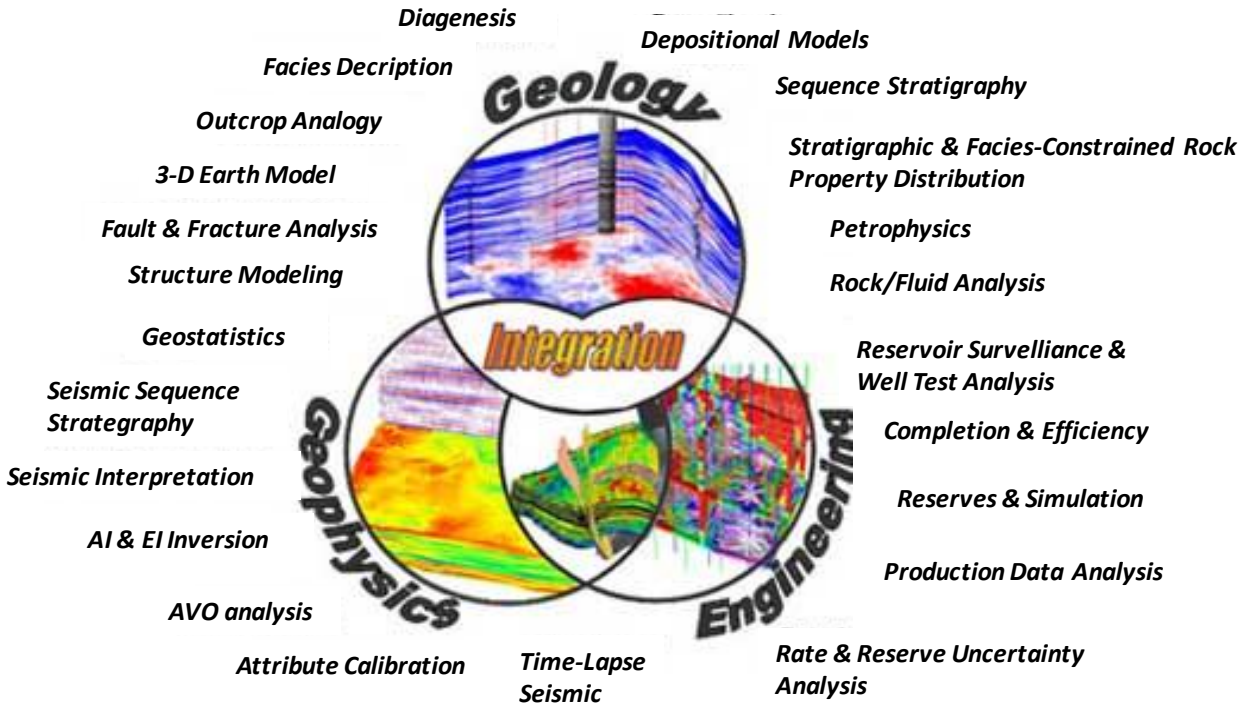

Figure 2.8 Schematic illustration of the information in the geology, geophysics and engineering domain integrated into the simulation model (adapted from iReservoir, 2011).

error' – noise, which might stack up and lead to spurious information in the simulator prediction. Even so, the geological information in geological model is delivered at fine scale (i.e. horizontally similar to the seismic scale; vertically several metres) will be further distorted in the process of *upscaling*. This is due to the limited computational power available to simulate the complex fluid flow process on a fine scale model. Despite studies in the literature showing the benefits of running the fluid flow simulation model at the geological model scale (Aarnes & Hauge, 2007), upscaling the properties to grid blocks in the simulation model is still common practice. The *upscaling* of reservoir properties is performed using a range of averaging method (arithmetic, harmonic and geometric), and the upscaled

model should predict same flow behaviour as the fine-scale model. In practice, the challenge is to upscale with minimum loss of precision in predicted reservoir performance, owing to errors in the process of *upscaling* reservoir properties, e.g. capillary pressure (Desbarats, 1995), relative permeability and permeability (Almeida et al., 1996). Moreover, the *upscaling* operation also leads to a larger *numerical dispersion* effect – an inherent problem of the numerical simulation method (Peaceman, 1977). Consider a given grid block in the simulation model, any changes in dynamic properties (e.g. water saturation) that occur on one side of grid block will immediately be dispersed to the other after one computation step – resulting in wrong prediction of pressure and saturation changes. Edris (2009) showed an example of the one-dimensional effect of numerical dispersion on water saturation change (Figure 2.9). Due to *numerical dispersion*, the simulated water front becomes increasingly smeared out with a coarser grid model and the predicted water breakthrough is earlier than it does for the fine-scale model. Such an effect can be partially compensated with some engineering measures, for example reducing the transmissibility between gird cells. There are still some errors inevitably introduced into the final simulation results due to numerical dispersion.

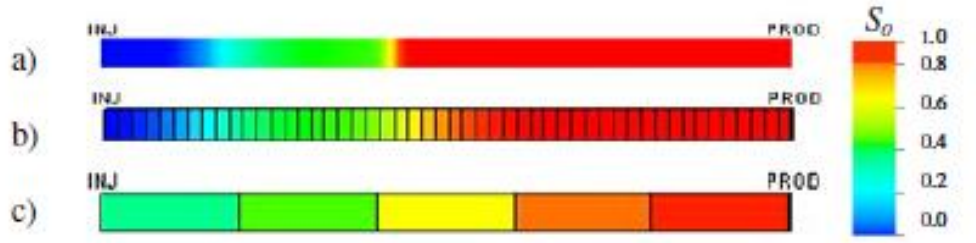

Figure 2.9 One-dimensional effect of numerical dispersion explains front resolution error and flow behaviour for different grid sizes. a) Fine grid cells, the closest to the analytical solution, b) coarse grid cells and c) Very coarse grid cells (after Edris, 2009)

Uncertainties in petro-elastic modeling

Petro-elastic models (PEM) are in the centre of the process of *simulator-to-seismic modelling* which links engineering to 4D seismic by transforming reservoir properties in each simulation grid to elastic properties as shown in Figure 2.10 . The *PEM transform* is based on the well-known fluid substitution equation proposed by Gassmann (1951). *Equation 2.10* shows the equation with the same explicit dependencies on parameters.

$$K_{sat} = K_{dry}(\sigma_{eff}) + \frac{\left(1 - \frac{K_{dry}(\sigma_{eff})}{K_0}\right)^2}{\frac{\varphi(\sigma_{eff})}{K_{fl}(T, P_f, C)} + \frac{(1-\varphi(\sigma_{eff}))}{K_0} + \frac{K_{dry}(\sigma_{eff})}{K_0^2}} \quad (2.10)$$

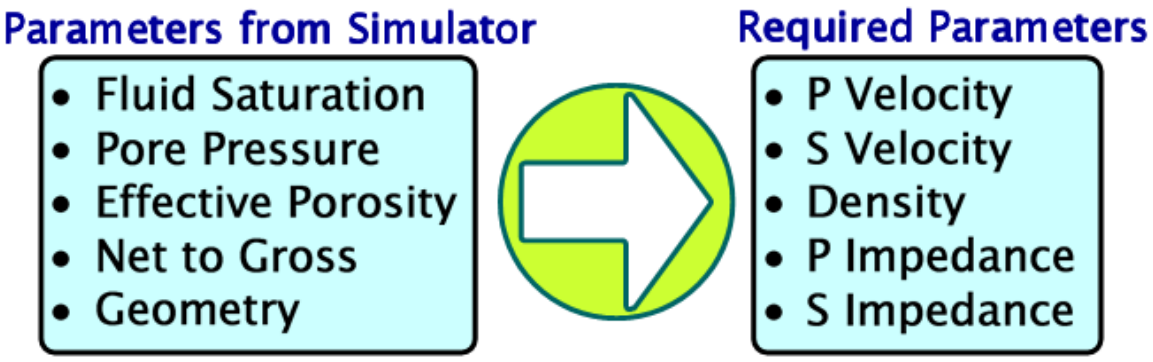

Figure 2.10 Input and output of petro-elastic modeling which transforms reservoir properties to petro-elastic properties (adapted from Amini, 2009).

where K_{sat} = the saturated bulk modulus, K_0 = the bulk modulus of the mineral matrix, K_{fl} = the bulk modulus of the pore fluid, K_{dry} = the bulk modulus of the porous rock frame, φ = porosity, P_f = average fluid pressure, T = reservoir temperature, σ_{eff} = effective stress and C is a vector containing fluid phase specific parameters for example API, salinity, solution gas/oil ratio. Indeed, this formula appears to be rather simple as it only includes simple algebraic terms. However, a considerable amount of effort needs to be made prior to its application to the simulation model. The major challenge lies in calibration of the parameters in this equation, which involves calibrating a large set of external elastic parameters of reservoir rock and fluid are needed (e.g. K_{oil} -bulk modulus of oil, μ_{oil} - rigidity of oil, K_{mineral} - bulk modulus of mineral, μ_{mineral} - rigidity of mineral). The values of these parameters are usually determined via lab measurement or empirical datasets. Some of these external parameters cannot be calculated independently such as σ_{eff} - the effective stress on the rock in-situ (the difference between overburden stress and a scaled version of pore

pressure), which requires the output from the simulator. Moreover, determination of K_{fl} requires an effective averaging method to calculate the average bulk modulus of multi-phase fluid in the pore space. The petro-elastic properties of mixed reservoir fluids are determined by a '*saturation law*' - 'Arithmetic (or Homogeneous)' or 'Harmonic (or Patchy)' average of individual phase's acoustic properties. These two types of averaging methods are written respectively as following:

$$K_{fl} = \sum_{i=1}^{n} S_i K_i \,, \tag{2.11}$$

and for the patchy approximation:

$$K_{fl} = \left[\sum_{i=1}^{n} \frac{S_i}{K_i} \right]^{-1} \tag{2.12}$$

where K_{fl} is the average fluid bulk modulus, S_i is the saturation of the i_{th} phase and K_i the bulk modulus of the i_{th} phase. Despite studies to improve *equation 2.11* and *2.12* (e.g. Hill, 1963), the *saturation law* is merely a mathematical approximation of the real fluid mixing phenomena and lack of real physical meaning. The same is true for '*stress sensitivity*' – the link between the effective stress σ_{eff} and the bulk modulus of dry rock frame K_{dry} (or μ_{dry}) as described by various equations in the literature, e.g. MacBeth (2004):

$$K_{dry}(\sigma_{eff}) = \frac{K_{\inf}}{1 + E_k e^{-\sigma_{eff} / P_K}} \tag{2.13}$$

The equation is controlled by three open parameters $K_{\inf}$, E_k and P_k are constants characterising a particular rock type. Again, these values are estimated based on the laboratory data measured under the laboratory conditions different from the in-situ. Furthermore, depending on the depositional environment a hydrocarbon reservoir can usually be divided into many *sedimentary facies* characterized by varied rock type (*lithofacies*). In order to apply Gassmann to the simulation model, the values of petro-elastic parameters in the equation need to be calibrated for each individual lithofacies as shown in Figure 2.11 – suggesting much effort on *facies analysis* (classifying reservoir rock according to lithology)

is needed. Amini (2009) presented an example in which he calibrated the set of parameters for each lithofacies using well log data.

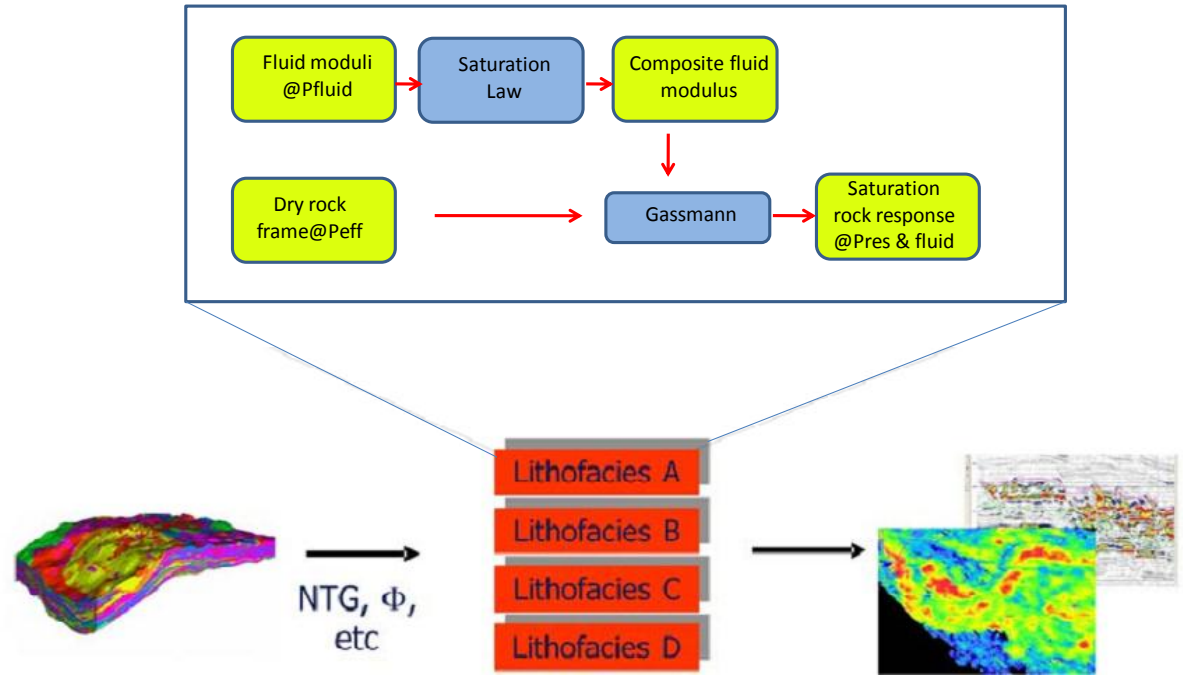

Figure 2.11 A schematic illustration of the petro-elastic transformation applied to different lithofacies in a reservoir simulation model (after MacBeth, 2007).

Seismic modeling uncertainties

Figure 2.7 shows, as part of *Simulator-to-Seismic modeling*, the need to generate synthetic 4D responses using rock and fluid properties output from fluid flow simulation and *PEM modeling*. This objective can be achieved by a variety of *Seismic Modeling* methods: *direct methods*, *integral-equation* methods and *ray-tracing* methods (see Carcione et al., 2002). Regardless of the differences between these methods, a common problem is the distinct geometry & size of computational grids of simulation model compared to that of the seismic grid blocks. Conventionally, the dimension of a simulation grid block - say 100×100 meters - is much coarser laterally than that of an elastic grid used for computing synthetic 4D (typically 12.5×12.5 meters or 25×25 meters), the typical size for a seismic grid.

Vertically, the thickness of a regular simulation cell (say 1m) is much smaller than that of the thinnest layer that can be resolved by seismic (see Figure 2.12). Hence, to produce synthetic 4D seismic in the seismic grid a downscaling and upscaling of information from the simulation grid are needed in lateral and vertical direction respectively in order to achieve the level of gird coarseness required. As discussed previously, it is inevitable that some information is distorted, thus this is another error source with respective to the final synthetic 4D result.

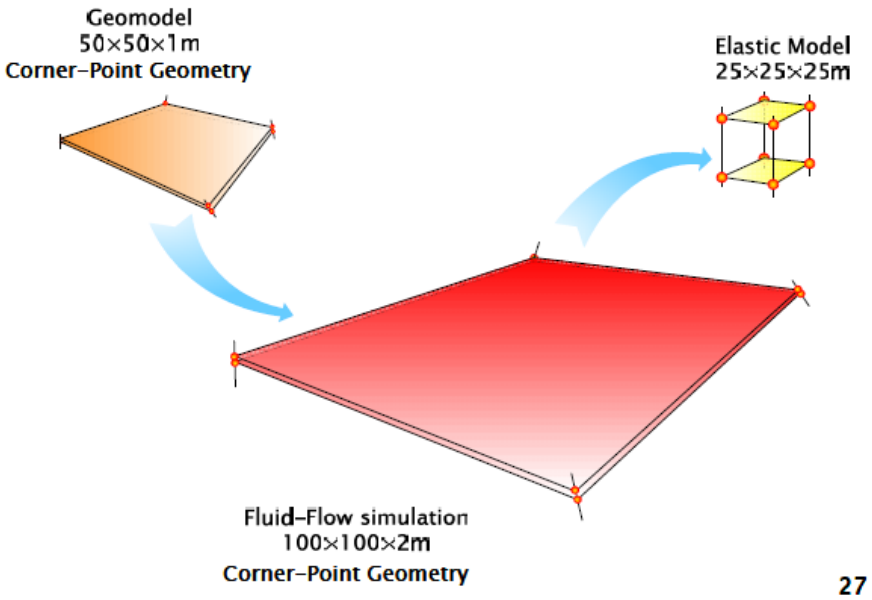

Figure 2.12 Relative scales and geometries of a grid cell in the geomodel, fluid-flow simulation model, and elastic model (seismic grid) after Amini (2008).

Moreover, each of these seismic modeling methods as mentioned previously has advantages and disadvantages as these methods are based on different levels of mathematical approximation to the propagation of seismic waves (Bullen & Bolt, 1985). Firstly, most of the published studies concerning *simulator-to-seismic modeling* utilised the *convolution method* because it is easy and quick to implement. This method in principle is considered to be the first order approximation of wave-field propagation – suggesting it cannot predict the whole spectrum of phenomena in the propagation of seismic waves (e.g. multiples and diffractions). As a result, the *convolution method* result has mainly been used as a rough guideline to interpreting observed 4D signals. Without considering computation and time cost, the most complete seismic modeling method available is the *Finite Difference* (FD) method which directly solves wave-field equations. As the result, FD method has obvious advantages

over other alternative methods: it can be used for complex reservoir and overburden velocity model where other methods may not be suitable, e.g. *ray-tracing* (see Carcione et al., 2002). Even with the most sophisticated FD method, it is also possible to expect large discrepancies between the synthetic and observed 4D data as the modeling of 4D response related to production in the reservoir is also dependent on the quality of the velocity model for the overburden. Domes et al. (2009) showed the level of error that one should expect in the synthetic 4D results given a poorly-modeled overburden velocity field. Indeed, the information related to layers above the reservoir is not the focus of most of the geophysical studies.

2.4 Summary

This chapter highlighted the fact that well activity defined by cumulative fluid volumes produced or injected is the cause of 4D seismic responses, and established a causal relationship which is the key to understanding the 4D signal. However, existing approaches for reconciling production and 4D seismic data are either excessively qualitative or quantitative. Although most of the 4D values are derived via *visual correlation* between well activity and the 4D response, the outcomes of this interpretation method are very subjective and do not allow quantitative analysis on the 4D seismic data. The quantitative approach based on engineering and seismic modeling tends to be affected by uncertainties from numerous sources as discussed in this chapter.

Therefore, there is need to explore new methods to achieve a better quantitative integration of well and 4D data. Most importantly, the integration should utilise the inherent causal relationship between these two data types, and in order to minimise errors related to modeling methods such integration is expected to be performed directly in the data domain despite the challenge to reconcile the distinctly different format of well and the production data. In addition, as discussed in Chapter one, frequently acquired 4D seismic surveys provide a wealth of dynamic reservoir information. It is considered that this new 4D development should also be taken into account in developing the new technique.

Chapter3

An engineering-consistent approach for enhanced dynamic reservoir interpretation by direct well-to-seismic correlation

In this chapter, an engineering-consistent method is developed aimed at extracting the underlying information in the causal relationship between well activity and the time-lapse response. This is realised through computation of *Normalised Correlation Coefficients* (NCC) between time-sequences derived from production data and multi-vintage 4D seismic data acquired from frequently acquired 4D surveys.

3.1 Direct correlation of the well activity with the seismic response

As discussed previously, interpretation of 4D signatures is dependent on understanding the causal link between well activity and the 4D response. A new engineering-consistent method is proposed in this chapter which converts these two data into an identical time-series format. This opens an opportunity to quantify the well-to-seismic causality by calculating the correlation coefficients between these time series.

Step 1: Generating sequences of seismic differences from multiple seismic attribute maps

With multiple seismic surveys, a time sequence can be created by making difference maps for all possible pairs of surveys (i.e. $\Delta A(x, y)$ for all ΔT_k). Indeed, for n surveys there are $\frac{1}{2}n(n-1)$ combinations of such differences. For instance, consider five surveys (baseline plus four monitor surveys), a sequence of ten seismic differences $\{\Delta A_k = \Delta A(x, y, \Delta T_k), k = 1,10\}$ can be generated at each location (x, y). The time sequence of 4D signatures consist of 4 differences made between monitor surveys and the baseline, and 6 differences between all possible pairs of monitor surveys as shown in Figure 3.1. It is the concatenation of these combinations that form the sequences used in this method. To clarify, the sequence can also be written in the following format:

$$(\Delta A_1, \Delta A_2, \Delta A_3, \Delta A_4, \cdots\cdots, \Delta A_9, \Delta A_{10}). \quad (3.1)$$

Seismic sequences of this kind can be computed using mapped seismic changes over all possible time intervals at every bin location. Unlike a usual seismic trace in 3D seismic cube, a seismic sequence generated in this way contains information about dynamic behavior of seismic changes at any given locations.

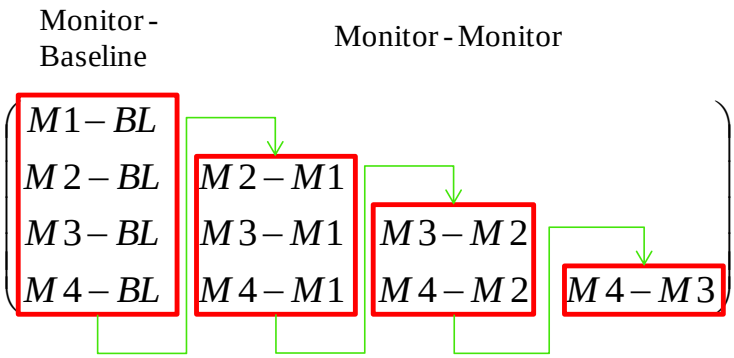

Figure 3.1 The pattern in which sequences of seismic changes are constructed given 5 repeated seismic surveys.

Step 2: Deriving sequences of cumulative volumes from production data

As discussed in *section 2.1*, cumulative fluid volumes produced or injected at wells over survey periods can be calculated from daily or monthly rates and they are considered to be better measures of well stimulus to the reservoir in the context of 4D interpretation. Consider the same five seismic surveys as discussed above, a well sequence of cumulative flow volumes for all ten combinations (see Figure 3.1) can be calculated and written into the following format:

$$(\Delta V_1, \Delta V_2, \Delta V_3, \Delta V_4, \cdots\cdots, \Delta V_9, \Delta V_{10}). \tag{3.2}$$

As an example, Figure 3.2 gives the plot for production data of two real wells in a North Sea field: P9 is a production well and W3 a water injection well. For P9, the cumulative fluid volume produced includes produced volumes of oil and water. Clearly, the production history of these two wells is distinctly different with regard to the time of activation and amount of fluid injected or produced. The sequences of cumulative volumes in the format of *equation 3.2* for P9 and W3 are plotted and shown in Figure 3.3. Clearly, well sequences of this kind defined by this method contain unique information about the production behaviors of the wells. Most importantly, the fluid volumes plotted at the sequence numbers (i.e. 1-10) of these two sequences are calculated over the time intervals defined by 4D surveys. As the result, these well signatures should be readily integrated with the seismic sequences in the same format as discussed above.

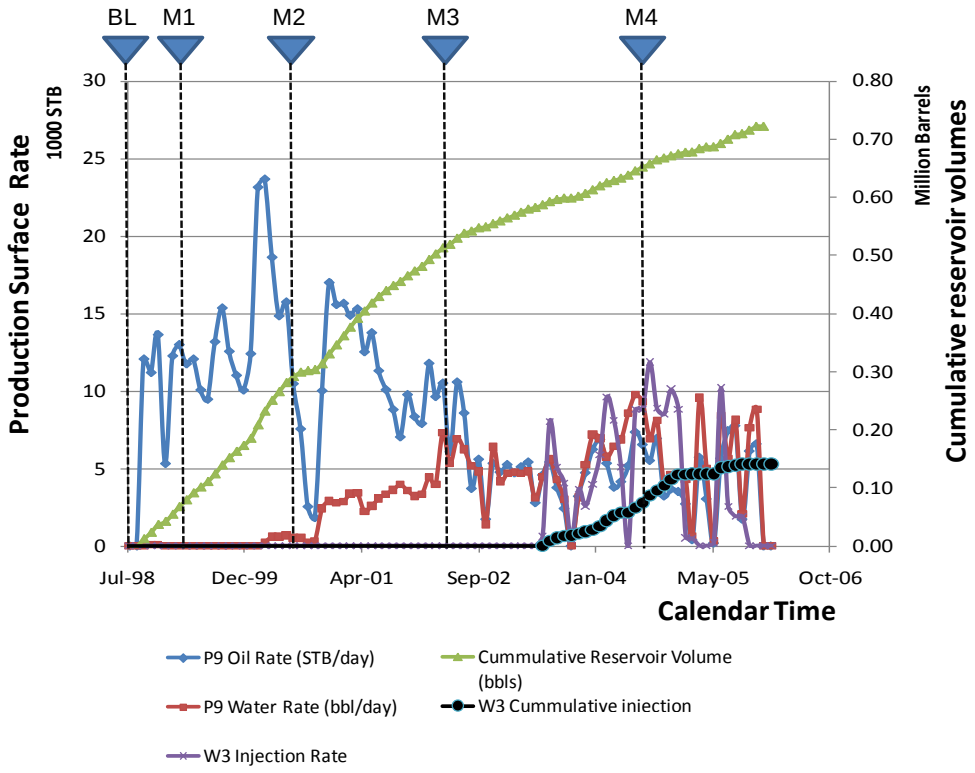

Figure 3.2 A real example of historical production data of two wells in a North Sea field: production well P9 and water injection well W3. Curves for cumulative volumes produced and injected and times of vintage seismic surveys are also shown.

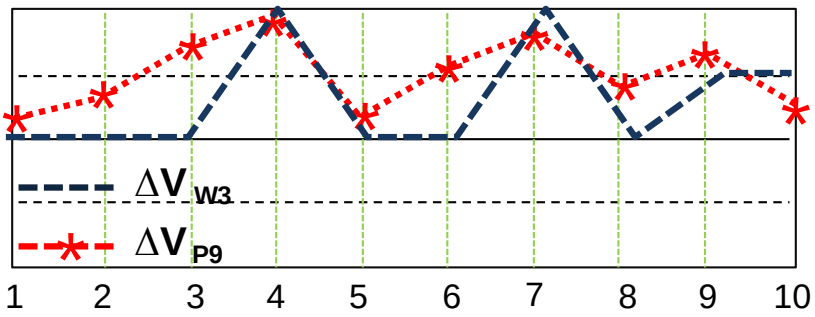

Figure 3.3 Correlation panel that displays the time sequences of normalised cumulative fluid volumes derived from the well activity of P3 and W3 shown above.

Step 3: Calculating the Normalised Correlation Coefficients (NCC)

In practice, the time sequence vector of 4D signatures $(\Delta A_1, \Delta A_2, \Delta A_3, ..., \Delta A_P)$ for each seismic bin location (x,y) is separately linked to the corresponding sequence of cumulative volumes $(\Delta V_1, \Delta V_2, \Delta V_3, ..., \Delta V_P)$ for a connected well group by calculating the *normalised cross-correlation* (NCC) statistic using (Bevington, 1975).

$$NCC = \frac{\sum_{k=1}^{P} (\Delta A_k - \overline{\Delta A})(\Delta V_k - \overline{\Delta V})}{\sqrt{\sum_{k=1}^{P} (\Delta A_k - \overline{\Delta A})(\Delta A_k - \overline{\Delta A})} \sqrt{\sum_{k=1}^{P} (\Delta V_k - \overline{\Delta V})(\Delta V_k - \overline{\Delta V})}} \tag{3.3}$$

The metric for *NCC* is that '1' indicates a perfect correlation and '-1' an anti-correlation. The sign assigned to the fluid volumes that constitute a well signature $\{ \Delta V_k = \Delta V(x, y, \Delta T_k), k = 1, P \}$ is determined by the polarity of resulting seismic responses. For instance, a particular water injection well can possibly produce two dynamic changes within its neighborhood, which result in opposite effects on rock compressibility – a 'softening' effect caused by pressure increase and a 'hardening' effect due to water saturation increase. Depending on the selected seismic attribute, the softening (or hardening) effect may be represented by either an increase or decrease in values of the selected attribute. Consider a particular seismic attribute, with a positive change indicating reservoir softening, and negative changes corresponding to reservoir hardening. Injected water volumes at this well are defined as the negative value, if the hardening effect due to water flooding is of interest. On the contrary, the volumes are defined to be positive if pressure increase is the interested effect.

This operation aims to eliminate negative correlation coefficients so that we can only focus on positive correlation coefficients from 0 to 1. A good well-to-seismic correlation implies that seismic changes occurring at (x, y) over time is very likely to be related to the activity of the well being correlated. The correlation procedure can be performed at each bin location (x,y) producing a map of *NCC* across the region of interest. When mapped, the *NCC* becomes a new seismic attribute with the same resolution as seismic. More repeat surveys or alternations in well rate lead to an increasingly complicated and finer scale time sequence, hence increasing statistical robustness of the normalised cross-correlation measure. To ensure stability, a minimum credibility threshold is needed for the *NCC* maps, as for a particular size

of time sequence the cross-correlation coefficient is only statistically significant above a certain coefficient value. Below this threshold there is a chance that samples drawn at random can yield the same coefficient (Bevington, 1975). However, the time sequences generated in this way

$$\begin{pmatrix} \Delta V(x,y,\Delta V_{M1-B}) \\ \Delta V(x,y,\Delta V_{M2-B}) \\ \vdots \\ \Delta V(x,y,\Delta V_{ML-B}) \\ \vdots \\ \Delta V(x,y,\Delta V_{ML-M(L-1)}) \end{pmatrix} \text{ and,}$$

$$\begin{pmatrix} \Delta A(x,y,\Delta A_{M1-B}) \\ \Delta A(x,y,\Delta A_{M2-B}) \\ \vdots \\ \Delta A(x,y,\Delta A_{ML-B}) \\ \vdots \\ \Delta A(x,y,\Delta A_{ML-M(L-1)}) \end{pmatrix}$$

only have L dependent variables. L is the number of monitor surveys and all the differences between monitor surveys $\{\Delta A_{Mk-M(k-p)}, k=2...L; p=1...L-1\}$ can be computed from the differences between monitor and baseline survey $\{\Delta A_{Mk-B}, k=1...L\}$. In another words, the vector has only L degrees of freedom. The probability of observing a value of the correlation coefficients larger than r for a random sample of N observation with v degree of freedom is given by (Bevington, 1975) in the following equation:

$$P_c(r;N) = \frac{1}{\sqrt{\pi}} \frac{\Gamma[(v+1)/2]}{\Gamma(v/2)} \int_{|r|}^{1} (1-x^2)^{(v-2)/2} dx \qquad (3.4)$$

For example, for the 45 points used in the Valhall study (9 degrees of freedom), the independent sequences with correlation coefficients greater than 0.58 are significant with a 90% confidence, whereas for 10 points this threshold becomes 0.54. Another reason for thresholding the *NCC* maps used in this PhD work is to focus on the 4D signature induced only by a particular well or group of wells, and to exclude the contributions from other wells.

The correlation coefficient between the selected well group of interest and the seismic sequence must in this case be higher than the sequence correlation between the excluded wells and the selected group. Thus, it should be noted that there is a compromise between removal of interesting features due to over-thresholding and having too much random features due to under-thresholding. In practice, the creditability thresholds for the NCC examples shown in this thesis are selected by trial-and-error approach so that the information content of interesting signatures can be maximized. But generally speaking, the two rules for threshold selection as described above are honored.

3.2 Model test for a compartmentalised reservoir

3.2.1 Model Description

We now evaluate the validity of the above prediction by considering numerical models of a simple idealised reservoir consisting of two compartments separated by a sealing and then a partially sealing fault (Figure 3.4). Model properties and dimensions are chosen to be typical of channelised turbidites in the North Sea (Leach et al.1999). The fault separating the compartments is assumed to be unforeseen during interpretation. Three flow simulations evaluate the consequences of possible leakage across the fault. In the lefthand compartment there are two injectors I1 and I2 and one producer P1, and in the righthand compartment there is one injector I3. The injectors and producer are sequenced according to what might be expected for a typical reservoir (Figure 3.5). The sequence is chosen to produce net total surface volumes for I1, I2, I3, and P1 that balance close to zero at any given time. Seismic surveys are shot every year (R1, R2, R3 etc..), with the baseline survey (BL) in January 1998.

3.2.2 Pressure changes versus cumulative fluid volume

The Appendix C describes in detail exactly how a pressure disturbance evolves in time. In this particular case, when the producer P1 begins its production at a constant rate q_{P1}, a pressure transient disturbance given by (C1) is created which propagates outwards from the well and then reaches a steady state. Based on the properties chosen for this model, the time taken for the component to reach a stable state is between 26 and 78 days - in comparison, for

the righthand compartment which is 25 to 65 days. In the steady state, the following equation from the Appendix applies to the lefthand compartment:

$$\Delta P = -\frac{1}{c_t V_{LH}}\left(q_{P1}\Delta T\right) \tag{3.5}$$

Where c_t is the constant total compressibility, V_{LH} the volume of the compartment, ΔT the time period over which the pressure change is measured (in this case the period between the baseline and first repeat survey. (For the purpose of this model-based example we take Bo=Bw=1.) Thus, the cumulative volume is $q_{P1}\Delta T$ and this can be correlated to the pressure change via the coefficient $1/c_t V_{LH}$. Pressure decrease in the compartment evolves linearly with time during this first year. After one year, I1 injects at a constant rate of qI1 such that the net volume produced and injected is now zero, thus holding the pressure constant. At later times injection stops in I1 and then starts up in I2, before finally starting again in I1 and reducing by a corresponding amount in I2. In the final year there is a fluid volume imbalance and pressure decreases slightly. Lastly, I3 injection increases the pressure in the righthand compartment in the final two survey periods. There are thus a range of cumulative rate changes in the period over which the multiple seismic surveys are shot, and hence variable pressure change. Each well rate change induces a small transient signal as observed in Figure 3.6, which shows the derivative of the pressure in the lefthand compartment.

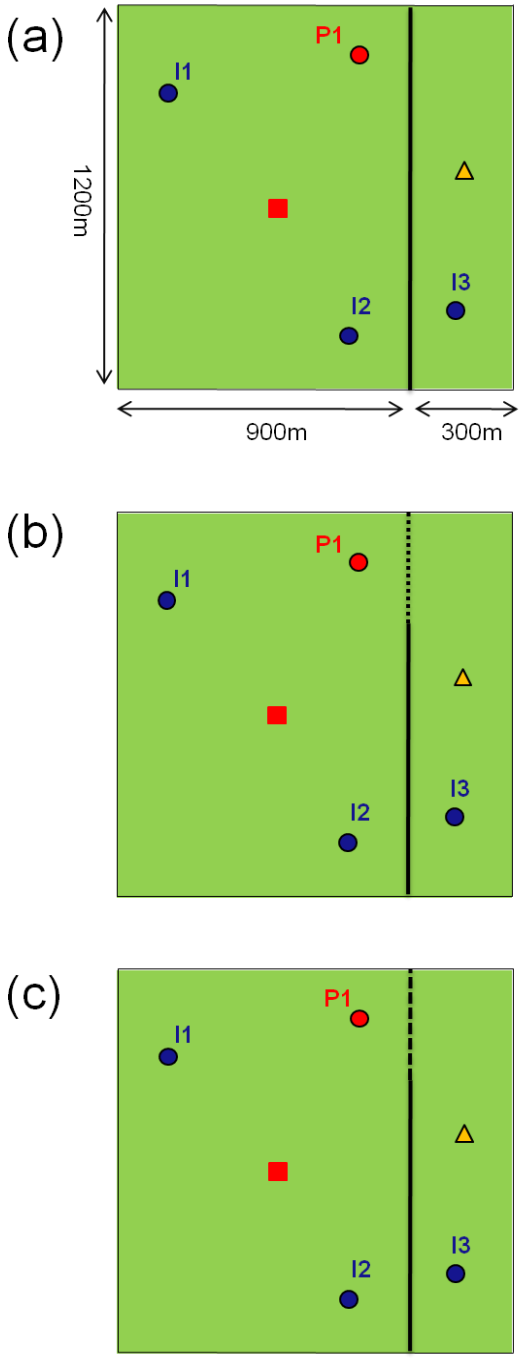

Figure 3.4 The three flow simulation models used to test our method of net well volume to pressure correlation taken over repeated seismic time intervals. The model properties are based loosely on Schiehallion field, North Sea: porosity of 28%, ct=2.210-5psi-1 and permeability of 280mD. (a) Model 1 – sealed compartments; (b) Model 2 – partially sealing fault with fault transmissibility of 0.005; (c) Model 3 –partially sealing fault with fault transmissibility of 0.01. Dimensions are 1200m x 900m for the lefthand compartment, and 1200mx 300m for the righthand one.

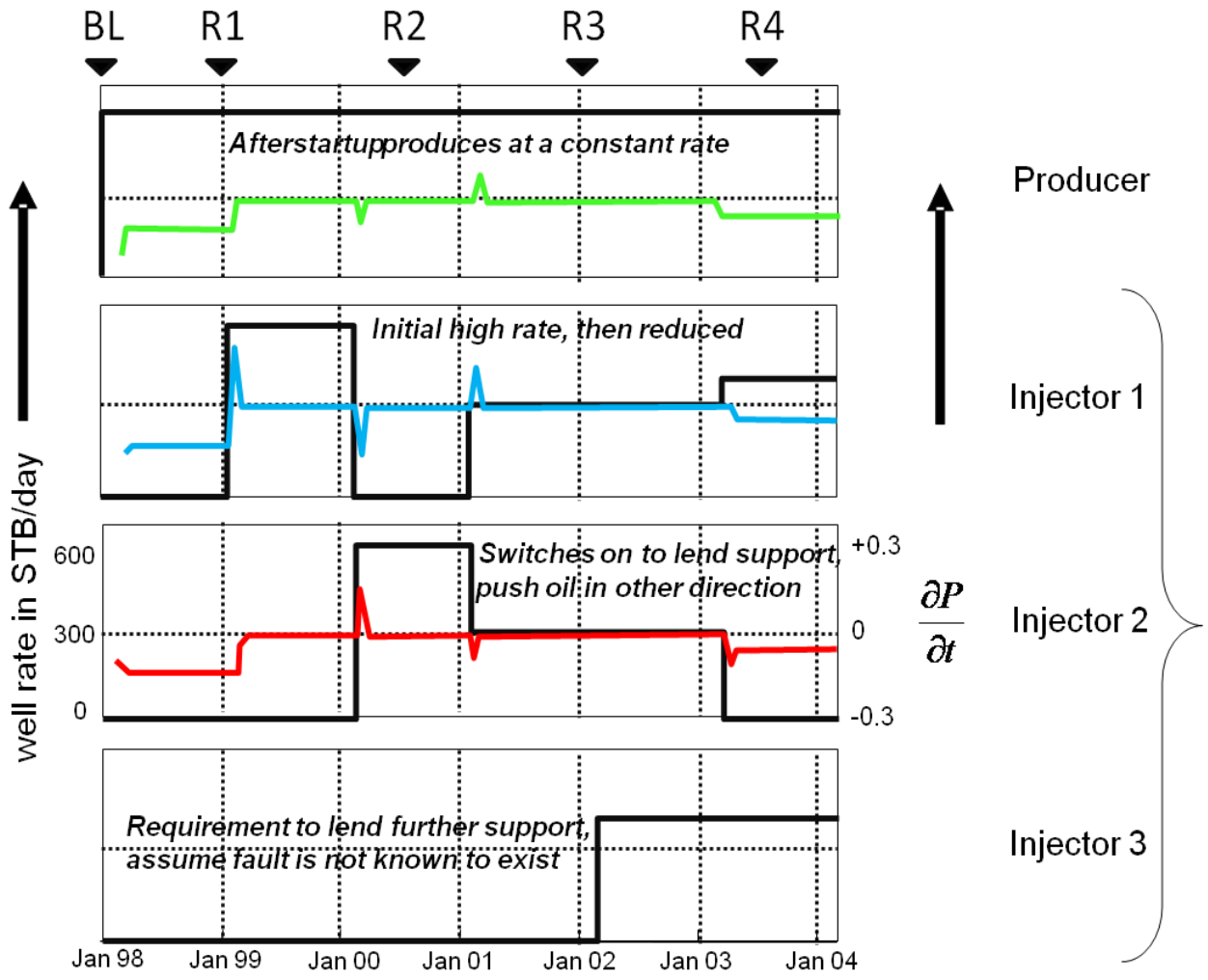

Figure 3.5 (Surface) rates for the four wells in the synthetic models of Figure 3.4 shown in black. Also shown are 4D seismic survey dates taken every 12 months (arrows), starting in January 1998 as observed along the horizontal axis. Well rates are overlain by the pressure derivative for reference purposes in colour (green, blue and red).

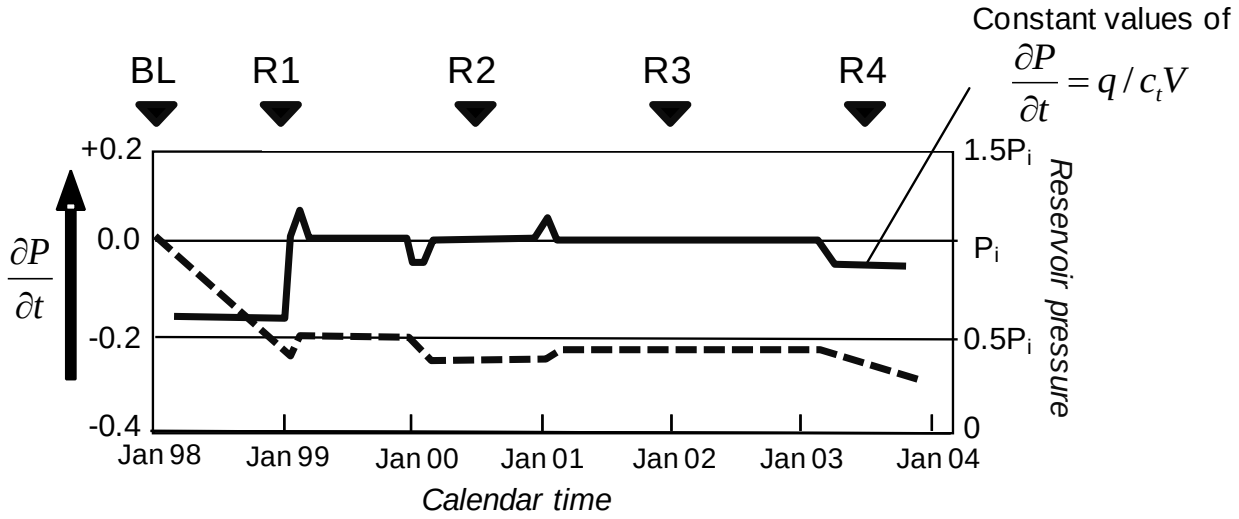

Figure 3.6 Time derivative of the evolution of the pressure field evaluated for the lefthand compartment of Model 1. The dashed line represents the change of pressure value against time at an observation point. The constant plateaus are related to the cancellation of the total cumulative well volumes. Transients can be observed at each well rate change.

In our example, the sequencing of the seismic surveys has been chosen to fortuitously miss these changes. When the pressure drop for each survey is plotted alongside the corresponding cumulative volumes, a correlation in their variation is apparent as in Figure 3.7 and Figure 3.8. Figure 3.7a shows that this is indeed the case for all locations in the lefthand compartment, whereas the pressure changes in the righthand compartment are not synchronised with wells P1, I1 and I2 as there is a barrier between the compartments. Clearly, an elevated pressure in the righthand compartment detected at the well will be indicative of the barrier. If the cumulative volume for I3 is used instead, then maximum correlation is obtained for the righthand but not the lefthand compartment (Figure 3.7b). Also, calculation shows that if the cumulative volumes for all four wells are used in error, the correlation coefficients are reduced from 0.90 to 0.55. It appears that the selection of wells is fairly critical in obtaining an optimal correlation coefficient.

If the fault barrier is made transmissible, then the pressure change in both the lefthand and righthand compartments is not only controlled by the wells. The mechanism of inter-compartmental hydraulic communication, itself a transient behaviour, is on a longer time scale than the duration of the intra-compartment transients. Calculations show that it takes 6 years to equilibrate between compartments in our model. ΔP will now not exactly correlate with ΔV over the repeated seismic surveys, as a fully stable state has not been reached. From

our model results it is observed that for the lefthand compartment the correlation coefficients between wells P, I1 and I2 and the pressure drop reduce slightly (Figure 3.8a). Interestingly, evidence of the leakage point in the fault is observed, through the structure of the correlation coefficient map. A similar conclusion is reached for the ΔP - ΔV correlation coefficients evaluated using well I3 activity alone (Figure 3.8b). Increasing the transmissibility again (Model 3) reduces the time taken to reach inter-compartment stable state (from 6 to 3.5 years), but produces a similar correlation result to Model 2. The coefficients reduce by roughly 15%, but this does not alter the ability to discriminate between compartments using this approach. Compartments can still be detected provided the correct selection of wells is made.

Summarising our understanding based on this modelling exercise, the application of a ΔP - ΔV correlation method appears generally possible as the transients are much shorter than the seismic repeat times. The time to reach a stable state in the presence of inter-compartment pressure communication may introduce a small reduction in the correlation coefficient. We conclude that our basic idea of correlating cumulative volumes to pressure changes remains intact.

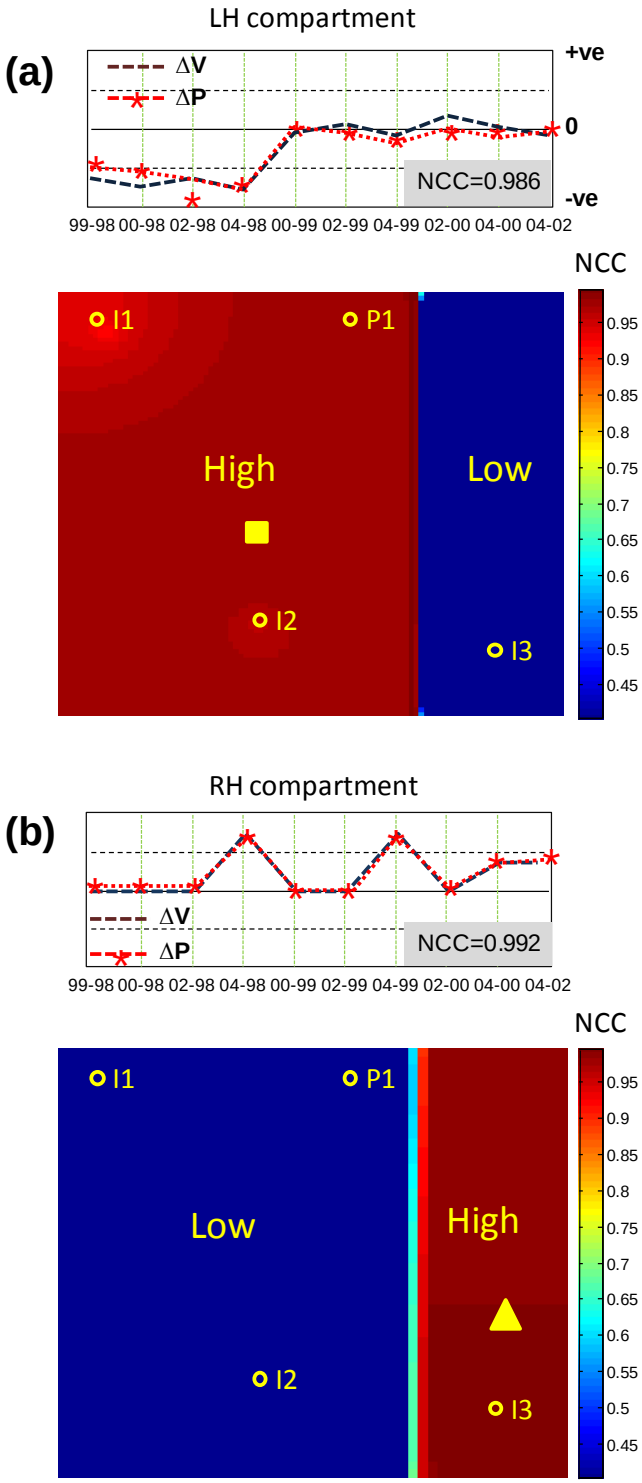

Figure 3.7 Normalised cross correlation coefficient constructed between the pressure change and well production/injection for the entire time sequence considered in Figure 3.1 (a) Correlation of the pressure drop at reference location indicated by square with wells P1, I1, I2 is shown in activity panel on the top; (b) Correlation of pressure drop with well I3. Reference points for activity panel are marked by the solid triangle.

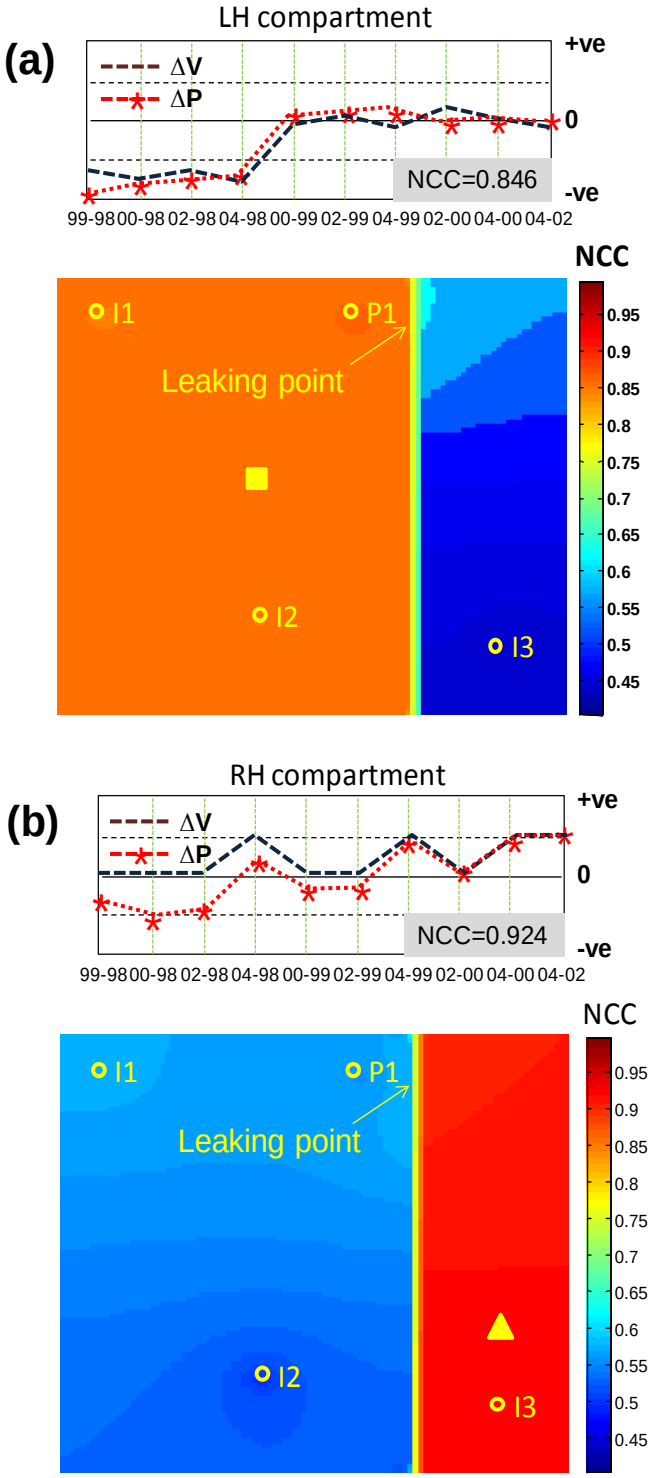

Figure 3.8 The effect of a partial break in the barrier, resulting in a reduction in the correlation between pressure change and cumulative volume. (a) Reduced correlation coefficients in the lefthand compartment indicate communication between the two compartments - the stable state has not been reached yet. (b) As in (a) but for the correlation with well I3 activity. Reference points for activity panel are marked by the solid triangle.

3.3 Summary

This chapter introduced an engineering-consistent method for integration of well and the 4D seismic data. Compared to the traditional approaches based on visual correlation or modelling techniques, this approach can achieve the integration of these two data types directly within data domain. In order for the proposed technique to succeed, several conditions must be met. Firstly, the field must be surveyed by multiple surveys, and in particular enough surveys for the well to seismic cross-correlations to be significant. If connected regions/compartments/geobodies around individual wells are to be 'imaged', these wells must also possess distinctly different well rates, such that the correlation coefficient between the well and the 4D signatures is higher than the well to well correlation.

The approach benefits from a sufficiently complicated well activity for each time series of activity (switching wells on and off provides a useful signal in our approach). Given the above, it is surprising how well the technique responds. Another important condition is that the chosen seismic attributes must be sensitive to reservoir pressure. The ideal situation for the application of the method is pressure-sensitive 4D signatures. For fields in which gas exsolves from solution or water saturation changes are a controlling influence over the seismic, then the technique requires some adaptation. This has been considered in the work of Huang et al. (2010) who have shown that in these situations the technique can still be used successfully. This lends support to efforts which attempt to separate the effects of both pressure and saturation in 4D seismic (for example, Landrø, 2001; Tura and Lumley, 1999; MacBeth et al., 2006). Finally, most production and injection volumes used in this procedure to date have been measured as comingled flow, and as such the volume rates refer to the whole interval completed rather than the particular reservoir over which the seismic attribute is defined. This is the correct approach if the overall reservoir interval is thinner than the seismic wavelength, but will not be appropriate for thick reservoir sequences. This could be improved if smart well technology is in place to observe the flow rates in specific flow units. However such technology is not commonly available in many mature fields.

The proposed technique resembles an extended well test, in that response to volume rate changes (not in this case build up or draw down however) induced at the well are detected. The scale for the extended well test is several months, whereas for the seismic it ranges from several months (the Valhall field) to a few years (the Schiehallion field). However, pressure

sensors in the well are now replaced by mapped seismic attributes. In both, the steady state condition is applied in a decline curve analysis, with the same objectives – to delineate barriers, volumes of compartments or geobodies in the reservoir. Once such regions have been identified, it is now possible to use these to update the simulation model and hence production forecasts. Of particular value in this process is that the map of *NCC* maintains the resolution of the seismic and therefore usually has a higher lateral resolution than the simulation model.

Chapter4
Application to the Schiehallion field

Reservoir pore pressure may evolve linearly in a compartment with respect to the net volumes produced or injected at all the wells within the compartment when stable pressure state is established. The proposed method has been applied to the multi-vintage 4D seismic data acquired over the Schiehallion field, which is characterised by numerous isolated and partially communicating compartments. This chapter focuses on examining the results from several selected areas and the results reveal that uncertainties in the interpretation of dynamic reservoir connectivity using conventional 4D attributes can be solved by this correlation technique.

4.1 General field description

Field background: The Schiehallion field is a UKCS field situated about 200 km to the west of Shetland (see Figure 4.1), and holds most of the hydrocarbon reserves in that area. Total recoverable oil reserves are estimated to be between 350 to 500 million barrels (BP, 2009). A partnership of BP, Shell, Amerada, Hess, Statoil, Murphy and OMV currently own the field. The field was discovered in 1993 by 3D seismic interpretation and exploration drilling. The production started in 1998 through subsea horizontal wells, which are tied back to the Schiehallion FPSO (Floating Production Storage and Offloading vessel). The estimated production life is 17 years, with a total output peaking at 117,000 barrels/day (Gainski et al., 2010).

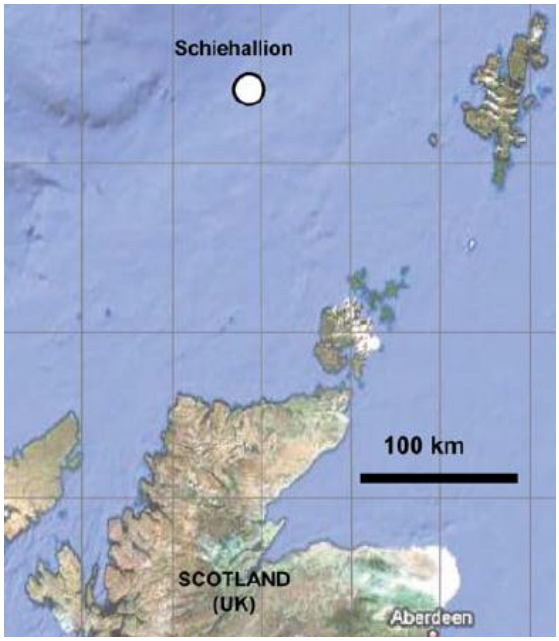

Figure 4.1 The location of the Schiehallion field; West of Shetland in North Atlantic Ocean, UK continent Shelf (after Gainski et al., 2010) .

Strategraphics and closure: the reservoir of the Schiehallion field consists of several layers of turbidite channel sands of Tertiary age, 10 to 50 m thick in total and lying at approximately 2000 m subsea (Leach et al., 1999). The sequence is named as 'T-sequence' by the operator, which comprises a number of sub-sequences (e.g. T30, T20). They can be further divided into smaller stratigraphic units using well log and 3D seismic data. For instance, the T30 sequence

is subdivided into ‘T31’ and ‘T34/35’ as shown in Figure 4.2. The geological model based on the information from the baseline 3D seismic shows that the Schiehallion reservoir sands are deposited in a deep water fan complex composed of highly channelised and amalgamated units (see Figure 4.3).

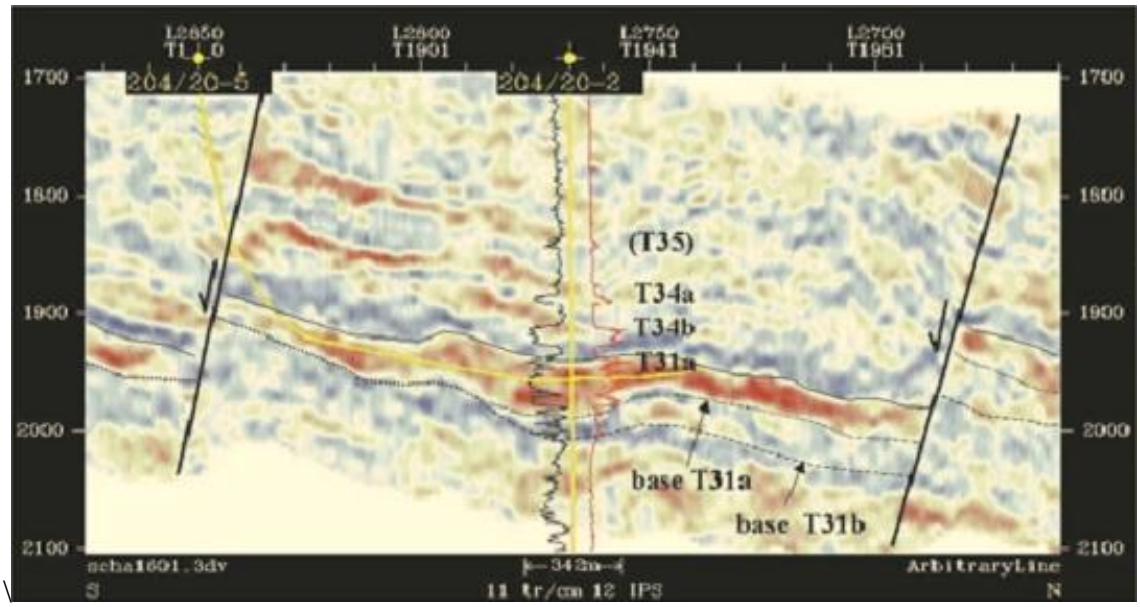

Figure 4.2 An inversion seismic section and well log showing subdivision of T30 sands. Hydrocarbon in high quality sand units produces bright seismic response in red colour (after Chapin et al., 2000).

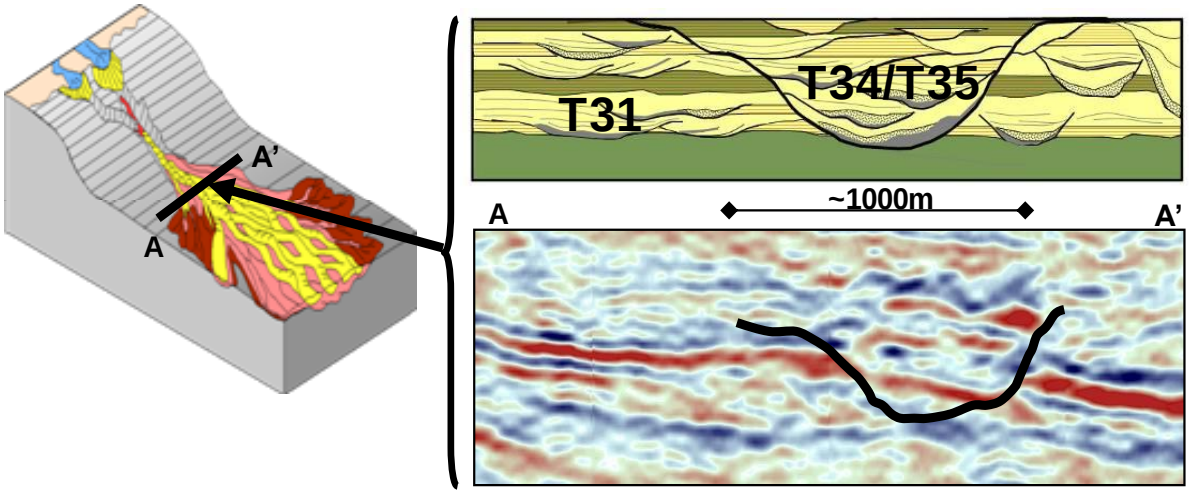

Figure 4.3 Geological model of the Schiehallion field: the cross-section *A-A’* shows the amalgamated sands of T30 sequence in the deep water channalised complex.

It should be noted that the focus of this chapter is on the upper unit of the T31 sequence, named as T31a or T31U which is most extensive and contains most of the reservoir sands in the field. The T31a reservoir dips west at about 20^{o}, and is sealed updip by stratigraphic pinch-out of the sands between top-seal and bottom-seal mudstones. The southern edge is defined by east-west normal faults that completely offset the reservoirs. The northern and western margins of the fields are defined by dip closure to an oil-water contact (OWC). The channelized sands are sub-divided into several segments by several normal east-to-west faults with large throw. The operator named them from north to south respectively as segment 3, 2, 1 and 4 (Figure 4.4). In this thesis, this convention is used to refer to these segments.

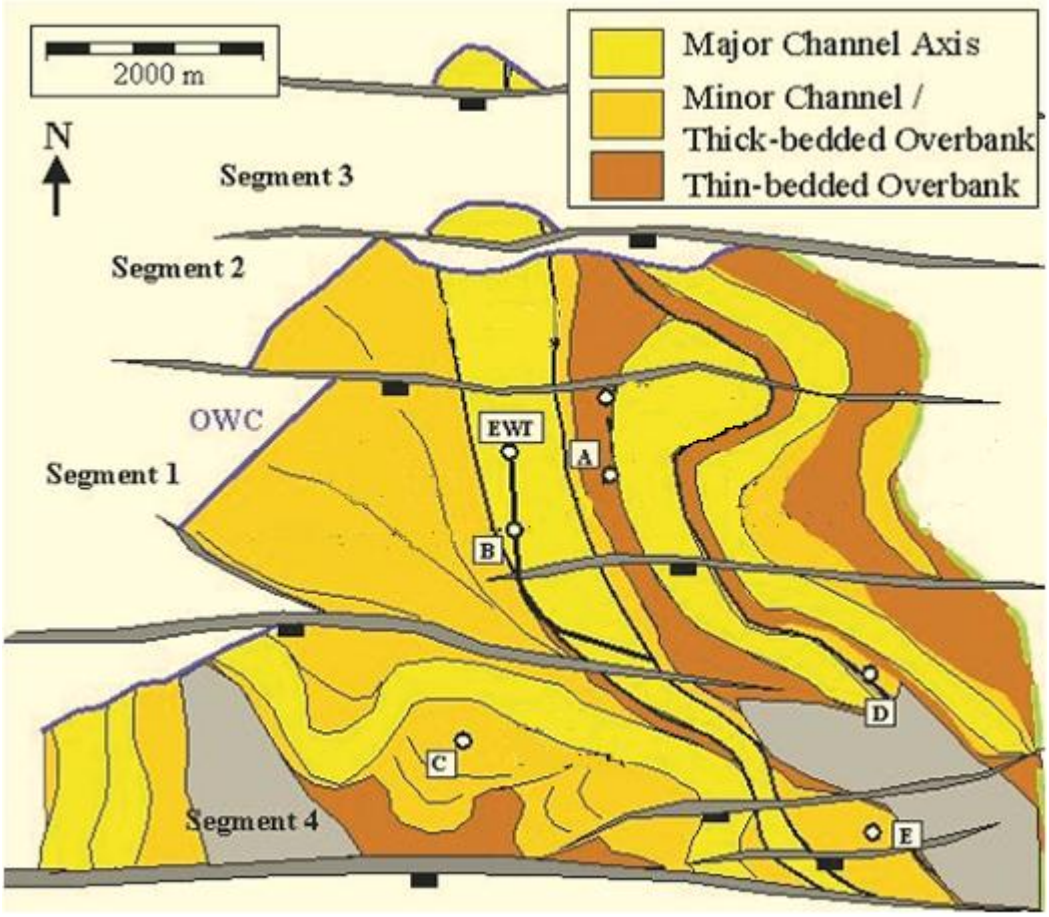

Figure 4.4 Facies map showing the layout of T31a channelised sands and the dip closure to OWC in the west. Four major east-to-west trend faults completely offset the reservoir and divide the channels into four segments.

Reservoir conditions: Reservoir quality varies in character from thinly interbedded sands to massive sands (Lancaster et al., 2000), with the massive sands being of better quality. Classically, the sands are fine to medium grained, with 23–30% porosity and 250–2000 mD

permeability. The oil is close to bubble point with oil gravity in the range of 22–28° API. The Schiehallion field has experienced poorer than predicted connectivity since start-up in 1998. Poor connectivity results in reduced well performance and high solution gas levels (Parr et al. 2000). To control gas breakout by pressure recovery, became the major task for the subsurface team in the early stage of field management (1998-2000). As a consequence, many sub-vertical water injectors were drilled during that period to recover reservoir pressure. There are evidences that most of liberated gas between 1998 and 2000 had subsequently come back into solution due to water injection. Due to complexity in reservoir connectivity at Schiehallion, the focus of the subsurface group was shifted to identifying and quantifying key factors affecting reservoir connectivity and managing water sweeping since 2000.

4.2 Reservoir connectivity

In individual segments, lithological contrasts caused by faulting and facies changes behave as baffles and barriers to flow, giving rise to a large number of compartments. In Schiehallion, flow barriers can be geologically subtle, and difficult to image and interpret within existing 3D seismic data. Poor connectivity in a few wells was quickly observed in poor well performance and high level of gas produced from solution. A limited aquifer to the west and low initial GOR means that the reservoir lacks energy, and water drive from appropriately positioned injectors is critical to good well performance (Govan et al., 2006).

It is also found that reservoir connectivity is the largest uncertainty to planning of new production and water injection wells, and reservoir management in Schiehallion. A good understanding of field connectivity is therefore essential as the geological complexity gives rise to a wide range of possibility for injector-producer communication. Complexity of the reservoir connectivity is increasingly appreciated with the help of dynamic reservoir surveillance data acquired during production. Integration of varied surveillance data from all the sources is the key to identifying reservoir compartmentalization (Gainski, Macgregor and Freeman, 2010). For instance, Dobbyn & Marsh (2001) presented a study aimed to determine the communication between compartments using material balance calculation and dynamic pressure measurement. The types of surveillance data available and the information each type of data may provide are summarised in Table 4.1.

Survelliance data source	Description
Permenant Downhold Gauge (PDG)	Installed in each produciton well
Well-head pressure and temperature gauge	Installed in water injection wells
Well tests	To allocate flow rates to individual wells
Isotopic tracer elements	Incorporated into injected water and detected at production well. An important measure to confirm and calibrate seismically defined compartments
Production logging tools (PLT)	Performed only in two wells due to high cost. To determine the producing zone and type of fluid
Formation pressure test	Detecting the existence of vertical barriers and thinner flow unit, important for infill well targeting
4D seismic data	Multiple 4D seismic surveys have been acquired to confirm reservoir compartments

Table 4.1 Surveillance data sources in Schiehallion, and the information each individual data provide.

In previous studies, fine-scale geological details and subtle barriers have been found through multi-disciplinary study. The latest dynamic full field simulation model was built in 2003 (Freeman et al., 2008). The model has been regularly updated to incorporate the new geology information derived from continuously acquired surveillance data. Figure 4.5 shows the flow barriers and baffles used in the 2005 history matching of the Full Field Model (FFM) built in 2003 (Gainski et al., 2010). New geological objects are usually inserted into the model by adjusting the location and transmissibility of the flow barriers. With a considerable departure to the initial picture of the reservoir in 2003/4, a new FFM was built in 2009 to reflect the latest knowledge about the reservoir. With modeling individual geobodies in the center of the workflow, the 2009 model used an improved gridding system where channels and geobodies are identified with discrete channel index. It is reported that this modeling method allows a rapid implementation of further revisions of the model, aimed to incorporate new geological, surveillance data (Martin and MacDonald, 2010). As new compartments were identified in the continued studies, the level of known reservoir connectivity reduced, meanwhile, this represented an opportunity for new in-fill wells (Gainski et al., 2010).

As discussed in Chapter 3, after a pressure stable state is reached, correlation may exist between the pressure-driven 4D response and the net fluid volumes produced from a given compartment. In the Schiehallion field, the reservoir contains a number of compartments of varied size and with different levels of communication to neighboring areas – providing a good ‘test field’ for the proposed technique.

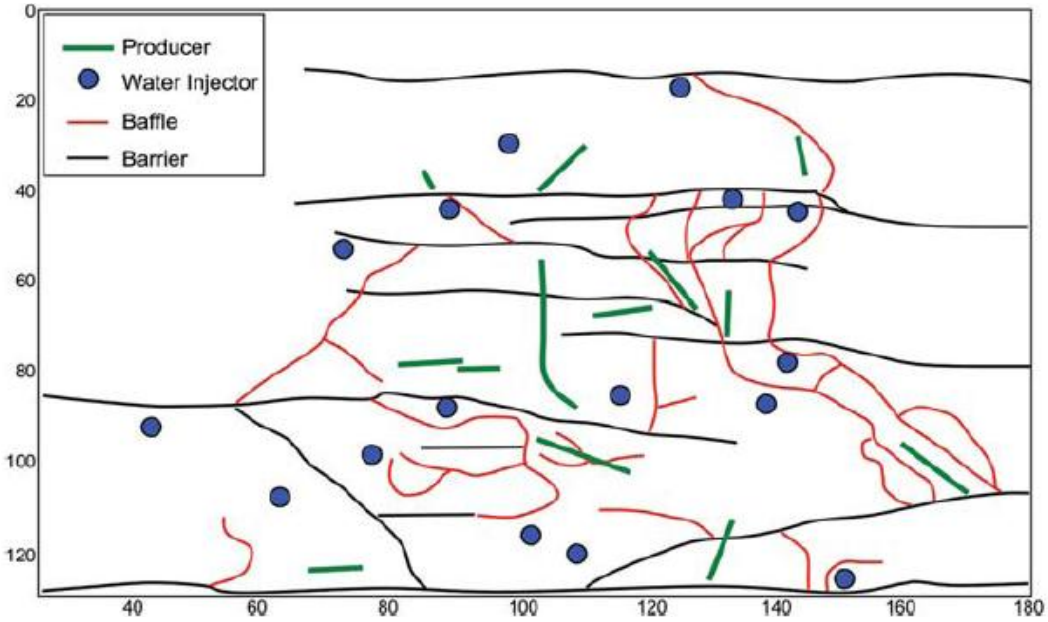

Figure 4.5 T31 sand barriers (black) and baffles (red) to flow used in 2005 history matching of 2003 Full Field Model. Also shown are field production wells and water injectors (blue dotes) (after Gainski et al., 2010).

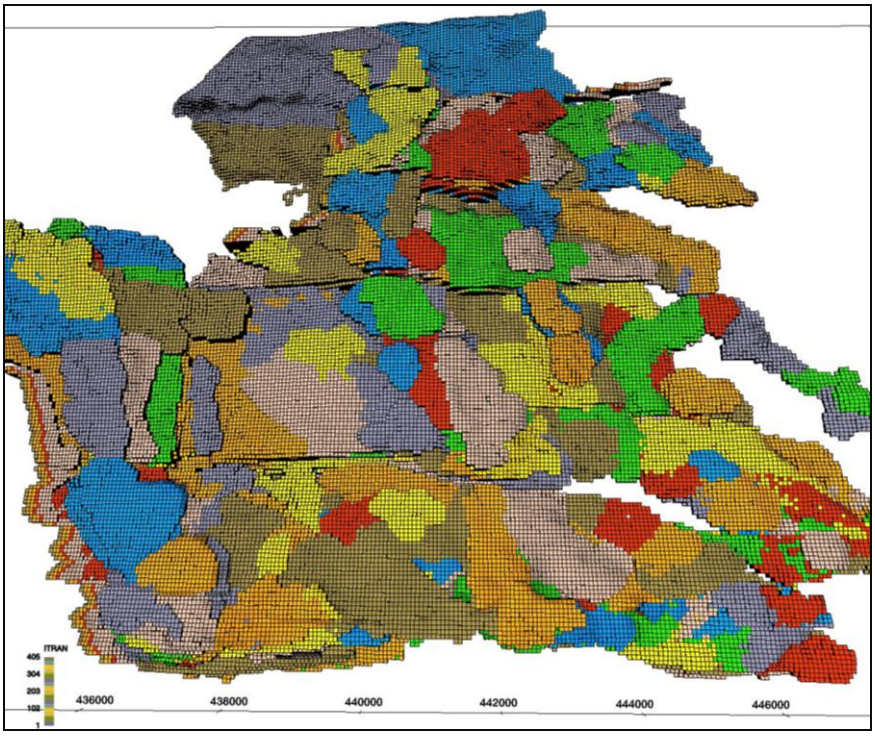

Figure 4.6 The geobodies index for the 2009 Schiehallion FFM built using a geobody-oritented workflow (after Martin and MacDonald, 2010)

4.3 Development and production history

At the time of writing, the Schiehallion subsea development (see Figure 4.7) consists of 5 subsea drill centers with 22 oil producers and 24 water injectors tied back to the Schiehallion FPSO. The Schiehallion is developed jointly with the neighbouring Loyal accumulation as they are 15 km distance from each other. Oil from the field (currently production rate at 220,000 bll/day) is exported by 14 cargo tanks to the Sullom Voe terminal. Gas (peak production 140 million scfd) is exported by pipeline to the Magnus field for re-injection (BP asset portfolio, 2009). Due to the proximity of the An'Teallach gas reserves, produced gas from this field is also exported by sharing the pipeline and network of the Schiehallion The location of An'Teallach gas reserves and Schiehallion field infrastructure is shown in Figure 4.7.

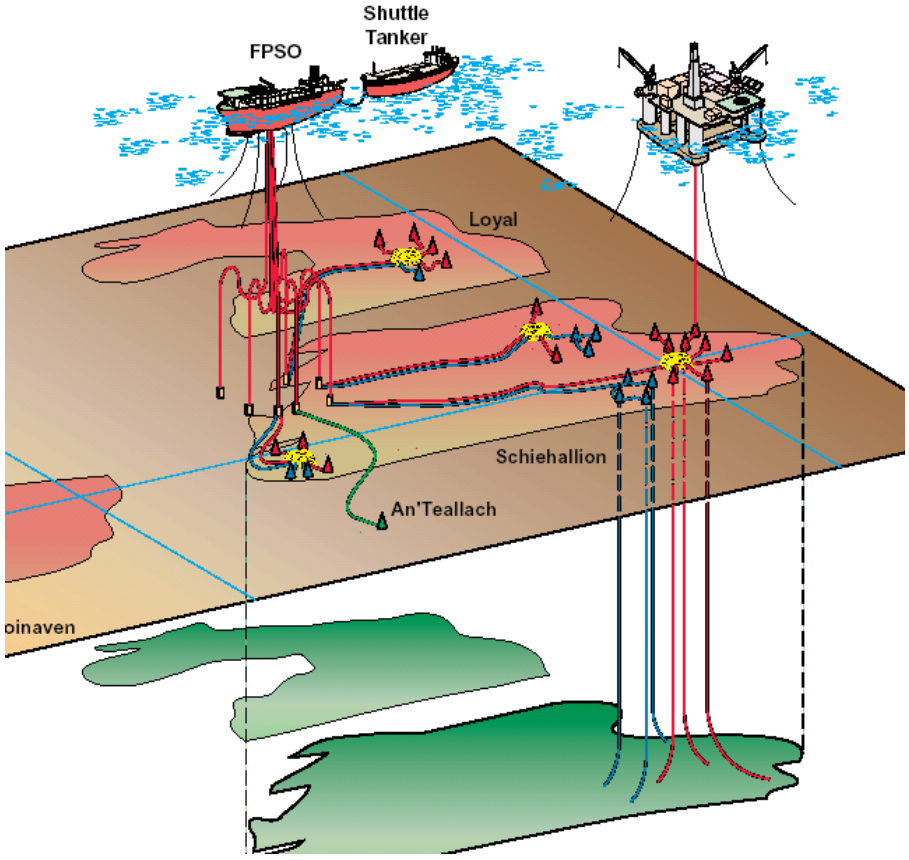

Figure 4.7 Schematic of field infrastructure showing main components: four drill centers, production wells and injection wells are connected through a system of well head and flow lines to Schiehallion FPSO (Martin & MacDonald, 2010).

As stated previously, reservoir connectivity in the Schiehallion field is rather complex due to a high level of compartmentalisation and faulting. Thus, the actual influence area of each planned well has been recognised as a high risk for field development in the early project life. Seismic attribute maps extracted from 3D seismic data reveal the reservoir sands are highly channelized, and an important observation from seismic is that 'bright' signals correspond to sand-rich channels and stacked overbank sandbodies. Considering the high level of geological discontinuity, most of the producers are horizontal wells and majority of them are placed in the core of the channels imaged by seismic in order for each well to gain maximum exposure to net pay. The horizontal section of the horizontal producers can reach as long as 1500 meters. It turned out that this strategy is correct after some time of production as the appraisal data from monitoring techniques indicate that many of these horizontal producers are producing from several intersected compartments.

The initial production strategy was to avoid early water breakthrough by not placing injector and producers in the same channel. After first oil in 1998, it is realised that this strategy was not successful because the connectivity is much poorer than expected. Many injectors and producers are placed in poorly connected compartments, thus expected pressure support from designed injector-to-producer pairs were not achieved. As a result, pressure in these compartments intersected by producers decreases dramatically in the early period of field life, causing a considerable amount of gas liberating from solution. The main task for the first stage of field management (1998-2003) was to manage gas by drilling in-fill water injectors while shutting down the injectors placed in the compartments disconnected to the producers. With these effort made, reservoir pressure is recovered to the level above the bubble point four years after production start-up in 2003 and the measured GOR suggests that most of the liberated gas comes back into solution when pressure is recovered. However, the downside of this drilling campaign is that water breakthrough was soon observed. The impact of the series of field management activities as discussed above are clearly shown on the historical production data as shown in Figure 4.8. Thus, the second stage of field development (2003 onward) focuses on monitoring water flooding. During this stage, new in-fill water injectors continued being drilled as new flow barriers are identified to further improve the sweeping efficiency and enhancing pressure support whilst new producers were also drilled to access the unswept zones. For instance, two examples for the identification of in-fill drill targets supported by multiple surveillance data are discussed in Gainski et al. (2010). The strategy of

integration of varied surveillance information is always used in order to offset the impact of the geological complexity on the field production.

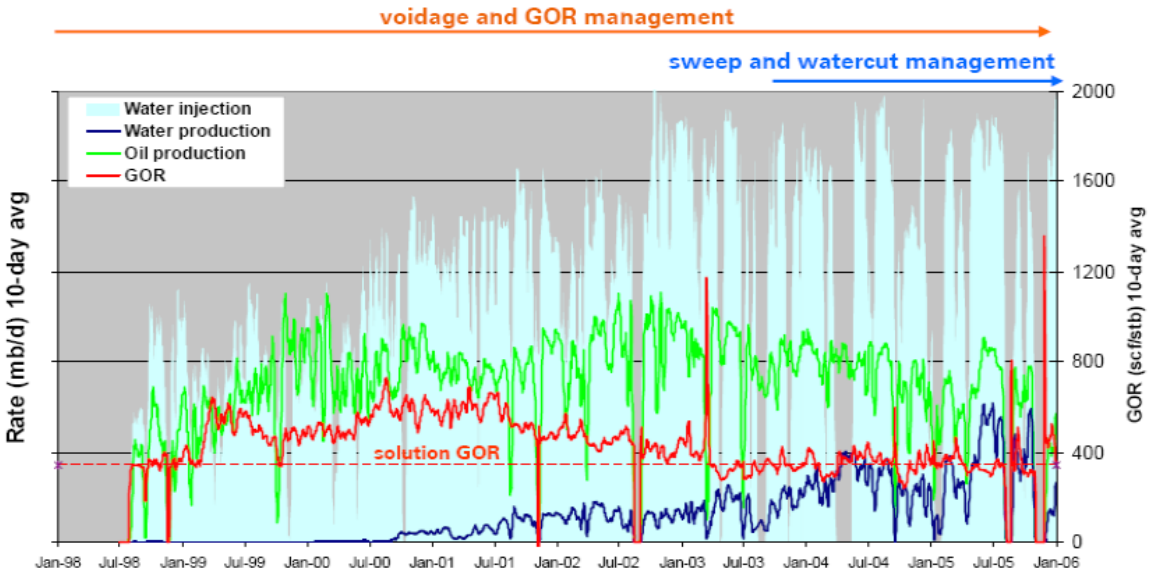

Figure 4.8 The Schiehallion voidage history shows GOR (red line), water injection (shaded areas), water production (blue line), and oil production (green line) from the production start-up to January, 2006. The variation of these measurements corresponds to the effects of the development strategies taken in different phases of reservoir management since the first oil in 1998: a considerable amount of liberated gas observed as a high GOR level between 2003 and 1998 due to poor pressure support has been successfully controlled as the result of massive injection activity aimed to recover the reservoir pressure (after Govan et al., 2006).

4.4 Seismic surveys

Two pre-production seismic surveys were acquired over the Schiehallion field: the first was shot in 1993 for 'exploration' purpose, and the second in 1996 used as a baseline for subsequent 4D surveys. As a result, different acquisition configurations were used for these two surveys and they were processed with different 'sequences' at the time. With improved data quality compared to that of 1993 data, the 1996 baseline data was used to identify most of the drilling targets in the early field life (Parr & Marsh, 2000). Figure 4.9 shows the time slices taken from 1993 and 1996 data at 2000 ms, and a comparison of these two images reveals that the 1996 data show more 'coherent' features of geological structures and relatively lower noise level (Altan et al., 2001). To research the impact of different acquisition configurations on the 4D signatures, these two baseline data were passed through

an identical processing ‘sequence’. As shown in Figure 4.10, the results showed an improved consistency in imaged reservoir structures, however, a quantitative comparison reveals the difference (~6%) between these two baseline data can still be observed.

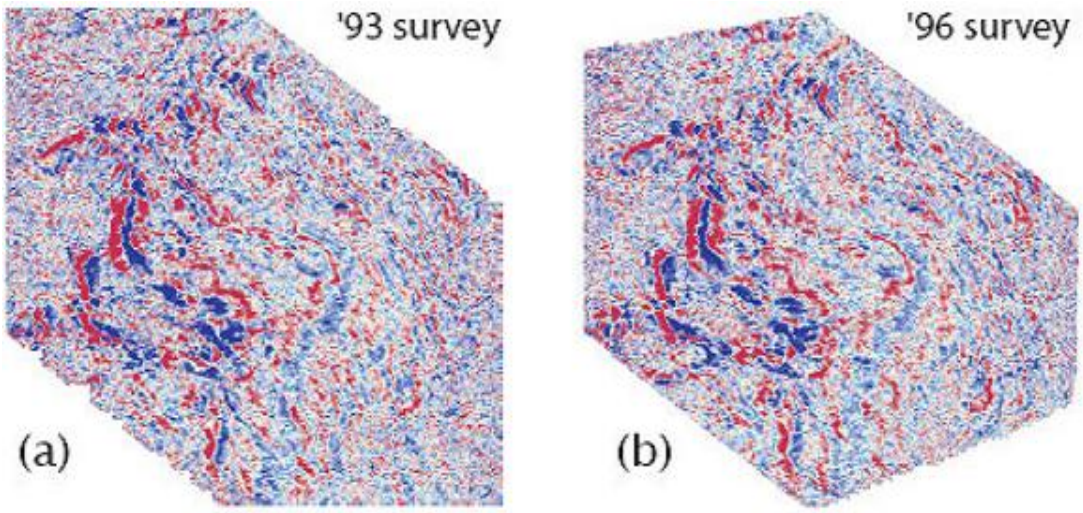

Figure 4.9 Time slices extracted from seismic data volume from (a) 1993 and (b) 1996 surveys at 2000ms (Altan et al., 2001).

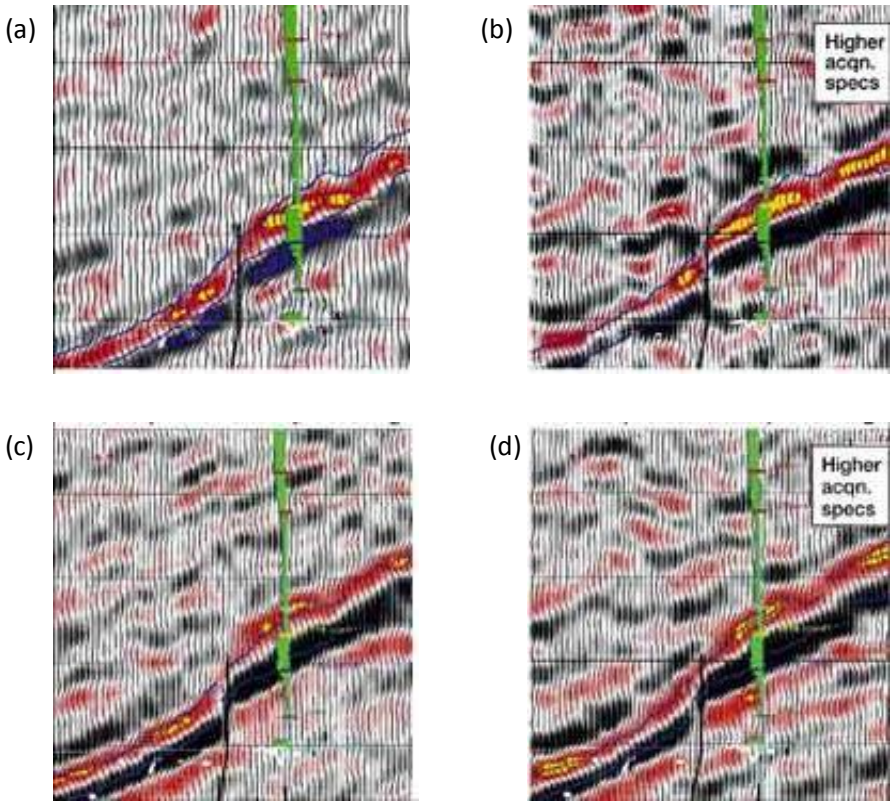

Figure 4.10 A selected section from (a) 1993 and (b) 1996 baseline processed with different ‘sequences’ compared to the reflection in the same section from (c) 1993 and (d) 1996 passed through

an identical sequence. Clearly, (c) and (d) show more consistency in imaged reservoir structures (adapted from Parr & Marsh, 2000).

Prior to 4D acquisitions, a series of feasibility studies based on log data, rock physics measurement and seismic modeling were carried out to estimate the 4D seismic differences corresponding to typical fluid-substitution cases (e.g. approximately 13 - 30% amplitude change for water replacing oil and 20 to 30% for gas coming out of solution) – suggesting the magnitude of 4D responses should be greater than noise threshold (see Floricich, 2006; Parr & Marsh, 2000). Following the feasibility studies, the 4D surveys were shot at time intervals of 1 to 2 years with the acquisition parameters of 1993 baseline repeated in the 1999 and 2000 surveys and those of 1996 survey repeated in 2002, 2004 surveys. The first three monitor surveys acquired in 1999, 2000 and 2002 mainly served to support in-fill drilling of water injection wells in the over-depleted regions where gas comes out of solution and the later surveys are used in management of water sweep. Figure 4.11 shows the amplitude difference between 2002 and 1996 in which 'softening' signal in red caused by gas breakout are the dominant effect.

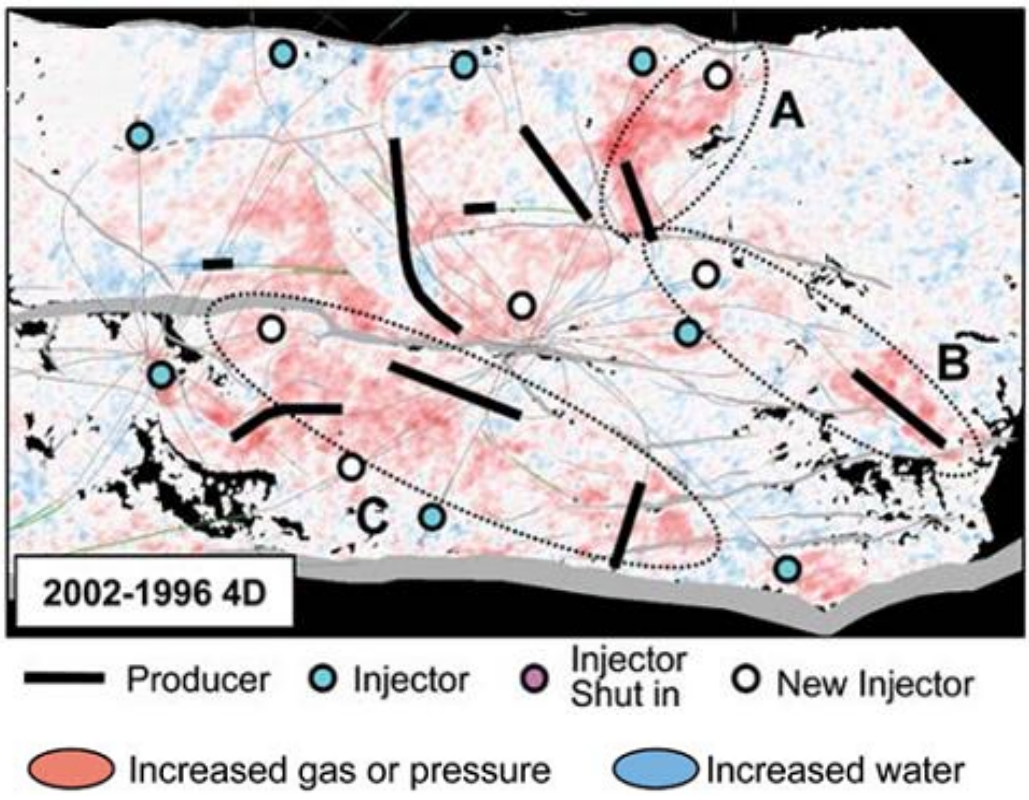

Figure 4.11 Amplitude difference between 2004 and 1996 with blue signals indicating increasing water saturation and red signals indicating increase in gas saturation or pressure (after Gainski et al., 2010).

In a wider context, 4D seismic has rapidly gained wide acceptance among major oil companies all around the world since the first 4D monitor survey was acquired in 1999 over the Schiehallion. Thus, the momentum of 4D is continued in the Schiehallion and three more surveys were acquired in 2006, 2008 and 2010 with installation of the *Permanent Reservoir Monitoring* (PRM) being considered. The repeatability of these surveys is excellent and data quality is generally very good (Campbell et al., 2005). As shown in Figure 4.12, the 2006 survey has shown its value in verifying the effect of water flooding between 2006 and 2002. The gas signatures clearly observed in 2002 4D difference map (Figure 4.11) has greatly reduced in 2006 4D seismic as a result of increased pressure and gas coming back into solution. The 2006 seismic has also indicated the water sweep between water injector/producer pair by amplitude dimming observed in channel sands (Gainski, Macgregor and Freeman, 2010).

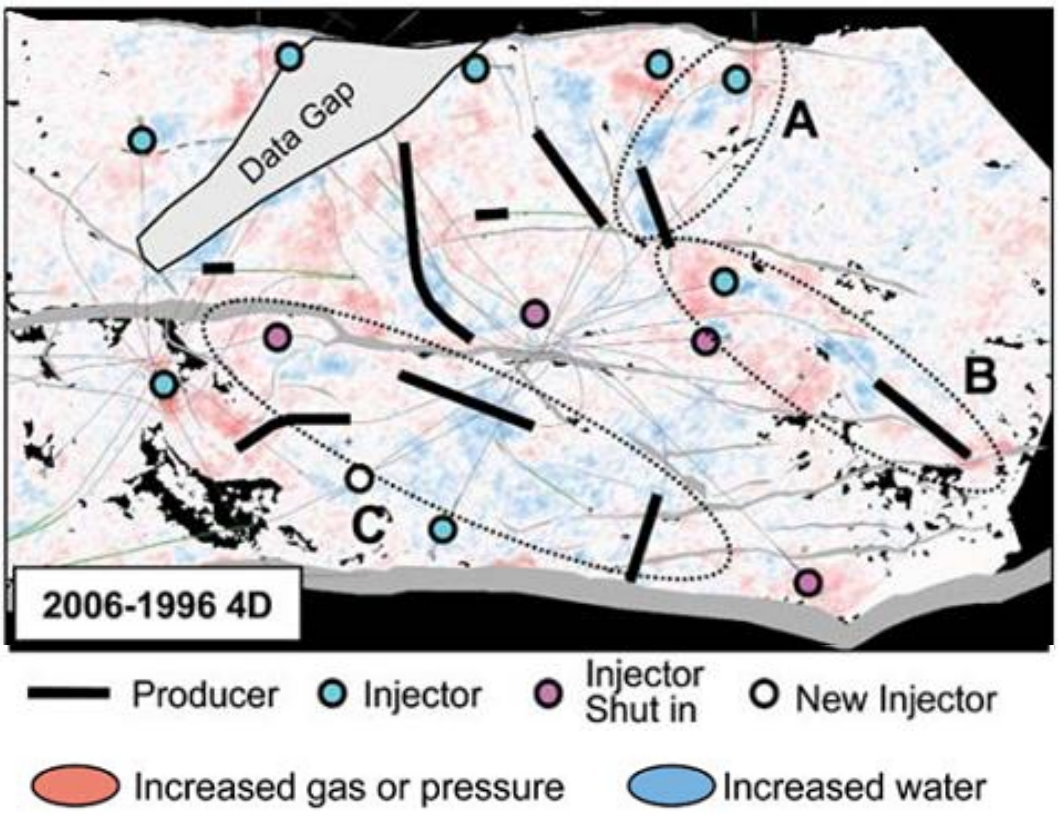

Figure 4.12 4D amplitude difference between 2006 and baseline survey; increasing 'blue' signals verify the effect of water injection between 2006 and 2002 and recovered reservoir pressure (after Gainski et al., 2010).

4.5 Selection of data in this study

As discussed previously, the Schiehallion field is a large hydrocarbon accumulation (approximately 10 ×12 km) and structurally divided into several isolated segments by major faults. In terms of 4D, there are many remarkable 4D anomalies on the difference map of seismic attribute. In order to carry out detailed studies, this chapter focused on selected area of segment 4 in the field (Figure 4.13), in which several compartments are believed to be almost closed. As explained in Chapter 2, such geological settings are favorable for testing the well-to-seismic correlation technique proposed in Chapter 3.

The Segment 4 is enclosed on three sides by faults and pinch-out and on the fourth side by active aquifer, thus is considered to be a hydraulically independent sector from the other segments of the reservoir. Compared to other segments, the segment 4 contains less high-quality channel sands and there is a higher level of heterogeneity in the studied area. The quality of channalised sands in this segment varies from thinly inter-bedded sand to massive sands, and massive sands with better quality (Floricich, 2006). In general, the sands are characterised by excellent flow properties, high porosity with average 25.7% and permeability 250-2900mD and 40-1300mD in horizontal and vertical direction respectively (Meadows et al., 2005). Oil in this segment is of good quality and primarily composed by light components with API° 22-28.

Interpretation of 4D signals in this area is considered to be challenging – owing to a combined effect of relatively poor data quality and complicated patterns in the pressure and saturation distribution due to complex reservoir connectivity. Due to complex patterns in the 4D signature, interpretation of the 4D response genuinely related to a particular well is usually complicated by the seismic difference caused by other factors such as the 4D responses of the neighbouring wells. As a result, there is large uncertainty in the interpretation of reservoir connectivity using 4D seismic alone especially when insufficient surveillance data sources are available or effective in the area of study. Thus, it is hoped that the technique proposed in this thesis can reduce some interpretational ambiguities by integrating production data directly with frequently acquired 4D seismic data available in Schiehallion. Such examples are shown in the remaining part of the thesis.

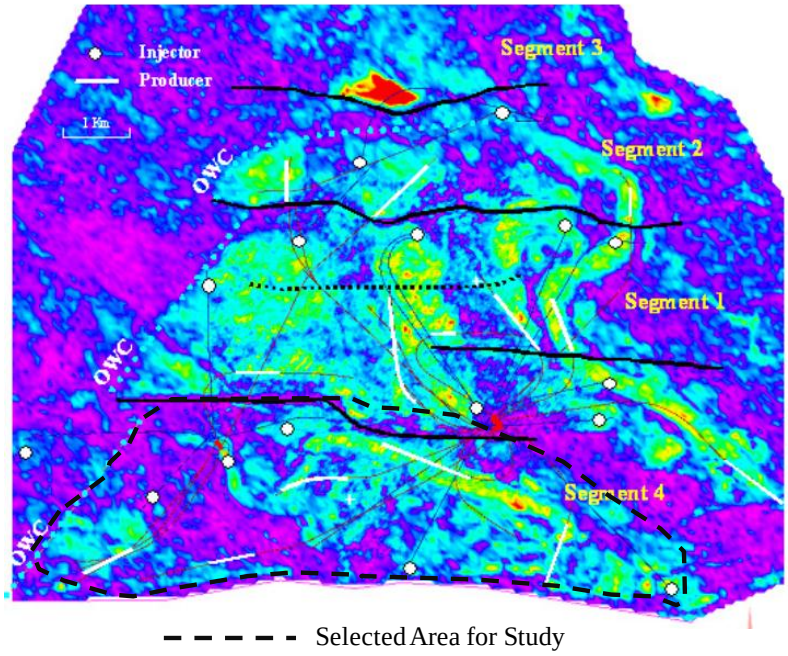

Figure 4.13 RMS average amplitudes taken from 1996 baseline survey**.** The selected area of study is outlined by black dashed line, in which several compartments are believed to be completely or nearly closed, after Floricich (2006).

As stated previously, the 4D data needs to be interpreted in conjunction with predicted simulation or pressure from the simulator. This imposed another constraint on the selection of seismic vintages for the testing. Thus, the five time-lapse vintages shot in 1996, 1999, 2000, 2002 and 2004 are used for this study due to the availability of production data and simulated results over the corresponding survey periods (Figure 4.14). These data have been cross-equalised by the field operator and are of satisfactory repeatability. For each survey, RMS amplitude is mapped between the picked top and base of the T31 interval. These surveys are cross-equalised to the pre-production 1996 survey through a simple normalisation operator derived from the histogram of the amplitude in a selected area where no production change is expected. In this study, the simulation model of the segment 4 was cropped from the full field model built by operator and used as guidance to interpretation (Edris, 2009). As a result, prediction errors due to model cropping were anticipated but found to be minor after comparing predicted dynamic reservoir performance from the cropped model with that from FFM (Edris, 2009). Five oil production and five water injection wells have been active in Segment 4 between 2004 and 1998 as shown in Figure 4.14. Additionally, the simulation model was up-scaled from the original model in the vertical direction by a factor of four,

aiming to reduce the CPU time for simulation. Arithmetic averaging was used for upscaling NTG and porosity, and geometric averaging was used for upscaling permeability. The dimension of the model is now 146×44×7 with the number of grid cells totalling 44,968. The predicted distributions of water, gas saturation and pressure in the reservoir in 2004 are shown in Figure 4.15 in comparison with the initial in 1998.

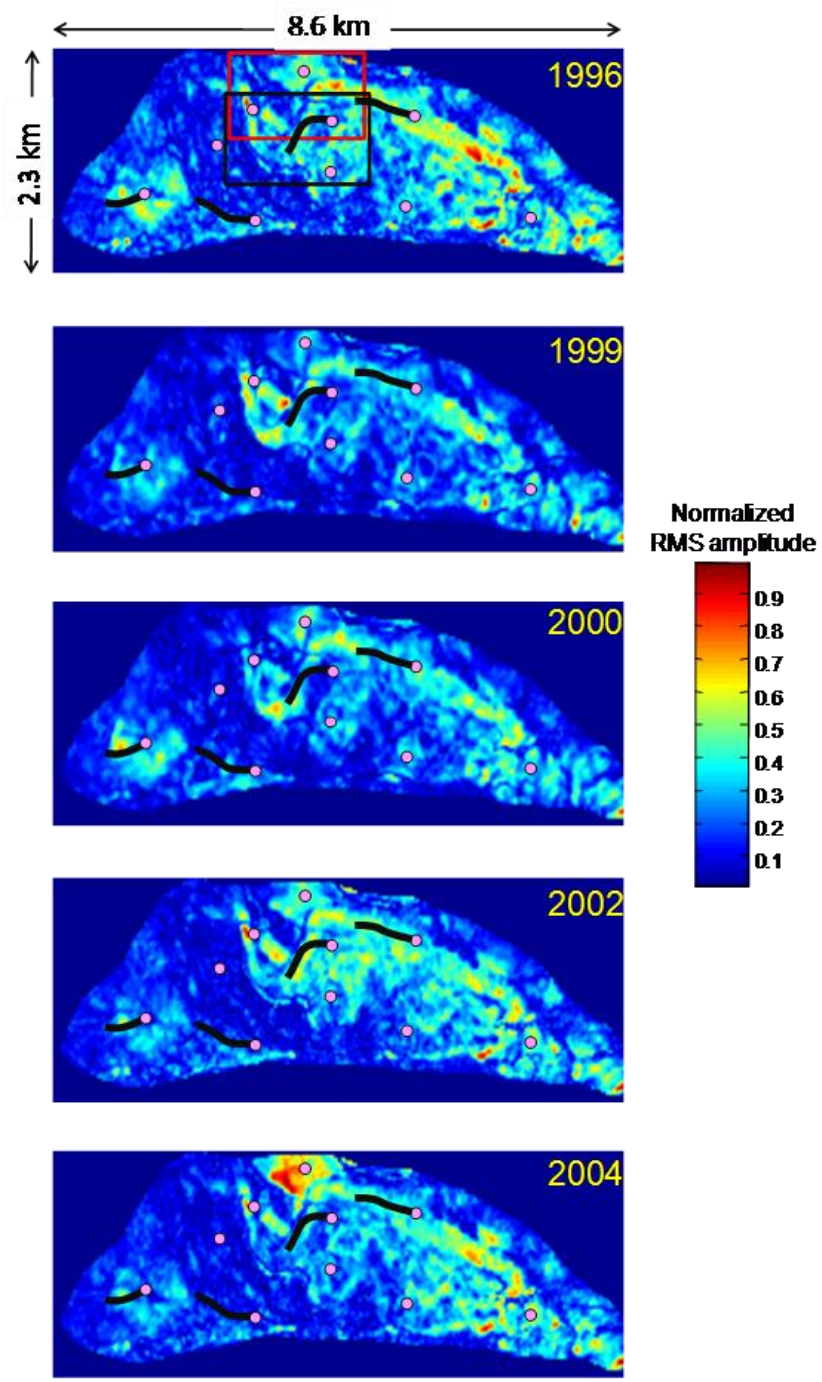

Figure 4.14 The five seismic maps used to generate the time sequence for cross-correlation analysis. Maps are of normalised RMS amplitude derived from the coloured inversion product. Squares in the topmost diagram indicate study areas for examples 1 and 2.

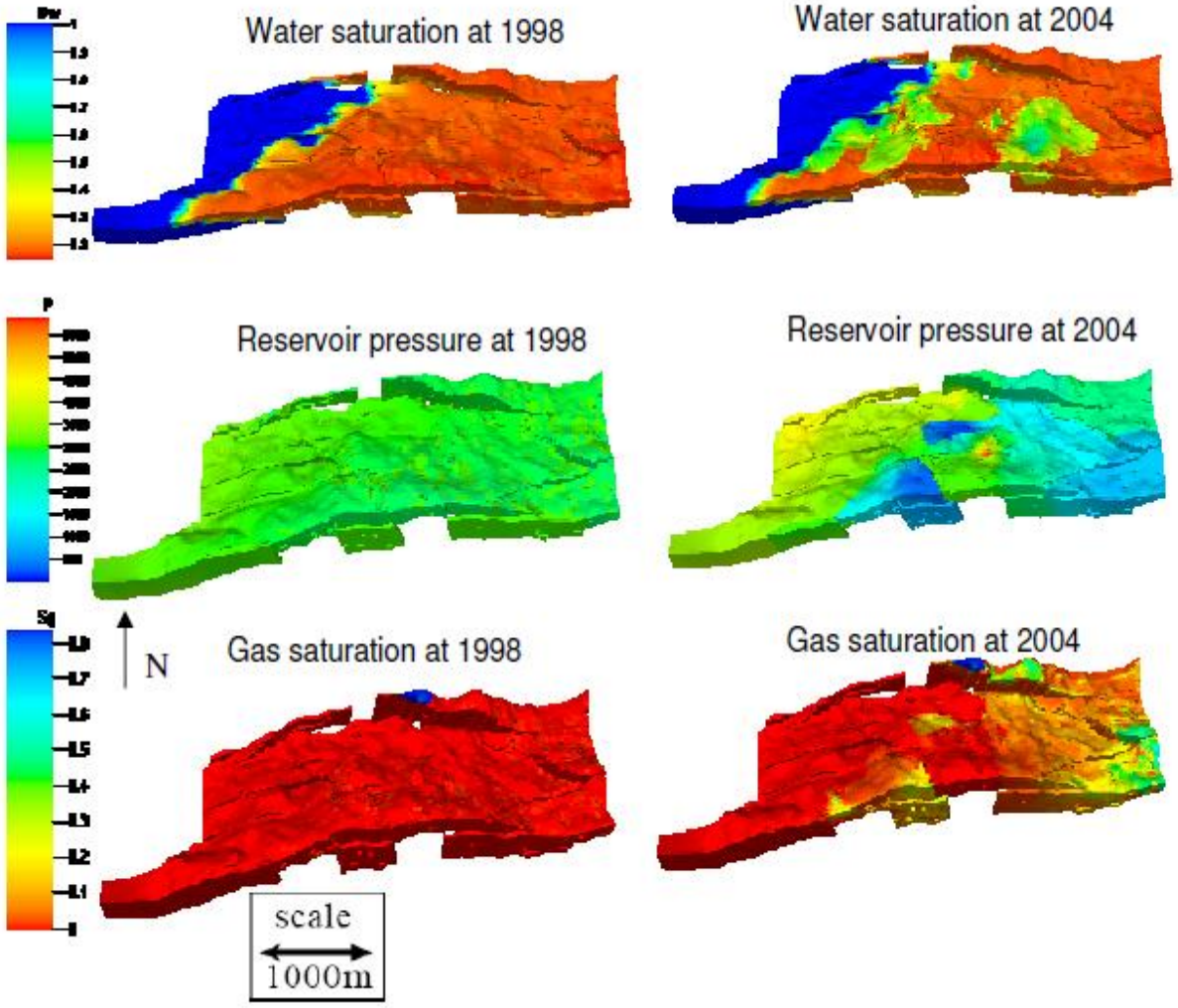

Figure 4.15 From the top row to the bottom, the picture shows the estimated water saturation, reservoir pressure and gas saturation distribution in 1998 (the left column) compared to those predicted in 2004 (the right column) from the cropped full field model (after Edris, 2009).

4.6 Identification of production related signal

In this chapter, our focus is on Segment 4 in the south eastern portion of the field, which lies between two major sealing faults. In this segment, the 4D seismic displays a softening of impedance at the injectors, consistent with a dominant pressure up response rather than a hardening from water invasion (Stephen and MacBeth 2006). Around some of the producers, gas out of solution creates a clear softening effect - however these wells are not considered in the current analysis (for this reason we exclude the lower right area of the segment as we wish to concentrate only on the pressure effects). Over most of the selected segment the pressure signal is the main control over the seismic amplitudes.

The selected five repeated seismic surveys as shown in Figure 4.14 generate in total ten distinct mapped 4D signatures, and these are arranged as a time sequence for each spatial location. Not all of these wells are active nor maintain constant rates for the full duration from production start-up until the last survey date. This variation of well rates provides the diversity in the time sequence necessary for the application of our method. To guide the analysis, pressure and saturation changes corresponding to the time sequences defined above are also extracted from the flow simulation model. Initial qualitative inspection of the seismic data reveals a reasonable correlation between the 4D seismic signatures and the well activity. To ensure stability, a minimum credibility threshold is needed for the *NCC* maps, as for a particular size of time sequence the cross-correlation coefficient is only statistically significant above a certain coefficient value. Below this threshold there is a chance that samples drawn at random can yield the same coefficient (Bevington, 1975). For example, for the 10 points used here, sequences with correlation coefficients greater than 0.77 are significant with a 99% confidence. Another reason for thresholding the *NCC* maps used in the current work is to focus on the 4D signature induced only by a particular well or group of wells, and to exclude the contributions from other wells. The correlation coefficient between the selected well group of interest and the seismic sequence must in this case be higher than the sequence correlation between the excluded wells and the selected group.

We select two examples from the segment to describe the resultant interpretation in detail. These two specific areas studied are outlined on the top image of RMS map in Figure 4.14 by red (example 1) and black (example 2) rectangular. Well data from the wells in these two

areas are also available to determine the fluid volumes produced or injected over each of the selected time intervals (Figure 4.16).

4.6.1 The *NCC* signal around an injector: W3 example

Injector W3 is in the central north portion of Segment 4, and was drilled to provide more support to the producers in that locality (Figure 4.17). At0 a sector level it is intended to supply pressure to P8 in the south and P9 in the east (outside the figure perimeter). Unfortunately for the oil production, W3 injects into a small isolated triangular fault block of roughly 1km x 0.5km, bounded along its northern edge by a major east-west sealing fault, and along its remaining edges by smaller faults or stratigraphic barriers. Transmissibility multipliers assigned to the simulation model along the block edges suggest that a small amount of leakage to the west is anticipated. W3 becomes active just before May 2003 and injects at a relatively constant rate up to September 2005, beyond the time of the last monitor survey in 2004. The well activity thus forms a step function in cumulative volume change between the 2002 and 2004 surveys. The 4D seismic response shows a strong pressure up (softening) signal (Figure 4.17a) and the prediction of pressure change (2000psi or 13.8MPa) from the simulator (Figure 4.18a) agrees with this response. Figure 4.19(a) shows the time sequence of cumulative fluid volume changes alongside the seismic RMS amplitude changes for two reference locations inside the fault block. It should be noted that W3 was only injecting for 1 year from 2003 to 2004. Meanwhile, there is no significant 4D signal observed in the surrounding area of W3 before it started injecting in 2003 that seems to correspond to the 'zero' injectivity of W3 during this period. However, the area outside the well compartment of W3 exhibited 4D changes before 2003. Thus, the different behavior of 4D seismic in the neighbourhood of W3 and beyond between 2002 and 1996 is thought to be useful for identifying the true influence area of W3. Thus the 4D seismic from 2002-1996 is also used for the well-to-seismic correlation for this example. The normalised cross-correlations (NCC) are high and the known fault block is readily delineated by mapping this attribute across the entire area. The mapped *NCC* attribute based on the predicted pressure changes from the simulator are also shown for visual comparison only (Figure 4.19b). This diagram validates the strong linear correlation between the pressure change spread across the entire fault block and the change in cumulative fluid volumes at well W3. It is the pressure

change component of the 4D signature (and hence the *NCC* attribute) that detects the boundaries of the fault block.

In contrast with the pressure, the water flood moving outwards from W3 is confined to only a small region of approximately 100m in size around the injector (Figure 4.19b). There is a visible drop in the *NCC* measure around the well observed in Figure 4.19b that is likely to have been caused by the effects of saturation. The shape of the saturation anomaly is governed by the net-to-gross within the block, whereas the spread in pressure change is unaffected by this heterogeneity and is defined by the transmissibility at the barriers. As there is no imprint of the net-to-gross on the overall *NCC* map, it is concluded that the result from Figure 4.19 is controlled by pressure. The mapped *NCC* attribute indicates that the barriers inserted during history matching of the simulation model appear consistent with the 4D seismic. There are some points of discrepancy with the simulator to the south and an extension of the signal suggests a re-positioning of the barriers could be necessary. Secondly, to the west, there is a similar extension of the signal, beyond that defined in the simulation model, suggesting another update to the barrier position. Interestingly, incorporation of the P8 and P9 produced volumes in the correlation calculation does not improve the results – suggesting that any leakage points are outside the compartment and are on a larger time scale than the survey repeat times.

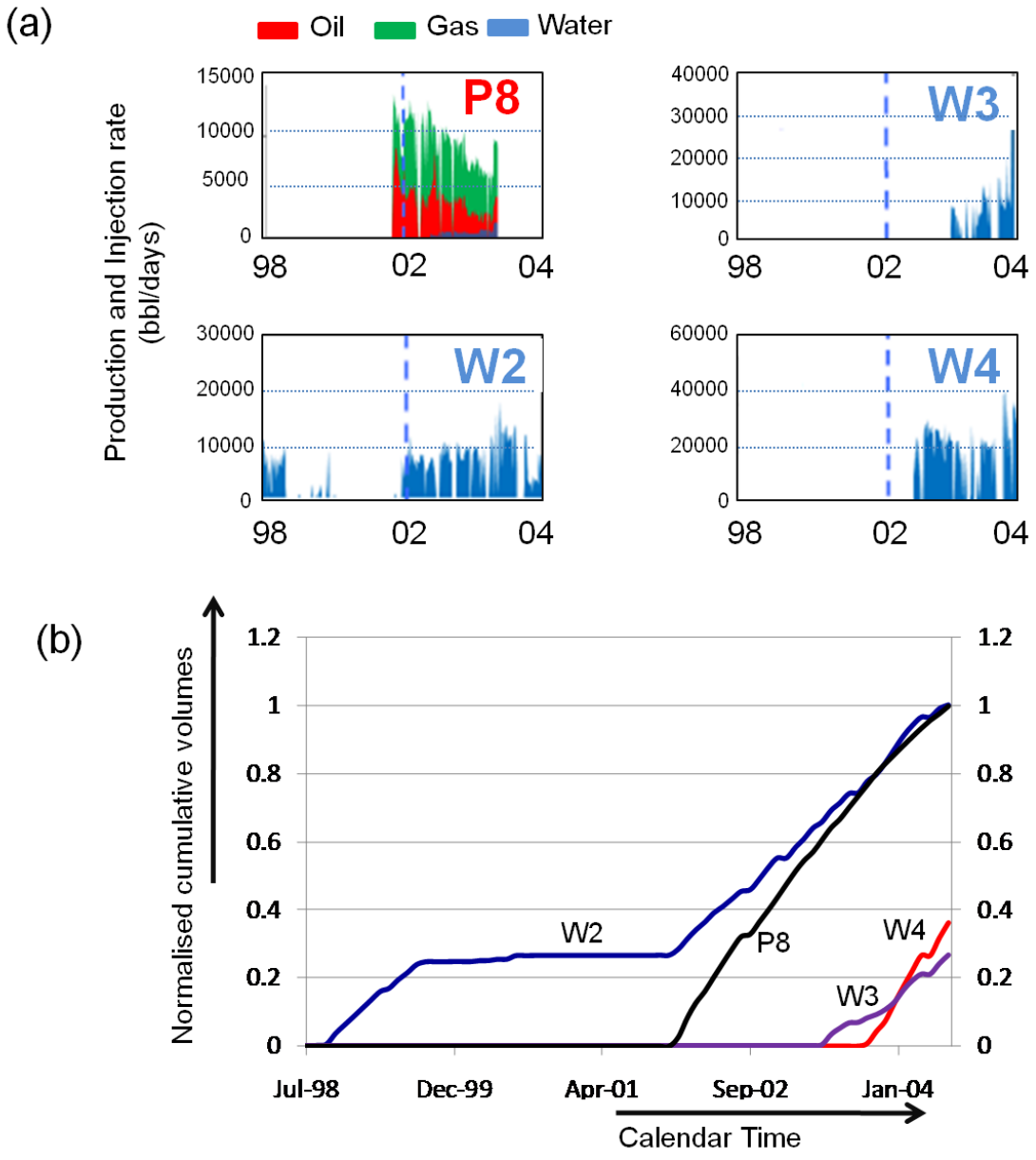

Figure 4.16 (a) Instantaneous well production and injection (redrawn after Edriz 2009); (b) Cumulative volume for the wells of interest in our work.

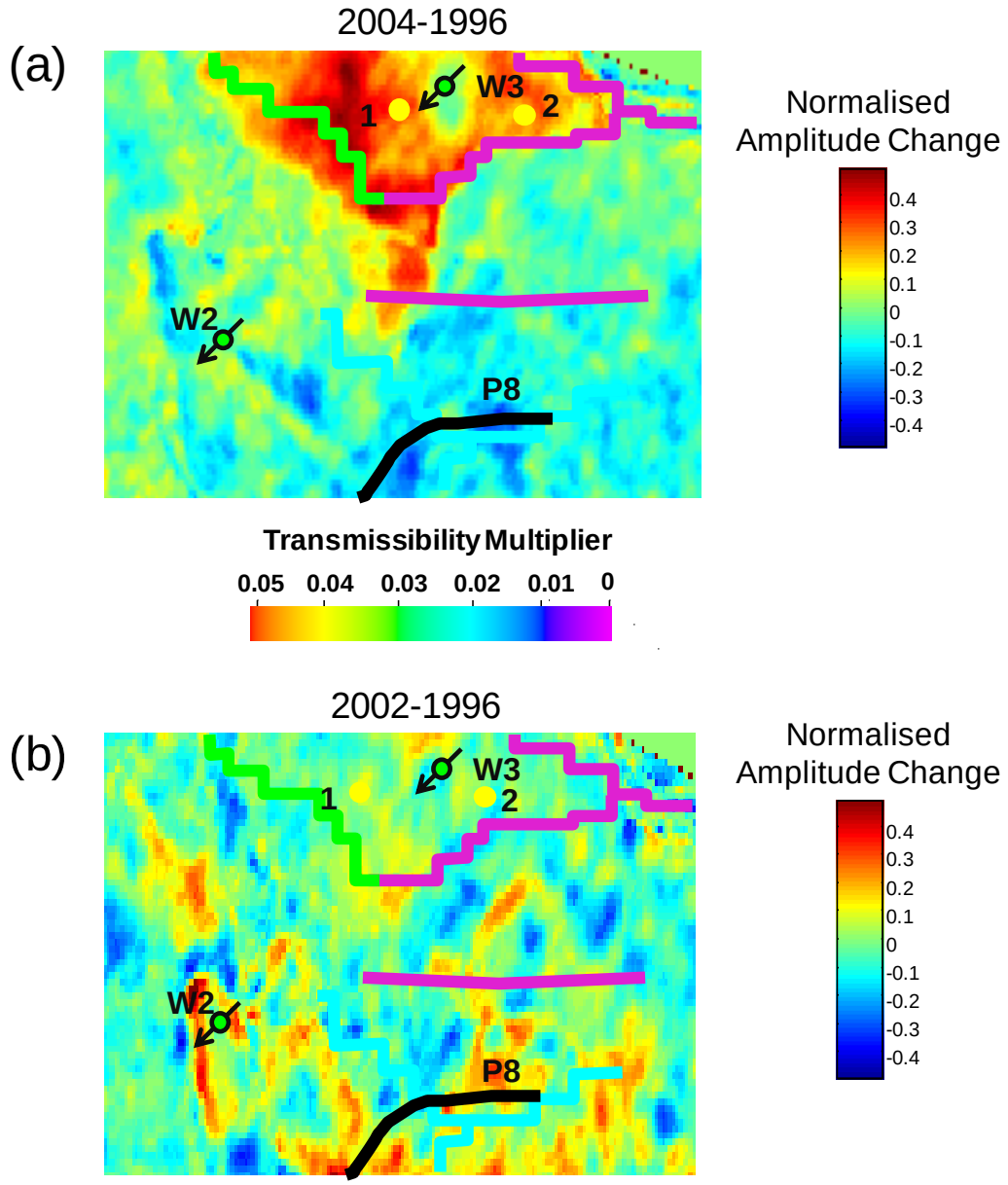

Figure 4.17 Two 4D seismic signatures selected from the sequence of available data, with transmissibility barriers from the simulator superimposed for reference in the selected area for example 1 (a) signature for 04-96; (b) signature for 02-96.

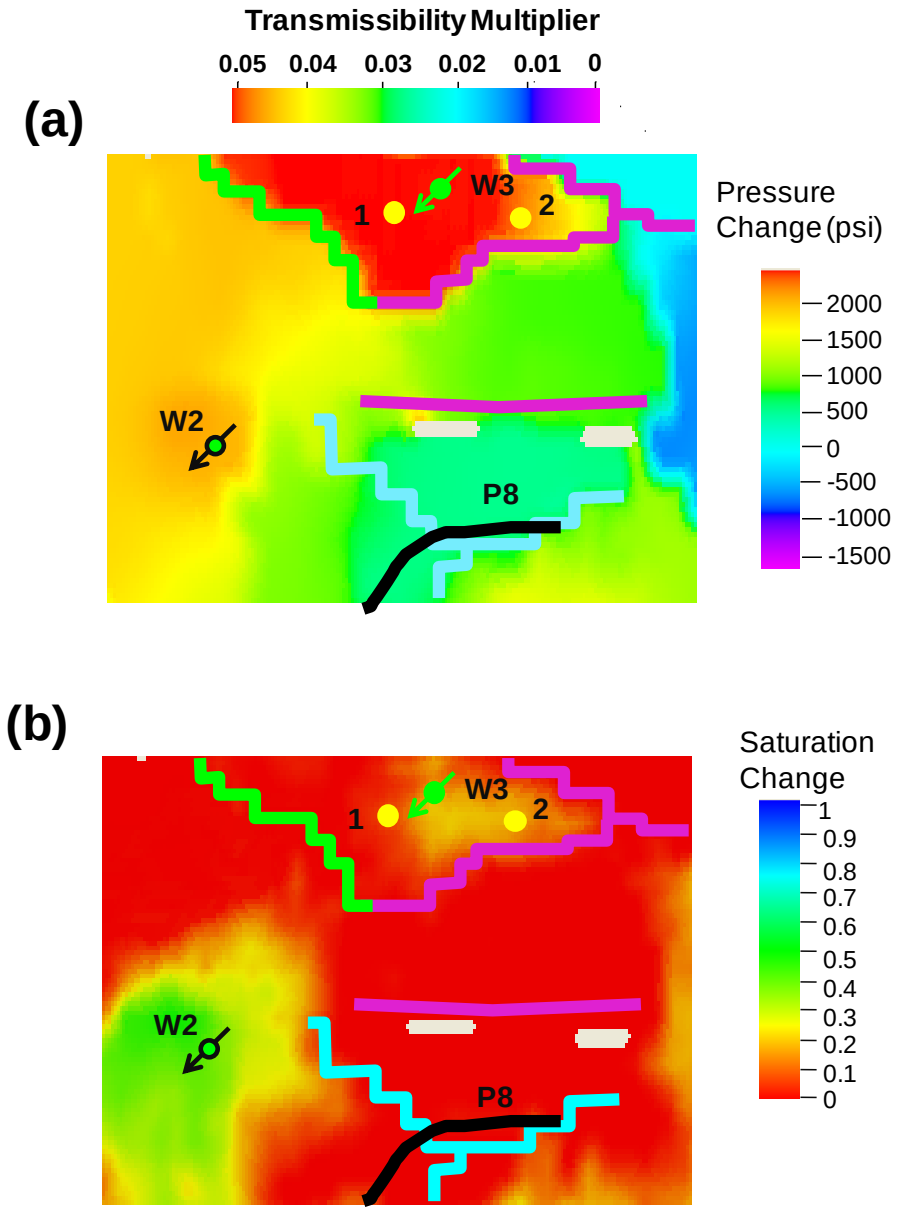

Figure 4.18 (a) Pressure change predicted from the simulator for the 04-96 period; (b) Corresponding saturation change. White regions are inactive cells in the model.

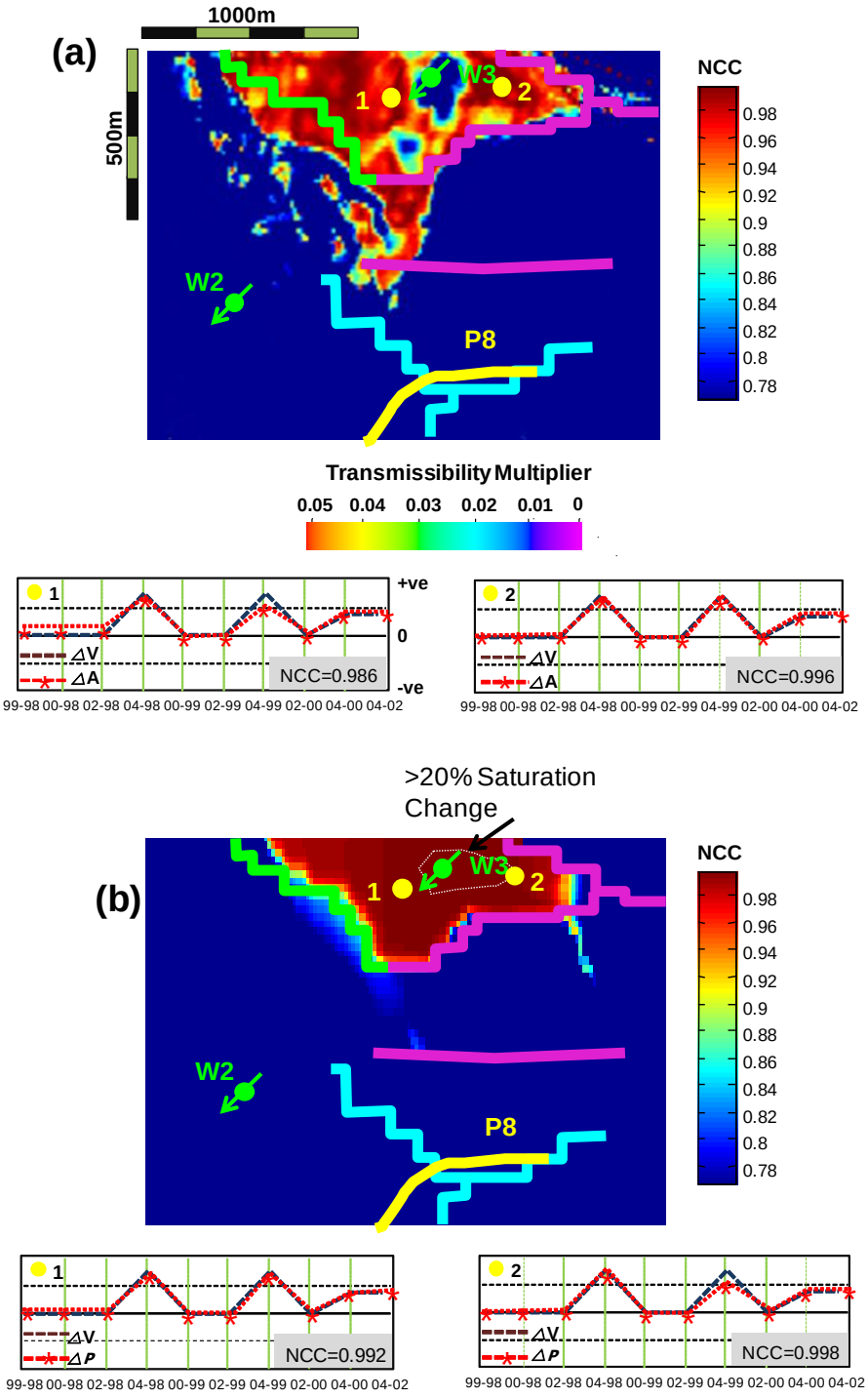

Figure 4.19 Right - correlation panels (right) for two specific locations (marked as 1 and 2 filled circles on the maps) around the injector W3, comparing cumulative fluid volume changes (black dashed lines) and the corresponding 4D signatures (red dashed lines). Left - map of the normalised cross correlation attribute thresholded at a 99% confidence level. (a) results for observed 4D signatures; (b) map for the corresponding pressure change from the simulator. Coloured lines are transmissibility barriers extracted from the simulator – barriers in both the x and y directions are combined.

4.6.2 **A newly outlined compartment: P8 example**

The horizontal well P8 produced from September 2001 at an almost constant rate for the entire duration of the seismic surveys considered here. In its vicinity there are two injectors, W2 and W4 (Figure 4.20). W4 started injecting in June 2003 and was active at an almost constant rate after that date, whilst W2 was closed immediately after September 1999 after it was found that it had been placed in an area with poor connectivity. W2 was later re-activated at several fixed rates. In the simulation model this lack of connectivity was expressed as a north-south barrier (transmissibility of 0.01) separating W2 from P8 (see Figure 4.20 and Figure 4.21). Only a small amount of the water injected at W2 is produced at P8 in agreement with the barrier in the model. Figure 4.20 shows that the 4D seismic signatures contain alternating areas of apparent hardening and softening, and it is difficult to obtain a satisfactory dynamic interpretation which disentangles the pressure and saturation effects. There is evidence of both hardening due to pressure depletion and softening due to gas saturation. In the simulation model a clear zone of reservoir depletion due to P8 is anticipated around the upper part of the reservoir (upper section of well trajectory) (Figure 4.21b). It is possible to observe a softening effect due to gas in the 2002 – 1996 difference map, slightly to the east of this predicted depletion (well W4 is not active at this time, and thus gas saturation is the only explanation for the 4D seismic signature). However, the flow simulation model predicts only a small degree of gas saturation (Figure 4.21a) around the toe of P8. This is in agreement with the measured well data, which reveals gas production at P8, suggesting low critical gas saturation and high vertical gas mobility (Falahat et al., 2011). Figure 4.22 shows the results of applying the *NCC* attribute calculation to the seismic (correlating with P8 production only) and also the pressure changes from the simulator. The *NCC* image is confined to the toe of P8, whilst the simulated pressure shows a distinctly different anomaly confined to the upper triangular compartment next to the heel of the well. The shape of the seismic-derived anomaly suggests that the northern compartmental barrier may not be present, and that the north-south barriers between W2 and P8 need to be shifted. Interestingly, the most recent fine-scale simulation model for this field (Martin and MacDonald 2010) shows an arcuate body around the toe of P8 of similar dimensions and shape to the connected region imaged by the NCC attribute Figure 2.3. The body is part of the channel that has been imaged by RMS amplitude map as shown in Figure 1.14. There is evidence of a vertical barrier in our work in agreement with the geobody interpretation. There is also evidence of a separate connected region to the east of this feature into which W4

injects. It appears that our proposed technique reveals dynamically active geobodies connected to wells.

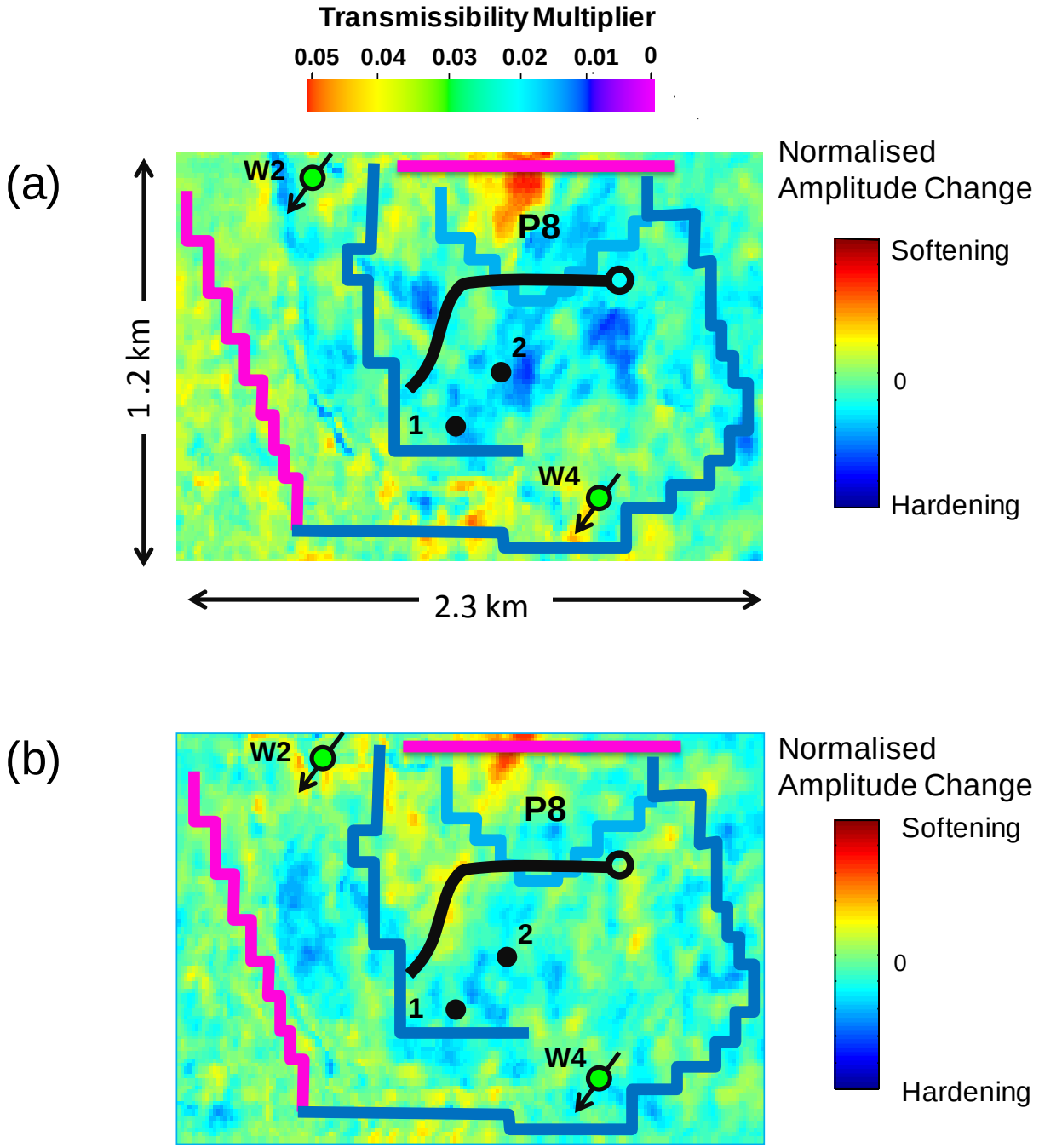

Figure 4.20 Two 4D seismic signatures selected from the sequence of available data in the selected area for example 2, with transmissibility barriers from the simulator superimposed for reference. (a) signature for 04-96; (b) signature for 02-96.

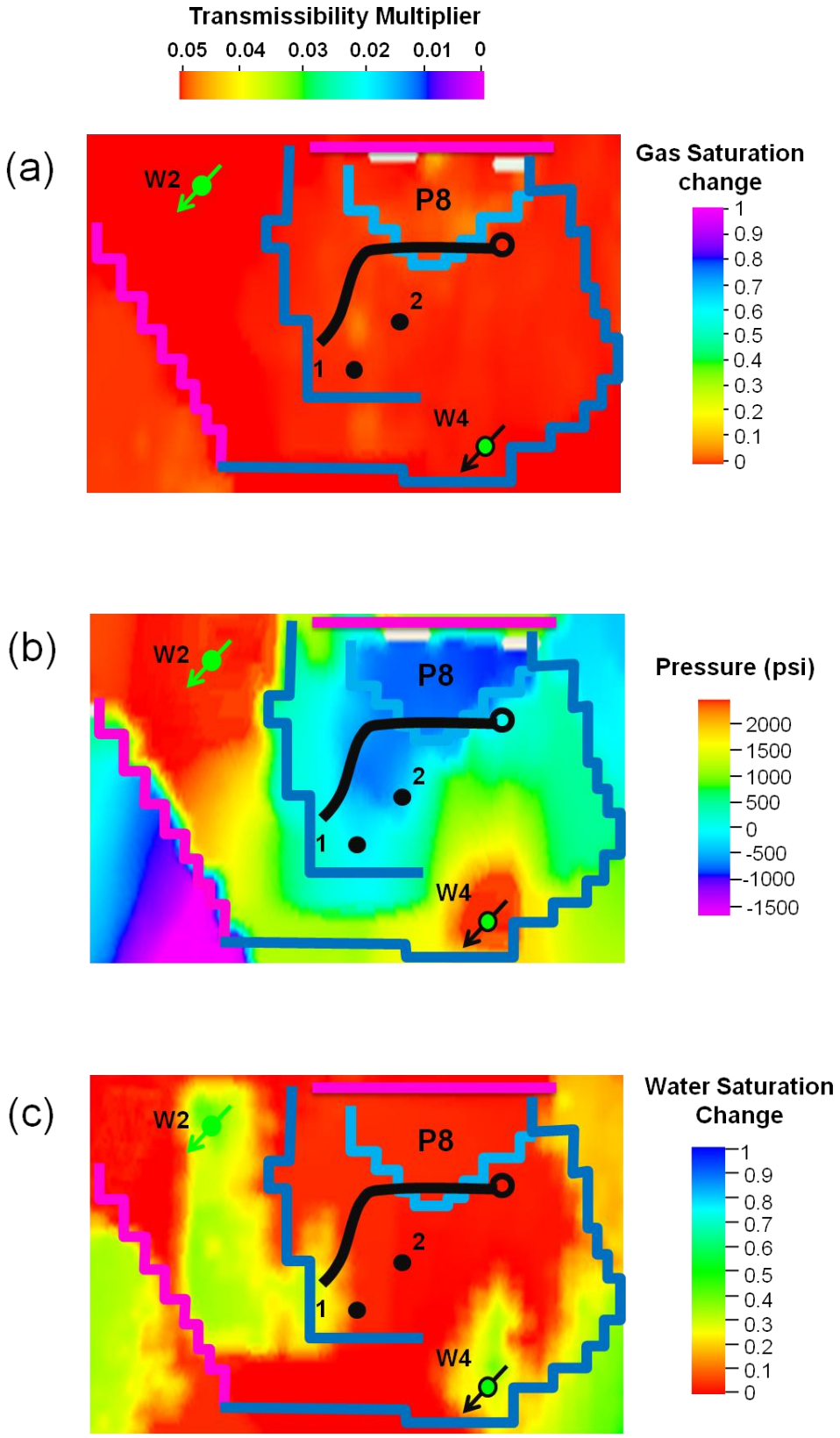

Figure 4.21 (a) Gas saturation change predicted from the simulator for the 04-96 period; (b) Corresponding pressure; and (c) water saturation change. White regions are inactive cells in the model.

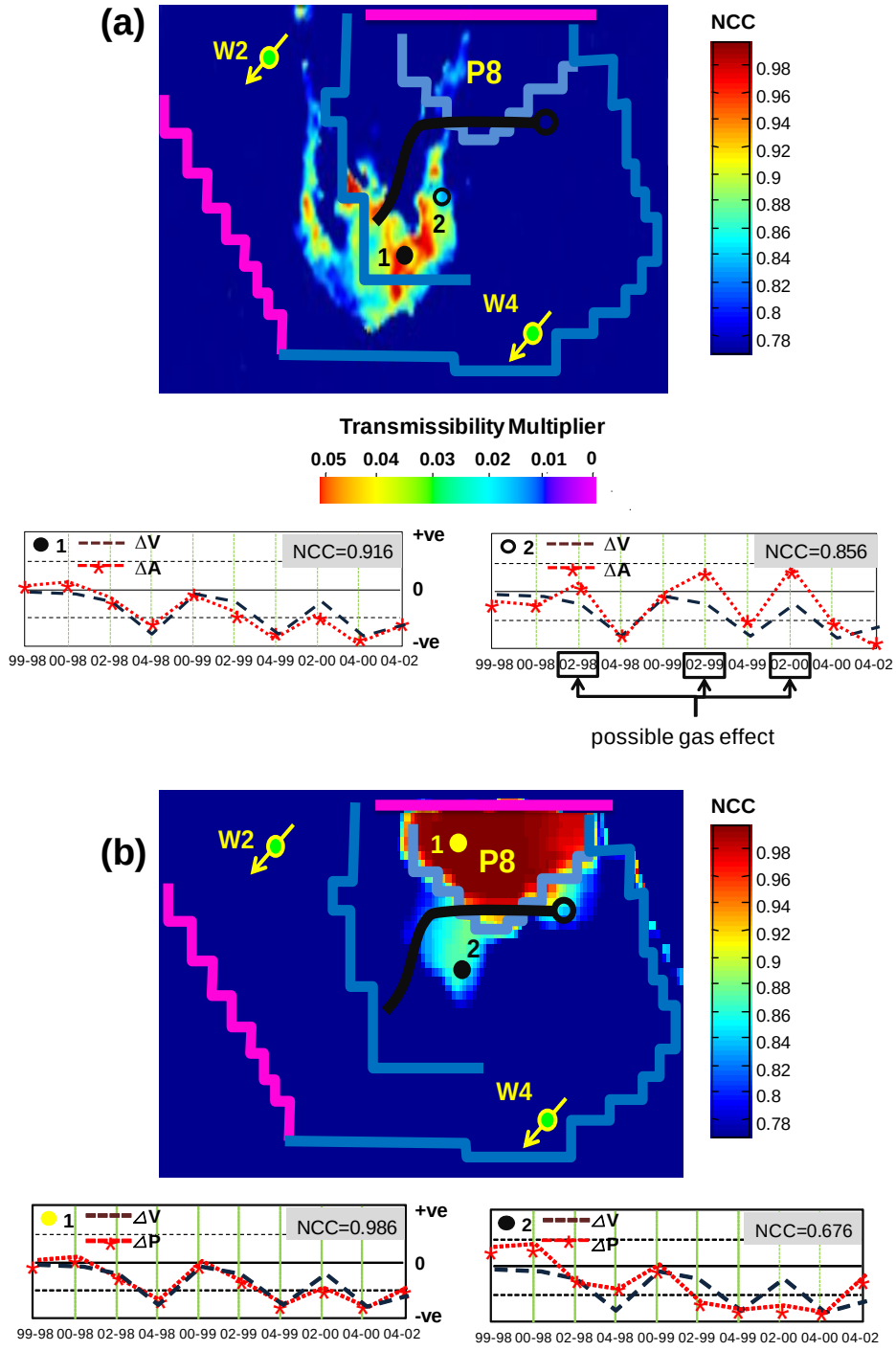

Figure 4.22 Correlation panels (right) for two specific locations around the producer P8(marked as 1 and 2 filled circles on the maps), comparing cumulative fluid volume changes (black dashed lines) and the corresponding 4D signatures (red dashed lines). Left - Maps of the normalised cross correlation attribute thresholded at a 99% confidence level. (a) NCC results for observed 4D signatures; (b) map for the corresponding pressure change from the simulator. Coloured lines are transmissibility barriers extracted from the simulator – barriers in both the x and y directions are overlapped.

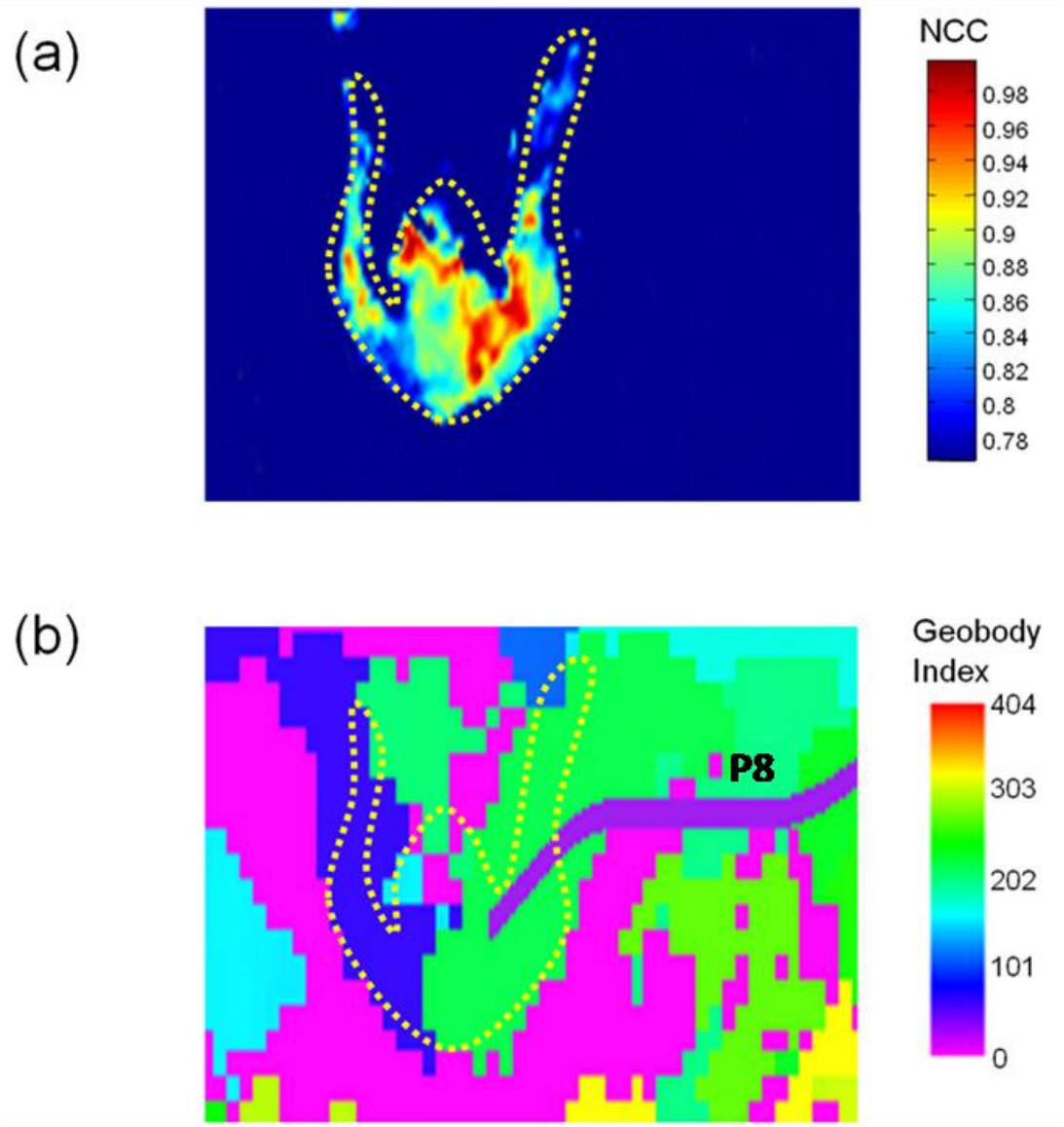

Figure 4.23 (a) *NCC* map for example 2 around producer P8; (b) Most recently developed fine-scale simulation model based on geobodies (after Martin and MacDonald, 2010) with *NCC* dynamic geobody outline superimposed.

4.7 Discussion and summary

The technique introduced previously in this thesis, outputs as a final product a thresholded map of cross-correlation values associated with the activity of a particular well or well groups. The resulting NCC maps from two examples for the application of this technique to the Schiehallion field reveal signal that appears to show more well-centric, spatially contiguous, and dynamically connected regions than those seen in individual 4D seismic signatures. This can be explained as the action of cross-correlation is to stack and enhance all mapped seismic attributes which linearly correlate with the well/well group. Of course, as these cross-correlation values are thresholded, it should also be noted that noise is still present in these results but it manifests itself differently from the input seismic. This noise gives rise to small zones of high cross-correlation lying outside the main signal which are non-production related. Stacking the 4D signatures for multiple surveys (Figure 4.24) does not show the same character, as random noise may be suppressed in this process but amplitudes unrelated to well activity are still present and are reinforced. Indeed, the pattern of the anomalies from stacking is also revealed to differ somewhat from the NCC output, suggesting that our proposed technique is also preferentially selecting that part of the 4D signature related only to pressure. It thus appears that the NCC method derives the benefit of enhancing seismic signal around the wells by 'stacking' a large number of frequently repeated seismic in a specialised, engineering consistent manner.

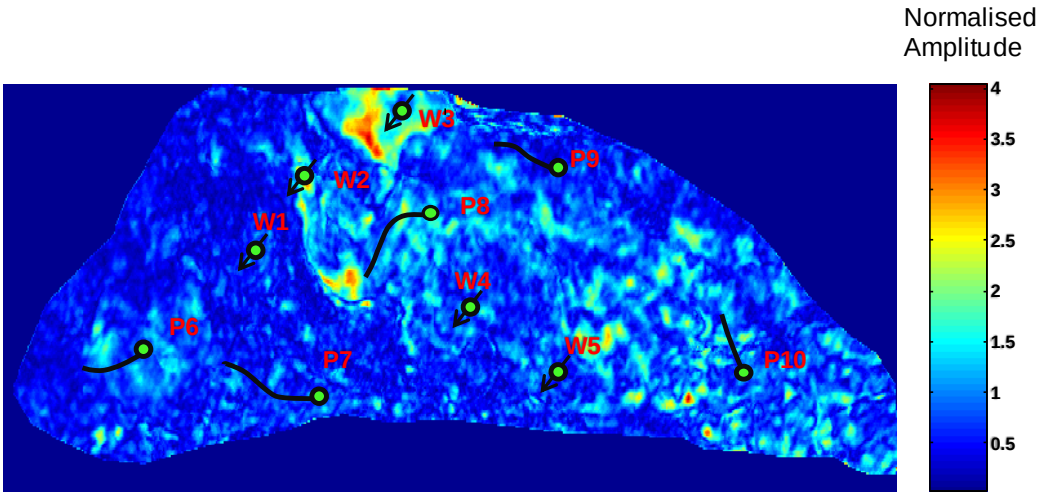

Figure 4.24 Stacked difference maps for all time intervals with all negative values being converted to positives.

Chapter5
Application to Valhall field

In this Chapter, the technique proposed in this thesis is applied to 10 sets of Life-of-Field Seismic (LoFS) data acquired from BP's first permanently installed seismic monitoring system over the Valhall field. The Valhall field is characterised by compacting and extremely low permeability chalk reservoirs, yield fundamentally different 4D signals in character from those observed in the Schiehallion field. However the results from the application to various regions in the field have shown some value in to resolving interpretational ambiguities.

5.1 General description of the Valhall field

The Valhall field is an overpressured, undersaturated Upper Cretaceous chalk reservoir located about 270km in the North Sea's Central Graben, in the southernmost corner of the Norwegian continental shelf (Figure 5.1). The water depth is 70m. The current owners of the field are BP Norge AS (36%) and Hess Norge AS (64%). The nearby producing fields include Ekofisk, Eldfisk, Tor, and Hod. The field is considered to be one of the most challenging in the North Sea due to the complex structure, geomechanical effects and very thin reservoir (Dyer et al., 1999).

The Valhall field was discovered in 1975 with the drilling of Well 2/8-6 and has been on production since 1982 with three platforms at the time, the majority of which has been produced under primary depletion. As is typical of chalk fields, the reservoir rock is characterised by a high porosity and low permeability and naturally fractured in the crestal area of the field. Approximately 50% of the drive mechanism has come from the rock compaction and active geomechanical effects which directly affect the production activity (Barkved, et al. 2003, van Gestel et al., 2008). The recovery factor is 40% and there are still 500 MMSTB remaining to be produced from the original 2.6 BSTB in place. The production is expected to continue until 2050.

The trap of the Valhall Field is an asymmetric anticline trending NNW-SSE. The western flank is more steeply dipping than the eastern limb (Figure 5.2). The Valhall Field is divided into compartments by WSW trending sinistral strike-slip faults. Most productive area accounting for an area of 8 km^2 is located on the crest of the Valhall structure. Most production from the Valhall field comes from two oil-bearing laterally extensive reservoir layers: Upper Cretaceous Tor and Coniacian-Turonian Hod formations (Figure 5.3). The Tor formation, the youngest chalk is the main pay interval and contains 70% of oil in place and 85% of the production. The thickness of Tor formation varies from 0-164 ft across the field area, and porosity approaching 50% are common on the crest but decrease to around 30% on the flank. The high porosity on the crest is primarily attributed to reservoir overpressuring, with the net confining pressure at the initial condition reported to be only 500 psi. The Tor Formation has been divided into five-reservoir zones base on detailed biostratigraphy: Tor-D, Tor-M1, Tor-M2, Tor-M3 and Tor- Camp. The Tor Formation is bounded by unconformities

at the top and base. The formation underlying Tor formation is Age Hod formation chalks with lower porosity. The lower portion of this formation contains most of the remaining oil. A low porosity zone known as *Hard Chalk* is located between the base of Tor formation and the top of the Hod formation. In seismic or well logs, the Hard Chalk serve as clear marks to distinguish between two stratigraphical layers with sharp increase in P-wave velocity.

The matrix permeability in the Tor Formation generally ranges from 2 to 10 mD, whereas it is less than 2 mD in the Hod Formation. This is due to the fine-grained nature of reservoir chalk and small pore throats (1 to 5μm). However, high production rates exceeding 10,000 BOPD from wells on the crestal area of the field suggest the likely contribution to flow of a nature fracture system .The Tor Formation was deposited in a series of erosional channels. It is impossible to clearly define the Oil-and-Water Contact (OWC) in the Valhall field due to significant capillary pressure effect – water saturation gradually increases with depth, while porosity and permeability decrease gradually. Connate water saturations in the crestal Tor formation are typically less than 5% - suggesting that crestal Tor formation is intermediate oil wet reservoir.

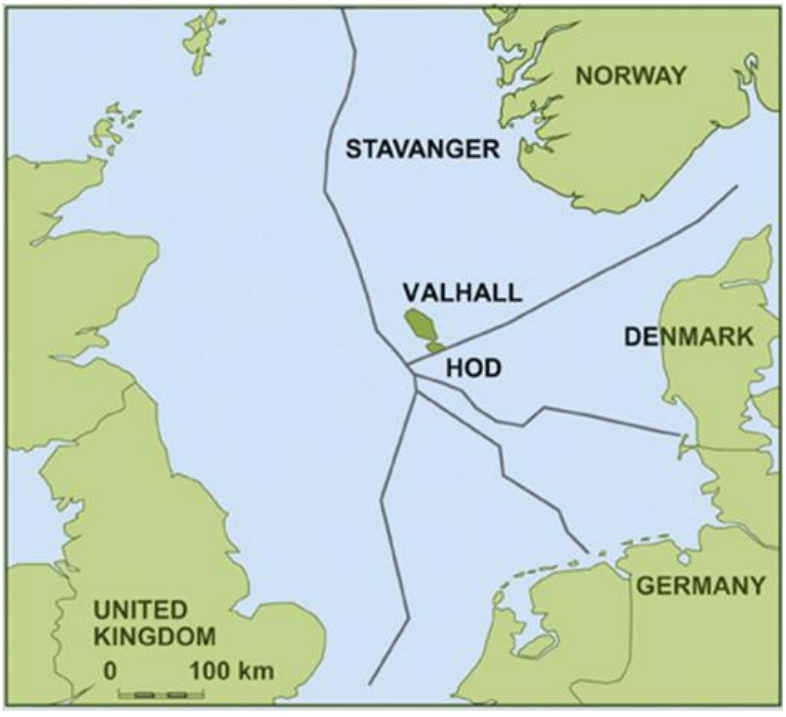

Figure 5.1 The Valhall Field location. The Valhall Field is located approximately 290 km offshore southernmost corner of the Norwegian continental shelf. The Valhall structure is associated with the Lindesnes Ridge, a NNW trending elongate antiformal feature which also contains other Chalk fields such as Hod, Eldfisk, Edda and Tommeliten (after Rogers et al., 2007).

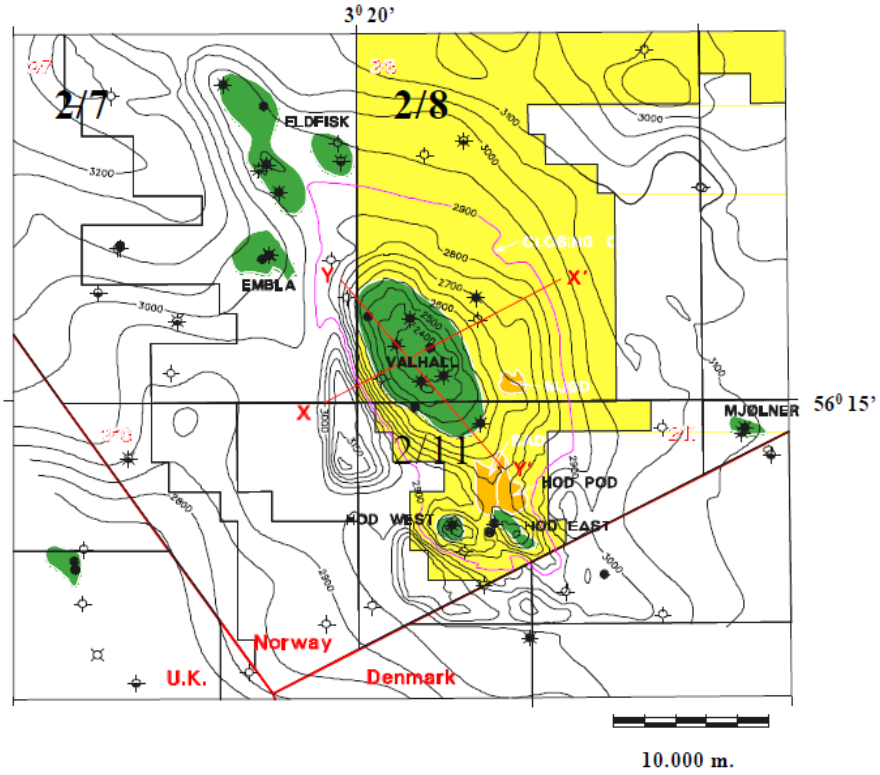

Figure 5.2 The field is a double plunging anticline trending NNW-SSE with the western flank more steeply dipping than the eastern one (after Barkved et al., 2003).

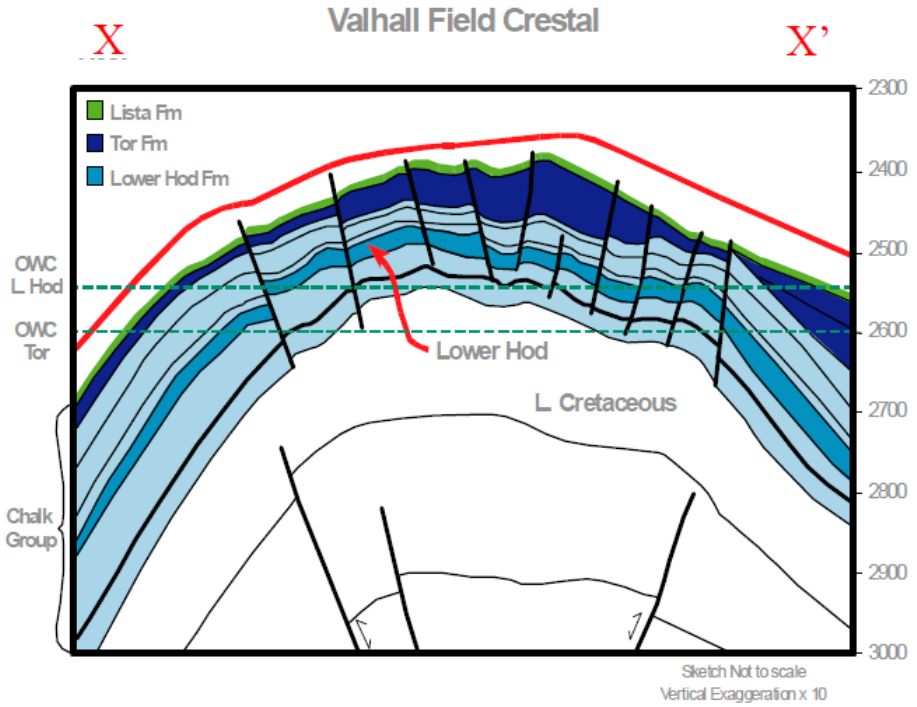

Figure 5.3 Schematic representation of a cross section (X-X' on Figure 5.2) that cuts through the crest of Valhall field.

5.2 Compaction of the field

Reservoir compaction in the Valhall field is a positive contributor to reservoir energy and hence hydrocarbon recovery. Reservoir compaction above certain magnitude, however, will result in major production problems such as casing deformation and well failure. It is also the most distinctive feature of the Upper Cretaceous Chalk in the field. The associated seafloor subsidence, approximately 50cm, was first measured only three years after production. Currently, the subsidence had reached 8 meters at the platform complex in 2008. Reservoir compaction is considered as a result of combined effects due to overpressure, high initial porosity and weak grain network (York, Pong and Joslin, 1992). The special characters of the reservoir rock are caused by the depositional process that the Valhall reservoir has undergone. The measured pore pressure (44.5MPa) at reservoir formation is only 3.4MPa less than the overburden pressure, and much larger than the estimated value (22.5MPa) using typical hydrostatistics gradient (10.5kPa/m), implying only minor formation compaction during burial (Rudy, et al. 1989). It also suggests that the highly porous chalk is weak and can lose a significant part of its original porosity when the effective stress increases during hydrocarbon production (pore pressure depletion) (Ruddy et al., 1989). This pore collapse occurring in the reservoir rock triggers reservoir compaction and seafloor subsidence.

In a cemented sandstone reservoir, rock grains are assumed to be strong enough to take the stress transferred from de-pressurised fluid during production, and reduction in porosity is minimal. The effective vertical stress acting on the reservoir rock is approximately the difference between the weight of the overburden and the pore pressure (*equation* 5.1).

$$\sigma_{eff} = \sigma_{ob} - \alpha P_{pore}, \tag{5.1}$$

where, σ_{ob} is the overburden stress, P_{pore} the pore pressure change, and α effective stress coefficient. In non-compacting reservoir, σ_{ob} is considered to be constant before and after production. Thus change of the effective stress $\Delta\sigma_{eff}$ can be directly related to pressure change, as shown in the following equation:

$$\Delta\sigma_{eff} = \sigma_{eff}' - \sigma_{eff} = \alpha\Delta P \qquad \text{Equation 5.2}$$

where, σ_{eff}' is the effective stress after production and ΔP the reservoir pore pressure change. In the case of a compacting reservoir, pressure reduction occurring in the reservoir induces the re-distribution of stress in the overburden, thus a different overburden stress σ_{ob}' at the time of monitor survey. The change in effective stress can be calculated using the equation set out in (Hettema et al., 2000).

$$\Delta\sigma_{eff} = (\gamma - \alpha)\Delta P \qquad \text{Equation 5.3}$$

where, γ is Hettema stress transference factor and α is effective stress coefficient. The combination of porosity change and geomechanical effects suggests that the interpretation of the 4D signal in a compacting reservoir is very different from that in a conventional clastic reservoir. For instance, 4D effects due to pressure depletion are usually weak in sandstone reservoirs, but are strong in the Valhall field due to enhancement of the compaction effect. However, gas breakout is typically a dominant effect over the 4D signature over a non-compacting reservoir, but cannot be distinguished from the compaction effect at Valhall due to similar magnitude of these two effects.

5.3 Description of seismic programme over the field

5.3.1 Historical Use of seismic at Valhall

In 1992, the first 3D seismic survey was acquired across the Valhall field. Due to the presence of overburden gas charge, this survey has failed to image the area in the reservoir under the gas cloud. The second survey therefore employed the 3D/4C OBC acquisition technology and was acquired between 1997 and 1998. The recorded converted S-wave from incident P-wave at the reflector is largely unaffected by the gas cloud and improves the imaging quality (Barkved et al., 2005). The P-wave volume of the 3D/4C survey was also referenced to the 1992 3D streamer survey in attempt to produce any meaningful 4D signal. However, poor repetition between the acquisitions of these two surveys did not generate

reliable seismic differences. The second conventional streamer 4D was acquired in 2002 and referred back to 1992 3D survey, producing significant signals.

In addition, the active geomechanical process induced by reservoir compaction at Valhall generates micro-seismic events within and above the reservoir, which are measured and recorded by installed micro-seismic devices (Caley et al., 2001). Clusters of microseismic events located within the reservoir interval reveal unseen reservoir structure and injection-induced fracturing; while in the overburden these events are believed to stem from drilling activity through the overburden layers, thus can be used to monitor potential zones of wellbore instability. The fact that events are concentrated at certain locations indicates that the microseismic events are caused by production rather than random background seismicity (Dyer et al., 1999).

5.3.2 Installation of Life of Field Seismic (LoFS) system

Although the field has been produced for more than 20 years since the first oil in 1982, there is still 2.2 BSTB oil in place and the aim is to recover 40% of oil in 2027 (Barkved et al., 2005). The production in the first 20 years focused on the crestal area of the field which accommodates reservoir sands with the best properties in the reservoir. As the reserves in the crestal area had been gradually drained up, production in the northern and southern flank of the field was accelerated in 2002. Additionally, water injection was planned to further enhance the oil recovery from the crestal area. These development targets are supported by 5 billion NOK investment and 20 production and injection wells are to be drilled in a 20-years span of time from 2002 (Barkved et al., 2005). Further ambitious development plans are likely to drill up to 100 injection and production wells over the field life to 2040's (Barkved, Amundsen and Landrø, 2009).

To ensure the investment in infrastructure pays off with the main production target met in 2027, the 'Life of Field Seismic (LoFS)' system was installed during the summer 2003 at Valhall (Barkved, Amundsen and Landrø, 2009). It is aimed to lend support to the injection programme by carefully monitoring water flow between wells, to improve final oil recovery through optimal positioning of production wells (e.g. to avoid production wells placed into water flooded areas), and to reduce the cost of drilling and maintenance by actively monitoring of geomechanical processes.

In the centre of the system are the permanent seismic cables (OBC) laid down on the seabed. The selection of permanent OBC technology for LoFS monitoring is made, taking account of the need to resolve the reservoir underlying the gas charge in the reservoir. During the summer of 2003, more than 120km cable covering 45 km^2 was trenched into seabed during the installation. The cable is equipped with approximately 2400 receiver units, each with 4C sensors. The spacing between each two of the receiver units is 50 meters in-line and 300 meters cross-line. The cable is connected to a recording system on one of the central platform. The acquisition system is controlled by acquisition vessel, data are sent onshore via the optical network after quality check.

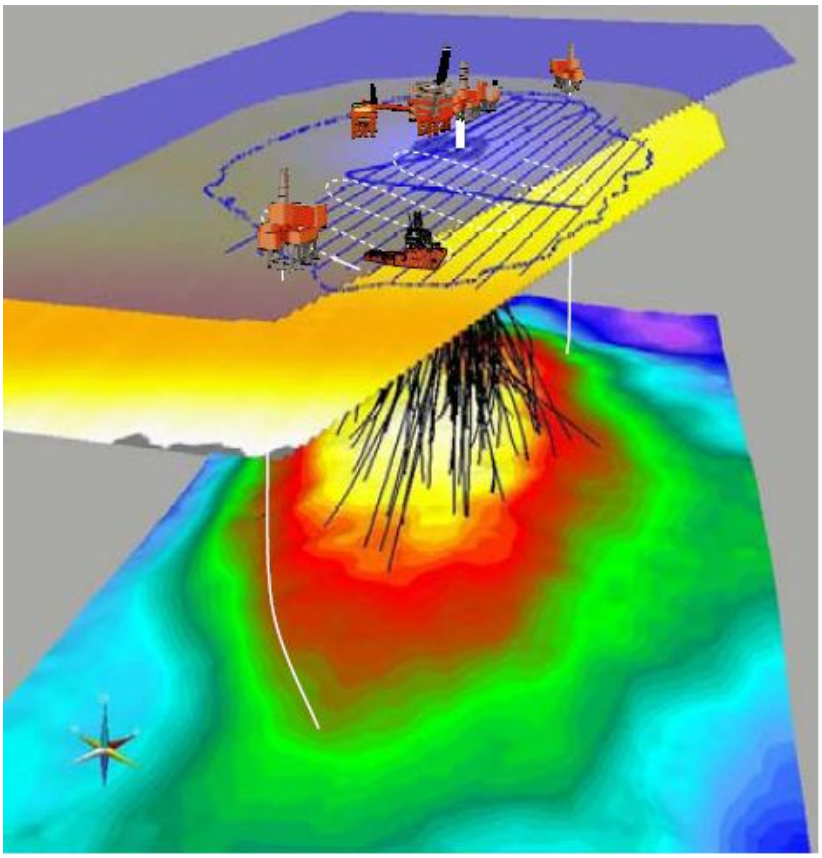

Figure 5.4 A schematic view of the infrastructure and LoFS monitoring system that equip Valhall. The level of water surface (semi-transparent blue plane), seabed (yellow plane) and top structure maps are shown (yellow-red-green-blue)

5.3.3 **Repeatability**

In general, excellent repetition of shot and receiver positions in different surveys is key factor to obtain high quality 4D seismic data. In the case of the permanent system installed at Valhall, the positioning of receiver arrays is optimum, and the seismic vessel that previously needed to accommodate both kilometers long streamers and source arrays, now only needs to be equipped with shot arrays. The simplicity of the acquisition setting leads to excellent positioning of shot arrays with an approximately +/- 5 meters achieved for planned shot positions.

With errors due to positioning minimised, tidal and seasonal water velocities and sea state appear to be the main source of non-repeatable energy. The water depth over Valhall is only 70 meters – suggesting the tidal level can impose a big difference between surveys. The seasonal temperature change may cause a huge velocity difference in the water table. These non-repeatable conditions are carefully monitored and dealt with through the corresponding processing effort. The overall repeatability is controlled within a range of 8%-20% at Valhall.

5.3.4 **Timeline of 4D acquisition**

The baseline survey was acquired immediately after the installation of the LoFS system in summer 2003, and 11 subsequent surveys have been acquired to date (July 2011). It takes an average 16 days to complete the shooting of the target area during surveys, and the following processing time is as short as 3 to 4 days due to the fact that processing workflow is largely simplified as a result of excellent positioning repeatability (Barkved et al., 2005).

The data available for our study are the first ten LoFS seismic surveys, shot between November 2003 and April 2008 at varying time intervals ranging from 2 to 10 months (see Table 5.1). The ten repeated seismic surveys produce a total of forty five seismic difference maps as shown in Figure 5.5. These maps are indicative of dynamic reservoir changes occurring over 45 corresponding periods defined in Table 5.1. To implement the correlation technique proposed in Chapter 3, sequences of seismic attribute changes are generated for

each location on the map. The order, in which the values of these seismic differences are arranged in such a sequence, does not affect the final correlation result.

5.3.5 Seismic attributes

Two seismic attributes are primarily used for interpretation of 4D data at the Valhall field: Acoustic Impedance (AI) and Time-shift attribute. Here, 'AI' refers to relative impedance directly inverted from the seismic data using coloured inversion (CI) procedures, which is realised through derivation of the CI operator from the AI logs and sufficient seismic traces in the region of interest (Conolly, 1999; Lancaster and Whitcombe, 2000; Lancaster and Conolly, 2007). Time shift attribute is defined as the change in the travel time for the top reservoir before and after production. With only several hours required to invert a 3D volume, apply colour inversion, this scheme is an easy and effective procedure to apply, and contributes to the short turnaround time achieved for the ultra-frequent seismic acquisitions over this field. Figure 5.6 shows the section and map view of the 4D effects from a well in the Valhall field for these two types of attributes. Additionally, it has also been understood that these two seismic attributes respond to different types of dynamic changes in the reservoir, with AI changes driven by both saturation and pressure change effects, and time-shift attributes predominantly related to pressure change and resultant reservoir compaction (Huang et al., 2010).

	L1 Nov,2003	L2 Apr,2004	L3 Jun,2004	L4 Nov,2004	L5 Apr,2005	L6 Nov,2005	L7 Jun,2006	L8 Apr,2007	L9 Dec,2007	L10 Apr,2008
L1										
L2	L2L1									
L3	L3L1	L3L2								
L4	L4L1	L4L2	L4L3							
L5	L5L1	L5L2	L5L3	L5L4						
L6	L6L1	L6L2	L6L3	L6L4	L6L5					
L7	L7L1	L7L2	L7L3	L7L4	L7L5	L7L6				
L8	L8L1	L8L2	L8L3	L8L4	L8L5	L8L6	L8L7			
L9	L9L1	L9L2	L9L3	L9L4	L9L5	L9L6	L9L7	L9L8		
L10	L10L1	L10L2	L10L3	L10L4	L10L5	L10L6	L10L7	L10L8	L10L9	

Table 5.1 The pattern of the well activity signature. The first entry to the well signature is the first nine entries in the first column and followed by the entries of the second column and so on (indicated by red rectangular and blue arrowhead).

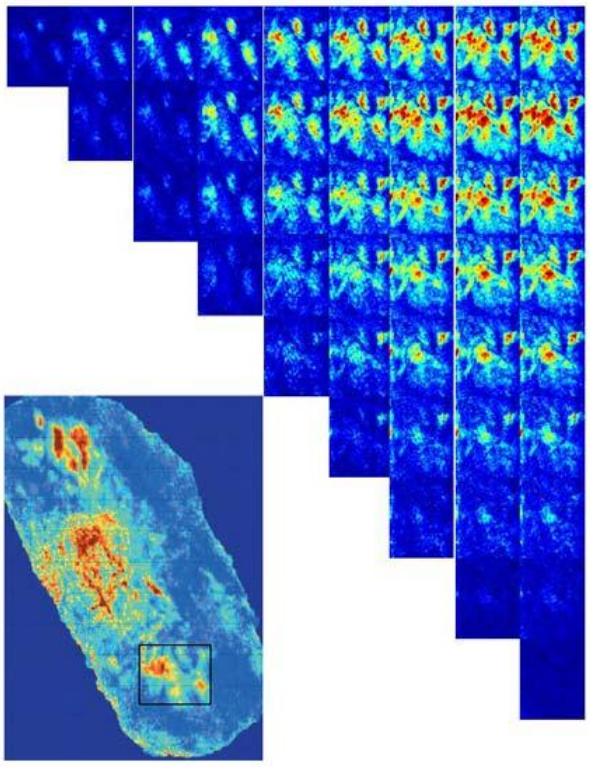

Figure 5.5 Matrix view of total forty five seismic difference maps made between each pair of surveys. First row: difference between LoFS1 and baseline, LoFS2 and baseline, etc. Second row: difference between LoFS2 and LoFS1, LoFS3 and LoFS1, etc. The bottom left figure is the map of difference between LoFS9 and baseline over full-field. The area for which all 45 difference maps are shown is highlighted by black rectangle (after Barkved et al., 2009).

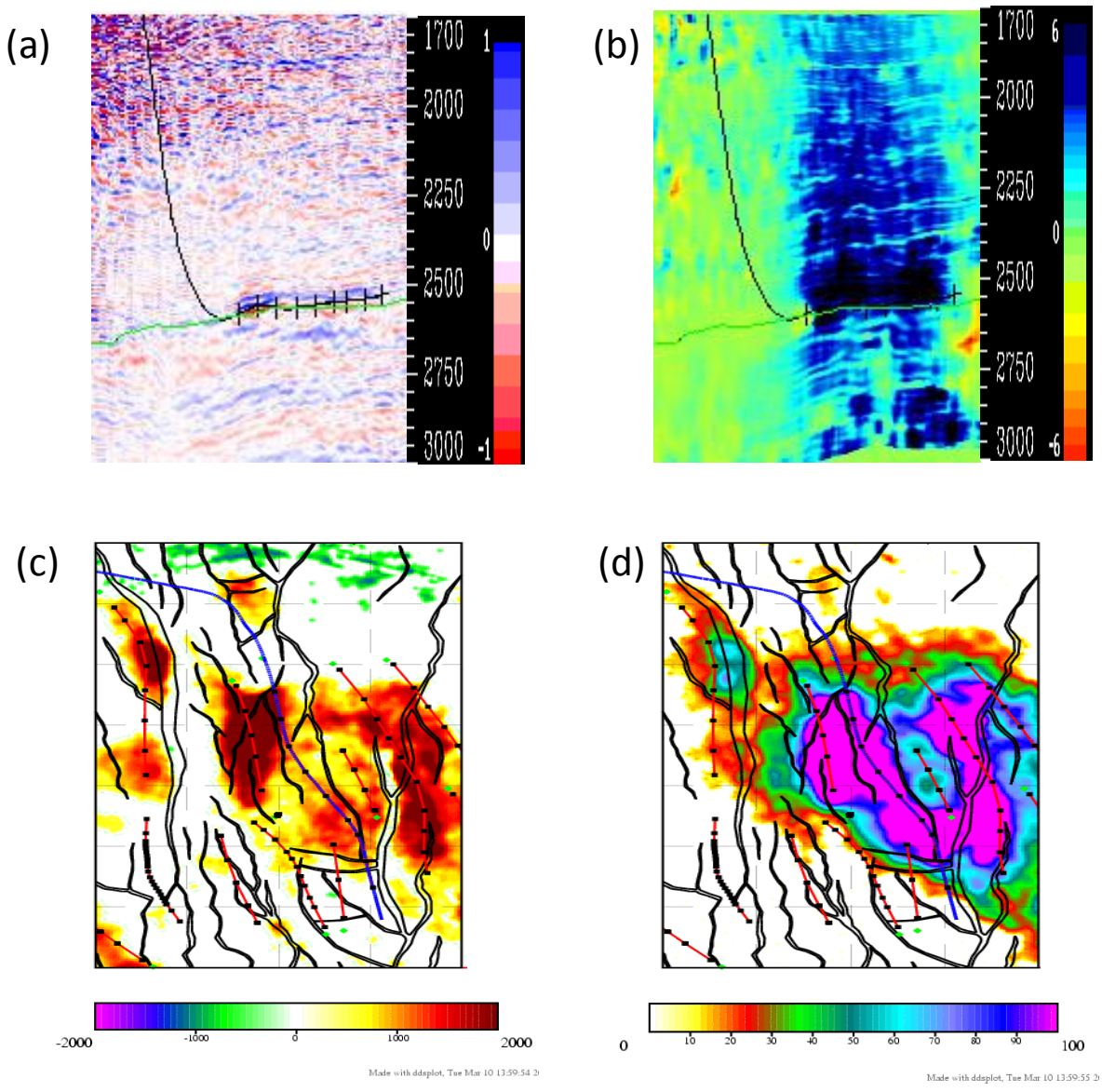

Figure 5.6 A sectional view of 4D responses of a well in (a) AI change and (b) time shift attribute. Mapped differences of these two attributes generated within the optimal time windows for this example are shown in (c) and (d).

5.4 Areas of interest

In 2003, a water injection programme was initiated over the crestal area of the Valhall field, and development campaign launched to accelerate the production in the less productive north and south flank of the field. Since 2003, objectives of field management have been the optimisation of the water sweep in the crestal area and to maximise production in the flank areas of the field through optimal well positioning. Thus, the crestal area, the north flank and south flank of the field are the areas of interest in our study (see Figure 5.7).

Over these three areas of interest, the seismic response is strongly related to the pressure reduction and resulting compaction, and the response of pressure depletion is very strong on 4D attribute maps due to the enhancement of compaction effect. To implement detailed interpretation, there are several problems to overcome. Firstly, the most common problem with interpretation of 4D signatures on different areas in the Valhall field is the difficulty of identifying influence area of individual wells, owing to the dense positioning of horizontal production wells in the field. On the South Flank, where gas breakout is anticipated and the locations of which are crucial to asset management, the compaction effect is as strong as the effect of gas coming out of solution which resulted in ambiguity for interpretation. On the South Crestal area, the hardening signals on the 4D signature (saturation-driven) of the newly activated water injection well interferes with that of neighbouring production wells which produce similar hardening signal (but caused by pressure reduction). These challenges will be addressed using the correlation technique proposed in this thesis and examples from the application of the technique to the three areas are to be shown in the following sections of the chapter.

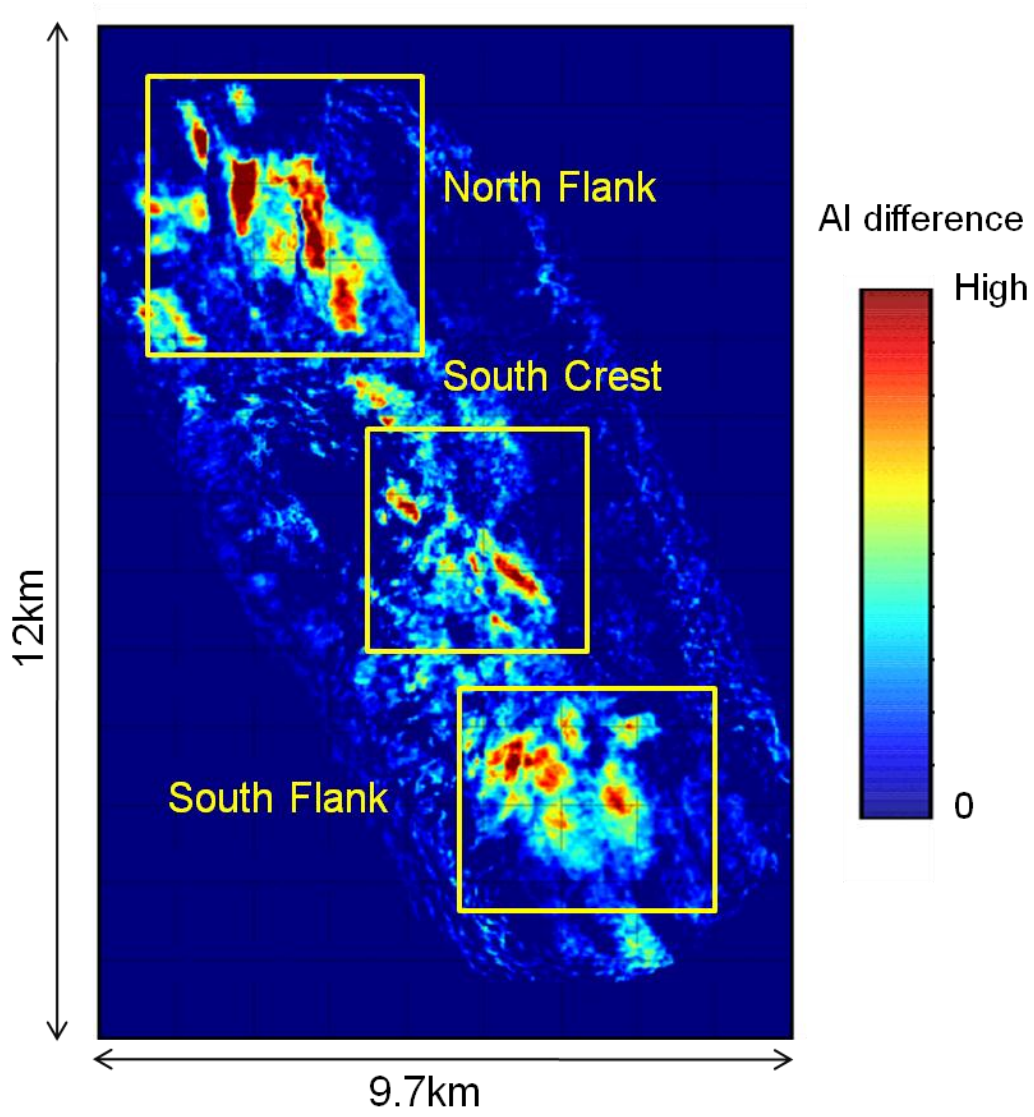

Figure 5.7 Map of AI change between LoFS10 and the baseline showing the outline of the Valhall field. Three major production regions in the Valhall field are identified: the North Flank, the South Flank and the South Crest where the technique proposed in this paper is applied.

5.5 Selected examples from the areas of interest

5.5.1 Separation of the responses of densely positioned wells: an example from North Flank

The field is mostly produced by many long reach horizontal wells (Barkved et al., 2009), and the 4D seismic signatures can be observed to be clearly associated with individual perforations (Figure 5.8 shows how the time shifts behave over this area relative to the wells). However it is found that due to the dense positioning of the wells it is difficult to precisely resolve the individual well responses using conventional 4D seismic attributes, as the closely positioned responses overlap and interfere. Plots for the cumulative volumes obtained from all seven wells in the North Flank are shown in Figure 5.9a. Comparing and correlating these well activity sequences is an important prerequisite reference step for this study and we identify two distinct groups of wells each with similar characteristics (Table 5.2). In the first group are wells N-5, N-7 and N-15 (Figure 5.9b) with an intra-group correlation coefficient of between 0.94 and 0.99. In the second group are wells N-11, N-12 and N-14 (Figure 5.9c), with a similar intra-group correlation, but a correlation with the first group of 0.87. It appears just possible to separate the two groups on the basis of their different behaviour. Proceeding with the seismic to well correlation analysis, all wells correlate strongly with the time-lapse signatures when plotted over calendar time or sequence number defined by different combinations. Figure 5.10 shows a map of the *NCC* statistic defined from the previous section, relating the well activity of Group 1 (as characterized by well N-15) to the 4D time-shift attribute. In this case, the threshold for the map is set at 0.87 to eliminate any undesirable correlations with well Group 2. Interestingly, a major feature strongly concentrated around well N-15 is revealed, with smaller concentrations around the other Group 1 wells N-5 and N-7. The correlation process has separated the original seismic response into the discrete drainage areas influenced by the wells in Group 1. Figure 5.11 shows the corresponding *NCC* map for the correlation between Group 2 wells (as characterized by well N-14) and the time-shift attribute, with an identical threshold set. The major anomalies now concentrate on N-11, N-12 and N-14. In both maps, the boundaries of separation between the drainage areas of N-15 and N-14 are now clearly visible, and these are quite different from any interpretation that might be made on the observed seismic response in Figure 5.8. It should be noted however that although the desired separation is achieved

between major producer N-14 and N-15, a response at N-12 from Group 1 and at N-5 due to Group 2 is still observed, this being an artifact of the narrow margin between intra- and inter-well correlation that exists for this particular case (note both correlations are still higher than the statistical significance threshold of 0.38 at 99% confidence). It should be noticed that well grouping performed in this way has no physical meaning and high intra-group correlation between the sequences of cumulative volumes does not imply the wells are dynamically connected. The main reason for doing this is to reduce the number of resulting NCC maps shown in this chapter as similar NCC result will be obtained if the wells with similar sequence of cumulative volumes are used as input to this technique. Thus, in practice a detailed study as such should preferably utilize the NCC result computed for each individual wells.

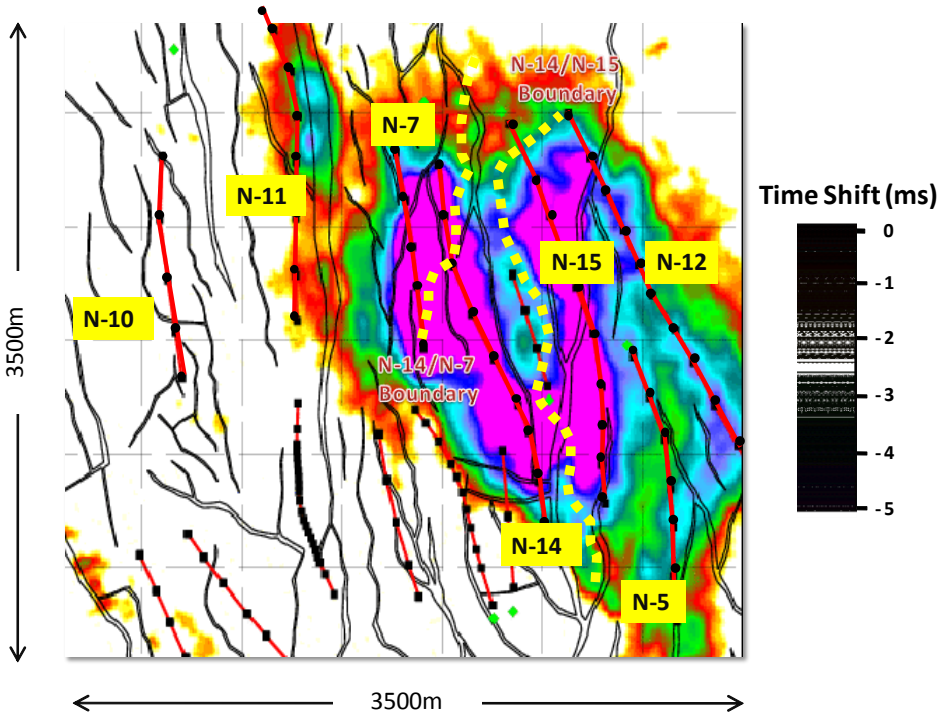

Figure 5.8 Major production wells (in red) on the North Flank superimposed on mapped time shifts between LoFS10 and the baseline survey. Black squares indicate perforations and black lines are interpreted faults. Dotted yellow lines are the common boundaries of separation between the N-14 and N-15 responses obtained by applying the technique in this paper.

		Group 1			Group 2		
		N-5	**N-15**	**N-7**	**N-11**	**N-12**	**N-14**
Group 1	**N-5**	1					
	N-15	0.958	1				
	N-7	0.992	0.945	1			
Group 2	**N-11**	0.916	0.926	0.912	1		
	N-12	0.875	0.905	0.870	0.988	1	
	N-14	0.835	0.878	0.830	0.972	0.993	1

Table 5.2 The matrix of the Normalised Correlation Coefficients (NCC) calculated between time sequences of cumulative well from the North Flank. High values of correlation coefficients between most of the wells indicate a similar production behaviour shared by most of the wells but two distinct groups.

		Group 1				Group 2	
		S-11	**S-12**	**S-14**	**S-15**	**S-3**	**S-10**
Group 1	**S-11**	1					
	S-12	0.988	1				
	S-14	0.991	0.983	1			
	S-15	0.971	0.983	0.982	1		
Group 2	**S-3**	0.516	0.573	0.833	0.448	1	
	S-10	0.516	0.573	0.76	0.448	0.943	1

Table 5.3 Normalised correlation coefficients calculated for cumulative volume time sequences from the South Flank.

	G-24	**A-16**	**F-17**	**A-3**	**A-2**	**A-18**
G-24	1					
A-16	0.768	1				
F-17	0.768	1	1			
A-3	0.965	0.903	0.903	1		
A-2	0.816	0.987	0.987	0.935	1	
A-18	0.799	0.962	0.962	0.924	0.984	1

Table 5.4 The matrix of the Normalised Correlation Coefficients (NCC) calculated between each pair of the time sequences of cumulative volumes derived from the production data of the wells in the South Crest of the Valhall field. The injector has noticeably different well activity compared to the other wells in this area.

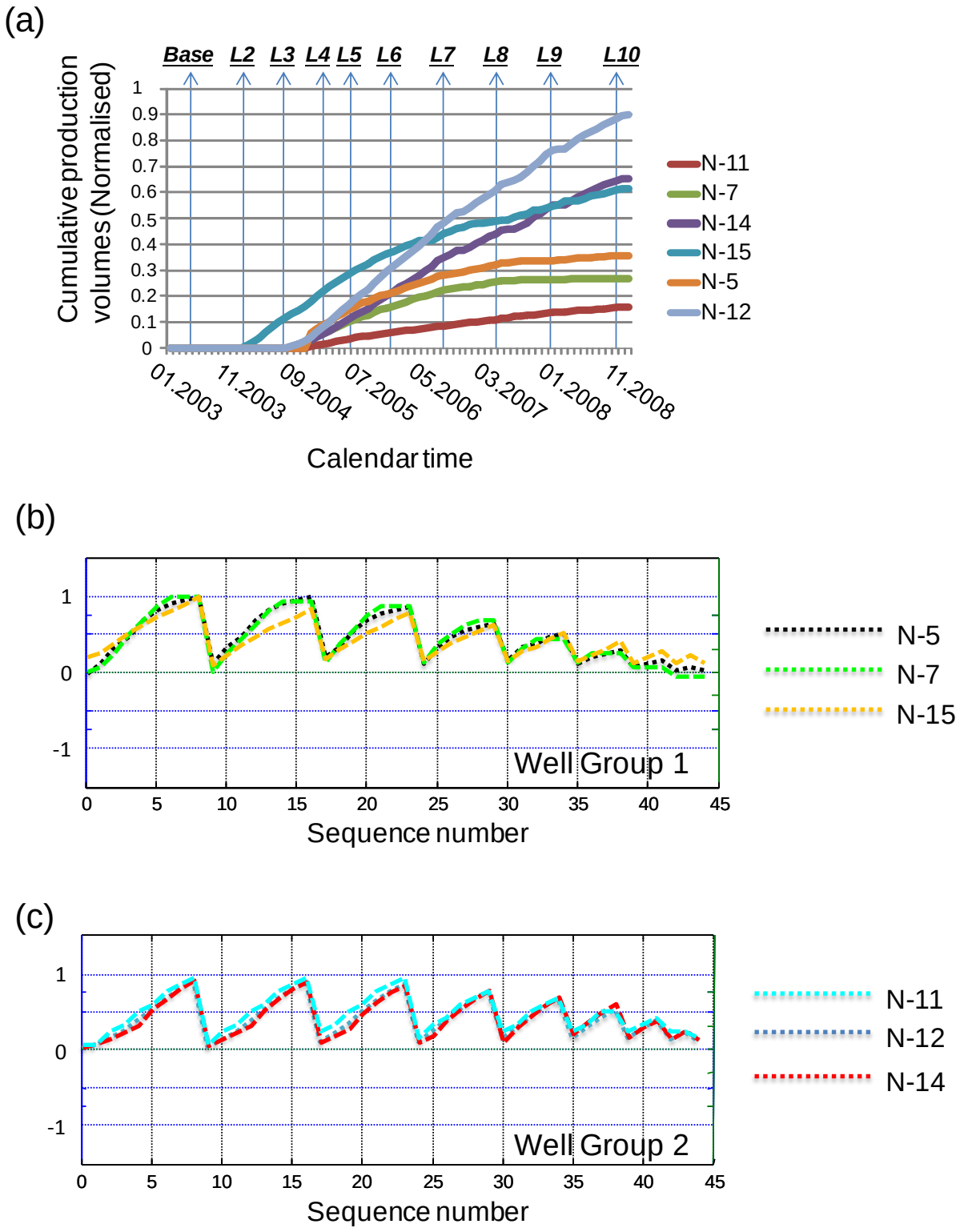

Figure 5.9 (a) Cumulative fluid volumes produced from wells of the North Flank. The plots are converted into the time sequences of cumulative volumes. Wells with similarly sequenced cumulative volumes are shown together (b) Group 1 – N-7, N-15 and N-5; and (c) Group 2 – N-11, N-12 and N-14.

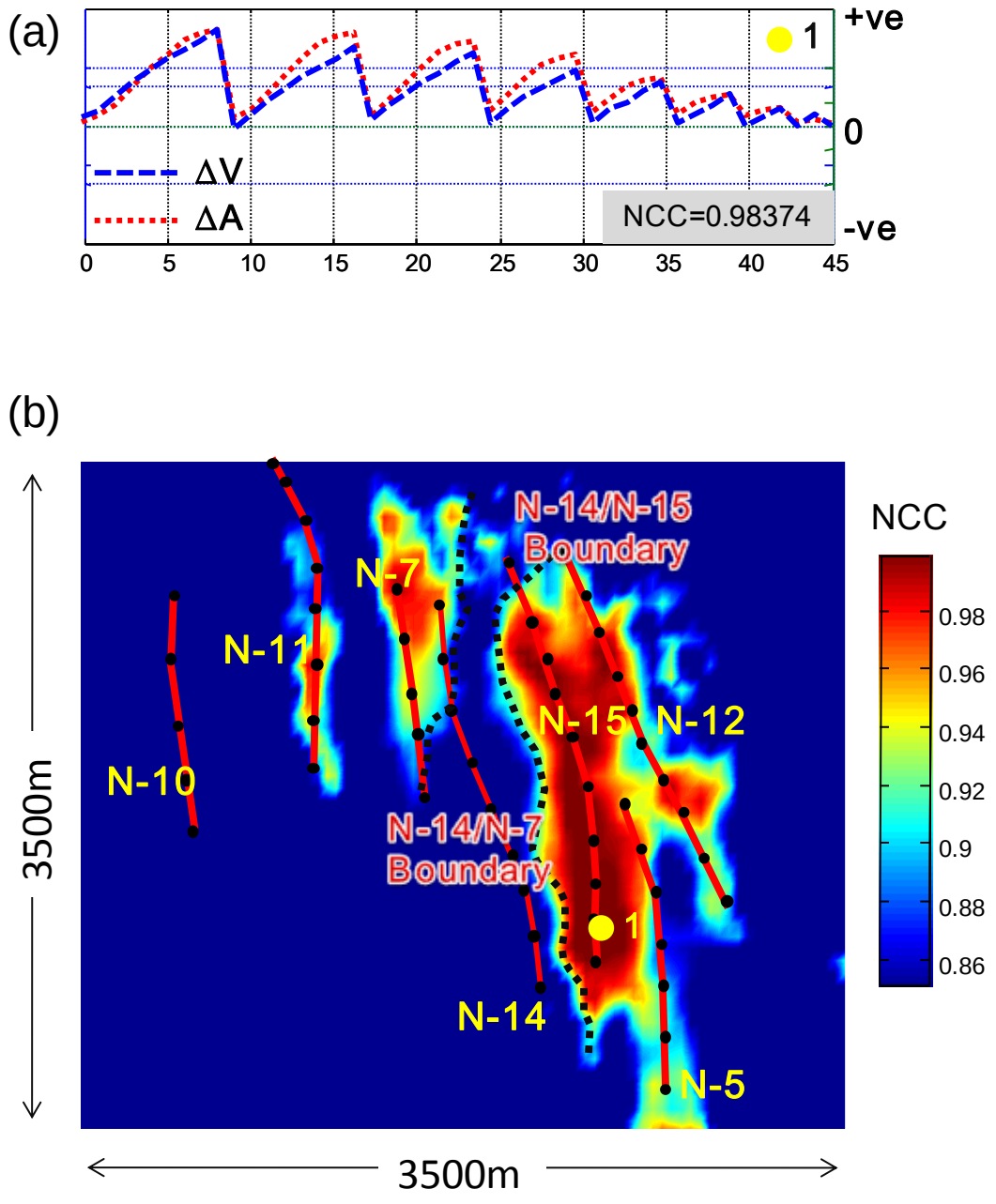

Figure 5.10 (a) The time sequence of seismic changes ΔA and well group cumulative volumes ΔV extracted from the observation point 1 in the reservoir. (b) Mapped and thresholded *NCC* correlation statistic generated using the well activity of N-15. The NCC result for N-5 and N-7 are very also generated (not shown). Dotted lines are interpreted boundaries between the areas of influence from N-15 and N-14, and between that from N-14 and N-7. These lines are common with Figure 5.11.

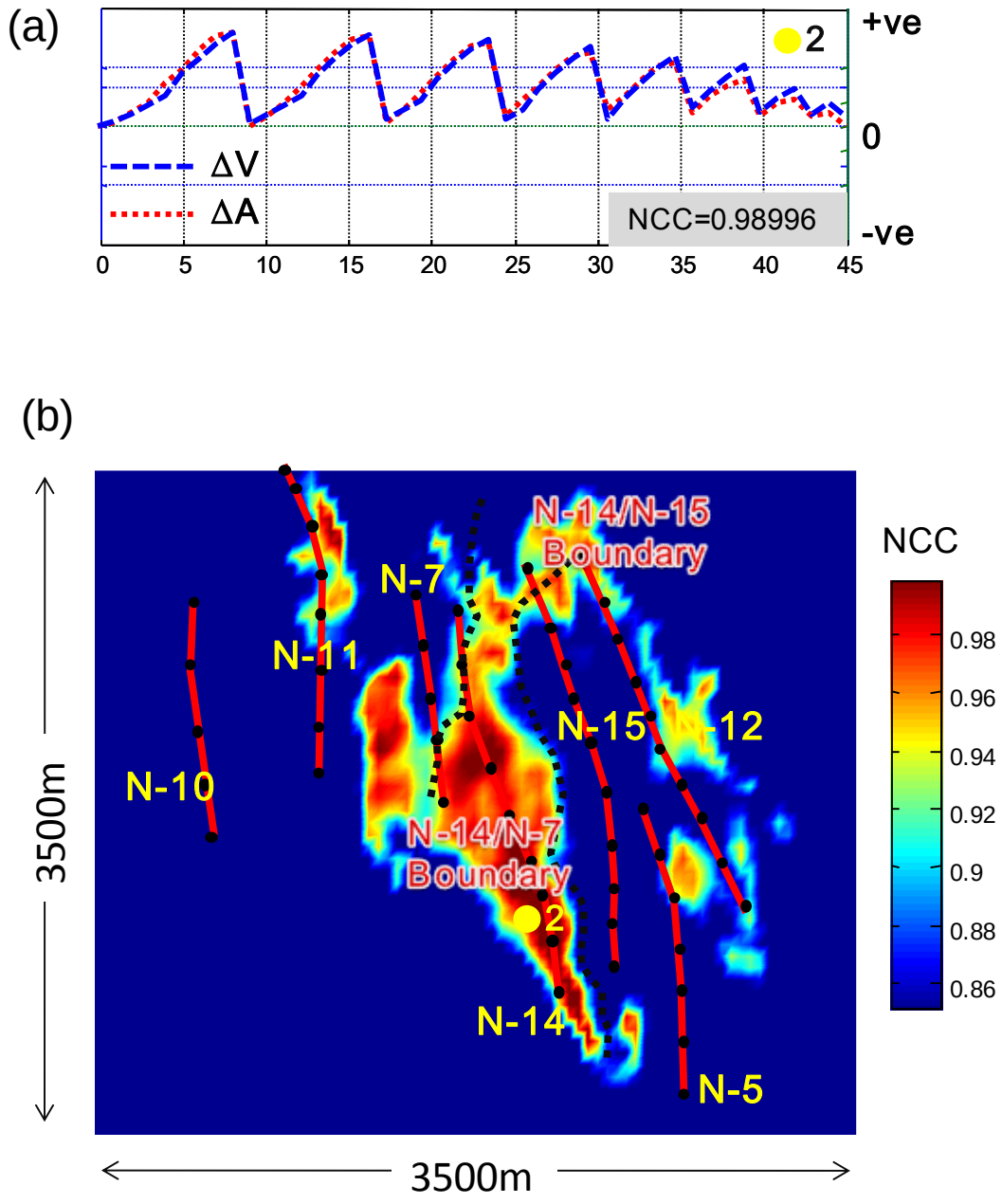

Figure 5.11 (a) The time sequence of seismic changes ΔA and cumulative volumes ΔV extracted from observation point 2 in the reservoir. (b) Mapped and thresholded *NCC* correlation statistic generated using the well activity of N-14. Dotted lines are the interpreted boundaries between the areas of influence from N-15 and N-14, and from N-14 and N-7 – these are identical to those derived in Figure 5.10.

5.5.2 Gas exsolution signal complicated by compaction effect: an example from the South Flank

Figure 5.12 shows the general development of positive AI changes across the South Flank, indicative of a reservoir hardening effect related to pressure reduction and the resulting compaction. However it is also known that at some of the well perforations, gas comes out of solution due to localised pore pressure decline below bubble point, causing a reduction in impedance. The exact position of these localisations is difficult to detect in the AI attribute due to the masking effect of compaction and inter-well interference. To tackle this problem, again the wells in this area influencing the seismic response are divided into two groups according to their distinct well activity, this gives wells S-11, S-12, S-14 and S-15 in Group 1, and S-3 and S-10 in Group 2. Table 5.3 shows the resultant well to well correlation which indicates that in this case there is a larger difference between the intra- and inter-well correlations. Figure 5.13 shows the resultant seismic to well correlation *NCC* map thresholded at 0.75, generated by correlating the AI signatures with S-12 (characterising Group 1). The maps reveal two strong zones of correlation related to wells S-11 and S-12 and a weaker zone related to S-14, but also small circular regions of reduced correlation that are positioned over the well perforations. This correlation weakening is caused by the exsolved gas disrupting and reversing the systematic hardening trend established between pressure depletion and the AI attribute. These zones are not evident at all in the map of AI change in Figure 5.12, however a separate study (Barkved et al. 2009) has shown that complex multiple attributes can be designed to specifically illuminate gas can detect zones at identical locations as shown in Figure 5.14. The areas where GOR has seen an increase show a good correlation with those as identified in the NCC attribute. These zones correspond to particularly active and competent perforations, with good connection to the formation, high reservoir quality, and hence well developed pressure depletion.

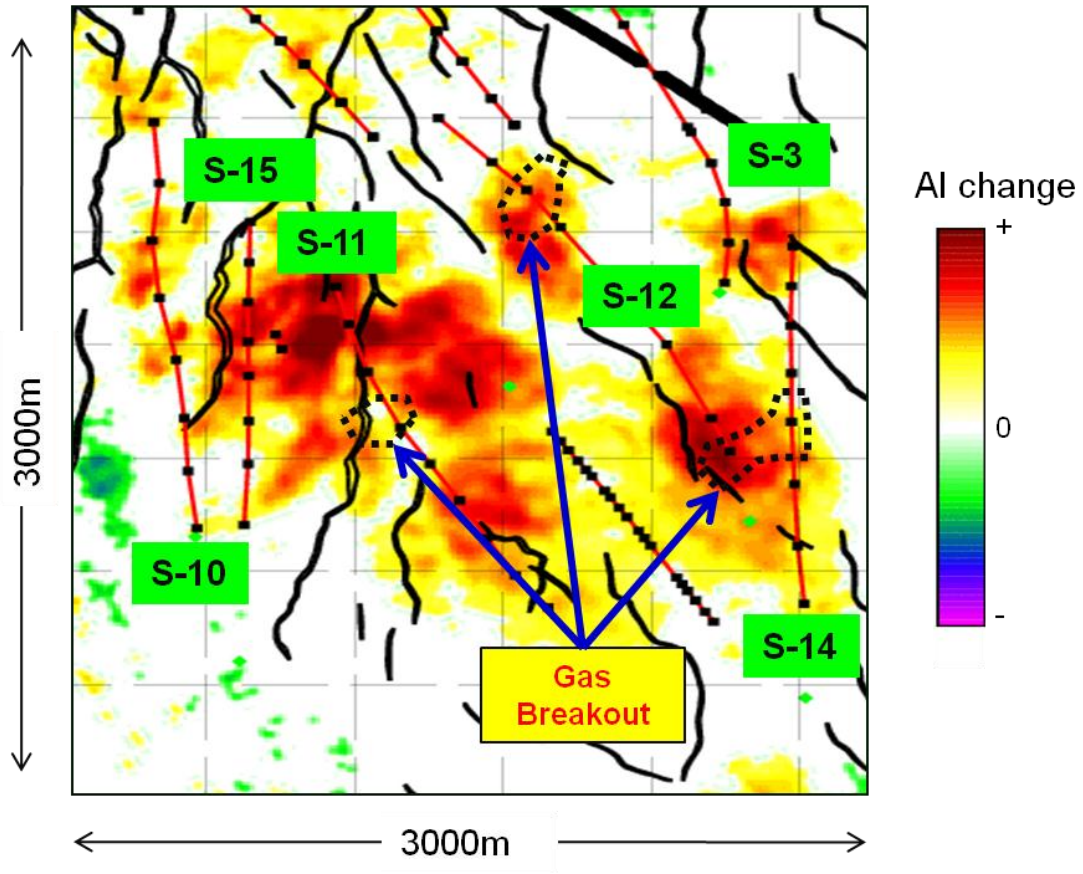

Figure 5.12 The well paths and perforation locations for the major production wells on the South Flank over laid on the mapped AI change between LoFS10 and the baseline survey. The positive AI change indicates the reservoir hardening caused by strong reservoir compaction due to pressure depletion in the reservoir. The dotted circular areas correspond to the zones of gas exsolution identified by the correlation technique in this paper.

.

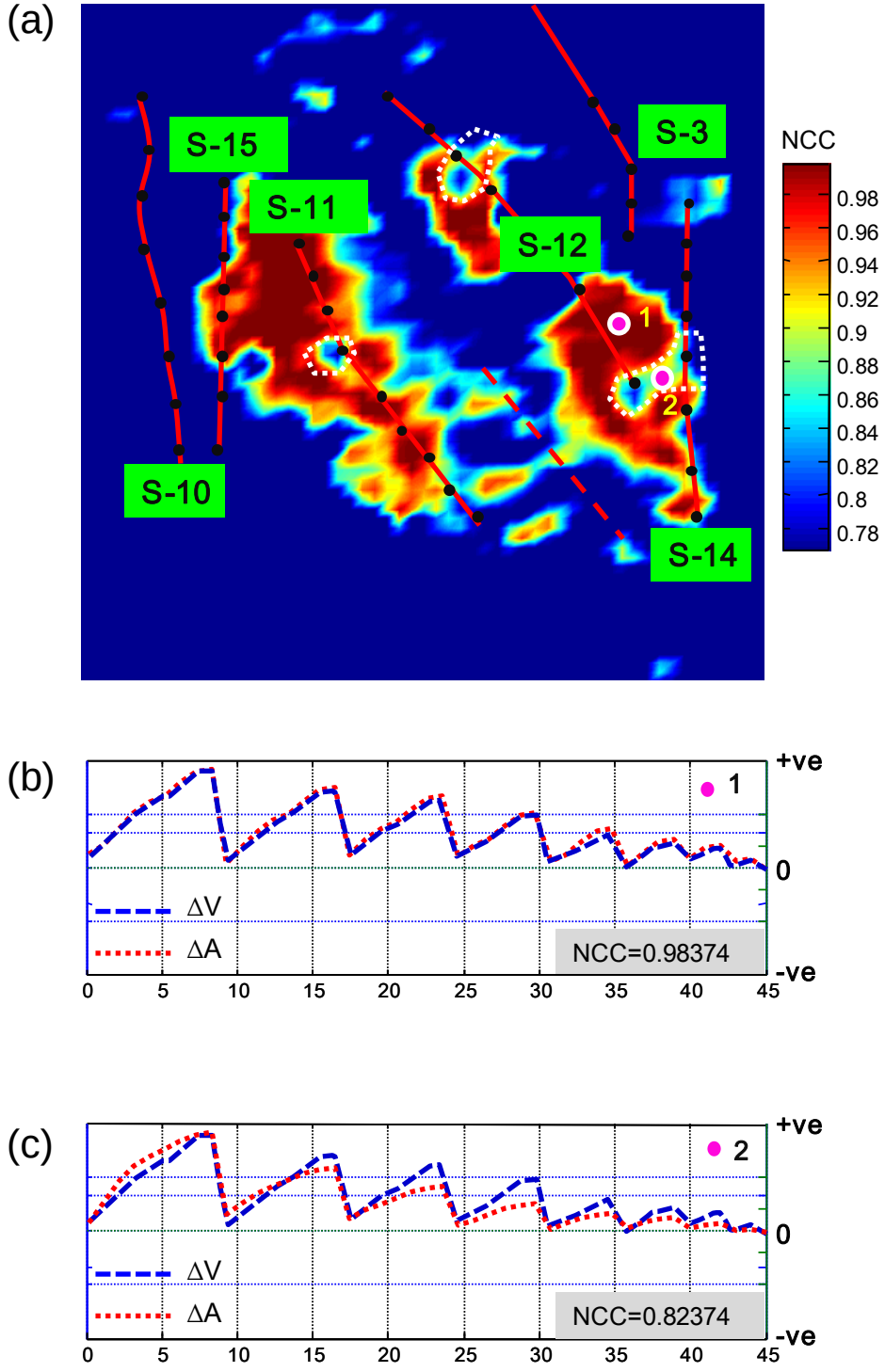

Figure 5.13 (a) *NCC* map computed using the well sequence of S-12. Low correlation regions are observed and highlighted using dashed lines. The time sequences of seismic change and cumulative volume are computed for two observation points 1 and 2, where the 4D seismic changes are dominated by (b) reservoir compaction, and (c) a combination of reservoir compaction and the gas breakout effect.

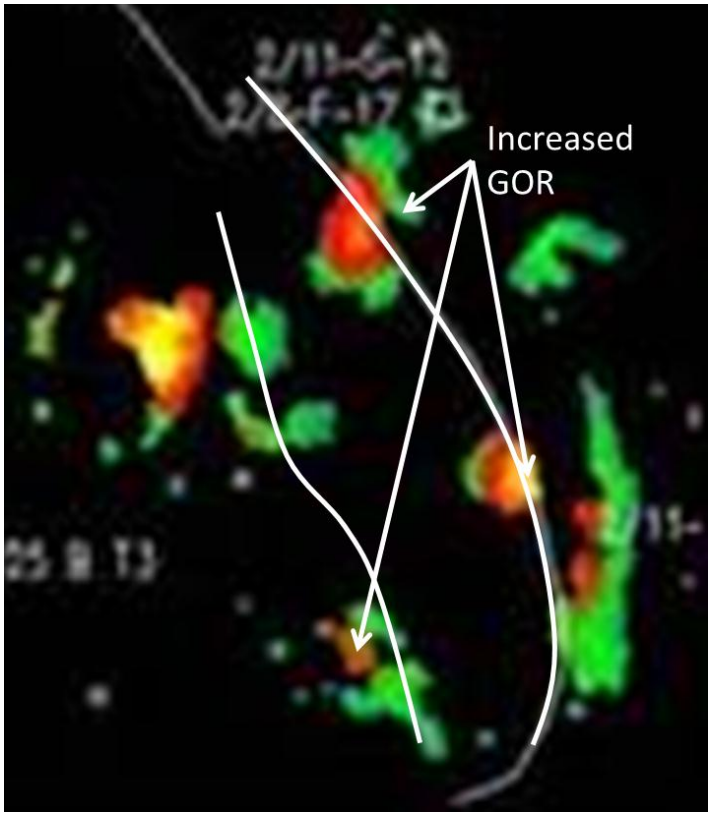

Figure 5.14 Increased GOR predicted using time-shift attribute by BP

5.5.3 Identification of water flooded region surrounded by producers: an example from the South Crestal area

Our third example is based on injector G-24 on the South Crest, surrounded by a number of producers A-2, A-3, A-11, A-16 and A-18 (Van Gestel. et al., 2010). G-24 starts injecting after the sixth LoFS survey and then injects at a constant rate. To detect the resultant waterflood precisely, the reservoir hardening effect caused by water influx must be identified in the AI response (Figure 5.15). Unfortunately, reservoir hardening of a similar magnitude can also be induced by pressure depletion from the neighbouring producers. This interference makes it very difficult to delineate the water flooded zone using this attribute. This is particularly true in the region between G-24 and A-16 or F-17. However, the inter-well correlation coefficients between G-24 and A-16, and between G-24 and F-17 are 0.777 (Table 5.4), and hence separation of the response with the neighbouring producers is possible only for high *NCC* thresholds. Further, it is found here that the *NCC* attribute is predominantly affected by the water flooded zone around G-24 and is less sensitive to pressure. Preliminary modelling studies support this finding and show that the pressure signal

defined by *NCC* is lower and more spatially diffuse in comparison to the stronger and more compact saturation signal. Figure 5.16 shows the *NCC* map thresholded at 0.90, generated by correlating the G-24 well activity with the AI changes. This highlights a strong connection around G-24 possibly that is interpreted to be related to the waterflooded zone, and a variation in concentration associated with the individual perforations (perhaps related to the performance of the injector completions). The zone delineated by this approach is also in general agreement with the results of coupled fluid flow and geomechanical simulation shown in Figure 5.17a and the resultant *NCC* map in Figure 5.17b.

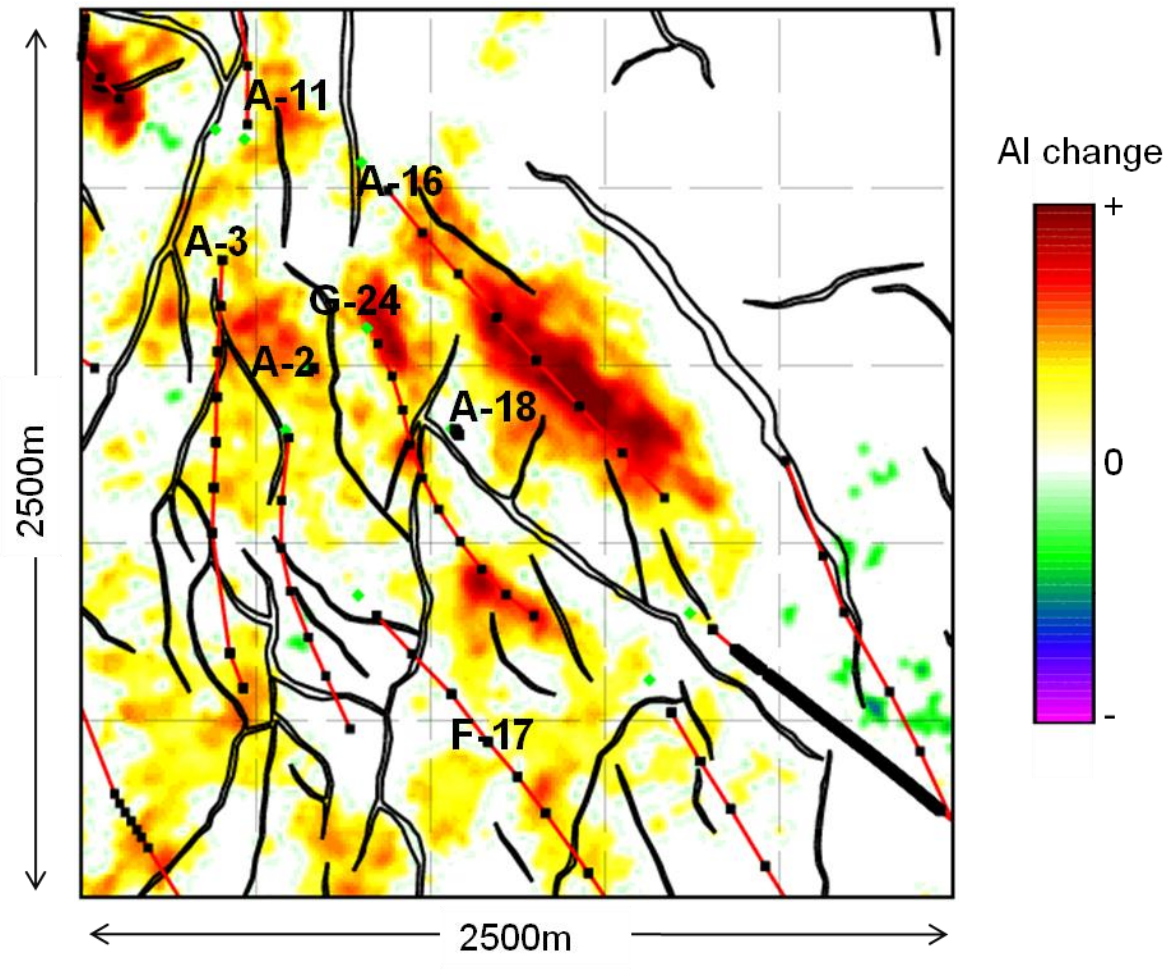

Figure 5.15 Mapped AI change on the South Crest of the Valhall field. G-24 is a water injector, the remainder of the wells are producers.

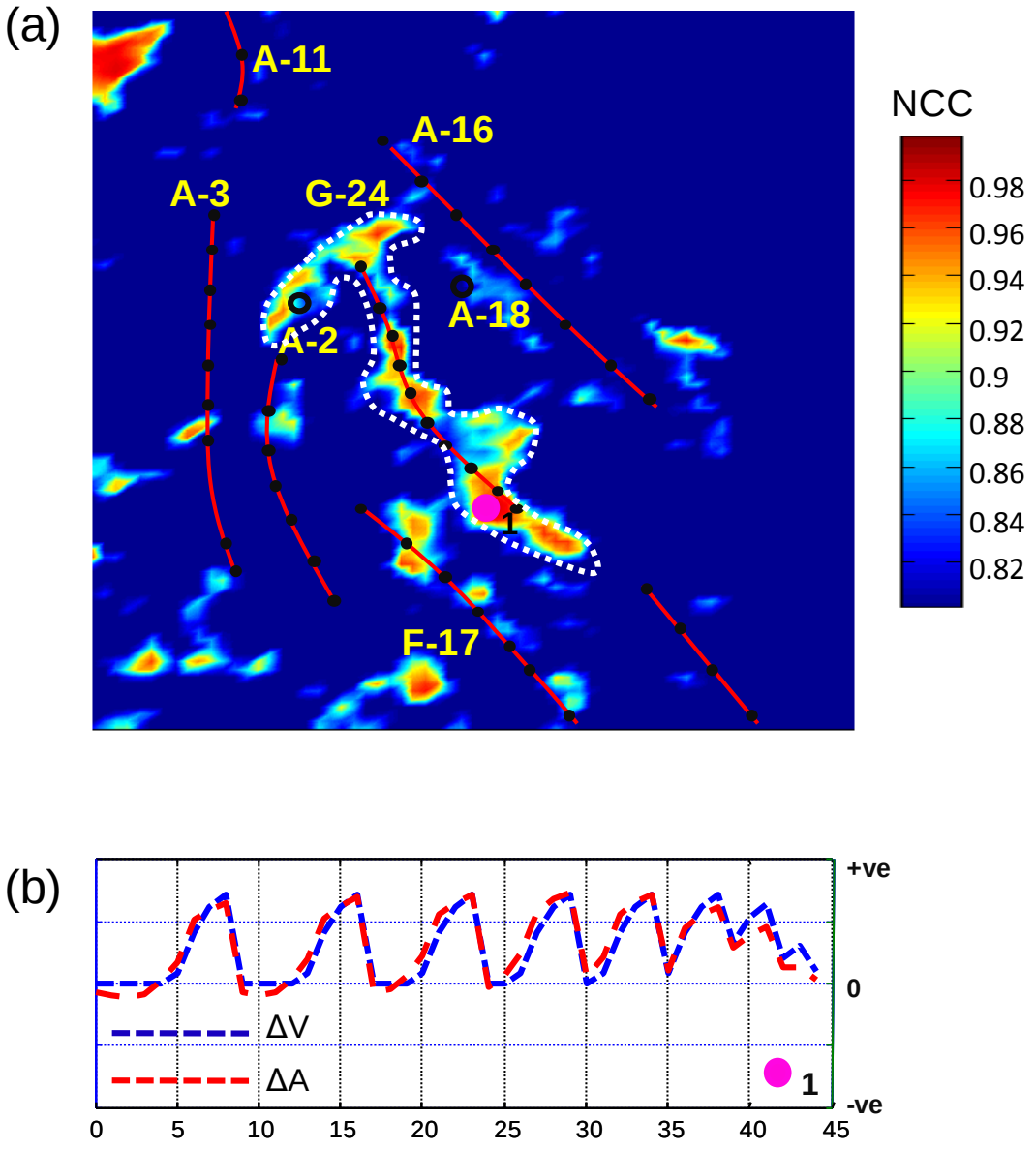

Figure 5.16 (a) Normalised Correlation Coefficients (NCC) generated using the well activity of G-24. Shown also is a rough interpretation of the water flooded zone in the neighbourhood of G-24 (dotted white line). (b) The time sequence of seismic changes and cumulative volumes extracted from the observation point 1. Red lines delineate the well trajectories.

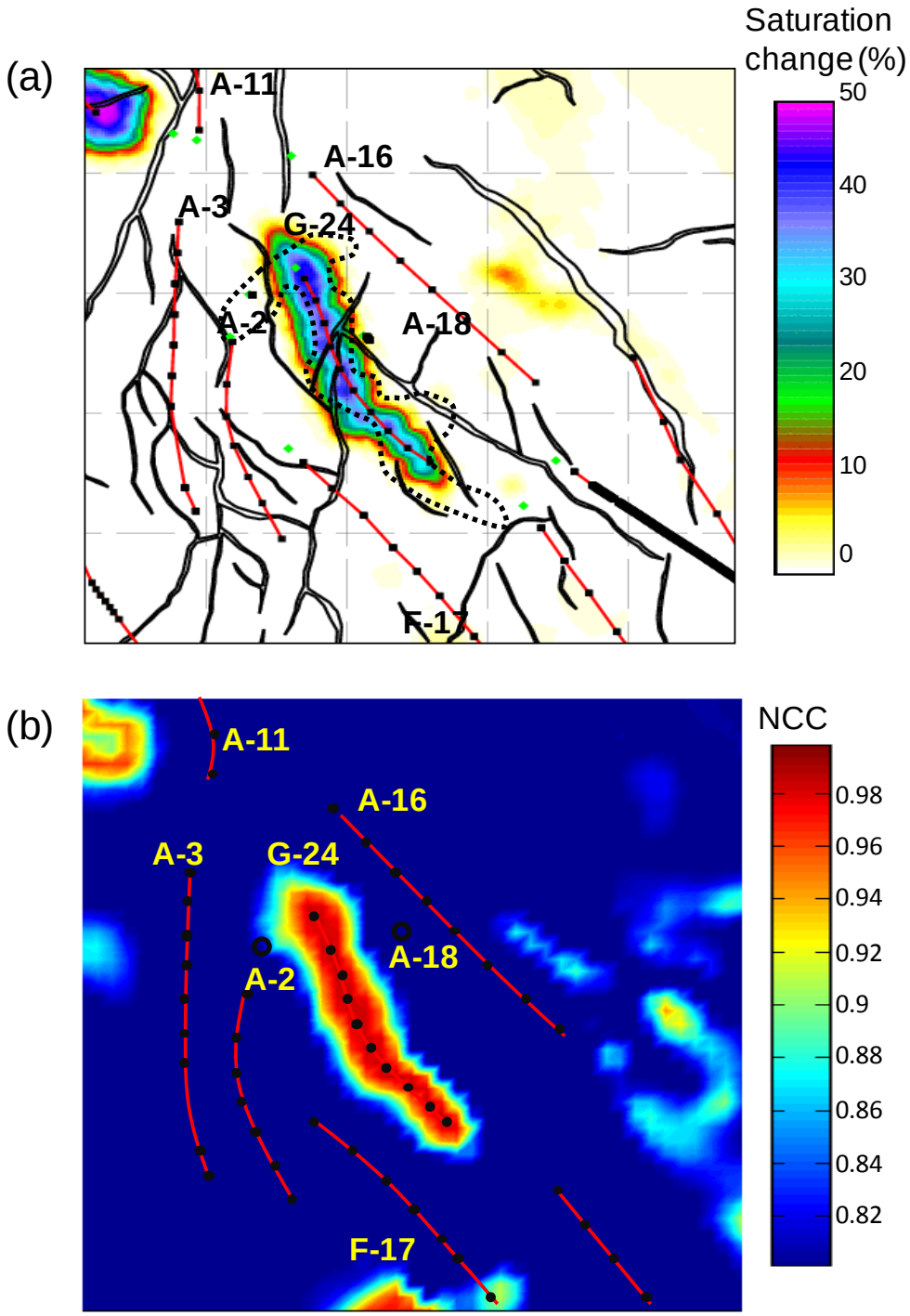

Figure 5.17 (a) Interpreted water flooded zone from Figure 5.16 (indicated by black dashed line) using the seismic to well correlation superimposed on the map of simulated water saturation difference between LoFS10 and baseline survey, compared to (b) *NCC* map calculated by correlating simulated water saturation and the well activity sequence of G-24. Red lines delineate the well trajectories.

5.6 Discussion and summary

Application of the well to seismic correlation method to Valhall reveals strong, localised signals around the wells. The spatially confined nature of these signals appears quite specific to the compacting chalk, as a previous application of the technique to Schiehallion has revealed a different more extensive character. The cause of this localisation is probably the low permeability of the chalk and perhaps the compaction mechanism. The shape of the Valhall anomalies has been verified by comparison with results obtained from synthetic seismic for the field (not shown). Importantly, the unique well signatures on Valhall give rise to higher cross correlation coefficients than seen with previous applications of the technique. The effectiveness of the technique, improves with the number and frequency of 4D surveys and the greater the complexity of well activity.

The resultant signals identify only those areas of the seismic which are strongly consistent with the well activity, and hence define portions of the reservoir connected to the wells. This is true regardless of whether the 4D seismic signatures are dominated by pressure or saturation. This information unites the seismic and well domains without the use of the simulation model. The signal tends to be quite robust and informative when compared to the individual 4D seismic difference signatures. The signal is not a conventional 4D seismic attribute, in the sense that it does not compare selected pairs of vintages but rather averages over multiple repeat surveys. As such, the distribution of the ‘attribute’ and its statistical significance will vary with the number of multiple surveys available and their overall time intervals. This seismic attribute can be used as a diagnostic tool for examining reservoir connectivity and constraining the simulation model. In the future such signatures may permit analysis of drainage patterns and conditioning of the simulation model to avoid well failure. This leads to the outrageous suggestion that, despite the practical consequences, more attempts should be made to fluctuate well production and injection during survey periods to aid in dynamic interpretation of the reservoir. This can be implemented, for instance, during the same period a particular well may be given heavier production workload while the neighboring wells being chocked back a little bit. This may create different sequence of cumulative volumes for the adjacent wells. In practice, if 4D surveys are acquired frequently, this may not so big an impact on field production.

Chapter6
Application to the Norne field

Multiple time-lapse surveys with good repeatability were acquired over the Norne field. The interpretation of the time-lapse difference signals in the G segment represents various challenges due to multiple complicating factors (e.g. the 4D response in neighboring areas). In this chapter, the well-to-seismic correlation technique is applied to the G-segment of the Norne field. In this study, it is demonstrated that the *NCC* method provided additional information content which helped enhance the conventional 4D interpretation based on examining the individual difference maps. The new information from the *NCC* results has also been incorporated into the reservoir simulation model. A better match between observed and simulated well performance has justified the modifications made to the simulation model. In addition, the character of 4D noise at reservoir level is studied using the *NCC* results, aiming to evaluate the effectiveness of non-repeatability measures (e.g. *NRMS*) computed in a time-window above the reservoir in predicting the 4D noise in the observed data.

6.1 General Description of the field

The Norne field is in the southern part of the Nordland II area in the Norwegian Sea approximately 80 km North of Heidrun field or 100 km North of Åsgard field (Figure 6.1). It produces from an FPSO. The field is owned by a partnership of Statoil, Eni and Petoro, and operated by Statoil. The Norne field was discovered in 1991 and the hydrocarbon reserves contained about 160 million SCM of oil first in place. Six well templates (4 production and 2 injection templates), each with 4 slots were installed on the seabed at water depths of 380 m. The Norne field's satellite fields include: ALVE, STAR and Svale field. The productions from these fields are all tied back to the FPSO over Norne field (Figure 6.2).

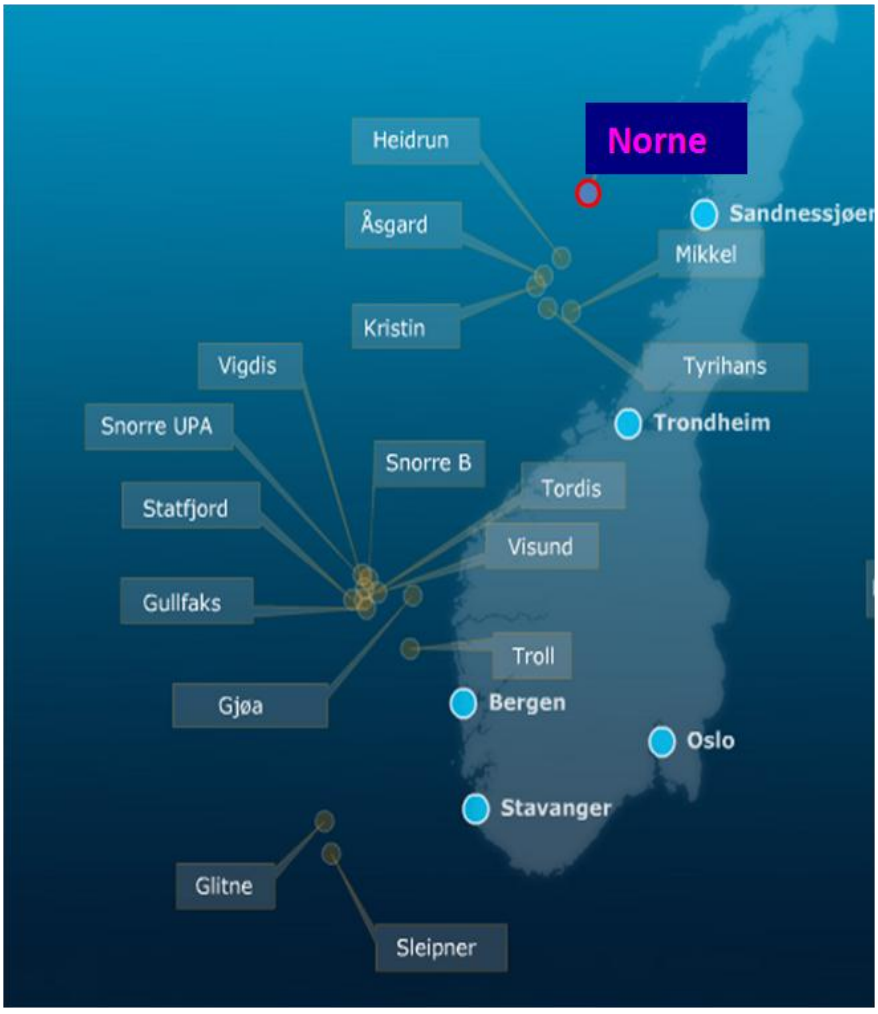

Figure 6.1: Location of the Norne field (after Cheng et al., 2007)

The Norne field is a horst block (Figure 6.3) approximately 9×3km (Osdal et al., 2006). Not all the segments are oil-filled. The main producing areas include C, D, E (main Norne structure containing 95% oil) and G segments; I and H segments are considered to be water filled. An initial gas cap was found to be stretched over C, D, E segments. Pressure exchanges through non-sealing barriers are found between C, D and E segments and the rest of the reservoir; G segment is considered very much isolated though. The Jurassic Not, Ile and Tofte Formations constitute the reservoir (see Figure 6.4) of very good quality with porosity and permeability of 25-32% and 200-2000mD, respectively. The gas cap (75m) is mainly situate in the Not Formation, and the oil leg (110m), mainly in Ile and Tofte formation. Non-continuous and thin carbonate cements have a significant impact on the vertical flow pattern.

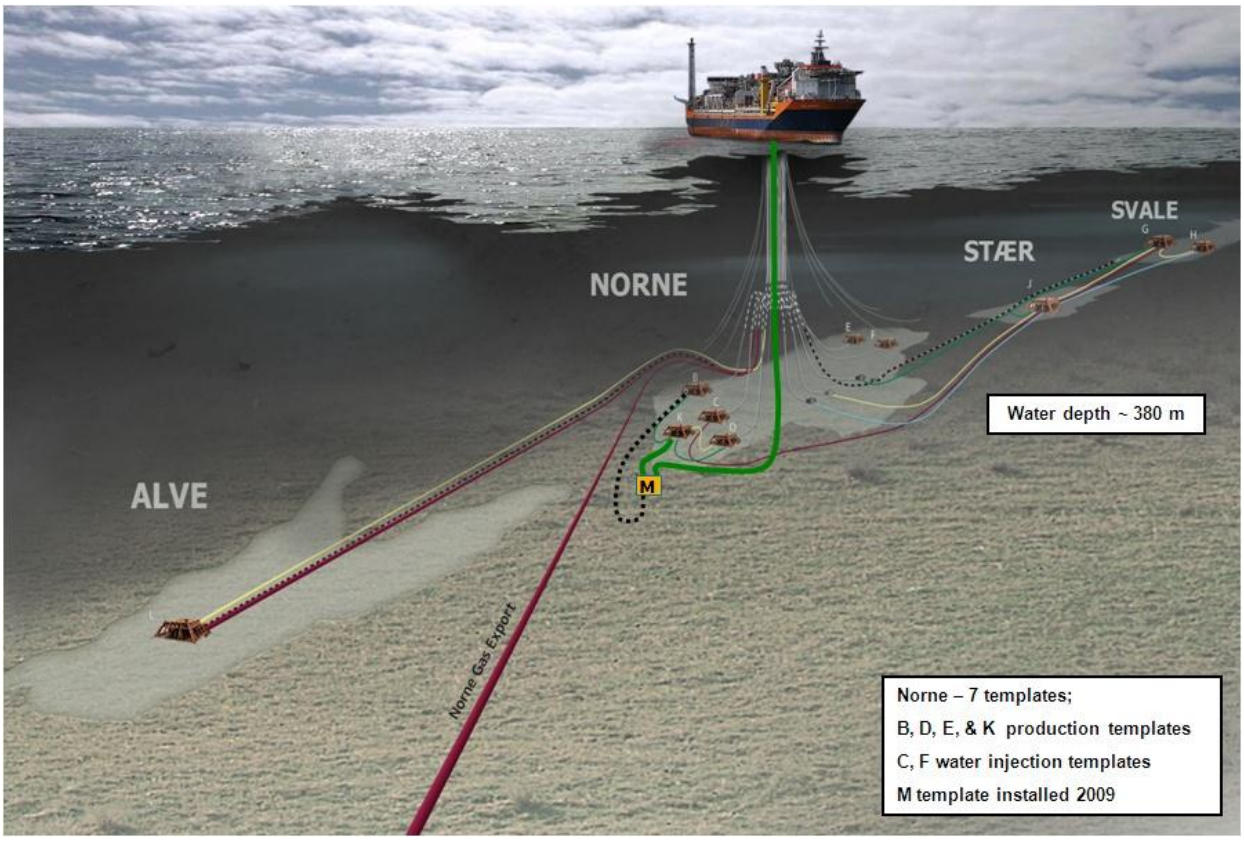

Figure 6.2 Production infrastructure for Norne and its satellite fields.

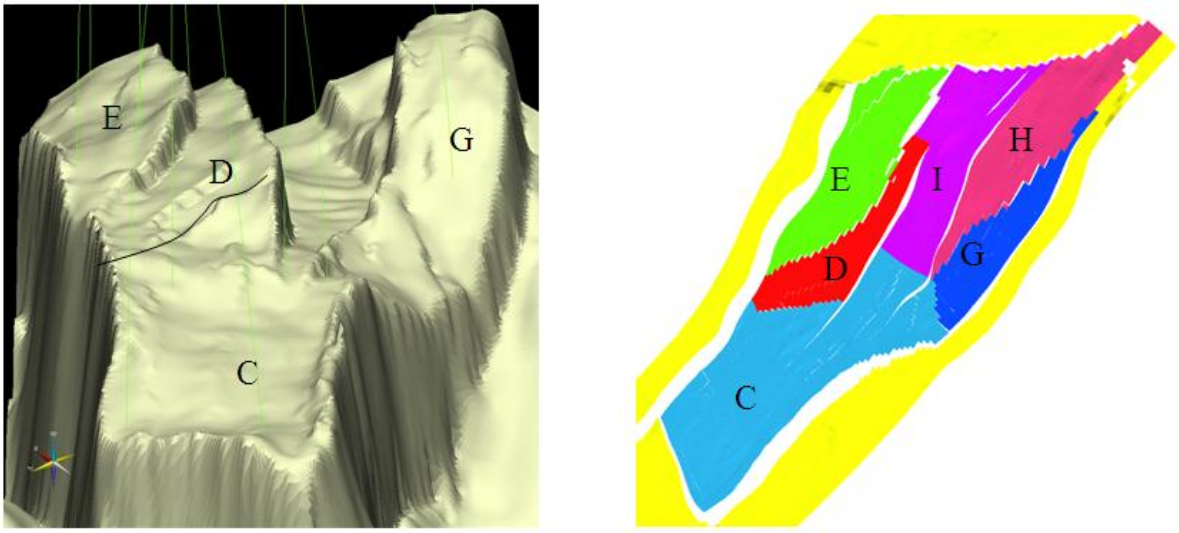

(a) Top reservoir map

(b) Reservoir segments in simulation model

Figure 6.3 (a) Norne horst structure and major segments shown on the top reservoir map and (b) plane view of segments in the simulation model

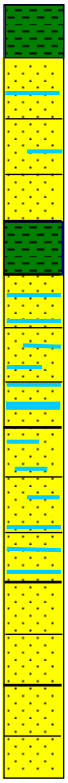

NORNE 2006			Reservoir Pressure
Not 3	Upper Not Shale		-
Not 2 (Not sandstone)	Not 2.3		236 bar
	Not 2.2		
	Not 2.1		
Not 1	Lower Not Shale		-
Ile 2	Ile 2.2	Ile 2.2.2	250 - 318
		Ile 2.2.1	
	Ile 2.1		
Ile 1	Ile 1.3		
	Ile 1.2		
	Ile 1.1		325
Tofte 2	Tofte 2.2		327
	Tofte 2.1		
Tofte 1	Tofte 1.2		329
	Tofte 1.1		
Tilje 4			330
Tilje 3			343

Figure 6.4 Geology formations and their subdivisions in the Norne field

6.2 4D seismic acquisition and interpretation

The first seismic survey on the Norne Field was acquired in 1992 with a configuration of dual source and three streamers of 100 m spacing. Subsequent 4D surveys were acquired in 2001, 2003, 2004, 2006 and 2008 using *WesternGeco* Q-marine[2] system with single source and 6 steerable streamers of 50 m spacing. Instead of steering the streamers to repeat the feathering of the base survey, the subsequent Q-surveys all repeat the geometry of the 2001 survey. This may cause a relatively higher level of non-repeatability noise in the differences between the base survey and the Q-acquisitions, than between the Q-acquisitions (see Figure 6.5). However, in general, 4D data in Norne Field have good quality: with an average of *NRMS* 40% for base versus Q-surveys and 19%-21% for Q versus Q surveys. Osdal et al. (2006) gives more information about repeatability between time-lapse seismic surveys on the Norne field.

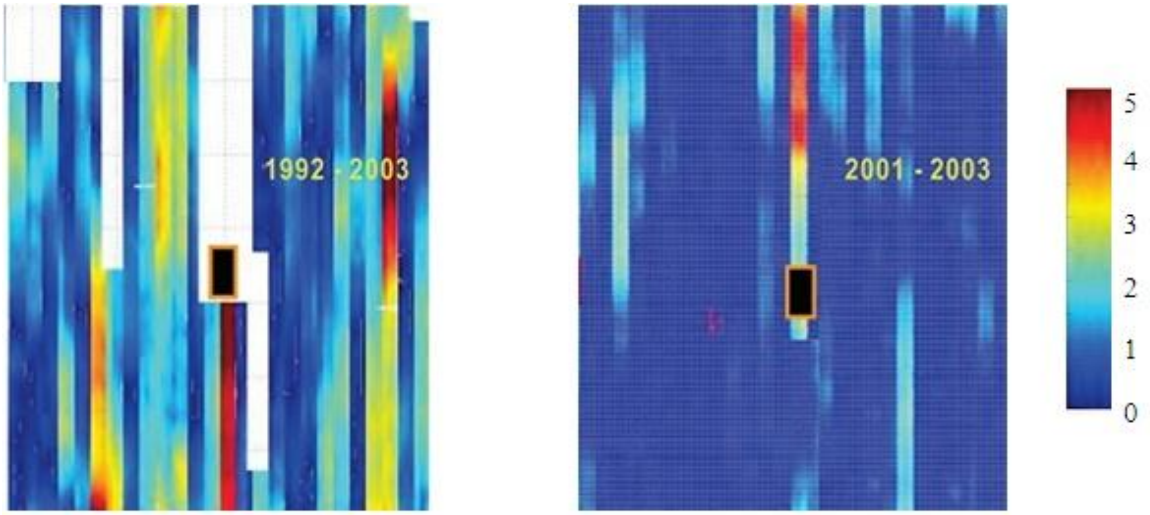

Figure 6.5 Significant improvement in repeatability is achieved between Q surveys (b) than between base and Q surveys (a)

Very thin and non-continuous carbonate cements, which can serve as vertical flow barriers, were found in the core plug from Ile and Tofte sands. The vertical flooding pattern during

[2] The Q-Marine seismic system is developed by WesternGeco with a series of technology designed specifically for marine time-lapse seismic acquisition.

production, therefore, could be very difficult to predict but very important for field exploitation. With the excellent vertical seismic resolution of the Norne data sets, the primary use of 4D information has been monitoring the vertical OWC movement. In order to implement this work efficiently, seismic modelling for a variable rise of 0 to70m were carried out. The OWC movement can be clearly interpreted in both synthetic (Figure 6.6b) and observed difference data (Figure 6.6d). The signature of the OWC movement (black to red pattern) in Figure 6.6b can be validated by the synthetic modelled difference data in the injector based on repeated saturation logging in 2000 and 2002. A complete flushing of the oil with water causes an acoustic impedance change of 7%-8% (Osdal et al., 2006).This 4D interpretation strategy has proven successful in C, D and E segment where the oil leg is up to 110m thick.

6.3 Field development and production history

The early field development strategy was dominated by a concept that Statoil itself referred to as 'Fast Track' field development. This strategy involves an array of new and integrated approaches to project management. It is aimed at a reduced cost of 30%-40% and to minimize time from discovery to production (Steffensen and Karstadt, 1996). The initial stage of field development involved drilling of 6 wells (5 horizontal producers and 1 gas injector). To maintain the reservoir pressure around the initial level, the produced gas was re-injected into the gas cap until 2001 when a network was set up for gas export. The production plateau was reached shortly after production as expected and lasted for almost 4 years under first recovery. The second drilling phase started in 2001 was aimed to prolong the plateau period of production and to improve areal sweep. During the second drilling phase, another 5 water injectors were put in place to re-inject the produced water from the reservoir and unprocessed sea water into the reservoir. Up to the present, a total of 50 wells have been drilled in the field with 33 producers (16 active), 10 injectors (8 active) and 7 pilot wells (NTNU, 2010). The field has produced 82.7 million Standard Cubic Metre (SCM) of oil in total up to March 2010 and 12.0 million SCM remains unproduced up to the present (NPD website, July 2010). The production is currently declining at a considerable rate. Infill drilling has been identified as the key measure to extend the field life to 2021 - a goal set by its asset team. An infill-drilling campaign is set to be launched in near future targeting the by-passed hydrocarbons identified using integrated information from adopted reservoir monitoring

technologies. With new satellite fields tied in and new IOR (Improved Oil Recovery) measures are being actively taken, the ambition is to extend the field life to 2021 with ultimate oil recovery to reach 60% (see Figure 6.7).

(a) Model for rising water of different levels

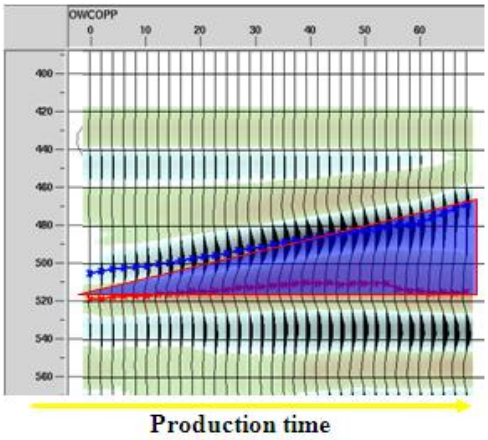

(b) Synthetic seismic response

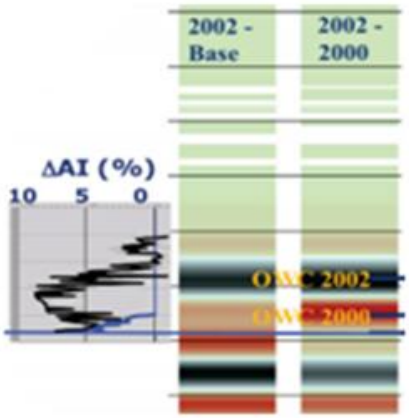

(c) Synthetic seismic response of rising water level based on repeated saturation logs

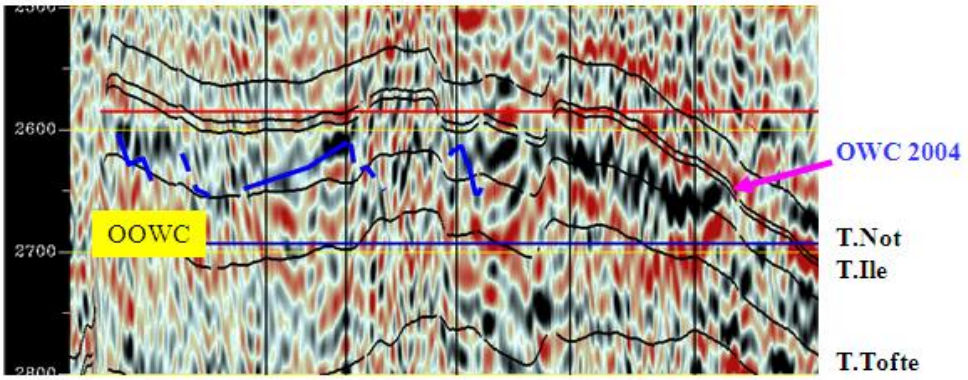

(d) An example of observed difference section between 2004-2001 with original and new Oil-water-contact highlighted

Figure 6.6 (a) Model for rising water level. (b) The synthetic seismic response of the model shown in (a). The pattern in which new and original OWCs are represented by black (peak) and red (trough) events is validated by (c) the synthetic seismic response is based on the measured saturation from time-lapse log data. (d) An example of the real difference section shows clearly the water-and-oil contact movement between 2004 and 2001 (after Osdal et al., 2006).

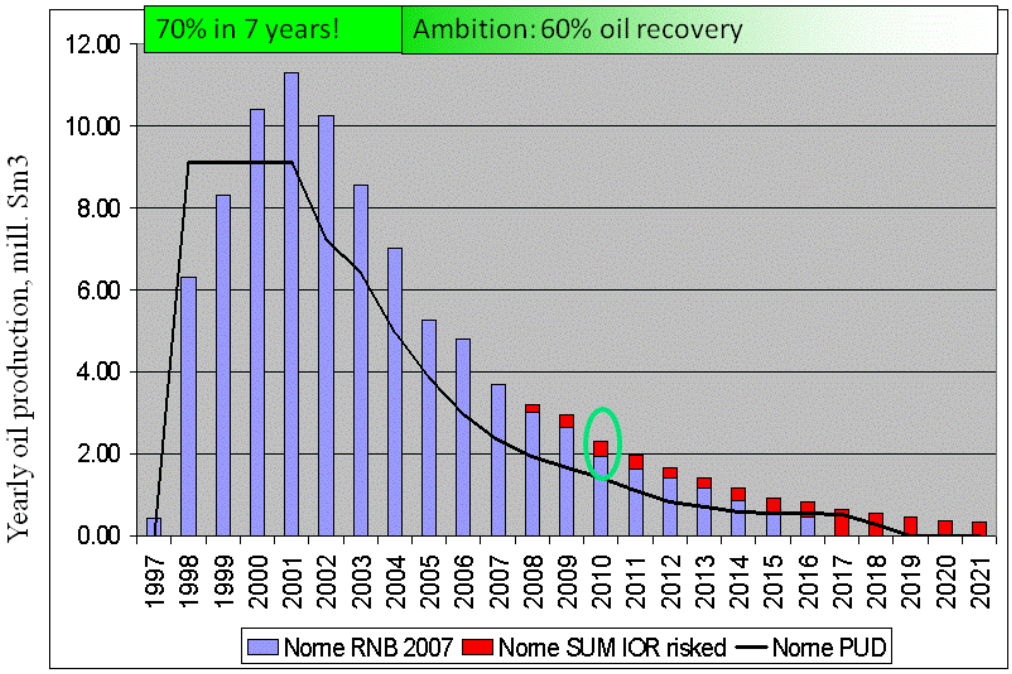

Figure 6.7 Estimated production throughout the Norne field life cycle including the portion contributed by IOR measures. Ultimate oil recovery of 60% is the target set by the Norne asset team (Statoil, 2001).

Use of time-lapse seismic is a routine in Statoil with 70% percent of the fields it operates covered by more than two repeated seismic surveys. The feasibility studies of time-lapse surveys demonstrate that the cost of time-lapse surveys is a small fraction of their value in terms of minimizing development-drilling costs and in recovering additional hydrocarbons (Osdal and Alsos, 2002). During field appraisal, acquisition of baseline 3D seismic survey helps the operator to accurately map the field and plan development drilling. Early in the production cycle, gas comes out of solution and the decreasing pressure produces an obvious seismic response. Time-lapse seismic surveys early in the production cycle offer vital information about future performance. As the field reaches maximum production, a time-lapse survey helps detect bypassed hydrocarbons and guides development well-location selection. As the production declines, additional surveys help the operator manage injection operations to maximize recovery from mature fields (Osdal et al., 2006).

6.4 Description of the G segment

This chapter mainly focuses on 4D seismic data over Norne G-segment. Compared to other segments, the situation in the G segment is relatively simple: there is no initial gas, and oil is only contained in the uppermost Not Formation (25-30m). The sands in the Not Formation in the G segment, similar to those in most of the reservoir, are of very good quality with high permeability and porosity (100-10000mD and 24%-28% respectively). It was also believed that G segment has little pressure interference with other parts of the Field; and aquifer encroachment is not significant. Thus, it is expected to see each unit of volume injected in and produced from the G segment and a corresponding pressure response. The reservoir simulation model for the Not formation Sands in G segment comprises three layers, which correspond to the subdivision of the Not Sands into Not 2.1, 2.2 and 2.3. The average size of the grid cells is 75m×100m×15m. There are three wells that have been drilled in the G segment: E-4AH (producer) is a horizontal well and placed in the up-dip part of segment; F-4H (injector) in downdip aquifer and its sidetrack well F-4AH were drilled in the central part of G segment (Figure 6.8). Another sidetrack well targeting the western G segment is also being considered. The initial oil reserve in G segment was estimated to be 180 mbbl and more than half of the oil has been extracted up to now.

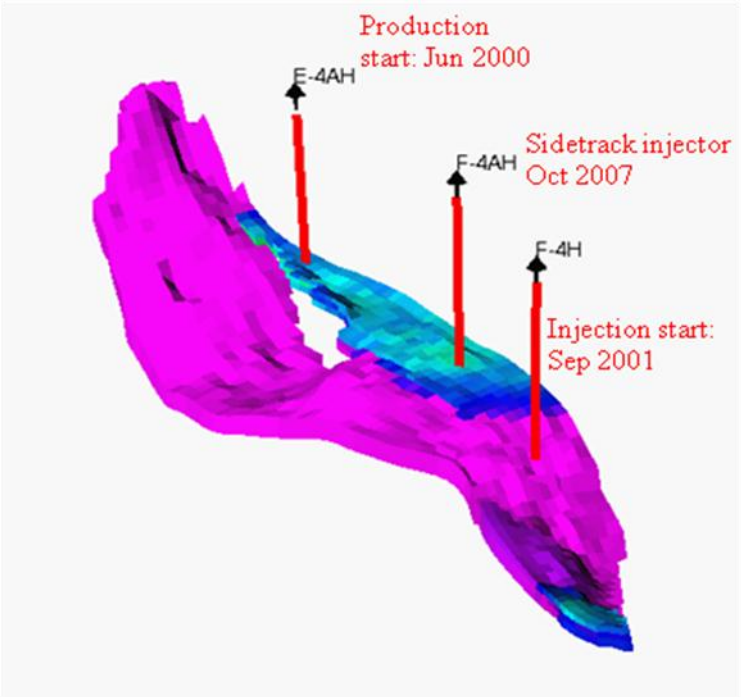

Figure 6.8 Reservoir simulation model (initial oil saturation) for Norne G-segment. Three wells including two injectors and one production well have been placed in G-segment so far.

6.5 Qualitative 4D interpretation of the G segment

4D signatures from high quality and multiple repeated seismic surveys over the G segment provide ample information of dynamic reservoir change due to production. AVO modelling was performed by Norne geophysicists in order to understand the seismic response of different production scenarios in different angle stacks. The AVO responses for gas saturation and pressure change were examined with particular attention because they were the primary production effects observed during production. To make things simple, the results from AVO studies are only shown using schematics in Figure 6.9. It is noticeable that near offset stack data see stronger pressure-driven 4D response while far offset stack data see stronger gas-saturation-driven 4D effects.

In this section, a number of time-lapse difference maps between seismic surveys with remarkable signals are given as examples to familiarise the readers with the previous interpretation carried out by the Norne asset team. The first example is the difference map between 2001 and 1992 survey (Figure 6.10), the reduced seismic amplitude (reservoir softening) was interpreted as the effect of gas coming out of solution due to pressure depletion in the early stage of the production cycle. The features of 4D difference signal in G-segment seem to suggest a good connection across the entire segment. There is also some evidence from downhole pressure measurements that can support this observation. Moreover, it can be inferred that the pressure change between 2001 and 1992 should be approximately the same everywhere in G-segment.

The 4D difference map between 2004 and 2001 however shows a polarity difference in different areas of G-segment (Figure 6.11). In the area close to the injector F-4AH (highlighted by the yellow polygon), the decrease in amplitude is interpreted as the seismic response of dramatic pore pressure increase due to injection from F-4H. In the area highlighted by the blue polygon, the opposite amplitude change is interpreted as a combination of the effect of gas back into solution and water replacing oil. A higher pressure was expected in the area highlighted by the yellow polygon than that in the area highlighted by the blue polygon.

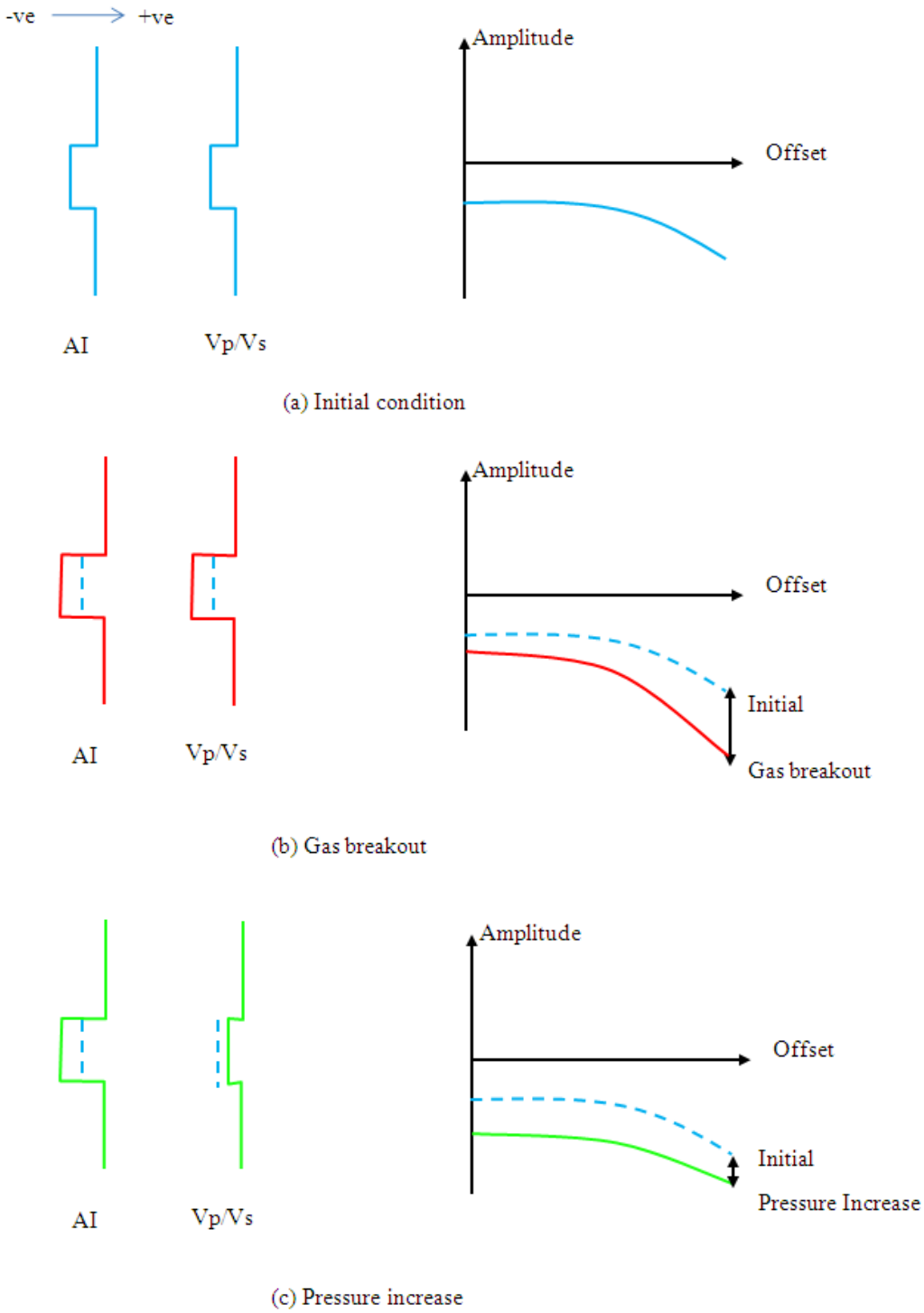

Figure 6.9 Schematic results from AVO modelling: AI, Vp/Vs ratio changes for Gas breakout (b) and Pressure increase (c). The AVO response of these two types of reservoir change compared to the initial state (a).

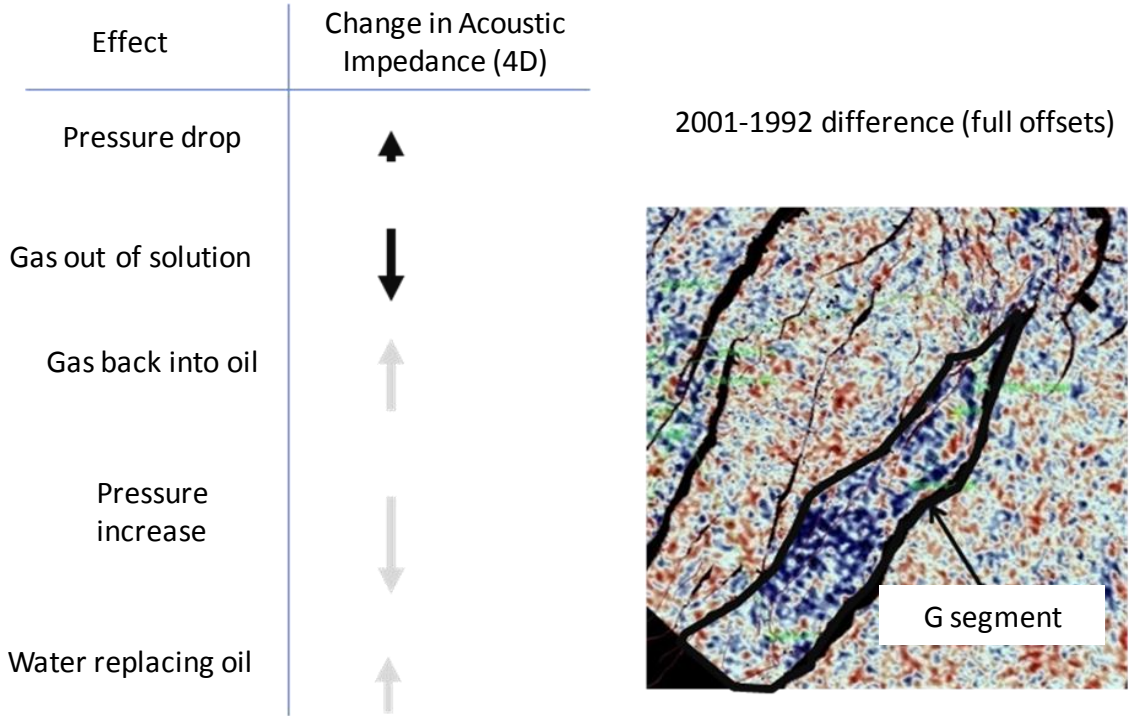

Figure 6.10 The effect of gas out of solution dominates the amplitude difference between 2001 and 1992 in G segment (Statoil, 2008).

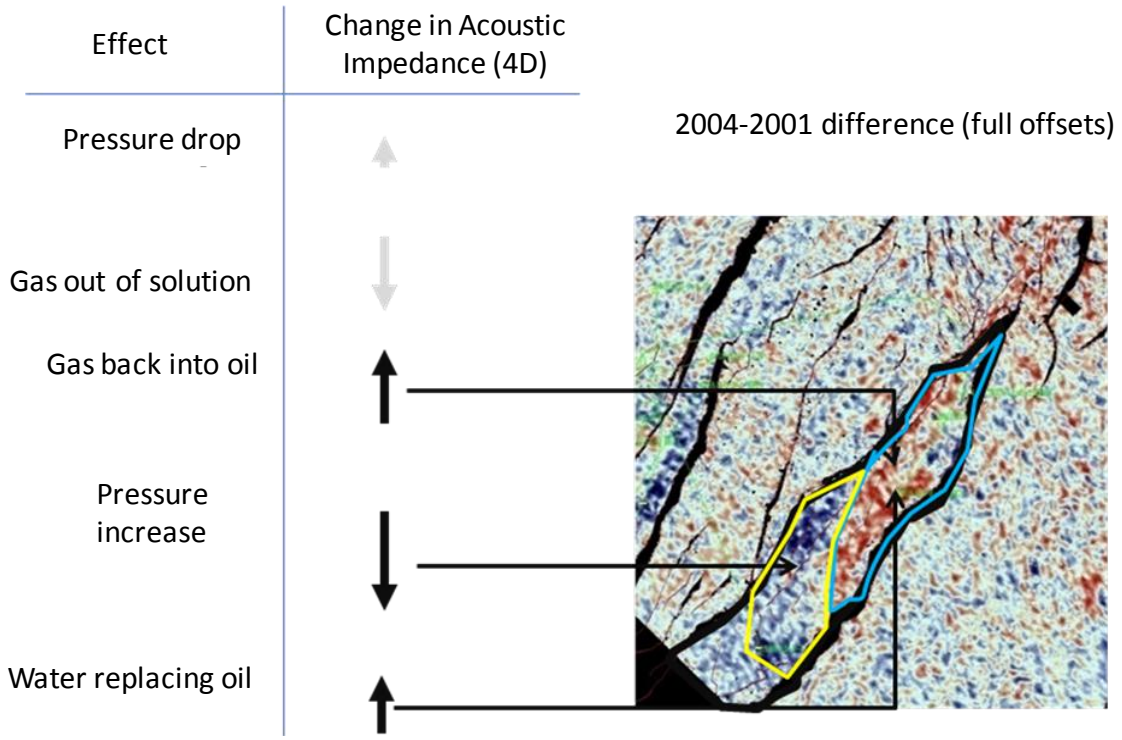

Figure 6.11 Amplitude difference map between 2004 and 2001 shows both saturation and pressure driven 4D signatures (Statoil, 2008).

Another two difference maps for example are shown in Figure 6.12 and 6.13. They are derived from the near offset differences between 2006 and 2001 surveys, and between 2006 and the most recent 2008 surveys. As mentioned early in this section, with near offset data dominated by pressure-driven 4D signals, these two difference maps show clean pressure-driven 4D signatures. The reservoir softening observed between 2001 and 2006 is interpreted as a result of significant pressure increase caused by massive water injected; the reservoir hardening between 2006 and 2008 as pressure depletion caused by production over the same period. The signatures in both difference maps seem to validate the previously mentioned interpretation which pointed to a good communication over the entire segment.

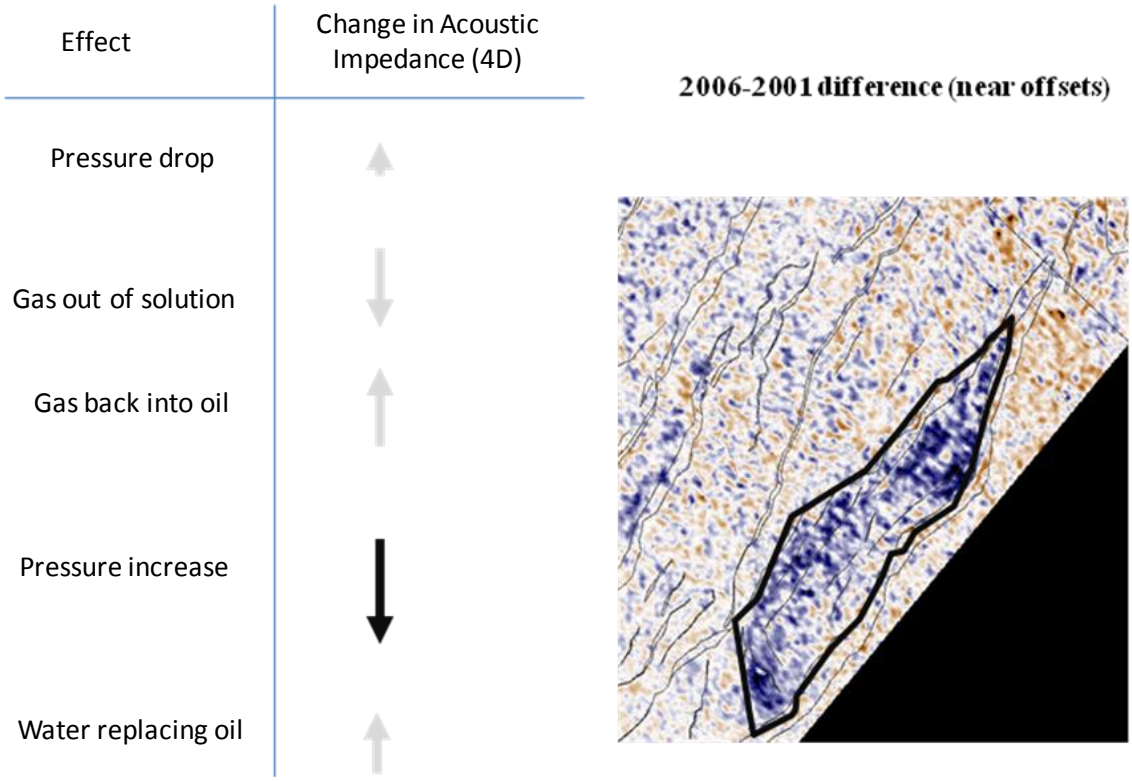

Figure 6.12 Near offset differences between 2001 and 2006 show strong reservoir softening (Statoil, 2008).

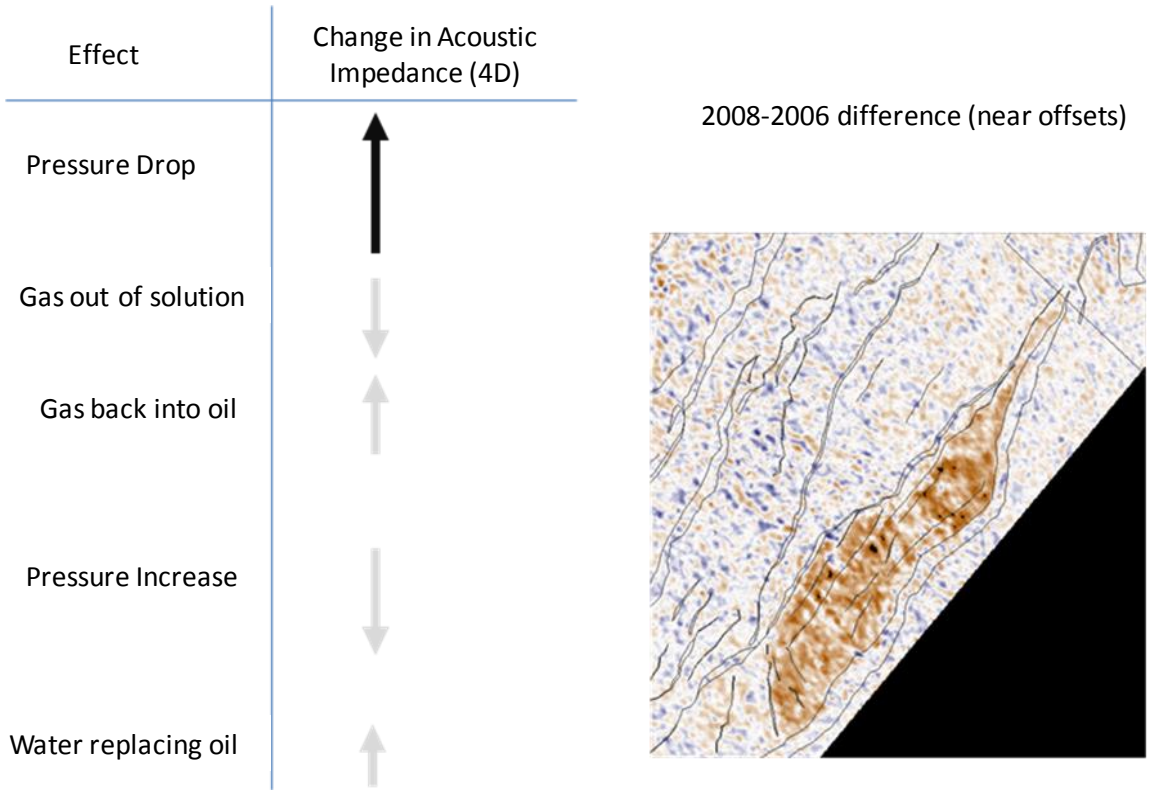

Figure 6.13 Near offset differences between 2006 and 2008 show strong pressure depletion effects (Statoil, 2008).

6.6 Data used in this study

The focus of this study is to identify pressure-driven 4D signals, thus only those time-lapse seismic vintages, between which the differences primarily exhibit pressure-driven signals, were used for this study. As explained previously, near offset seismic data in the Norne field is more sensitive to change in pressure in the reservoir. Hence, the study in this chapter was focused on the near offset data. Nevertheless, the 2003 and 2004 surveys were not used for this study because the differences between these two surveys and the other seismic vintages contain strong saturation effects which may comprise the use of the proposed technique. Moreover, the 2001-1992 difference dominated by the effect of gas out of solution has been converted to its pressure-driven component, through a simple scaling factor derived from the petro-elastic relationship deduced from the observed seismic (see Appendix D). Figure 6.14 shows the four surveys selected as input to our well-to-seismic correlation algorithm. The differences between each of them are dominated by the pressure-driven 4D signature. The net

segment volume (the summation of injected and produced fluid volumes with opposite signs) was used to compute the sequence of cumulative volumes for this study.

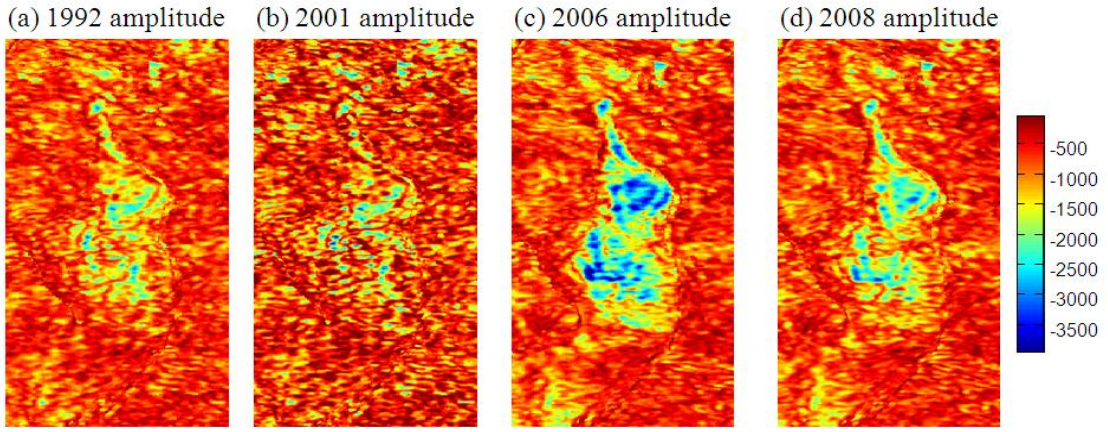

Figure 6.14 Four time-lapse surveys selected for well-to-seismic correlation technique

6.7 Identification of the true connected area

The first and the most important use of the well-to-seismic correlation technique is to identify the 'real' 4D signal from noise. Unlike in other scientific fields, a coherent and strong anomaly in 4D seismic data that clearly stands out from the noisy background does not necessarily contribute 'Signal'. On the other hand, 4D signatures that appear noisy may not be real 'Noise'. Any definition of 'signal/noise' in 4D data should respect a basic fact that the real '4D signal' is the consequence of well activity. That is to say that no matter how strong a 4D anomaly is, it is simply not a meaningful 4D signal if it is not the consequence of any well activity.

An example of this use of the well-to-seismic correlation technique is shown in Figure 6.15. On the left hand is the amplitude difference between 2006-1992. It was noticed that the amplitude changes at two locations ***a*** and ***b*** in the reservoir are in the same order. This appeared to suggest a potential connection to the location ***b*** from the wells in G segment. It is unlikely to rule out this possibility if we only look at this difference map by itself. Nevertheless, the plotting of the sequences of mapped 4D differences and cumulative volumes for all the time steps revealed that the systematic behaviours of amplitude change at location ***a*** and ***b*** are distinct: the one at location ***a*** correlates with the sequence of cumulative

volumes; the one at location ***b*** not. Hence, the 4D difference between 2006 and 1992 at location ***b*** is just noise; the one at location ***a*** is signal.

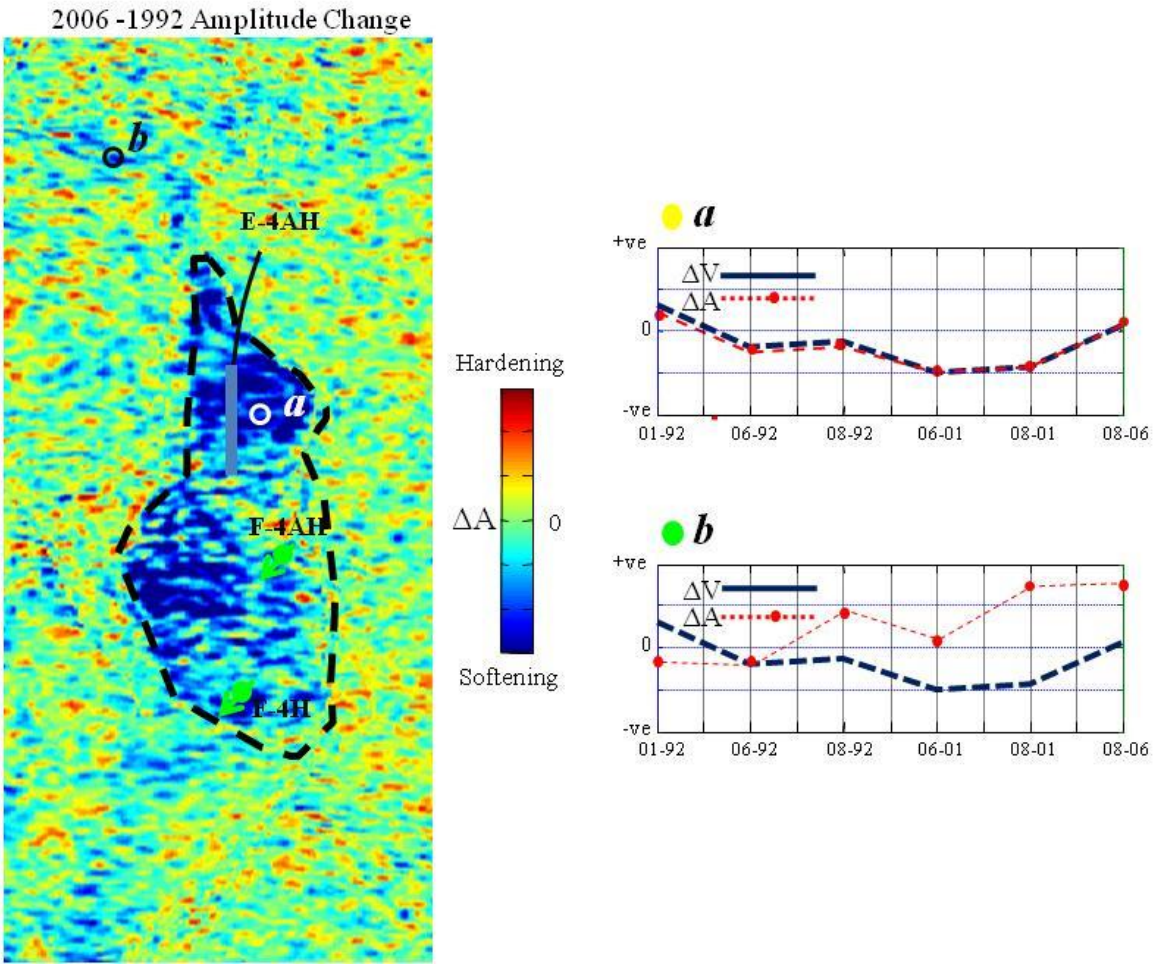

Figure 6.15 The amplitude change between 2006 and 1992 (left) and the sequences of 4D signatures and cumulative volumes at two observation points a and b (right). The G segment is delineated by black dashed line.

6.8 *NCC* map and 4D noise at the reservoir level

A normalised correlation coefficient (*NCC*) map between the 4D seismic signatures and the change in well volumes was calculated (see Figure 6.16a). The 4D changes in the G segment correlate remarkably with well activity defined by the cumulative volumes. Out of the G segment, little correlation was found except for a channel-like region on the South West (Figure 6.16a). This section focuses on the characteristics of the *NCC* inside the G segment. Despite the majority of G segment occupied by high *NCC*s, low *NCC* is clearly visible. The

reduction in *NCC* was caused by the portion of amplitude changes that does not correlate with well activity defined by the cumulative volumes. In order to highlight low *NCC*, a binary map which highlights low *NCC* (NCC <0.6) with value '1' was generated (see Figure 6.16b). Indeed, this map pinpoints the 'unexpected' 4D changes at the reservoir interval according to well activity. Apart from saturation, 4D noise (non-repeatability oriented) was considered as the main factor responsible for low *NCC*.

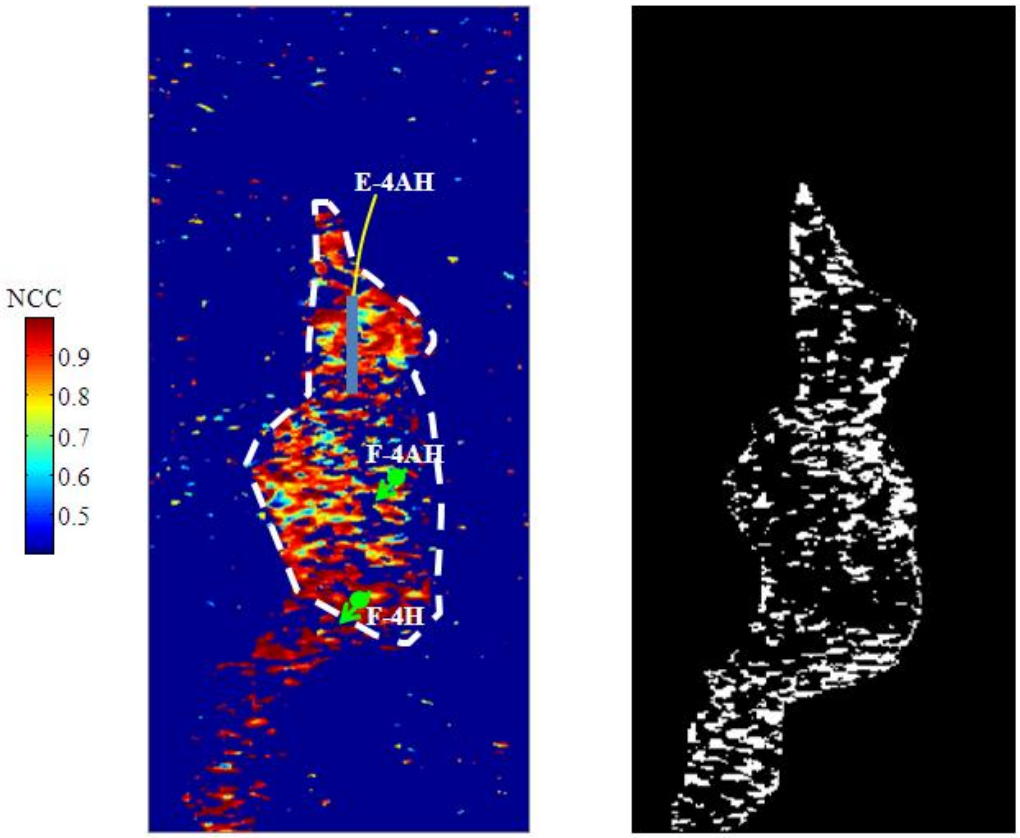

Figure 6.16 (a) *NCC* map (thresholding NCCs<0.4) and (b) Binary map highlighting the location with where *NCC* value is smaller than 0.6.

However, 4D noise in the reservoir has yet been fully looked at in any publications. Indeed, it is very difficult to distinguish 4D noise from the production-related 4D changes in the reservoir. Thus, almost all the published studies concerning 4D noise look into the overburden, where no production occurs. The most well-known non-repeatability measure calculated from overburden is Normalised RMS difference (*NRMSD*), which was introduced by Kragh & Christie (2002). However, how well *NRMSD* can predict the level of 4D noise in the observed data at the reservoir level is still an open question.

6.8.1 Measure of non-repeatability versus 4D noise

Since the low *NCC* map can highlight errors in the observed data at the reservoir level, a comparison is made possible between the non-repeatability measures derived from a time window above the reservoir and the low *NCC* map. However, *NRMS* is defined based on the difference between two sets of data only. The *NCC* map that is generated using multiple surveys can therefore not be directly compared with *NRMS* maps. To overcome this difficulty, a few new measures of non-repeatability were proposed by Kommedal & Barkved (2005) for the cases where the number of repeats goes beyond two. Among which, one measure referred to as *Normalised Mean Squared Error* (*NMSE*) was calculated for the Norne data sets (see Figure 6.17b). In the *NMSE* map, the 'highs' indicate where acquisition and processing were poorly repeated. Further, another simple 'binary' approach was used where the value '1' is used to highlight the location where the *NRMS* value of any of the six time intervals exceeds a defined threshold (e.g. Figure 6.17c shows the result using a threshold 0.6). This method seems to yield a similar pattern in the results to that in the *NMSE* map, but clearly more detail can be observed. This level of detail was found necessary when compared to the *NCC* map.

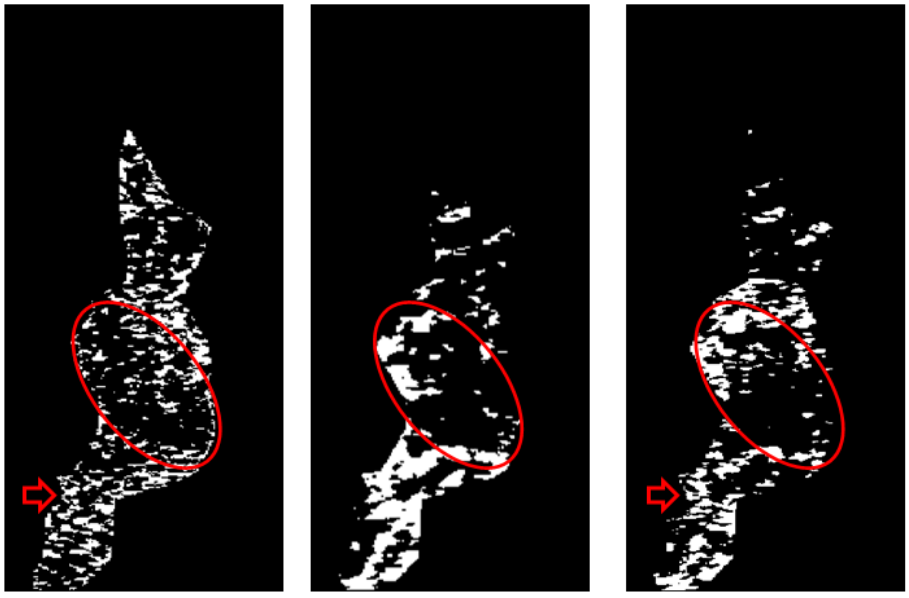

(a) Binary map highlighting Low NCCs (0.6)

(b) NMSE measure

(c) Our measure of average non-repeatability level among multiple surveys

Figure 6.17 The binary map with the highs indicating the distribution of noise, compared to (b) binary *NMES* map where high values are indicative of locations where the repetition of surveys is poorly achieved, and (c) the map of averaged *NRMS* values generated for each pair of surveys.

There is some degree of correlation between the features in Figure 6.17a, b and c. Firstly, the high *NCC*s in the central area of the G segment seem to correlate with the generally high level of repeatability in the same area. Secondly, an east-to-west trend is present in both Figure 6.17a and c. However, it should be noted that the features in these maps are just loosely correlated. The causes are discussed in the following part of this chapter.

6.8.2 Poor correlation between non-repeatability measure and 4D noise

The reasons why the correlation between non-repeatability measures and the low *NCC* map is poor are discussed in this section. One obvious reason is the saturation change response, which as mentioned above is considered as noise and thus it should yield poor correlation between time-lapse signatures and well activity. However, the 4D changes are dominated by pressure change in G-segment except in an area where the low *NCC*s are interpreted as water flooding.

Secondly, geology is unchanged from survey to survey. In reality, the residual differences between imaged geology in different surveys cannot be fully eliminated due to poor repetition and equalisation. The residual difference is often referred to as '*Geology Noise*', which can be clearly seen in the difference maps between the baseline survey and subsequent Q surveys (Figure 6.18). With its geology dependent nature, the mapped time-lapse differences extracted from different time windows in the overburden may show changing features, this also leading to the discrepancies between the characters of the non-repeatability measure and the *NCC* map.

Thirdly, with good repetition of source and receivers, in the difference between the subsequent Q surveys, '*Geology Noise*' becomes insignificant with respect to diffracted multiples that are widely present in the Norne data. It was found that this type of noise was rather localised in the area right below ice scourings at the ocean bottom, and the errors it causes correlate quite well from one level to another in non-migrated volumes; while no such evident correlation can be seen in migrated volumes (Figure 6.19). It suggests that migration can considerably change the spatial characteristics of noise in 4D data. This is also indicated by different mean values of *NRMS* between non-migrated (mean *NRMS*=0.75) and migrated case (mean *NRMS*=0.45) - diminishing the vertical correlation in noise features at different levels.

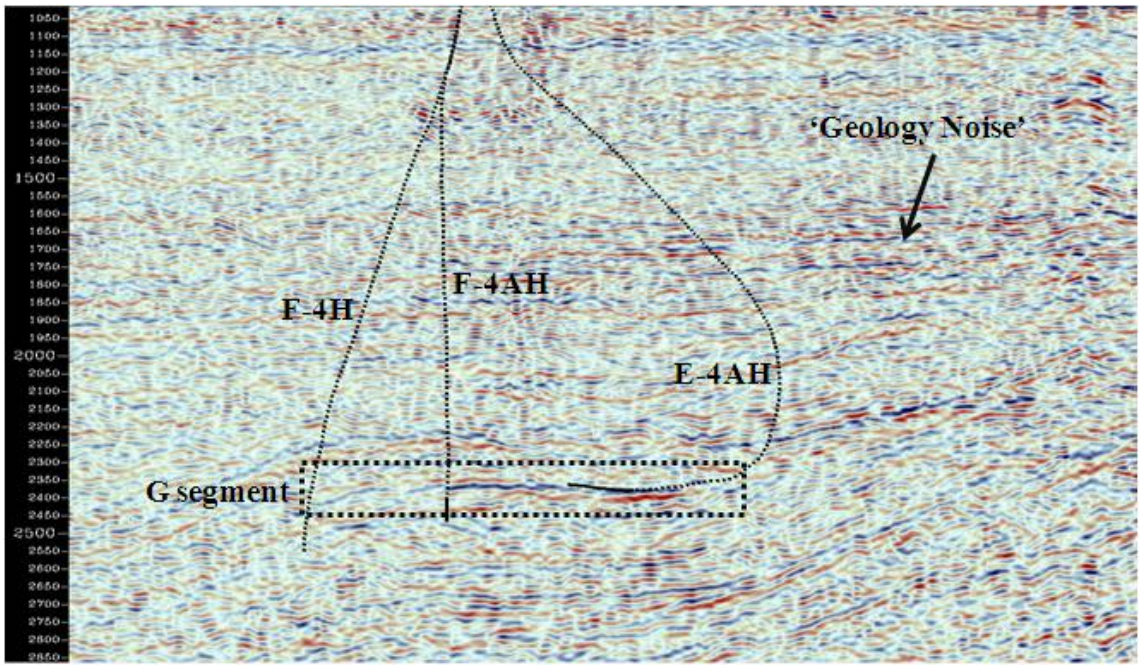

Figure 6.18 Strong 'geology noise' observed in a section across G-segment in the difference volume between 2001 and 1992

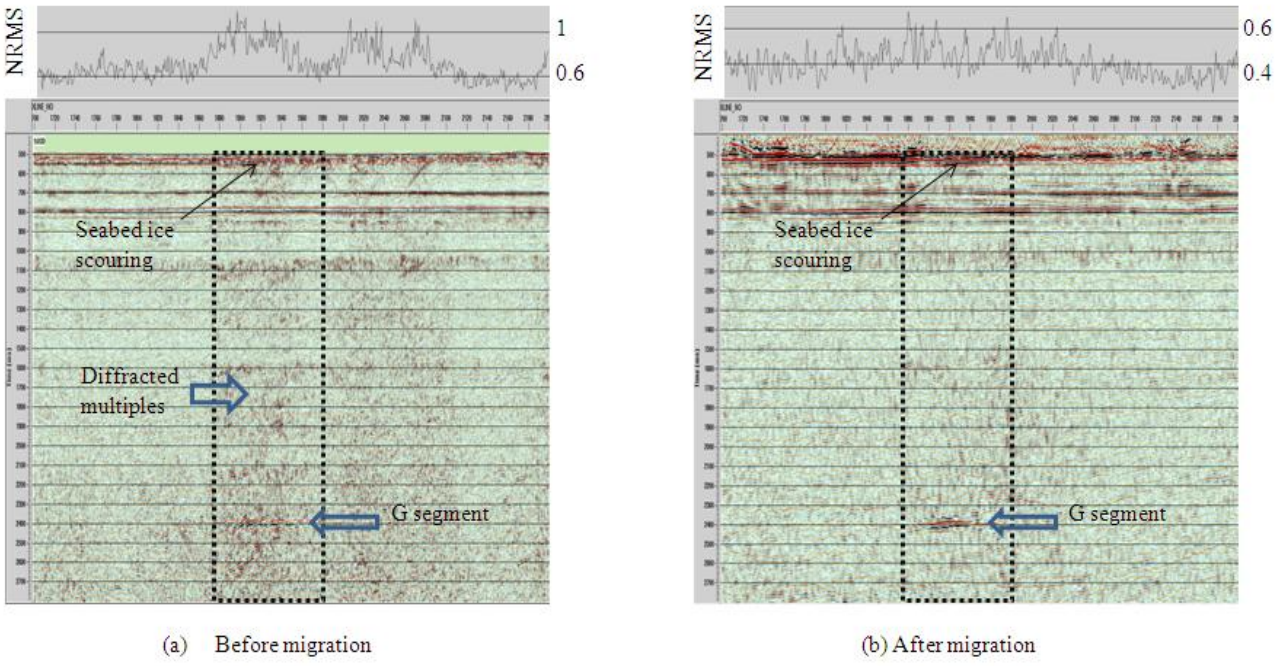

Figure 6.19 A clear stripe of diffracted multiples (noise) can be seen in un-migrated difference section (a). This can cause a similar distribution of errors in the amplitude difference at different levels. In the migrated section (b), the consistency in the noise pattern at different levels is much reduced.

6.9 Improved history matching using the *NCC* result

6.9.1 Interpreting the *NCC* map

The well-to-seismic correlation technique has proven its value by pointing to and enhancing the same set of conclusions as were apparent when the individual difference maps were interpreted. The interpretation of water movement in the G segment has been a rather challenging work due to the masking effect of gas moving back into solution. This led to a misunderstanding in 2004 (Figure 6.20a): the eastern part of G segment was thought to be oil filled and water mainly flowed along a pathway in the western G segment (Osdal et al. 2006). Nevertheless, a subsequent sidetrack well F-4AH (date: Oct 2007) saw very high water saturation (60-70%), highlighting the fact that the eastern segment had been flooded. The saturation measurement, however, is consistent with the low *NCC*s in the eastern part of G segment (Figure 6.20b). A comparison with the signatures in this area in the far-offset stack has further proven this point.

The pathway in the western part of the G segment does not seem to exist. The latest study that also considered the new 2008 survey, led to the conclusion that the western segment should be oil filled (Statoil Internal Documents). The *NCC* map seems to converge, with this latest study, to the same conclusion: the relatively coherent signal in the *NCC* map suggests there is much less saturation change in the western than eastern part of the G segment. The decision-making to sidetrack the producer E-4H or drill a new well into this area has been largely dependent on the degree of confidence we have about how much oil is left there. Therefore, the extra confidence, added by the *NCC* map, has been considered valuable to decision making for future drilling activities. In addition, it was noticeable that a finger-like area out of G segment (highlighted by the ellipses in Figure 6.21c) also bears high *NCC*s different from the area in the previously delineated the G-segment. This may prove the previous postulation of the connection between this region and the G segment. A difference section (A-B) between 2008 and 2006 seems to be also suggested this connection (Figure 6.21a), but the likelihood of this connection is largely increased by well-to-seismic correlation because it shows the amplitude in the study area not only changes over time, but most importantly according to well activity (Figure 6.21b).

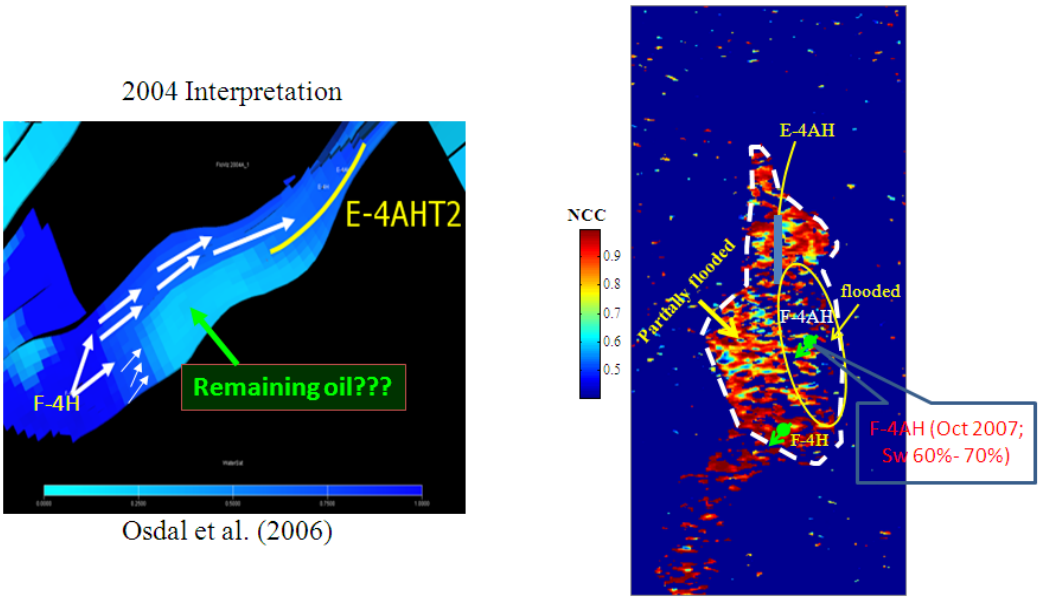

(a) Updated simulation model based on 2004 interpretation

(b) NCC map

Figure 6.20 Updated simulation model based on the previous interpretation which predicted high remaining oil saturation in the eastern part of G-segment (a), while (b) *NCC* map and saturation log suggest the opposite.

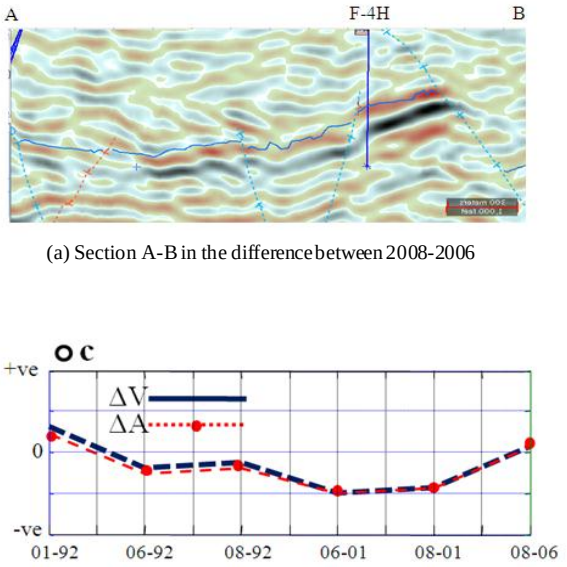

(a) Section A-B in the difference between 2008-2006

(b) The sequences of 4D signatures and cumulative volumes at the randomly selected location ***c***

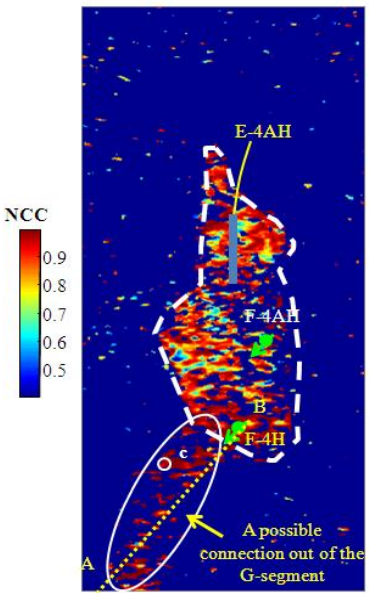

(c) NCC map highlighing a connected channel-like area to G segment

Figure 6.21 (a) A section (A-B) through the difference volume between 2008 and 2006, (b) Good correlation between the seismic responses and well activity in the studied area as outlined in (c) the *NCC* map.

6.9.2 Updating the simulation model using the *NCC* map

Having discussed the new information in G-segment obtained from the *NCC*s in the last section, modifications were made to the reservoir simulation model to see whether better matches between the observed and simulated well history can be achieved. It should be noted that: despite much effort made to history matching, the current version of the reservoir simulation model is still far away from a satisfactory one. The challenge in part comes from the complexity in the way the time-lapse effects with multiple types of reservoir change (pressure, gas, and water saturation) are combined - which led to the wrong interpretation made in 2004. Moreover, 4D seismic interpretation also considers the information in recent 4D survey in 2008. Therefore, the 'Baseline Model' (see Figure 6.22a) which is referred to in this chapter, is just an intermediate product from the Norne asset team. The predicted pressure in 2001 can be used to manifest the configuration and connectivity between the segments in the baseline model. No communication is allowed in the baseline model between the C and G segment; while considerable pressure exchange can be seen between the G and H segment. Inside the G-segment, no major flow barriers or baffles were in place. Mismatches can be found between the predicted and measured pressure and water cut as shown in Figure 6.22b and 6.22c.

Possible flow pathway to G segment

The first change made to the baseline simulation model is to reproduce the connection out of G segment as highlighted in the *NCC* map. Moreover, the connection between G and H segments in the baseline model should be shut off. As per the principle of material balance, such changes made to the total volume of a segment in simulation model will have significant impact on the predicted pressure response. In order to show the effect of each revision, an intermediate model is also shown in which all of the connections from G-segment to the neighbouring compartment are closed. Nevertheless, the predicted pressure response from the intermediate model is much too high and exceeds the reasonable pressure limit in the Norne field. However, the overestimation of pressure by the intermediate model reinforces our belief in the existence of this connection. It is obvious that the updated model with the

connection out of the G-segment yields the predicted pressure that matches better with the measurements from PLTs (Figure 6.23).

Suppression of early water flooding by adding a high permeability zone

As explained in Section 6.9.1, it is interpreted that water from the down-dip injection of the G-segment should have first flooded the eastern part of the G-segment. In order to incorporate this information into the simulation model, a scenario in which a high permeability zone situated in the eastern G-segment is tested (see Figure 6.24b). Injected water from the down-dip injectors in this version of model has preferentially flowed through this high permeability conduit. As highlighted in the red ellipse in Figure 6.24c, most of the saturation change occurs in the eastern part of the segment. Moreover, the predicted water cut exhibits a better match with the observed in the late period. Nevertheless, the mismatch in the early stage is also clearly noticeable (Figure 6.24d). This suggests more modifications of the model are still needed.

(a)

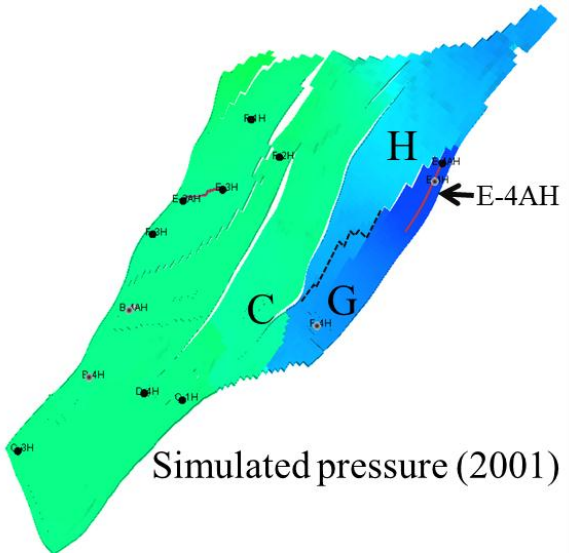

(b)

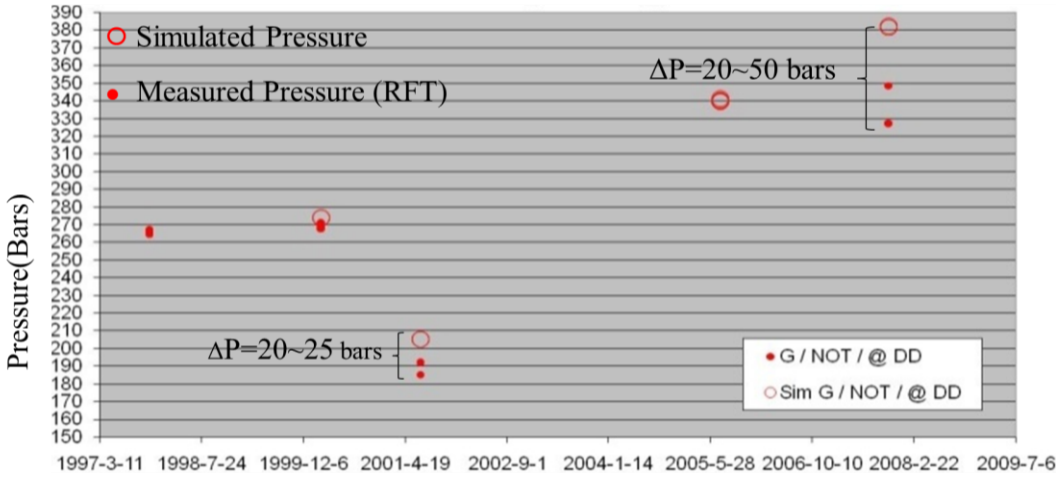

(c)

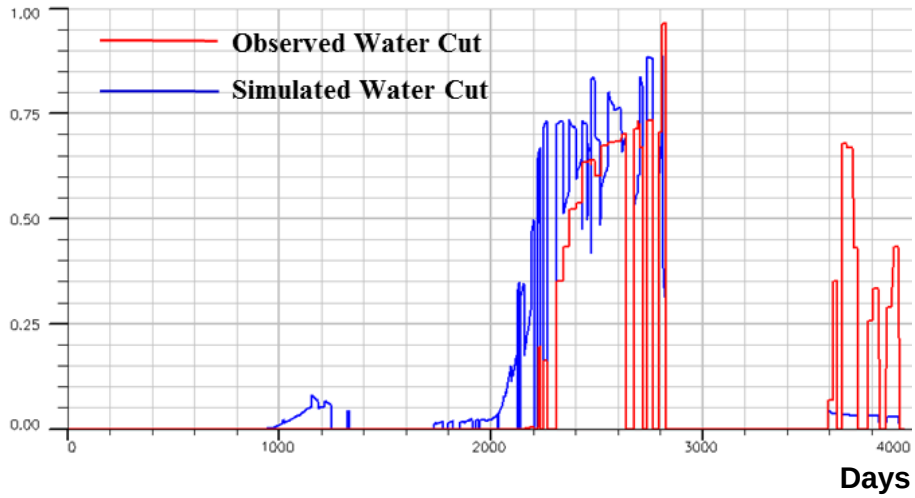

Figure 6.22 Connections between segments and the locations of major flow barriers in the baseline model can be visualized clearly in the simulated pressure map in 2001(a). The comparisons between simulated and observed pressure (b) and water cut (c) show clear mismatches.

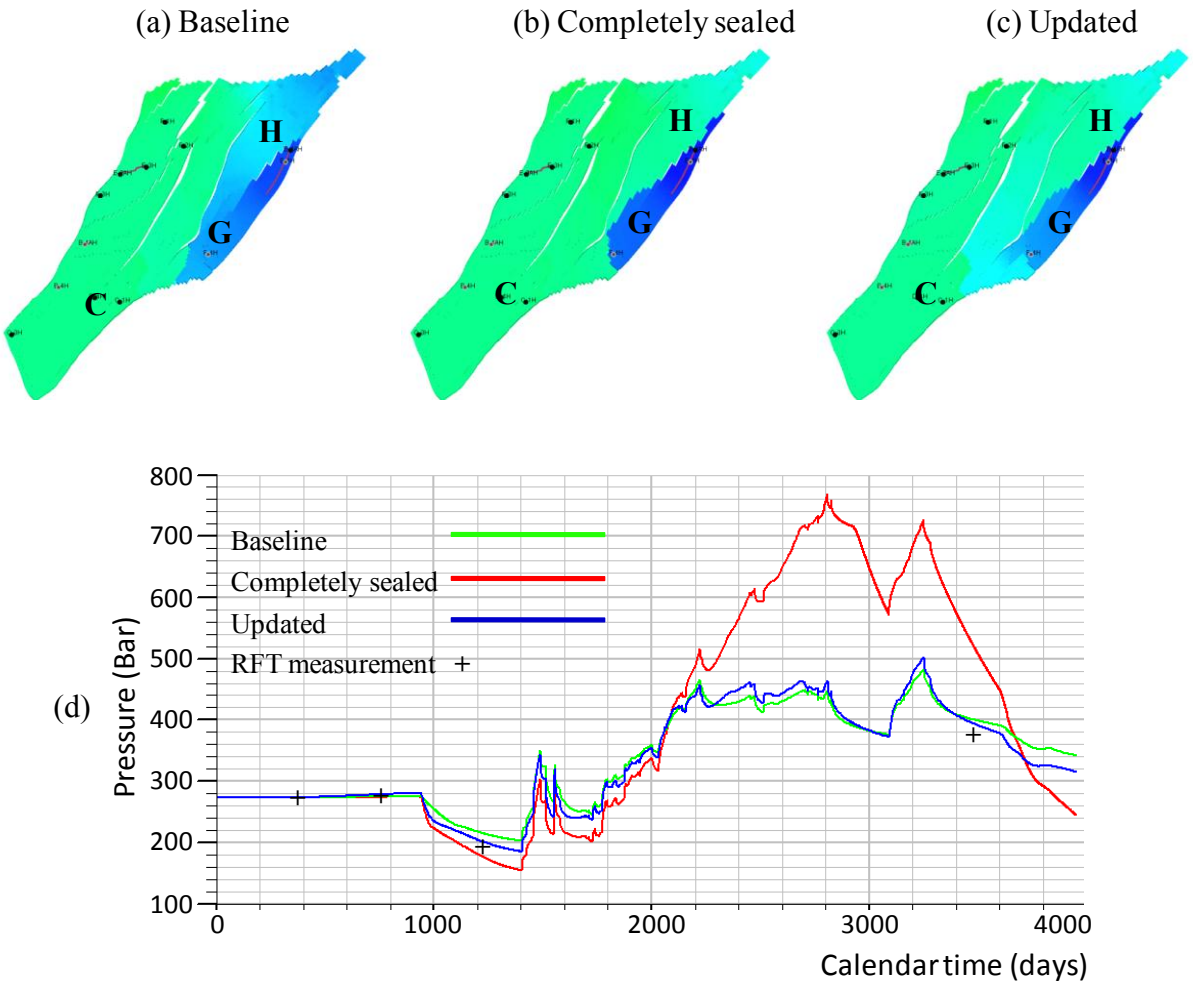

Figure 6.23 Maps of predicted pressure from (a) baseline model; (b) intermediate model with the enclosing faults of G segment all closed; and (c) updated model. The pressure predicted from the updated model exhibits a good match with the PLT measurements.

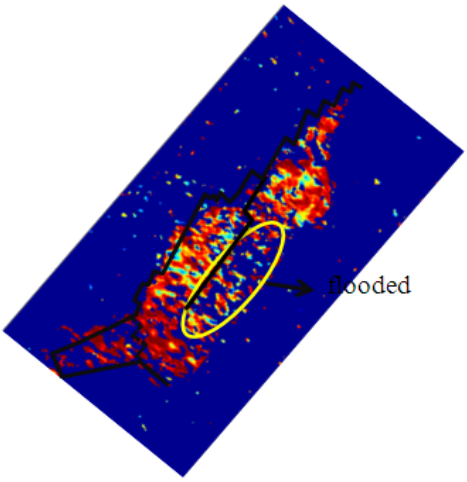

(a) NCC Map

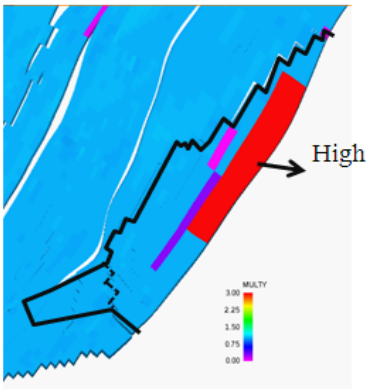

(b) Transmissibility Multiplier Y-direction

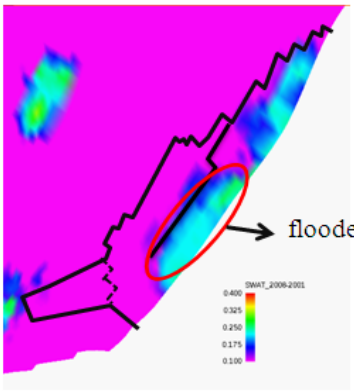

(c) 2008-2001 Predicted Saturation Change

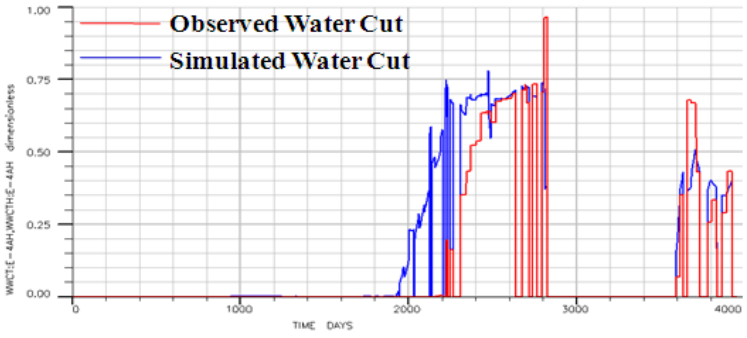

(d) Simulated versus observed water cut

Figure 6.24 (a) Low *NCC* in the eastern part of the G-segment (yellow ellipse) is interpreted to be related to significant saturation change. Based on this interpretation result, (b) a model featured by a high permeability conduit was made, and it predicts large saturation changes between 2001 and 2008 as shown in (c). (d) The simulated water cut shows a better match with the observed.

6.10 Business impact and discussion

Regardless of what seismic attribute is chosen to detect the change in the reservoir state, the 4D difference signature must always obey the principle of causality by virtue of its association with the fluid volumes input or extracted from the reservoir by the individual wells. The conventional 4D seismic interpretation approach focuses on each individual time-lapse survey, which fails to utilise the temporal information in multiple seismic surveys acquired over the Norne field. This chapter showed that the well-to-seismic correlation technique assembled the information from all the repeated surveys into a sequence of seismic differences at each image pixel and the *NCC* map generated by this method adds clarity to the interpretation of the 4D signal in the Norne field.

Furthermore, the *NCC* result opens up an opportunity to investigate 4D noise at the reservoir level. The factors that cause 4D noise are discussed following a visual comparison between the non-repeatability measures used in practice (e.g. *NRMS*) and the distribution of low *NCC* which is considered to be driven by non-production related 4D noise. The fact that only a poor spatial correlation exists between these represents a challenge when predicting the exact locations of the high noise level at the reservoir level. This has also been pointed out in recent publications, e.g. Domes et al. (2009) and Kommedal et al. (2005) – both suggest a need to carry out further studies on this issue.

By nature, the mapped *NCC* from well-to-seismic correlation is a new engineering-consistent attribute that integrates information in both well production and multiply repeated time-lapse seismic data. As shown in this chapter, the *NCC* map has lent support to the interpretation of 4D data previously made by the asset team in terms of reservoir connectivity and the distribution of reservoir fluids. The changes to the simulation model as suggested by the *NCC* map have also been made and justified by a better match between the observed and simulated historical production data.

Chapter7
Conclusions and recommendations for future research

7.1 Main conclusions on the well-to-seismic correlation technique

This thesis has provided a brief review on the current status of and development trend in the 4D seismic technology as well as practical challenges to the interpretation of 4D seismic data. It has been highlighted that the 4D signature should be interpreted in the context of well activity and the key being a seamless integration of these two data types whilst highlighting the causal link between them. Such understanding is the guiding philosophy in this thesis. Existing 4D-interpretation methods have been re-assessed in terms of how well the information from these two types of data can be fused and whether the causality between them can be used. A series of drawbacks recognised for each established methods has been discussed in this thesis. As a result, there is a need to develop a new technique which can provide a better solution to well-and-seismic integration as indicated in the thesis. This well-to-seismic correlation technique has been proposed in order to address some of the practical problems currently associated with 4D interpretation as discussed in Chapter 1. The method has been tested on data from a synthetic model of an idealised compartmentalised reservoir. The resulting NCC maps outline the edges of the compartments previously unknown to interpretation, and the structure in the NCC attribute better illustrates the non-sealing section of the barrier separating the compartments than standard amplitude attribute maps. The technique has also been applied to datasets from three fields in North and Norwegian Sea with encouraging results. From the results achieved, the following benefits of the application of this technique to the 4D interpretation have been recognised:

This technique integrates the production and the 4D seismic data in a direct manner without the need to implement 3D fluid flow modeling and seismic modeling (see Figure 7.1). This allows the information in well and the 4D seismic data be interpreted in a straightforward way without interference of the uncertainty from other sources. However, without the use of the simulation model, it is understood that the technique may not suit all engineering needs, but it is quite easy and quick to apply, and thus can serve as a fast approach for data inspection upon which direct reservoir management decisions are made.

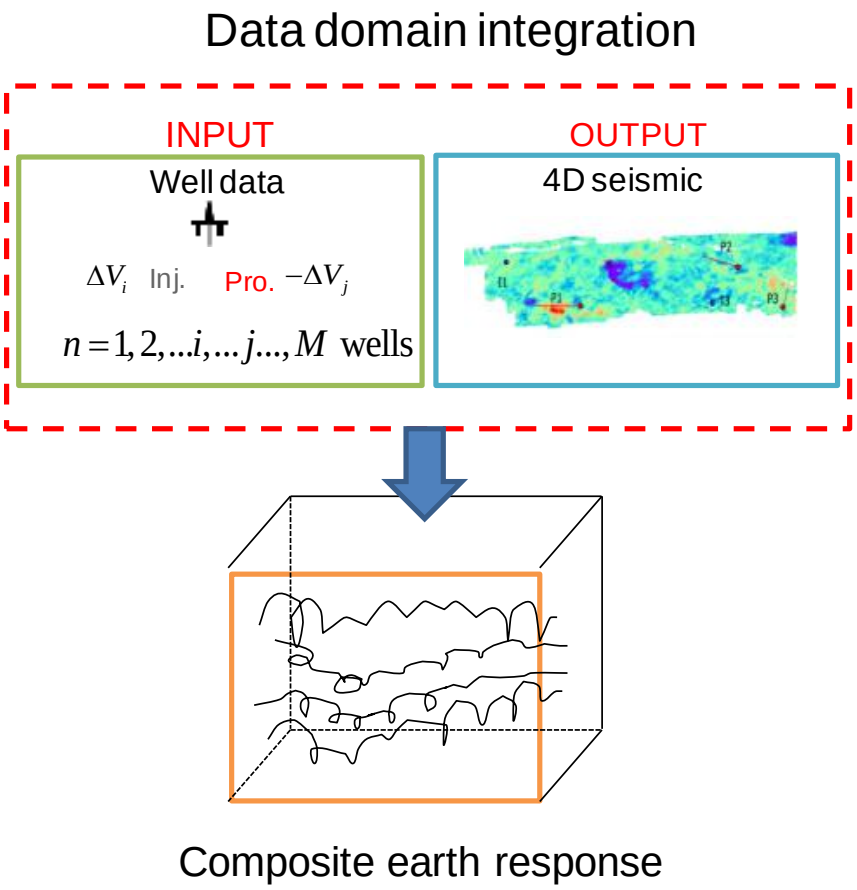

Figure 7.1 Direct integration of well and the 4D seismic information in the data domain via well-to-seismic correlation

2. By performing the correlation between unique sequences of volume rates and 4D signatures, the causal relationship between the well activity and the 4D response, which could only be determined subjectively, can be quantified. In another words, the well-to-seismic correlation technique can provide information on the origin of a particular signal observed on 4D signature. Similar questions to be asked by reservoir engineers are where the produced or injected fluid volumes come from or migrate to in the reservoir. Thus, the technique is very similar by nature to a biotechnology – DNA fingerprinting used to determine if two persons are related or un-related by comparing the DNA sequences. Moreover, this attribute is different from conventional seismic attributes as the NCC signatures contain both engineering and seismic information. It is the engineering-consistent nature of the technique that provides additional information of the reservoir previously undetected with conventional 4D attributes.

3. The above benefit has been demonstrated in the three field studies discussed in this thesis. In the Schiehallion and Norne examples, it has been demonstrated that reservoir connectivity that could not be unambiguously determined with conventional 4D attribute maps now have gained more clarification with the NCC maps. Further, it has also been shown in the Norne study that the prediction from the simulation model has been improved after new geological features identified in the NCC map have been incorporated. The results from the Valhall study have shown potential of the technique to separate the interfering responses of densely positioned wells so that the influence area of each individual well can be clearly resolved. This helps improve the understanding of the flow pattern between the wells so that drainage can be managed in an optimised way. In addition, the method has also shown value in revealing saturation responses obscured by changes due to pressure change as shown in the Valhall South Flank. This is achieved by utilising the fact that the 4D signals due to pressure and saturation changes respond differently to well activity.

4. Similar to other 4D seismic attributes, the interpretation of the NCC result should be validated to multi-disciplinary data. In this thesis, examples are shown where the information derived from the NCC result is validated by information from other sources. As example, the water flooded zone identified in the NCC map shown in Figure 4.19 shows a nice correlation with the predicted area of 20% water saturation change from the simulation model. Both of these areas are within a close proximity to the wells. The low NCC observed in Figure 5.13 which is interpreted as gas breakout has been validated by the result from another BP study based on overburden time-shift analysis. In the Norne study, the water flooded zone as suggested by the low NCC in the eastern part of the G segment in Figure 6.20(b) is confirmed by the newly drilled well data.

Meanwhile, the following issues need further discussion:

1. At the centre of this technique is an assumption that the 4D seismic signature should respond to the fluid volumes injected or produced in a linear manner. Indeed, the fields as shown in this thesis exhibit such a linearised behaviour due to the special reservoir settings. In the Schiehallion and Norne field, the linearity is considered to be the result of the established stable state of pressure in the closed compartments. In Valhall, the simple and linear ΔV - ΔA relationship is derived from empirical observation rather than vigorous theoretical derivation or a modeling study – this can be attributed to the special properties of reservoir chalk in the Valhall reservoirs. However, it should be noted that many other fields,

even other regions in the fields tested in this thesis (e.g. Schiehallion) illustrate a non-linearised ΔV - ΔA relationship due to many complicating factors such as partially communicating fault, which dramatically delays the total pressure stabilization over the entire reservoir as shown in Figure F.1. 2. In order for the technique to distinguish between the interfering responses of neighbouring wells, distinct well activities in terms of sequences of volume rates generated by the proposed method are required. For instance, the wells that possess distinctly different activation timings or shut-in timings are easy to separate in the NCC attribute. The examples from the three field applications in this thesis benefit from sufficiently complicated well activity.

3. Finally, most production and injection volumes used in this procedure to date have been measured as comingled flow, and as such the volume rates refer to the whole interval completed rather than the particular reservoir over which the seismic attribute is defined. This is the correct approach if the overall reservoir interval is thinner than the seismic wavelength, but will not be appropriate for thick reservoir sequences. This could be improved if 'smart well' technology (wells equipped with permanent downhole measurement equipment and valves) are in place to observe the flow rates in specific flow units. However such technology is not commonly available in many mature fields.

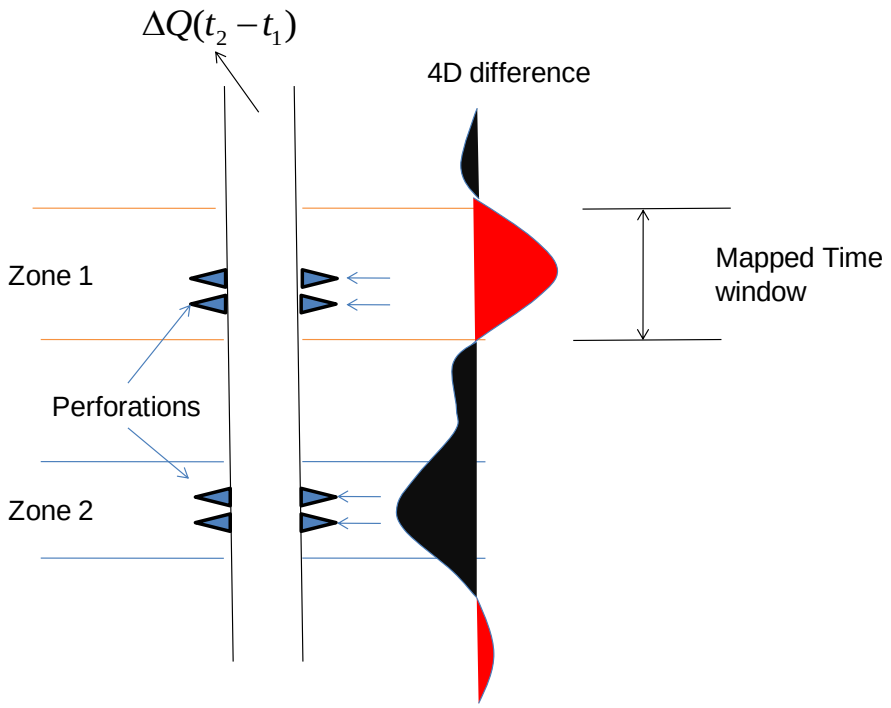

Figure 7.2 A schematic illustration of the situation where the proposed technique does not apply - production from multiple layers and the 4D seismic response.

4. In each example shown in this thesis, all the surveys available is used to compute the NCC map. A sufficient number of surveys are considered to be the prerequisite for the application of this technique. However, it is also noticed that the NCC signal will become 'smeared' when an extra survey with its redundant information is added for the calculation. This is particularly true when the 'independent' differences (the differences between monitor surveys) are included in the sequence of cumulative volumes. For keeping the statistical significance of the NCC result, the minimum number of survey to use in the analysis is 4 (with 3 surveys only two independent differences will be generated). As an extension, if the field of study is covered by more than 4 time-lapse surveys, it may be worthwhile testing the well-to-seismic technique using different combination of surveys so that the information content in the resulting NCC map can be maximized.

5. As discussed in the Chapter 1, it has gradually become a trend to acquire 4D surveys at more frequent intervals. This is underpinned by recent technological advances, e.g. permanent OBC system and short turnaround time for conventional streamer surveys. However, a new question pertaining to the minimum period between surveys arises: how often should we acquire 4D survey? As part of the effort to understand pressure-driven 4D signal, pressure behavior in the transience period is discussed in this thesis. As an example related to the Schiehallion field from the main text, if ϕ =28%, μ =3.2cP, ct=2.2.10-5psi-1, k=280mD and rb=900m, the time for the pressure disturbance to reach all the boundaries is approximately 26 days. The conclusion has some indication to the frequency at which 4D surveys need to be acquired if the 4D signal is pressure driven. If budget and technology permit, it is beneficial to implement seismic monitoring of the reservoir continuously. Such data will reveal the dynamic details in the evolvement of pressure disturbance and the reservoir heterogeneities it encounters. However, such data does not contain the very important information related to major reservoir compartments until significant regional pressure change occurs sometime after pressure stable state is established. In practice, choice needs to be made to determine what is the optimal period between surveys depending on the types of information expected to derive from 4D seismic, budget and historical use of 4D seismic.

6. In this technique, the correlation method has mainly been used as a screening technique with easiness and low cost to apply. The technique does not replace the conventional 4D interpretation approach but has proven its value as a data fusion method that provides

information otherwise that can not be obtained. More quantitative use of the NCC map may be possible in conjunction with the simulation model. For instance, the dynamic boundaries between the drainage areas of the major producers in Figure 5.11 can be compared to the same boundaries predicted by streamline simulation. The streamlines distribution is known to be mainly affected by permeability distribution therefore the information derived from the NCC map can lend help to improve the permeability distribution in the model.

7. It should be noted that the three fields tested in this thesis are characteristic of almost constant thickness of the reservoir. All the existing examples demonstrate that the correlation technique works nicely with mapped attributes. Depending on seismic attribute used, the thickness variation is anticipated to have some impact on the patterns in the extracted attribute due to the volumetric averaging nature of the seismic. The seismic attribute change is proportional to both thickness change and dynamic value changes (Falahat, 2011). The conventional vertical averaging of dynamic change may produce different patterns from the thickness-weighted dynamic attribute map (Figure 7.3). Nevertheless, a modeling work is needed to investigate the effect of the thickness if the technique is to be applied to thick reservoir.

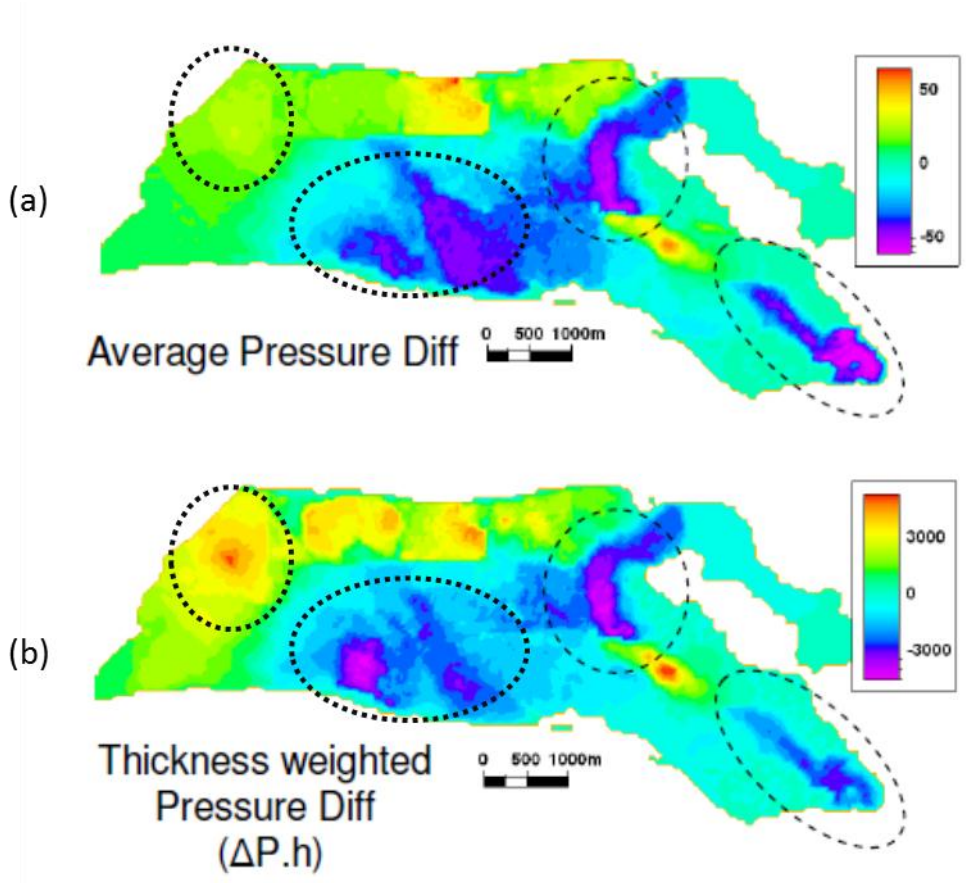

Figure 7.3 (a) Standard vertical averaging over a reservoir interval of pressure difference predicted by simulation model of a UKCS field, compared to (b) thickness weighted pressure difference map averaged from the same interval. The ellipses highlight the regions where noticeable disagreements exist.

7.2 Future work and potential applications

In this thesis, potential usage and limitations of the technique have been discussed. The three case studies and subsequent analysis of the NCC results could be used as a guideline for future applications of the technique. However, some further improvement should be made so that the technique can be even easier to apply and be integrated with other engineering or geophysical methods.

7.2.1 User friendly interface

To facilitate the integration of this technique into an integrated reservoir management workflow used in daily work, BP Norge has made some effort to develop a user-friendly interface for this code. The software is now capable of generating correlation panels in which a normalised sequence of 4D signature and well activity are displayed after specifying a location on the attribute map and selecting a well on the user interface. It also offers various options to calculate NCC maps at specified thresholds and using different seismic attributes (e.g. observed compaction, amplitude) in different areas of the field (see Figure 7.4). As stated in Chapter 3, prior to interpretation, the NCC map needs to be thresholded by a minimum threshold to guarantee the NCC signature is statistically significant and the actual thresholds employed are usually higher than the statistically-determined minimum threshold to resolve the wells with similar activity. However, in practice the threshold used is usually determined by trial-and-error to guarantee the NCC map is at its most informative. The user-friendly interface is found to be extremely useful for achieving the optimised threshold. However, this software is very much Valhall field oriented. In order to apply it to other fields, some adaptions are needed such as adding I/O modules that allow data and results to be read/saved directly in the formats accepted by other geophysical/engineering software.

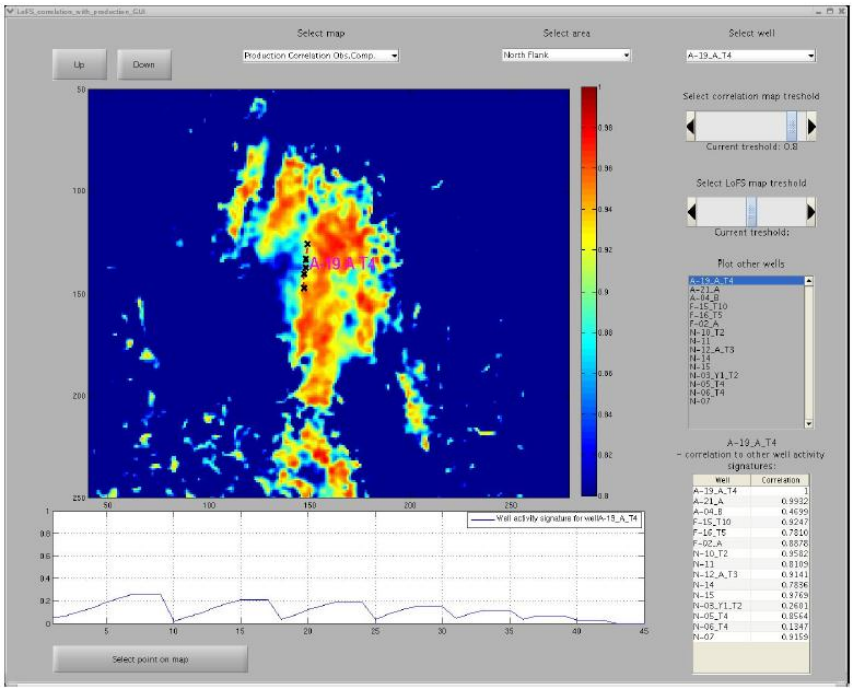

Figure 7.4 An illustration of the user-friendly interface made by BP Norge to the ETLP well-to-seismic code. The selection of wells, NCC threshold and attribute can now be made interactively.

7.2.2 **Application to other similar fields**

As discussed in Chapter 1, it is an industrial trend to shoot 4D surveys at increasingly frequent intervals – it is anticipated this will broaden the use of the technique. Take Statoil as an example, this company has reported its plan to further reduce the response and turnaround time for 4D seismic acquisition for the continued 4D projects on 75% of the fields in its portfolio so that more surveys can be acquired in a more cost-effective and efficient way (Sandø, Munkvold and Elde, 2009). This ambition is shown in Table 7.1 which summarises the existing and planned 4D surveys over Statoil fields.

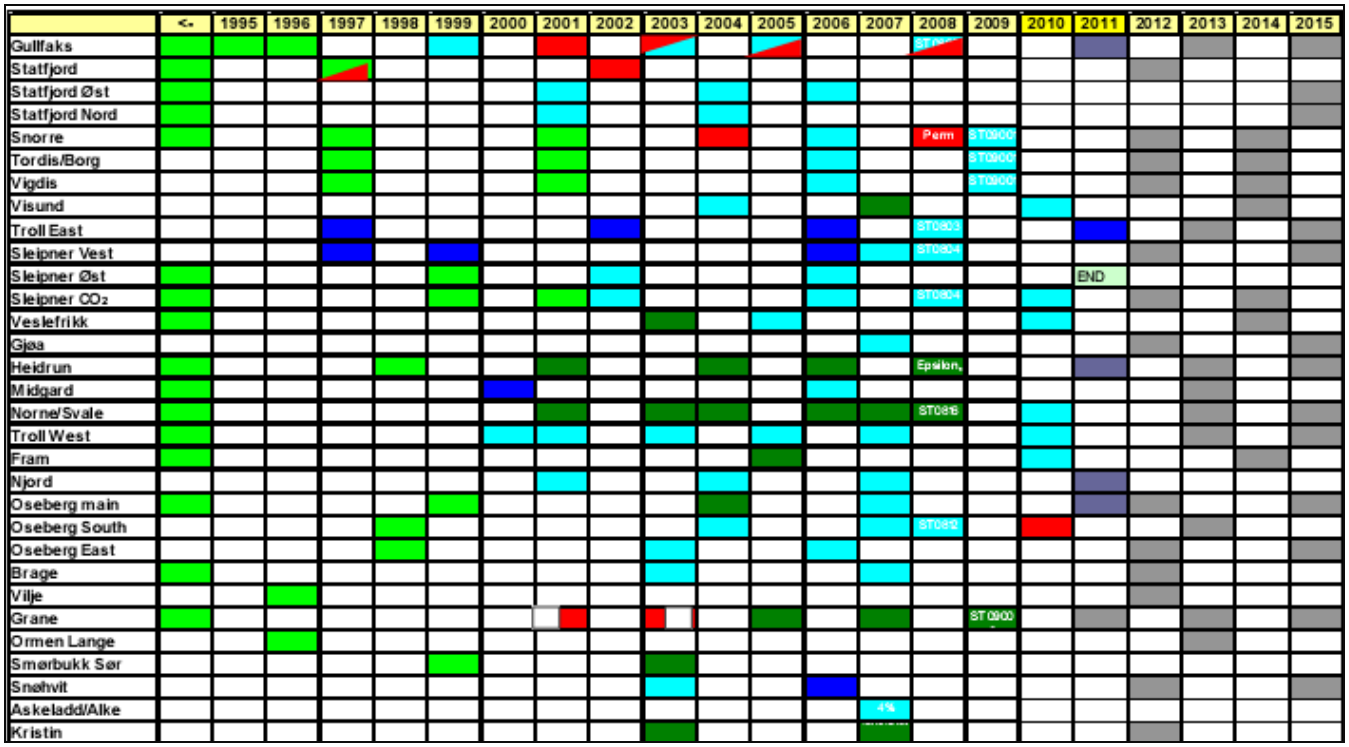

Table 7.1 The Statoil 4D ambition – acquisition and planning of 4D surveys over its fields owned (after Sandø et al., 2009).

Although the testing of the technique on the 4D data from 'high spec' towed-streamer surveys has shown some satisfactory results, it is understood this method is suited for highly repeatable data from a permanently installed OBC system. Following the success of the LoFS system on the Valhall field, the definition of long term seismic monitoring as part of the concept of Permanent Reservoir Monitoring (PRM) has obviously gathered momentum via a wider acceptance and application by companies around the world. For instance, the most recent application are on the Clair field (Foster, et al. 2008; Ricketts & Barkved, 2011), the Snorre field (Morton et al., 2009; Thompson, 2011), Jubarte field (Thedy et al., 2011), Gournay-sur-Aronde gas reservoir (Meunier 1998) and the Ekofisk field (Hoeber et al., 2011). The data yielded by the PRM systems installed on these fields are considered to be ideal for the testing and application of the technique in the future.

7.2.3 4D seismic noise

In the Norne study, low NCCs were interpreted to be 4D noise caused by poor repetition of the acquisition geometries between repeated surveys. Conventionally, prior to 4D

interpretation a comparison is usually made between the section of source-to-receiver positioning errors and that of NRMS, which in turn is used to guide the understanding of 4D signals derived from the data corresponding to the reservoir interval. The study shown in Chapter 6 has given an insight into the direct impact of non-repeated conditions on the 4D signal in the difference data. Although the analysis is dependent on special reservoir settings which yield a linear 4D response with respect to well activity, the study still implies that the NCC result may be useful for designing engineering-consistent processing sequences by which a desired type of 4D effect can be enhanced. This is driven by the view that processing sequences should evolve to better suit 4D needs through its integration with engineering activities (e.g. Lynch, 2011). Further, it may also lead to separation of 4D noise from production-related signals in the 4D data, and if this happens it would significantly increase our understanding of the 4D noise and signal.

7.2.4 Apply to other seismic attribute

In this thesis, all the NCC examples are calculated from only two types of seismic attributes: time shift and amplitude change. However, multiple seismic attribute can be used for the well-to-seismic correlation. Different features in the NCC map based on different seismic attribute gives insight into different dynamic changes in the reservoir. As an extension, a much broader range of attributes can also be considered if available. For instance, the saturation and pressure change may have different weight in the near and far stack data. Instead of amplitude attribute derived from a time window around reservoir reflectors, inversion attributes such as acoustic impedance may also be good candidate for the application of the technique. It is anticipated that some unconventional geophysical data such as gravity and Electro-Magnetic (EM) data should also correlate with well activity.

7.2.5 Pressure and saturation discrimination

As discussed in Chapter 2, overlapping of pressure and saturation signals is a problem that constantly challenges 4D interpretation. Existing methods rely on the petro-elastic relations to interpret pressure and saturation from the 4D signal. I think it may be possible to decipher pressure and saturation from 4D data using well-to-seismic correlation as they respond to the same well activity in different ways. For instance, if the 4D signal is driven by pressure

changes which may correlate to production volumes, the residual uncorrelated changes may be interpreted as either water or gas saturation change. In the three examples shown in this thesis, low correlations are observed in a background of 'highs', e.g. in Valhall the lows are interpreted as the regions of gas breakout and the results are validated by results from other studies carried out by the asset team.

7.2.6 Reservoir connectivity

A good knowledge of reservoir connectivity is almost certainly a key to optimising reservoir management. However, there is almost certainly a level of uncertainty associated with the interpretation of reservoir connectivity due to lack of information. The field applications in this thesis have demonstrated that the interpretation uncertainty from reservoir connectivity may be reduced by integrating data from multiple seismic surveys. For example, Floricich et al. (2008) overlapped trace-to-trace coherence between multiple vintage surveys for enhanced barrier interpretation in the Schiehallion field. With a similar principle, the seismic-to-seismic correlation technique has been developed (Appendix F) and the potential of this technique should be explored (i.e. what do the regions revealed represent? How can use them effectively to update the simulation model?) in future studies.

7.2.7 Application to the simulation volume

Instead of correlating seismic to the well activity as shown in this thesis, there is also a possibility to correlate the 4D signature to the mapped volume changes of each cell in the simulation model. It is an invalidated observation that the reservoir body which contributes more to the flow should cause a higher magnitude of dynamic changes in pressure and saturation (e.g. fluid expansion in the near-wellbore region contributes more volume than the areas in-between the wells). Thus, such kind of correlation between seismic and the simulation model may produce the NCC map similar to those shown in this thesis from well-to-seismic correlation, but the NCC will instead indicate the disagreement of simulation and the 4D seismic.

APPENDIX A

A review on non-repeatability between seismic surveys

To repeat seismic surveys is more complicated than thought. It has been understood that non-repeatability noise primarily originates from three sources: acquisition parameters, environmental conditions and processing workflows. To obtain high quality 4D seismic data, acquisition parameters required to be repeated include, not only those (such as acquisition geometry, streamer length, line spacing, receiver spacing) recognised to be important for conventional 3D seismic surveys but also those less obvious, such as sail direction and the characteristics of source signatures, receivers, equipment and field crew. Changing environment onshore, such as urban development, water table velocity seasonal changes, or offshore, such as tidal level, swells, ocean current will further compromise our ability to place the sources and receivers at the exactly the same location as the previous survey. Further, it is believed the noise in the 3D seismic data such as '*multiples'* will cancel out in the 4D data given that all the conditions for the surveys are perfectly repeated. The non-repeatability will lead to residual spurious information due to non-repeatable noise between 3D vintages. To repeat the processing sequences is also essential to generate meaningful 4D signals. This usually consists of the use of the same algorithms, velocity model and processing parameters for every pre- and post-stack processing step. As a result, the chance that the 4D difference is caused by different processing rather than the true changes in the reservoir can be ruled out.

It should be noted that seismic acquisition and processing in on- and off- shore environments can be very different. So are the non-repeatability factors concerned. For instance, data quality for onshore surveys is usually compromised by the presence of surface waves (ground roll) which is not significant in the offshore streamer data. Table 1.2 and 1.3 summarise studies of various non-repeatability noise published in the literature for marine and land seismic respectively. Generally speaking, most successful 4D projects are marine surveys; and land data tend to contain a higher noise level and conditions are relatively more difficult to repeat (Houston & Criss, 2006). Strong ground roll, diffractions of seismic energy by the near-surface unconsolidated soil, topography, diverse noise due to human activities will lead

to spurious energy in the final 4D signatures. Despite an increasing number of successful land 4D surveys published in the recent years, all the data analysed in my PhD thesis are from marine surveys.

Paper(Author, year)	Non-repeatability noise
Ross & Altan (1997), Morice et al. (2000), Naess (2006)	Non-repeatability of source-receiver position
Musser et al. (2006), Saunders et al. (2004)	Source signature + positional non-repeatability
Laws & Kragh (2002)	Swell noise
Bertrand & MacBeth (2005), Celine et al (2001)	Water column velocity change and tidal
Malme et al. (2005)	Overburden layers
Morice et al. (2000)	Source array and geophone fidelity

Table A. 1 Published papers and online materials concerning non-repeatability factors for marine surveys

Paper(Author, year)	Non-repeatability factors
Faure & Spitz (2006)	Weather change, ground roll
ION (2011)	Environmental change, receiver, near surface condition positioning(http://www.iongeo.com/Solutions/Land_4D/)
Meunier & Herculin (2003)	Positioning error, geophone coupling variation, ground rolls
Tura et al. (2006)	Near surface coupling, shot-and-receiver positioning
Yun et al. (2007)	Source type change, geometry, bin size, fold, processing sequence
EL-emam et al. (1998)	azimuth, offset, field statics, different phase conversion filter
Soroka et al. (2005)	Non-repeatable 3D noise, dust environmental change, source characteristics change

Table A. 2 Published papers and online materials regarding non-repeatable factors for land surveys

APPENDIX B *NRMS* as a measure of non-repeatability noise

In the last decade time-lapse seismic technology has been applied and proven useful in many fields worldwide. This trend is driven by the increasing use of dedicated time-lapse seismic acquisition and processing. However, there are still many 4D projects relying on old vintage data acquired at the time without 4D applications in mind. No matter whether a 4D project involves vintage data, minimisation of the non-repeatability noise is always the theme of 4D data acquisition and processing. Therefore, it is necessary to quantify the level of non-repeatability noise in the 4D seismic data so that it can be better controlled. The most commonly used metric to quantify the likeness of two traces in different generations of seismic data are the normalized root mean square (*NRMS*) value (Kragh & Christie, 2002). For a given time window $t_1 - t_2$ for traces a_t a_1 and b_t a_2, the *NRMS* value is defined as the RMS of the difference between a_1 a_t and a_2 b_t divided by the average of the RMS value of each, written in the following form

$$NRMS = \frac{200 \times (RMS(a_t - b_t))}{RMS(a_t) + RMS(b_t)}, \qquad (B.1)$$

where the *RMS* is defined as

$$RMS = \sqrt{\frac{\sum_{t1}^{t2} a_t^{\,2}}{N}}. \qquad (B.2)$$

N is the number of samples in interval t1-t2. The range of *NRMS* metrics is 0 to 200%. *NRMS* values for special cases are calculated by (Kragh and Christie, 2002):

- Two traces with random noise: *NRMS*=141%;
- 180 degree reverse phase or one trace with all zeros: 200%;

- One trace half the amplitude of the other: 66.7%.

However, it should also be noted that *NRMS* is just an indirect measure of 4D noise. Indeed, the value of *NRMS* is calculated for a defined window above the reservoir, while the reservoir interval is the true region of interest for the subsurface team. Using *NRMS*, it is not possible to precisely predict the location and impact of the non-repeatable conditions, expected to be observed on the attribute maps extracted from the reservoir interval – suggesting that it may be problematic to distinguish meaningful signal from noise. This is considered to be one of the key issues to successful interpretation and analysis of 4D seismic data by Foster (2008). A number of published examples based on different acquisition and processing technologies are ranked with their *NRMS* values and plotted against calendar time. A trend in which survey repeatability is gradually improved as the result of new technologies and meticulous operation is shown as the decreasing average *NRMS* level for a number of published cases (Figure B.1).

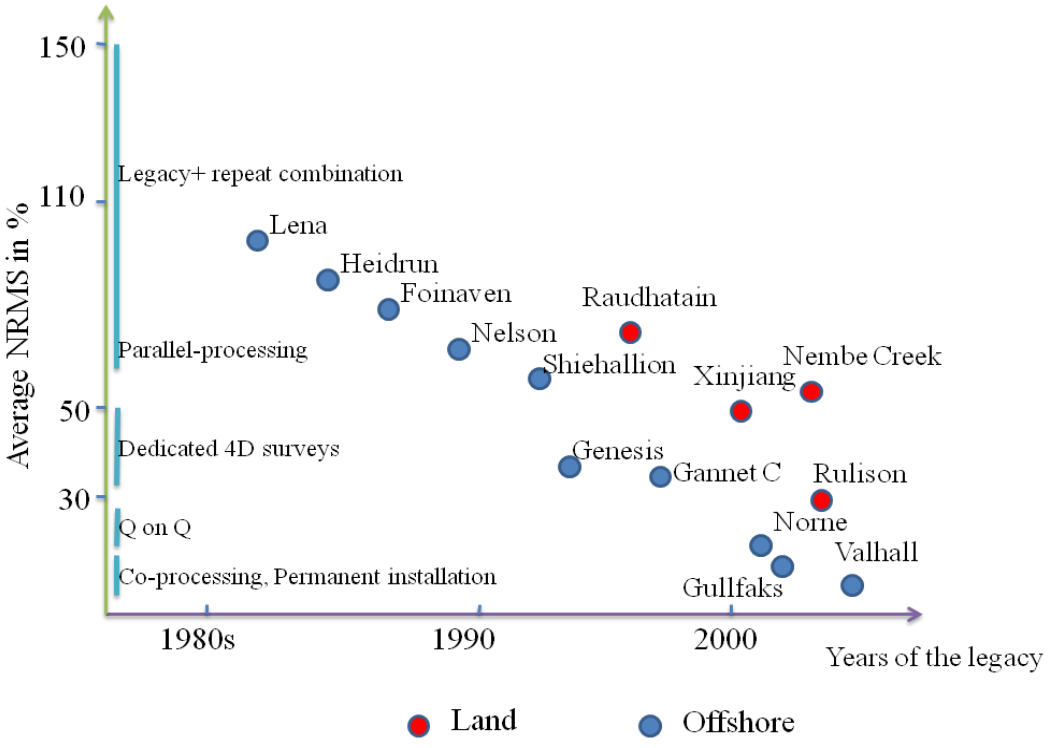

Figure B. 1 Published 4D project examples, which are ranked according to their *NRMS* values and times being shot. It is noticeable that the recent 4D data acquired with advanced technologies such as Q marine and OBC have very low *NRMS*, thus very good quality and offshore surveys are better repeated than land.

Appendix C Linking cumulative volume to pressure change: basic concepts

The objective of this appendix is to define a relationship between the pressure change, ΔP (as detected by the time-lapse seismic) and the change in the cumulative fluid volume ΔV produced and injected over time intervals similar to those of most time-lapse seismic surveys (typically years). For the purpose of this work, pressure changes are induced in the reservoir by the production of a volume of oil or water, or the injection of water or gas. It is shown below that the relationship between the well activity and the pressure changes is governed by equations normally used in the context of well testing. However it should be noted that well testing concerns itself mainly with pressures measured *in the borehole over periods of hours or days at most*, whilst our application considers pressure changes *in the inter-well space over tens of months or several years*. This difference in time scales and measurement location affects the choice of solution for our particular objective.

When the well is put on flow at time *t=0* the oil production rate is initially sustained by the expansion of fluid immediately around the well-bore. This expansion is accompanied by a reduction in pressure and a pressure gradient is established. Fluid from the next outwardly adjacent annular zone flows towards the wellbore and the process of fluid expansion and pressure decline is extended further into the reservoir. A progressively increasing zone of pressure drawdown develops out from the active well. The evolution of the pressure around and away from each well is governed by the pressure diffusivity equation, the particular well production/injectivity, well configurations, and the boundary conditions associated with the reservoir. Consider a well which has started to produce from an initially untouched reservoir at virgin pressure. In terms of the physical phenomena involved, several distinct time intervals must be distinguished (Figure C.1).

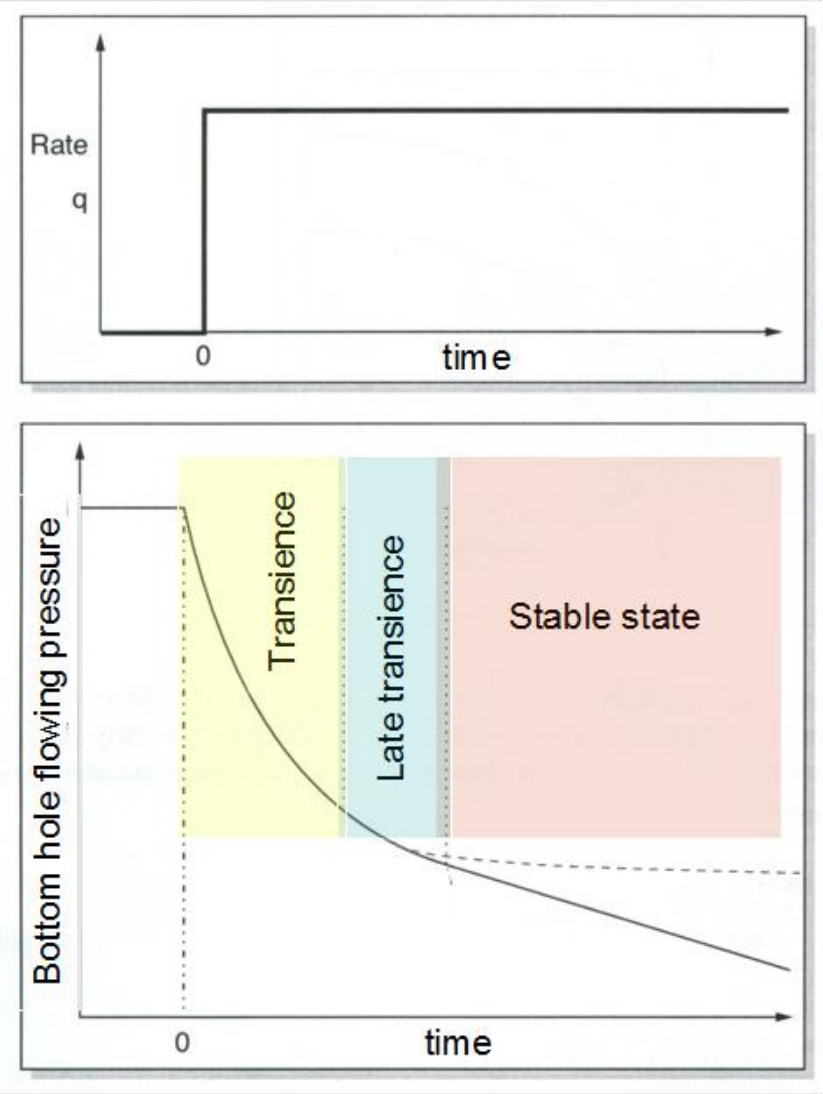

Figure C. 1 The regimes are defined by the different boundary conditions and different solutions to the problem of pressure evolution in the reservoir. Exact time periods are important when considering well testing versus 4D seismic monitoring. Full line and dashed line refer to different types of stable state flow.

At first a period of transient behaviour persists, the exact duration of this depending upon the diffusivity constant and hence the properties of the reservoir around the well, but being independent of the conditions and geometry of the external reservoir boundaries. During production, any disturbance in the wells such as changing the volume rate, or opening or closing a well to flow, will create a corresponding transient. This is analogous to the activation of an electrical switch and the subsequent electrical current settling into a stable state. In this early stage regime the pressure-transient solution to the diffusivity equation (see Section C.1 below) is relevant. This is also the region used for interpreting the wellbore

pressure changes in most well test literature (see for example, Dake 2001). Following this interval is a complicated region of late transience, which is seldom analysed in the literature due to the difficulties involved with obtaining an interpretable solution. Finally, when the pressure disturbance has propagated at last to the outer boundaries of the reservoir or reservoir compartment, the evolution of pressure settles down into a stable equilibrium state. In this *stable state*, the behaviour conforms to a well-defined predictable form dependent on the boundary conditions. It is this latter condition that is appropriate for the 4D seismic analysis in our study (see section C.2).

C.1 Pressure transient behaviour and well testing change

Consider a single producing well flowing at a constant rate q into a homogeneous and isotropic porous reservoir of uniform thickness h but infinite lateral extent. The reservoir is considered sufficiently large that the external boundary conditions are distant so that open flow boundary conditions can be applied laterally, although it is closed and sealed by the top and base of the reservoir. Until the start of the production the reservoir is initially at a constant pressure $P_{initial}$. Upon production, flow to the well is mostly radial and pressure drops rapidly quite close to the wellbore and more slowly away from the well. In this condition, the local oil flow varies from a maximum at the borehole to zero at the external boundary. The evolution of the pressure at an arbitrary observation point a radial distance r from the well and at time t is governed predominantly by the single phase, linearised diffusivity equation in a cylindrical coordinate system

$$\frac{\mu\phi c_t}{k}\frac{\partial P}{\partial t} = \frac{\partial^2 P}{\partial r^2} + \frac{1}{r}\frac{\partial P}{\partial r} \tag{C1}$$

where μ the viscosity, k the permeability, ϕ the porosity and c_t the total rock and fluid compressibility. In this equation all the rock and fluid properties are assumed to be pressure independent, and the fluids only slightly compressible. Treating the well as a line source and initial conditions, the solution to this equation is non-linear and given by (for example, Van Everdingen and Hurst 1949)

$$P(r,t) = P_{initial} - \frac{qB_O\mu}{2\pi kh} Ei\left(\frac{\phi\mu c_t r^2}{4kt}\right) \tag{C2}$$

where Ei is an exponential integral defined by $Ei(x) = \int_x^\infty \frac{e^{-s}}{s} ds$ and B_O is the oil volume formation factor. An approximation of (C2) arises for the case when $x = \phi\mu c_t r^2 / 4kt < 0.01$

$$P(r,t) \approx P_{initial} - \frac{qB\mu}{2\pi kh} \ln\left(\frac{1.781\phi\mu c_t r^2}{4kt}\right). \quad \text{(C3)}$$

This form of the equation is commonly used as the basis for well testing interpretation. Values of x for a range of radial distances and times for fixed permeability, porosity and fluid properties are typical of Schiehallion (Stephen and MacBeth 2006). From this it can be concluded that in the case of well testing, despite the times being only a few hours, x is typically less than 0.01 as all measurements are made at the well, so that r is the wellbore radius. Well to well interference tests, where the pressure is measured in an inactive observation well at some distance r from the flowing well, are taken over larger times and thus the approximate solution can thus be used for interpretation. If barriers or discontinuities defined by faults, stratigraphic pinchouts or shale barriers, are encountered, then small perturbations in the pressure decay profile of (C3) can be noted and used to infer their location and reservoir significance.

C.2 The stable state and global reservoir pressure

The stable state is mostly ignored by well testers, but is of value to those wishing to pursue decline curve analysis. The velocity with which the pressure disturbance moves through the reservoir is determined by the porosity, permeability, viscosity and total compressibility. The leading edge of this pressure disturbance, the pressure front, is usually defined loosely as the location where the pressure is 1% of the initial value $P_{initial}$. The time to propagate a radial distance r_b to the nearest boundary is (Stewart and Whaballa, 1988)

$$t \geq 497.6 \frac{r_b^2 \phi\mu c_t}{k}, \quad \text{(C4)}$$

where μ is in cP, c_t in psi^{-1}, r_b in metres, k in mD and t in days. As an example related to the Schiehallion field from the main text, if ϕ =28%, μ =3.2cP, c_t=2.2.10^{-5}psi^{-1}, k=280mD and r_b=900m, (C4) gives approximately 26 days. Note that the time at which the stable state solution becomes important, and a measure of the extent before the system is disturbed by the

outer boundary condition, is usually 1 to 1.5 times this number. Interestingly, the departure from the transient period can be used in transient well testing to determine the permeability of the reservoir if r_b and the reservoir properties are known. Importantly, the time period over which seismic surveys are repeated is always much greater than the duration of the transients. It thus appears that for most 4D surveys the steady state condition is immediately applicable.

The steady state solution of the diffusivity equation is observed by recognising the stability of the pressure distribution over time. In a balanced waterflood, for example, the total rate of water injection (and aquifer influx if appropriate) is equal to the total rate of oil produced such that for the pressure, *P*, at any location throughout the reservoir volume of interest the condition $\partial P/\partial t = 0$ is fulfilled. In many reservoir situations there is no natural water influx and in the absence of fluid injection, oil production results solely in the expansion of oil in place and the reservoir pressure is reduced. When the pressure disturbance propagates outwards and encounters the outer sealing boundary of the reservoir compartment, no flow is allowed and this leads to an overall pressure decline. The rate of pressure decline is obtained by equating the production rate, $q = \partial V/\partial t$, at the well to the overall volume rate of fluid expansion within the drainage region *V* and considering the total compressibility $c_t = -\frac{1}{V}\left(\frac{\partial V}{\partial P}\right)$. This leads to the relation

$$q = -c_t V \frac{\partial P}{\partial t} \tag{C5}$$

or

$$\frac{\partial P}{\partial t} = -\frac{1}{c_t V} q\,. \tag{C6}$$

Thus, if we produce a reservoir compartment at a constant rate *q*, after the period of transience the rate of pressure decline $\partial P/\partial t$ for all radial distances from the well is constant and uniform. Note that the pressure profile in the reservoir still remains relatively complex, but the pressure drop is quite simple and predictable. The condition for which there are regular changes with time, but pressure still declines as in (C6) is known as the semi steady state in well testing literature. From (C6) we observe that the rate at which the pressure declines depends on the compartment volume, and its total compressibility and the well rate.

C.3 Connection between pressure change and the wells

By rearranging (C6) and integrating over the time period ΔT between a baseline and monitor seismic survey, the corresponding pressure drop ΔP at all distances and locations in the compartment from the well (and hence the 4D seismic response) can be written in terms of the difference of the cumulative volume produced $\Delta V_f = q\Delta T$

$$\Delta P = -\frac{1}{c_t V}\Delta V_f . \tag{C7}$$

Thus, the pressure drop in the reservoir is proportional to the cumulative volume of oil produced from the formation. This equation can be extended to include *M* wells injecting into (constant positive rate q_I) and *N* wells producing from (constant negative rate q_p) the reservoir by applying the principle of superposition (Dake 2001) which permits linear combinations of solutions

$$\Delta P = \frac{1}{c_t V}\left(B_W \sum_{i=1}^{M} q_i^I + B_O \sum_{j=1}^{N} q_j^P \right)\Delta T. \tag{C8}$$

The produced volumes at the surface must be adjusted by formation volume factors, B_w and B_o, to the formation volumes. Furthermore, superposition states that if each well experiences a different sequence of constant rates, the equation can be generalised further

$$\Delta P = \frac{1}{c_t V}\left(B_W \sum_{i=1}^{M}\sum_{k=1}^{m_i} q_{ik}^I \Delta T_{ik} + B_O \sum_{j=1}^{N}\sum_{l=1}^{n_j} q_{il}^P \Delta T_{jl} \right). \tag{C8}$$

where m_i and n_j are the segments of times for the i^{th} injector and j^{th} producer over which the rates are held fixed. In the limit, the summations over time may be replaced by integrals. The equations are only valid provided the stable state holds. Thus, if several repeated 4D surveys are shot, the pressure drop measured at the time of each surveys can be related directly to the cumulative well data only if the surveys are not shot during a transient period (that is, the well startup, closure, or rate change). Interestingly, this predicts that for a constant rate throughout the period ΔT and for all repeated surveys, the pressure drop is proportional to the duration of the time period and can be correlated directly to the duration between surveys. If

the wells are producing at a constant rate during the time at which all surveys are being shot, then the pressure drops (and hence seismic) simply respond and are correlated to the length of the time period. If the wells change their rates frequently, then the pressure drops in the compartment can be directly correlated to the cumulative volumes produced and injected (the large bracketed term on the right hand side of (C8)). In practice this term may become an integral over time due to the small-scale well fluctuations. In the main text, this correlation can be utilised to understand the pressure signal for a sequence of many time lapse seismic surveys. Importantly, this equation holds regardless of the well positioning in the compartment, the shape of the compartment and the exact nature of the boundary conditions (the steady state solution naturally follows by setting $\Delta T = 0$).

Appendix D
Seismic-based petro-elastic model for pressure

The 4D difference for near offset data between 2001 and 1992 (see Figure D.1a) was interpreted as the combined effect of pore pressure decrease due to production and gas coming out of solution. The magnitude of these two effects is controlled by the physical properties of the rock frame and the fluids. If the ratio is defined as α , their relationships to the observed amplitude change ΔA can be written in the following format:

$$\frac{\Delta A\_gas}{\Delta A\_pressure} = \alpha , \tag{D1}$$

also

$$\Delta A = \Delta A\_gas + \Delta A\_pressure , \tag{D2}$$

where ΔA_gas and $\Delta A\_pressure$ are amplitude changes due to gas breakout and pressure change respectively. The ΔA is the observed 4D seismic difference which is a combined effect of ΔA_gas and $\Delta A\_pressure$. Thus a simple conversion can be performed between ΔA and $\Delta A\_pressure$ as the following equation shows

$$\Delta A\_pressure = \frac{\Delta A}{(1+\alpha)} . \tag{D3}$$

The conversion factor α can be estimated by calibrating the observed 4D attribute change to the estimated pressure-driven 4D change between 2001 and 1992 at well F-4H.

$$\alpha = \frac{\Delta A}{\Delta A\_pressure} - 1 . \tag{D4}$$

The PLTs installed in the well F-4H measured a pressure drop from 275bar to 200bar between 2001 and 1992. The 4D attribute difference caused by this 75bar pressure drop can be roughly determined using the petro-elastic relationship for stress-dependency of the rock framework. The measurement in the laboratory suggested a second order polynomial or exponential relation between change in pressure and acoustic impedance change. The polynomial form was written as following (Floricich, 2006):

$$, \Delta A\_pressure = a\Delta P^2 + b\Delta P \quad \text{(D5)}$$

where, ΔP is the pressure change, as recorded between the baseline survey amplitude and the repeat survey amplitude. The coefficients *a* and *b* are controlled by physical properties of rock framework. It is believed that the 4D seismic amplitude differences between the baseline survey and Q surveys acquired in 2003, 2004, 2006 and 2008 contain only pressure-driven 4D signatures. The coefficients *a* and *b* can be determined by calibrating the amplitude changes in an area around wells to pressure values from reservoir simulation in the same area. *Equation D5* can be applied to each well measurement at different times when seismic surveys are acquired. In this case, for 2 selected wells in 4 difference maps (2003-2001, 2004-2001, 2006-2001 and 2008-2001), a non-linear system of 8 equations and two unknowns (coefficients *a* and *b*) is obtained for each 4D seismic attribute. To solve this non-linear system, many optimization algorithms can be used. To avoid the result being biased by a particular algorithm, three different algorithms (Particle Swarm Optimization, Simulated Annealing and the Genetic Algorithm) were simultaneously used to compute the coefficients *a* and *b*. The same results: a=0.00014 and b=-5.20 were obtained. Hence the stress sensitivity curve can be plotted (see Figure D.2) and an estimation of pressure-driven 4D change between 2001 and 1992 ($\Delta A\_pressure = 176.4$) can be obtained. Meanwhile, the observed amplitude change between 2001 and 1992 around F-4H is -380 ($\Delta A = -380$). Using *Equation D4*, the value -3.1542 for the α factor can be solved. According to *Equation D1*, this is to say that pressure and gas out of solution have the opposite effect on the 4D amplitude change and the effect of the latter is almost three times stronger than the former in the near offset seismic data.

The map of the pressure-component of amplitude change between 2001 and 1992 (Figure D.3a) can thus be derived from the observed amplitude-change map (Figure D.3b) using the relationship depicted in *Equation D3*. The derived pressure component is then added to the baseline map to roughly estimate the amplitude level in 2001 without the fluid saturation

effect. A comparison between the observed 2001 amplitude map and the converted map with only pressure effect is shown in Figure D.3c and d. It should be noted that the estimation of this pressure-oriented 2001 amplitude map is a very rough one. This may not be able to reproduce the exact pressure-driven 4D signatures and noise pattern associated with the non-repeatability between 2001 and 1992 surveys. Therefore, this may introduce errors into the derived noise pattern at the reservoir level as discussed in Section 6.5.

This converted 2001 amplitude map is then used as one of the input maps to our well-to-seismic correlation algorithm to generate *NCC* maps. Since the converted 2001 amplitude map is also subject to uncertainties associated with the estimated value of the α factor, the *NCC* maps based on different values of the α factor are generated. It was found that these results are not so different from the main features (Figure D.4). This is attributed to the fact that the sequences of 4D signatures for different α factors hold more similarity after normalisation when the absolute amplitude level is removed. Thus, the dynamic reservoir interpretation based on the *NCC* map discussed in Section 6.6 is considered to be robust.

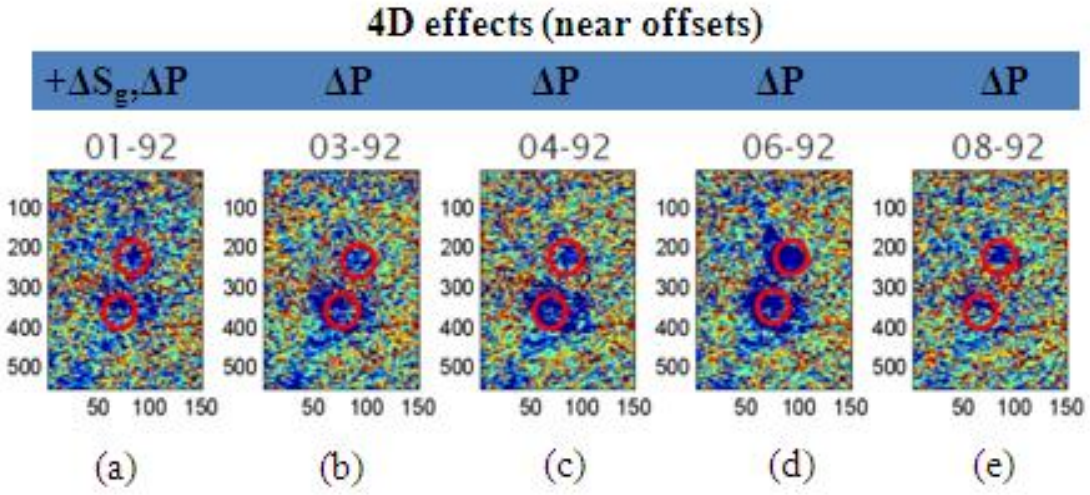

Figure D.1 Near offset differences between the time-lapse and baseline surveys. Except for the difference between 2001 and 1992 (a), the subsequent differences (b), (c), (d) and (e) are thought to contain only pressure-driven signals because all the gas in the reservoir in 2001 had gone back into solution by 2003 as indicated by the observed GOR.

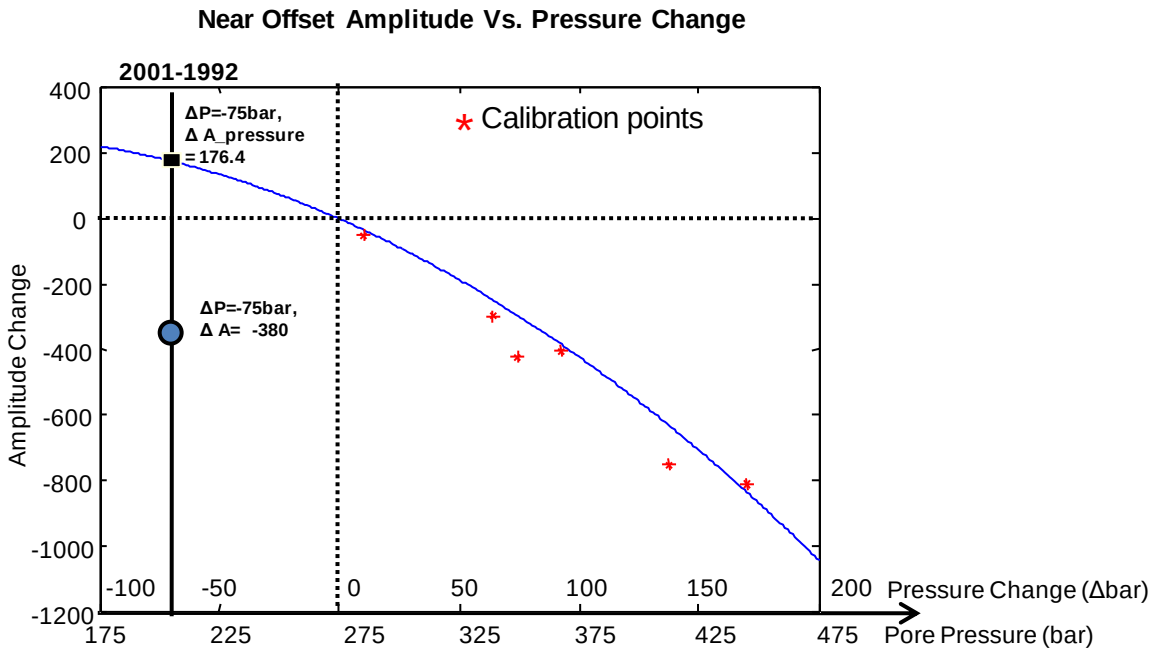

Figure D.2 Stress-dependency of the rock frame curve defined by the petro-elastic parameters determined from real time-lapse seismic responses using the calibration method proposed by Floricich et al. (2006). The estimation of the pressure component of the amplitude change is 176.4, in contrast to the value of the observed amplitude change (-380).

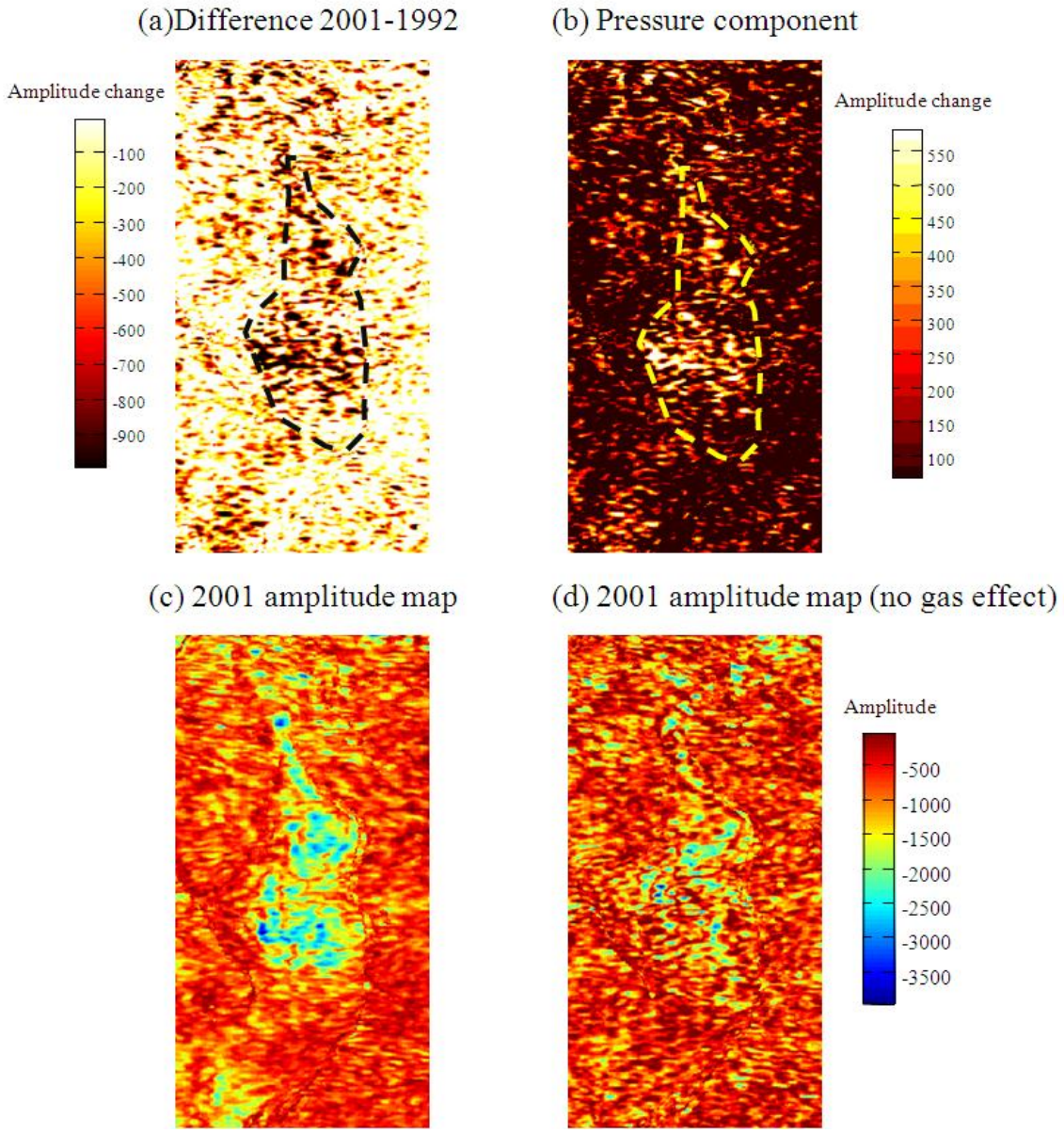

Figure D.3 Resulting maps in the process of removing the gas effect from the observed amplitude difference map between 2001 and 1992. (a) Negative amplitude changes (effective signal); (b) Amplitude change due to pressure changes; (c) Observed amplitude in 2001 and (d) Amplitude in 2001 that only contains pressure-driven 4D signals.

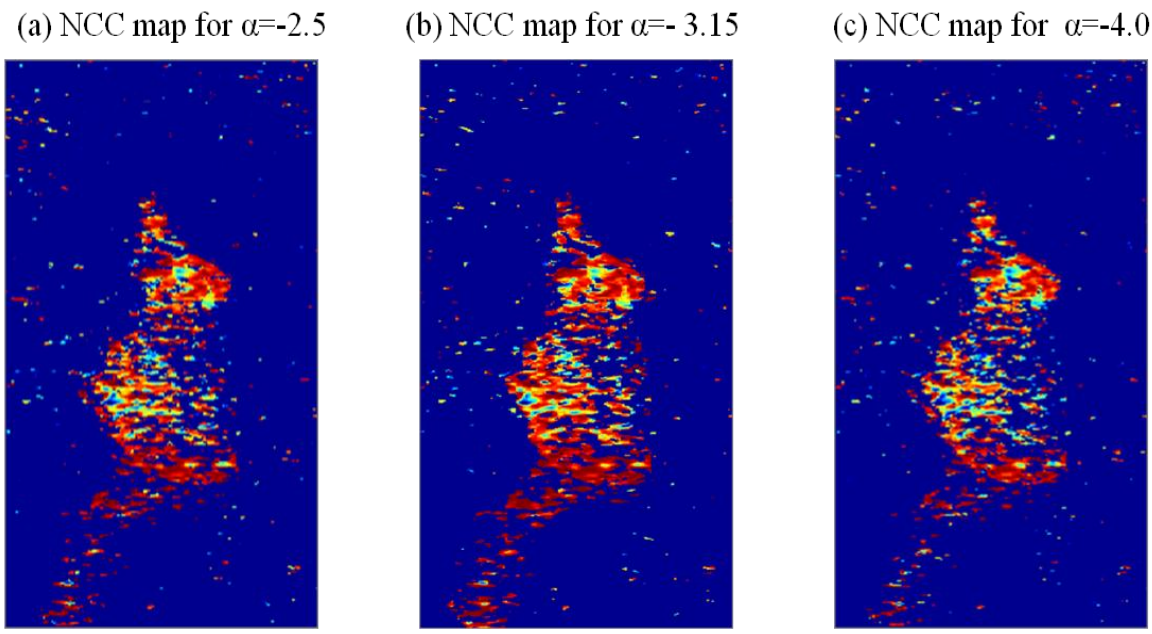

Figure D.4 The *NCC* results calculated for various values of the α factor.

Appendix E
Frequency analysis for the 4D signatures

An early attempt was made to understand the characteristics of the 4D signal and noise in this PhD thesis using frequency analysis of the mapped 4D signatures. It had been noticed that there is some scattered energy in the 4D signature for which it may be difficult to achieve reasonable interpretation. Thus, it was postulated that the low-frequency components of the 4D signal may contain more effective information of the dynamic reservoir change than the high-frequency components. Thus spatial frequency filtering based on the *Fourier transform* is applied to the observed field dataset.

E.1 What is spatial frequency?

Spatial frequency is the foundation of a broad range of image processing techniques, and is a measure of the distribution and character of the signal in the space, characterised by periodic troughs and peaks in a similar way to the one-dimensional time-series signal. Along a particular section, the 2D image distribution $I(x_i, y_i)$ can be represented by a 1D waveform $g(x_i, y_i^{'})$, which can be decomposed using *Fourier transform* into different constituent frequency components in the same way as if the signal is in a similar 1D time sequence (e.g. pressure vs. time) as shown in Figure E.1 (Boreman, 2001). The SI unit for *spatial frequency* is cycle/m, which is defined by two components in the *x* and *y* direction: $\xi = 1/X$ and $\eta = 1/Y$, where X,Y are spatial periods of the waveforms along the *x* and *y* directions respectively).

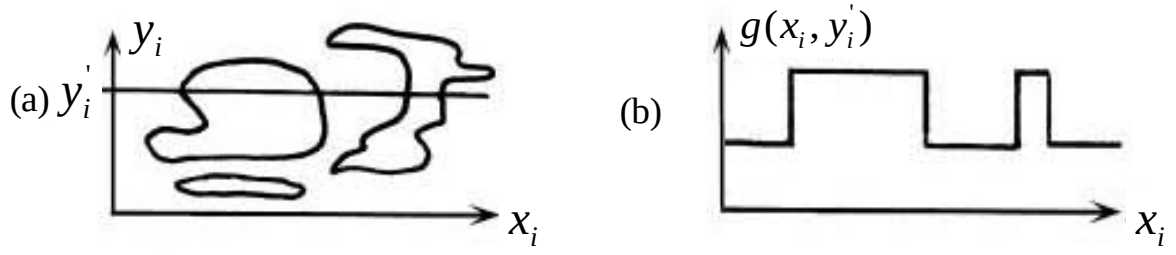

Figure E. 1 (a) Schematic illustration of a two-dimensional image distribution; and (b) one-dimensional profile along a selected cross-section (after Boreman, 2001).

E.2 Two-Dimensional Fourier Transform

In this study, the frequency analysis of the 4D signature is performed using the *fast Fourier transforms* (fft2) in the image processing toolbox of Matlab. If the 2D image is expressed as a real matrix A

$$A = \begin{bmatrix} a_{11} & \cdots & a_{1N} \\ \vdots & \ddots & \vdots \\ a_{M1} & \cdots & a_{MN} \end{bmatrix}, \tag{E1}$$

The Fourier transformed image A can be described as

$$Y = fft2(A) = \begin{bmatrix} y_{11} & \cdots & y_{1N} \\ \vdots & \ddots & \vdots \\ y_{M1} & \cdots & y_{MN} \end{bmatrix}, \tag{E2}$$

where

$$y_{rs} = \sum_{m=1}^{M}\sum_{n=1}^{N} a_{mn} e^{-\frac{2\pi i(m-1)(r-1)}{M} - \frac{2\pi i(n-1)(s-1)}{N}} \tag{E3}$$

To get the image back from its frequency representation y_{rs}, the inverse Fourier transform needs to be applied:

$$y_{mn} = \frac{1}{MN}\sum_{r=1}^{M}\sum_{s=1}^{N} y_{rs} e^{+\frac{2\pi i(m-1)(r-1)}{M} + \frac{2\pi i(n-1)(s-1)}{N}} . \tag{E4}$$

This formulation expresses an image as a combination of different *spatial frequencies* y_{rs}, phase and magnitude. Similar to the one-dimensional case, the *fft2* applied to the 4D signature will also deliver the magnitude and phase information of the frequency space function. To analyse the information for a specific range of frequency, a filter designed to restrict certain constituent frequencies is needed and applied in the spatial frequency domain.

Depending on the purposes of different studies, specific frequency bands may be of interest. Therefore, images will need to be filtered by '*low-pass*', '*high-pass*' and '*band-pass*' frequency filters.

E.3 Application to the observed signature

The spatial-frequency analysis is performed using the amplitude difference map from a selected area of Field A (see Figure E.2a). The field is composed of a typical turbidite reservoir rock, characterised by excellent porosity and permeability. The study area, approximately 6km×3.5km, is relatively simple in terms of geological structure and reservoir heterogeneity. Producers (blue circles) and injectors (blue dotes with black arrows) have been densely positioned in order to achieve maximum recovery. At many wells, the 4D signals are observed to correlate nicely with the well locations. Predominantly, strong 'hardening' signals are observed around the injectors placed in this area, indicative of a rising water saturation level as a result of water injection (Figure E.2b), e.g. the signals around I1, I2, and I3. The 4D response of pore pressure change is believed to be weak compared to that of saturation change since the excellent intra-reservoir hydraulic connection can quickly equilibrate any localised pressure changes occurring around a particular well. Therefore, around producers in this area, there appears to be no noticeable 4D signal, which can be attributed to production effects such as pressure depletion and gas coming out of solution. The red polygon outlines the areas of high source-to-receiver positioning errors, indicating that softening signals (in red) observed around the producers (e.g. P3, P8 and P6) are caused by poor repetition of the acquisition geometry between the monitor and baseline survey rather than other alternative explanations (e.g. gas breakout effect).

Figure E.3a shows the low-pass filtered (*0–6.84 cycles/km*) image of the 4D signature shown in Figure E.2a. Clearly, the water flooded zone around each injector indicated by the low-frequency 4D signals appears much more readily recognisable for interpretation. Interestingly, the low-frequency component reveals the larger extent of the water flooded areas than those in the original 4D signature. In addition, the size and geometry of the water flooded zones seem to be consistent with the prediction from the simulation model (Figure E.3b). There is little uncertainty associated with the estimate of reservoir thickness over this particular area, and it is believed that simulation predicted area of water flooded zones is fairly accurate due

to fundamental law of material balance in terms of injected water. In another words, it seems that the water flooded zones tend to be under-estimated using the original 4D signature since only the regions with water saturation change above a certain threshold can be seen in the *full-frequency* 4D signature. Intuitively, the threshold for detectable saturation change by 4D seismic should be controlled by the noise level in the data and the properties of the reservoir rock.

E.4 Summary

Although the saturation-driven signal seems to be enhanced in the low-frequency component and the volumetric estimation of injected water volume is more consistent with the production data, these results do not necessarily lead to the conclusion that the noise in the 4D signature has to be of high-frequency. For instance, the non-repeatability noise (noticeable as strong and 'patchy' soften 4D changes) distributed along the acquisition direction within the red polygon shown in Figure E.2a, has contaminated in the low-frequency component. In addition, the extent of the regions where water saturation changes occur is obviously dependent on the band-width of the low-pass filter. The smaller bandwidth that the filtered signatures occupy, the more contiguous the signal and noise appear (e.g. the water flooded zones appear to be larger in size on the *0–6.84 cycles/km* than *0–13.68 cycles/km* map). Therefore, special care is needed if one wishes to interpret 4D signals in terms of the constituent frequency components as the 4D signal and noise may not be distinguishable in a straightforward manner in frequency domain. However, this study also shows the potential of frequency analysis as a useful tool to deliver enhanced 4D results within a certain frequency width that might exhibit improved consistency with the engineering data.

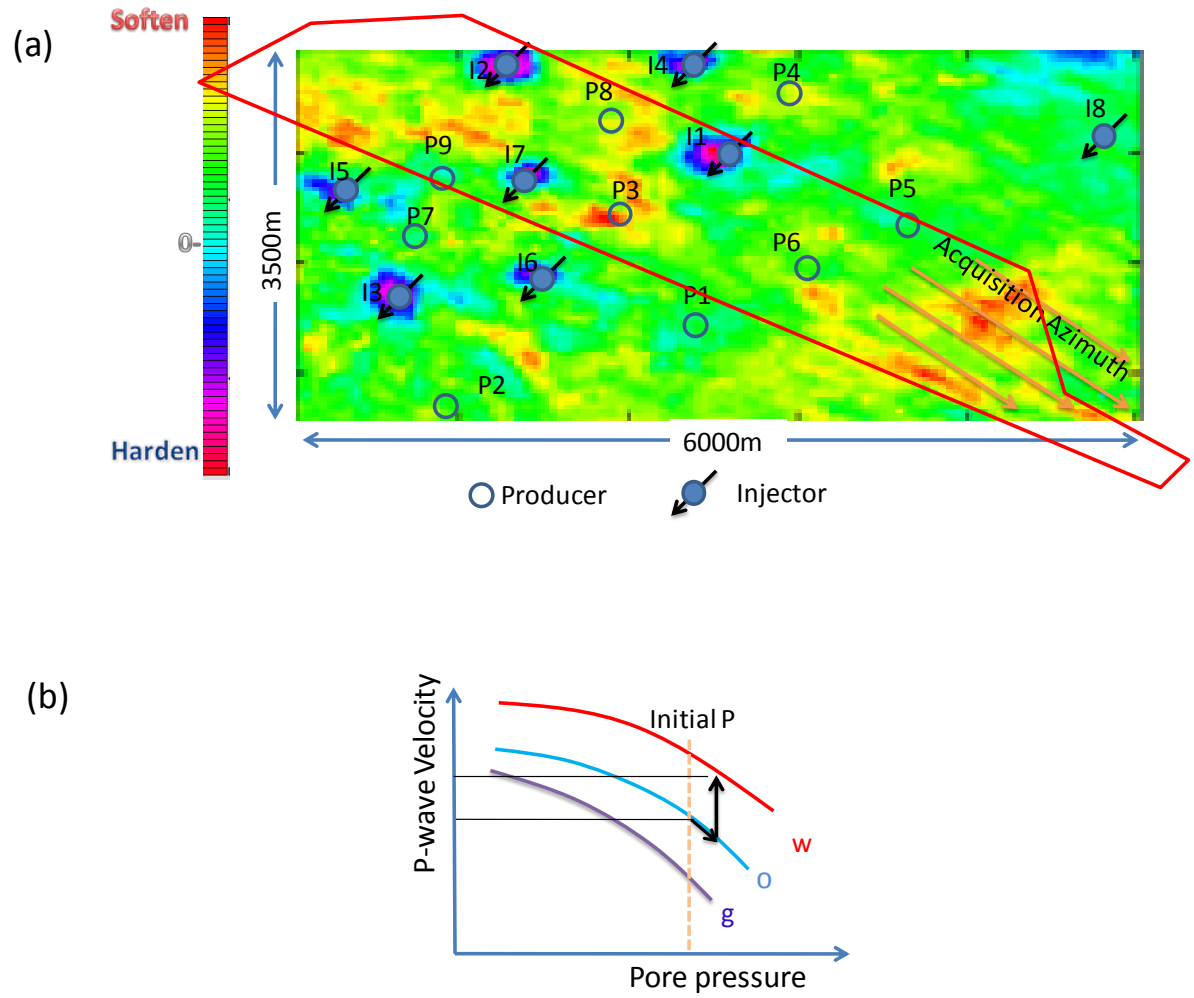

Figure E. 2 (a) Amplitude difference map over a selected area of Field A. (b) A schematic illustration of P-wave velocity change due to water saturation increase occurring around the injectors shown in (a).

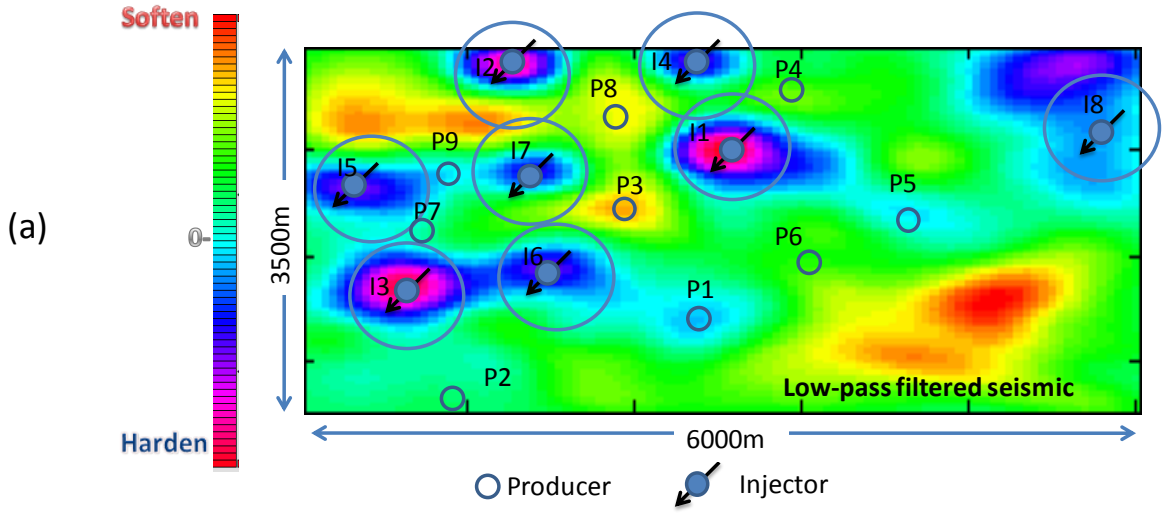

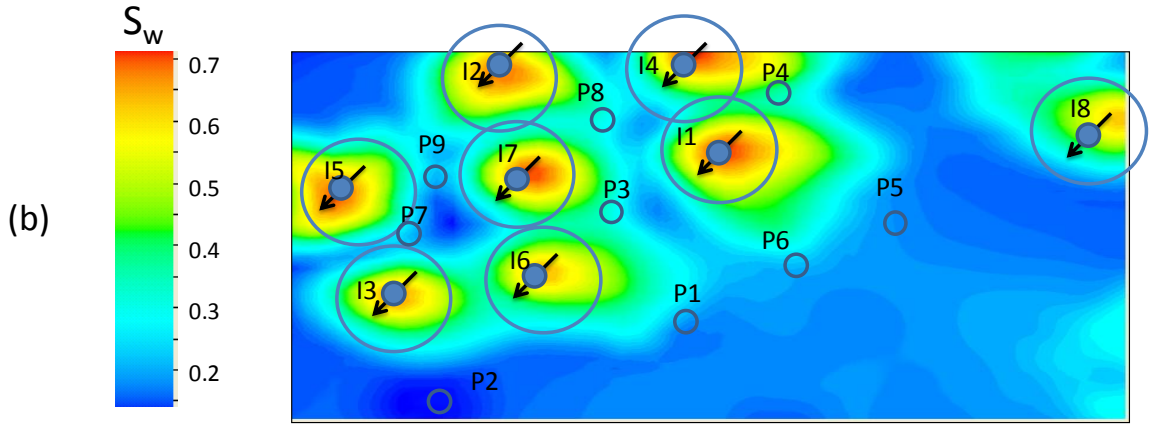

Figure E. 3(a) The Low-pass filtered 4D signature (b) Water saturation changes predicted by the simulation model.

Appendix F
A natural extension: Seismic-to-Seismic correlation

F.1 Pressure regime in communicating compartments

As discussed in Appendix C, the pressure regime in a closed fault block undergoes a transient period before reaching the stable state, during which the pressure profile shifts as a whole and at the rate in proportion to the total fluid volume produced from the compartment. The pressure transience usually only takes a short period of time so that the well-to-seismic correlation technique proposed in this thesis should be applicable and the results useful for enhanced interpretation of reservoir connectivity by highlighting flow barriers and baffles. However, it is also noticed that compartments are usually non-sealing on the edges and a low level of hydraulic connection may generally exist between these compartments. In this situation, the pressure response of production at a given time and location in the reservoir may be difficult to predict as it is not only controlled by the activity of the wells in the particular compartments of study but also those in neighbouring compartments. In other words, it may take a long time for pressure to stablise between all partially connected compartments. For instance, Figure F.1 shows an idealised reservoir composed of two compartments separated by a non-sealing fault with a transmissibility of 0.05. The reservoir parameters used in this model are exactly the same as those used for the model study shown in Figure 3.4. For simplicity, there is only one water injection well located in the centre of the left-hand compartment and injecting at a constant rate. Two observation locations are arbitrarily selected in both compartments at which the derivative of pressure versus time are calculated (see Figure F.1b). The blue curve corresponds to pressure derivative at the observation location in the left-hand compartment, and the purple curve to that in the right-hand compartment. The physical meaning of the pressure derivative is the rate at which pressure is changing at a given time. Clearly, the pressure regime induced by water injection into such reservoir settings is very dynamic and behaves distinctly for different sides of the flow barrier. However, it is noticeable that for a constant rate, pressure will eventually reaches equilibrium after approximately 3000 days.

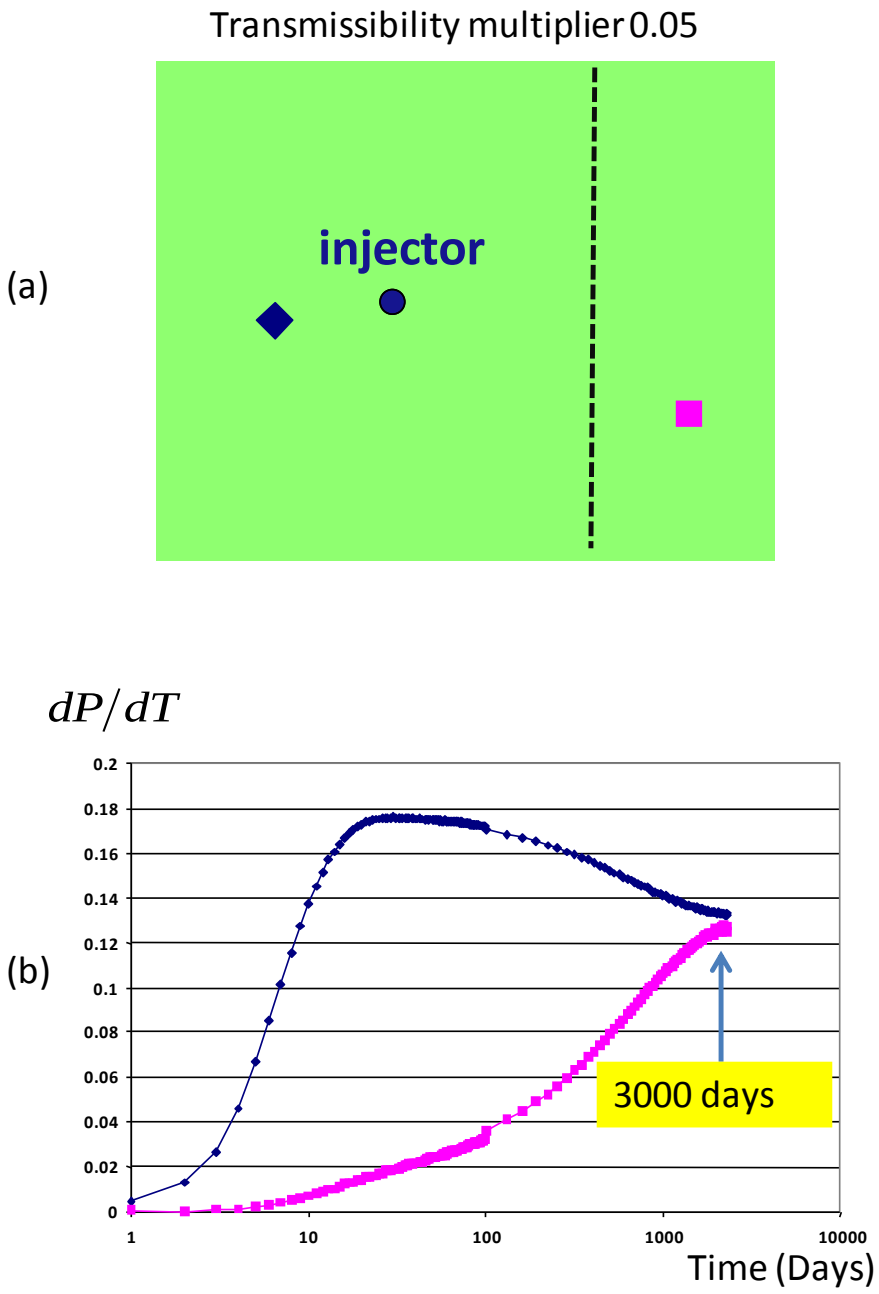

Figure F. 1 (a) The simulation model for an idealized reservoir composed of two compartments of different sizes that are separated by a non-sealing fault (transmissibility in x direction equals to 0.05).

F.2 Seismic-to-Seismic correlation

A method was proposed by Floricich (2008) who performed coherence analysis in a trace-to-trace manner on a time-lapse seismic data cube from five monitor surveys. This method delineated subtle reservoir barriers that were undetected in 3D seismic interpretation by analysing the temporal behavior of 4D signatures through production time. Indeed, flow barriers between compartments with 4D signals results in 'sharp discontinuities in trace-to-

trace coherence of the time-lapse seismic cube'. In other words, his work suggested that the traces on one side of the flow barriers in time-lapse seismic cube tend to possess a reasonably high level of correlation. In Chapter 3, this well-to-seismic correlation technique is proposed. At the centre of this method is the construction of the time sequences of volume rates and 4D signatures for all possible time intervals (Figure F.2). Instead of correlating all the sequences of 4D changes to the identical sequence of cumulative volumes of a well/well group, it is possible to correlate them ($\Delta A_k = \Delta A(x_i, y_i, \Delta T_{k=1\ldots P})$) to a reference sequence derived from 4D seismic changes at a fixed (reference) location ($\Delta A_k = \Delta A(x_{ref}, y_{ref}, \Delta T_{k=1\ldots P})$). Preferentially, the reference location is selected close to the well of study as it is in our interest to know the connected reservoir bodies controlled by this particular well. This idea stems from the modelling study which demonstrates that sequences of seismic changes generated at different locations in a well hydraulically connected to a reservoir volume possess similar characteristics (see Figure F.3). As a result, high correlation coefficients are expected between these sequences as they are reflections of the same pressure regime. Similar to the method proposed by Floricich (2008), this method is based on seismic-to-seismic correlation and benefits from the fact that the temporal coherence dimension is added to the 4D interpretation by analyzing the seismic dataset acquired from multiple surveys at the same time.

F.3 An initial test on Schiehallion

This method has been tested on the new batch of seismic data from the latest surveys on the segment 4 of the Schiehallion field. This includes data acquired by 2004, 2006 and 2008 surveys, which have all been cross-equalised with the baseline survey in 1996. Figure F.4(a) shows the *RMS* map (normalized by the maximum) derived from the baseline seismic. With excellent data quality, details of the reservoir channels can be resolved in the exploration stage, which offers a good opportunity to identify possible objects that may become the flow barriers after production start-up. However, a high level of uncertainty is found to be associated with interpretation of the dynamic properties of these targets. For instance, consider a detailed study of reservoir connectivity in the neighborhood of producer P8 using seismic data. Two discontinuities in the *RMS* amplitude can be clearly recognised as highlighted in the red circular areas in Figure F.4a. However, the actual flow properties of the objects cannot be determined with a satisfactory level of confidence if the interpretation is only based on the baseline seismic data. In addition, the channel in which P8 is positioned

seems to be connected to the area of relatively poorer quality (indicated by dimmer amplitude as indicated by the black arrow). Clearly, the level of connection is difficult to determine as result of lack of spatial continuity of the signal. Conventional 4D difference maps (e.g. 2004-1996 difference as shown in Figure F.4b) can resolve some of the interpretation uncertainties: the upper channel discontinuity previously recognised in baseline seismic map does seem to exist, whilst it is hard to determine whether the amplitude discontinuity highlighted in the lower circular area behaves as a flow barrier or not, also whether the influence of P8 can reach the area of interpretational uncertainty as discussed above. Figure F.4c shows the *NCC* result from the proposed seismic-to-seismic correlation technique. The reference signature for the 4D signatures is produced at a location close to the producer P8. Despite uncertainties that are still expected for interpretation, the *NCC* result does appear to provide reasonable answers to the questions initially raised regarding reservoir connectivity, which also confirms the two channel discontinuities and connection to the area below the well location of W4 in Figure F.4c.

F.4 Discussion

An extension of the method proposed in the thesis has been proposed in this appendix. It relies on correlation between sequences of 4D signatures and the reference sequence. Utilising the temporal behavior of the 4D signals at the same location, the method may have potential to improve the knowledge of reservoir connectivity obtained from the interpretation of baseline 3D and conventional 4D seismic data. However, one should also be aware of the risk that the *NCC* result might cause in the decision-making for reservoir management. Unlike the *NCC* result from well-to-seismic correlation technique, the *NCC* from the seismic-to-seismic correlation may not be consistent with engineering data and it may simply reflect similar errors in the 4D seismic data. Furthermore, it is anticipated that the temporal coherency of seismic changes may not have specific physical meaning in some cases. Thus, further study is needed to better understand the nature and explore the value of the temporal behavior of seismic changes over a dynamic reservoir.

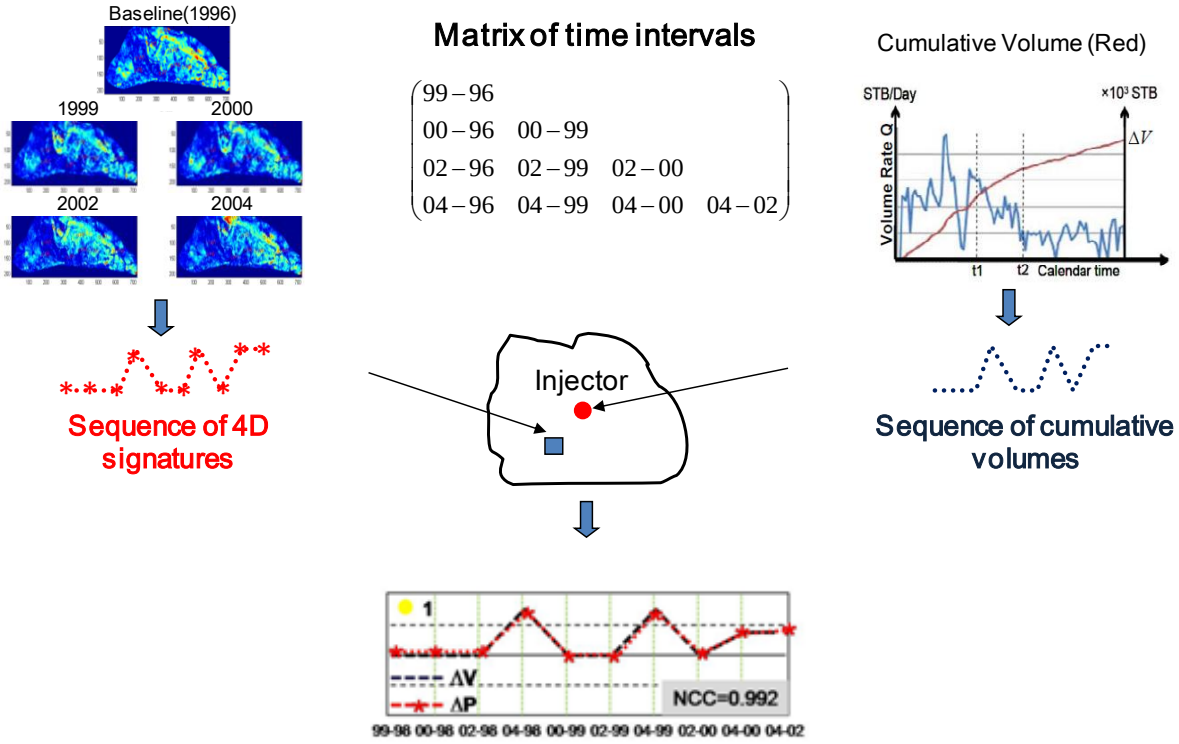

Figure F. 2 Workflow of well-to-seismic correlation proposed in this thesis

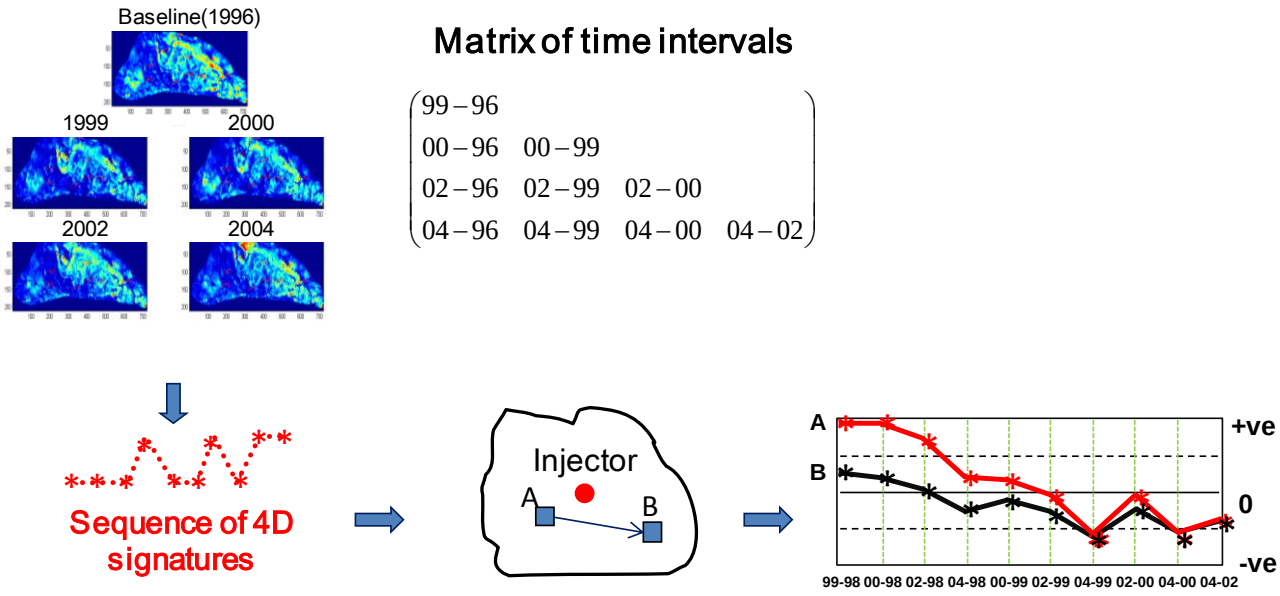

Figure F. 3 Workflow of seismic-to-seismic correlation

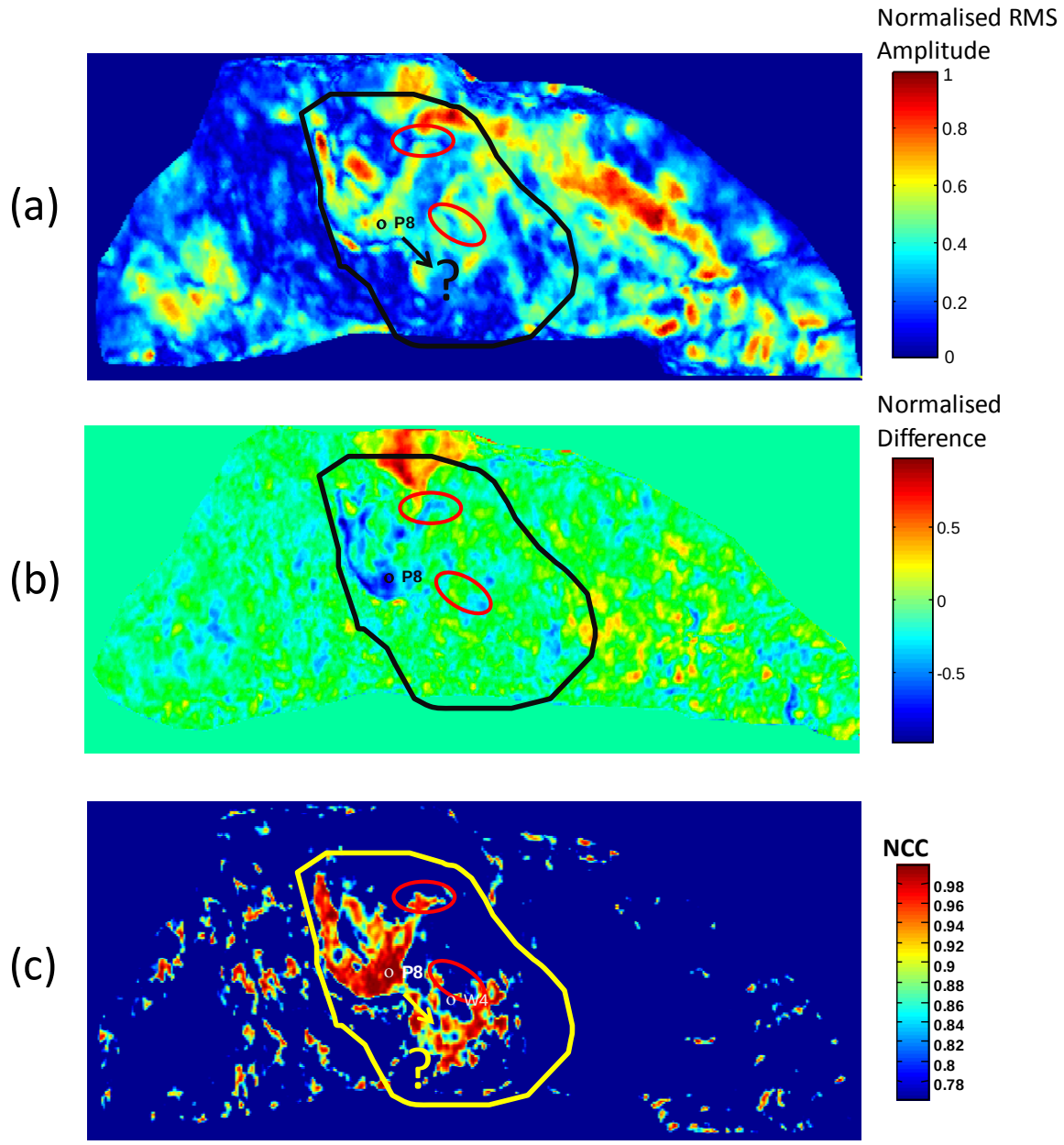

Figure F. 4 (a) RMS amplitude map from the baseline seismic survey in 1996 over the segment 4 of the Schiehallion field; (b) Difference between 2004 and 1996, normalised to -1 to 1; and (c) *NCC* map from seismic-to-seismic correlation, the reference sequence used for calculation is extracted from a location close to the toe of P8. The uncertain connections in (a) are highlighted by red ellipses and area of interest by yellow polygons

References

Aarnes, J.E. and Hauge, L.V. (2007) 'Coarsening of three-dimensional structure', *Elsevier Science*, 16 April.

Adrian, J. and Macfarian, G. (2008) 'Prospects for deepwater drilling: 2008-2012', *E&P*, 19 May.

Al-Maskeri, Y. and MacBeth, C. (2006) 'Extraction of permeability from time-lapse seismic data', *Geophysical Prospecting*, 54, pp. 333-349.

Almeida, J.A., Soares, A. and Pereira, J.M. (1996) 'Upscaling of permeability: implementation of a conditional approach to improve the performance in flow simulation', In European 3-D Reservoir Modelling Conference, Stavanger, Norway.

Altan, S., Zhu, X., Dillon, G., McArdle, J., Walker, C., Parr, R. and Westwater, P. (2001) 'Schiehallion 4D; From Time-Lapse Repeatability Study to Reservoir Monitoring', In SEG International Exposition and Annual Meeting, San Antonio, Texas.

Amini, H. (2009) 'Accurate simulator-to-seismic predictions: examples from modeling from full field simulators', ETLP sponsor meeting, Edinburgh.

Barkved, O., Amundsen, L. and Landrø, M. (2009) 'The Valhall LoFS Project', *Reservoir Monitoring Technology,Part IV, GeoExpro*, no. 32-34.

Barkved, O., Buer, K., Kristiansen, T.G., Kjelstadli, R.M. and Kommedal, J.H. (2005) 'Permanent seismic monitoring of the valhall field , Norway', International Petroleum Technology Conference , Doha,Qatar.

Barkved, O., Heavy, P., Kjelstadli, R., Kleppan, T. and Kristiansen, T.G. (2003) 'Valhall field - still on Plateau 20 years on production', *Society of Petroleum Engieners Reprint No.83957*, Sep.

Barkved, O.I. and Kristiansen, T.G. (2005) 'Seismic time-lapse effects and stress changes: Examples from a compacting reservoir', *The Leading Edge*, vol. 24, no. 12, pp. 1244-1248.

Benguigui, A. and MacBeth, C. (2008) 'Quantitative evaluation of reservoir fault communication using 4D seismic: An application to the Heidrun field', In EAGE conference and Exhibition, Rome, Italy.

Benguigui, A. and MacBeth, C. (2009) 'Updating the Simulation Model using 4D-derived fault transmissibility multipliers: An Application to the Heidrun Field', In EAGE Conference & Exhibition, Amsterdam, Netherland.

Bertrand, A. and MacBeth, C. (2005) 'Repeatability enhancement in deep-water permanant seismic installations: a dynamic correction for seawater velocity variations', *Geophysical Prospecting*, vol. 53, no. 2, pp. 1365-2478.

Bevington, Philip R., 1969, *Data Reduction and Error Analysis for the Physical Sciences*. McGraw-Hill, New York. Eq. (7-5), page 121. Chapter Four is on propagation of error. Includes many methods with full justification and FORTRAN subroutine codes.

Boreman, G.D. (2001) *Modulation Transfer Function in Optical and Electro-optical Systems*, Bellingham,WA: SPIE Press.

BP asset portfolio (2009) *The UK upstream asset portfolio*, [Online], Available: http://www.bp.com/liveassets/bp_internet/globalbp/STAGING/global_assets/downloads/U/uk_asset_schiehallion.pdf [14 Jun 2011].

Brain, J. (2007) 'Understanding 4D Noise at Nelson', Shell Exploration & Production Internal Presentation, Aberdeen, UK.

Bullen, K.E. and Bolt, B.A. (1985) *An introduction to the theory of seismology*, 4th edition, Cambridge: Cambridge university press.

Caley, A.J., Kendall, J.-M., Jones, R.H., Barkved, O.I. and Folstad, P.G. (2001) 'Monitoring Fractures in 4D using Micro-seismic data', In EAGE Conference and Exhibition, Amsterdam, Netherland.

Calvert, R. (2005) 'Insights and Methods for 4D Reservoir Monitoring and Characterization', *Distinguished Instructor Short Course*, vol. 8.

Campbell, S., Ricketts, T.A., Davies, D.M., Slater, C.P., Lilley, G.G., Brain, J., Stammeijer, J. and Evans, A.C. (2005) 'Improved 4D seismic repeatability - a West of Shetland towed

streamer acquisition case history, UKCS', SEG Annual Meeting, Expanded Abstracts, Houston, USA.

Carcione, J.M., Herman, G.C. and Kroode, A.P.E. (2002) 'Y2K Review Article - Seismic Modeling', *Geophysics*, July-August, pp. 1304-1325.

Chadwick, R.A., Arts, R., Eiken, O., Kirby, G.A., Lindeberg, E. and Zweigel, P. (2004) '4D seismic imaging of an injected CO2 plume at the Sleipner Field, central North Sea', *Geological Society,Memoirs*, 29 Jan, pp. 311-320.

Chapin, M., Terwoget, D. and Ketting, J. (2000) 'From seismic to simulation using new voxel body and geologic modeling techniques, Schiehallion Field, West of Shetlands', vol. 19, Apr, pp. 408-412.

Cheng, N., Osdal, B., Lygren, M., Husby, O. and Springer, M. (2007) 'Updating the Norne Reservoir Model with 4D Seismic Data', RESPRO Seminar, Stavanger,Noway.

Conolly, P. (1999) 'Elastic Impedance', *The Leading Edge*, 18, pp. 438-452.

Core, S., Lumley, D., Meadows, M. and Tura, A. (2002) 'A pressure and saturation inversion of 4D seismic data by rock physics modeling', SEG International Exposition and Annual Meeting, Salt Lake City, USA, 2475-2478.

Dake, L. (2001) 'The practice of reservoir engineering', Developments in Petroleum Science 36, Elsevier.

Desbarats, A. (1995) 'Upscaling Capillary Pressure-Saturation Curves in Heterogeneous Porous Media', *Water Resource*, pp. 31(2) 281-288.

Dijksman, N., Evans, A., Mccormick, D. and Stammeijer, J. (2007) '4D key to Schiehallion reservoir management', *Offshore*, pp. 88-90.

Dobbyn, A. and Marsh, M. (2001) 'Material Balance: A Powerful Tool for Understanding The Early Performance of The', *Society of Petroleum Engineers Reprint No.71819*.

Domes, F., MacBeth, C. and Brain, J. (2009) 'The Influence of Overburden on Time-lapse Saturation Interpretation', In EAGE Conference and Technical Exhibition, Amsterdam, Netherland.

Dyer, B.C., Jones, R.H., Cowles, J.F., Barkved, O. and Folstad, P.G. (1999) 'Microseismic survey of a North Sea reservoir', *World Oil*, March, pp. 74-78.

Edris, N.R. (2009) 'Identification of appropriate data, assimilation approach in seismic hisory matching and its effect on prediction uncertainty', *PhD thesis, Institute of Petroleum Engineering, Heriot-Watt University*, 1 April, pp. 63-64.

Eiken, O. (2003) 'Improvements in 4D seismic acquisition', *World Oil*, *Exploration*, vol. 224, no. 9, Sep.

EL-emam, A.H., Hughes, J.K. and Bunaian, H.A. (1998) 'Repeatability of land seismic surveys: A case study from Kuwait', In SEG International Exposition and Annual Meeting, New Orleans, USA, 5-8.

Falahat, R. (2011) 'A volumetric approach to interpret 4D seismic, *ETLP Sponsor Meeting*, May 2011

Falahat, R., Shams, A. and MacBeth, C. (2011) 'Towards quantitative evaluation of gas injection using time-lapse seismic data', *Geophysical Prospecting*, Mar, pp. 310-322.

Faure, P. and Spitz, S. (2006) 'Onshore 4D seismic repeatability at the gas storage geophysical laboratory', SEG International Exposition and Annual Conference, New Orleans, USA.

Floricich, M. (2006) 'An engineering-consistent approach for pressure and saturation estimation from time-lapse seismic data', *PhD dissertation, Institute of Petroleum Engineering, Heriot-Watt University*, p. 119.

Floricich, M., Evans, A., McCormick, D., Jenkins, G. and Stammeijer, J. (2008) 'Adding the temporal coherence dimension to 4D seismic data - assessing connectivity in the shiehallion field', EAGE Conference and Technical Exhibition, Rome, Italy.

Floricich, M., MacBeth, C. and Staples, R. (2005) 'An engineering-driven approach for separating pressure and saturation using 4D seismic: Application to a Jurassic reservoir in the UK North Sea', SEG International Exposition and Annual Meeting, Houston, Texas.

Foster, D.G. (2008) 'Lessons learnt from over 20 years of 4-D deployment', SPE Indian oil and gas technical conference and exhibition, Mumbai,India.

Foster, D., Fowler, S., McGarrity, J., Riviere, M., Robinson, N., Seaborne, R. and Watson, P. (2008) 'Building on BP's large-scale OBC monitoring experience - The Clair and Chirag-Azeri projects', *The Leading Edge*, 27, pp. 1632-1637.

Freeman, P., Kelly, S., Macdonald, C., Millington, J. and Tothill1, M. (2008) 'The Schiehallion Field: lessons learned modelling a complex deepwater turbidite', *Geological Society, London, Special Publications* , no. 309, pp. 205-219.

Furre, A.K., Nordby, L.H., Bakken, E., Kløv, T., Moen, A.S. and El Ouair, Y. (2006) 'Time-Lapse Seismic at the Heidrun Field: Advantages of Cross-Disciplinary Work', Offshore Technology Conference, Houston,USA.

Gainski, M., Macgregor, A.G. and Freeman, G.P. (2010) 'Turbidite reservoir compartmentalization and well targeting with 4D seismic and production data: Schiehallion Field, UK', *Geological Society, London, Special Publications*, pp. 89-102.

Gassmann, F. (1951) 'Uber die elastizität poröser medien', *Vierteljahrsschrift der Naturforschenden Gesellschaft in Zürich*, vol. 96, no. 23.

Gosselin, O., Aanonsen, I.S., Avavatsmark, I., Cominelli, A., Gonard, R., Kolasinsk, M., Ferdinand, F., kovacic, L. and Neylon, K. (2003) 'History Matching Using Time-lapse Seismic(HUT)', In SPE Annual Technical Conference and Exhibition, Denver, USA.

Govan, A., Primmer, T., Douglas, C., Moodie, N., Davies, M. and Nieuwland, F. (2006) 'Reservoir Management in a Deepwater Subsea Field--The Schiehallion Experience', *In SPE Reservoir Evaluation & Engineering*, Aug.

Hansen, H., Gommesen, L., Rasmussen, K. and Stronen, L. (2005) '4D quantitative estimation of dynamic reservoir properties for the Gullfaks Field', In EAGE Conference and Technical Exhibition, Madrid, Spain.

Hatchell, P. (2010) '4D seismic interpretation', SEG AM Recordings, Houston.

He, N., Inderwiesen, P. and Condon, P. (2005) 'Pressure and saturation inversion from 4D seismic constrained by production data', In EAGE Conference and Technical Exhibition, Paris, France.

Helgerud, M.B., Johnston, D., Jardine, B.G., Udoh, M.S., Aubuchon, N. and Harris, C. (2009) '4D case study in the deep water Gulf of Mexico: Hoover, Madison, and Marshall', In SEG Internation Exposition & Annual Meeting, Houston, USA.

Hettema, M.H.H., Schutjens, P.M.T.M., Verboom, B.J.M. and Gussinklo, H.J. (2000) 'Production-Induced Compaction of a Sandstone Reservoir: The Strong Influence of Stress Path', *In SPE Reservoir Evaluation & Engineering*, vol. 3, no. 4, pp. 342-347.

Hill, R. (1963) 'Elastic properties of reinforced solids:some theoretical principles', *J.Mech.Phys.Solids*, vol. 15, no. 357-372.

Hoeber, A.S.H.C., Berg, C.R., Buizard, S., Oexnevad, G., Tommerbakke, R., Bertrand, A., Folstad, P.G., Haugvaldstad, H. and Jeangeot, G. (2011) 'The Ekofisk Life of Field Seismic – An Integrated Operation', EAGE Workshop on Permanent Reservoir Monitoring (PRM) - Using Seismic Data, Trondheim,Norway.

Houston, M. and Criss, J. (2006) 'Challenges and Opportunities - 4D land permenant monitoring', EAGE Conference and Technical Exhibition, Vienna, Austria.

Huang, Y. and MacBeth, C. (2009) 'Direct correlation of 4D seismic and well activity for dynamic reservoir interpretation', In SEG International Exposition and Annual Meeting, Houston, USA.

Huang, Y., MacBeth, C., Van Gestel, J.-P. and Barkved, O. (2010) 'Correlation of well activity to time-lapsed signatures in the Valhall field for enhanced dynamic interpretation: application to Valhall field', EAGE/EUROPEC Conference and Technical Exhibition, Barcelona, Spain.

Huang, X., Meister, L. and Workman, R. (1997) 'Reservoir Characterisation by Integration of Time-Lapse Seismic and Production Data', SPE International Exposition and Annual Meeting, San Antonio, USA, In Society of Petroleum Engineers. Reprint No.38695.

ION (2011) *Land 4D*, [Online], Available: http://www.iongeo.com/Solutions/Land_4D/ [23 Jun 2011].

iReservoir (2011) *Home page of iReservoir consulting services*, [Online], Available: http://www.ireservoir.com/index.html [10 Jun 2011].

Johann, P., Sansonowski, R., Olivera, R. and Bampi, D. (2009) '4D seismic in a heavy oil, turbidite reservoir offshore Brazil', *The Leading Edge*, Jun, pp. 718-729.

Johnson, J.P., Rhett, D.W. and Siemers, W.T. (1988) 'Rock Mechanics Of The Ekofisk Reservoir In The Evaluation Of Subsidence', Offshore Technology Conference, Houston,USA.

Johnston, D.H. (2011) 'How PRM stacks up against conventional 4D', EAGE Workshop on Permanent Reservoir Monitoring (PRM) - Using Seismic Data , Trondheim, Norway.

Kommedal, J.H. and Barkved, O.I. (2005) '4D repeatability beyond twice - using variance', In SEG International Exposition and Annual Meeting, Houston, USA.

Koster, k., Gabriels, P. and Horvei, A. (2000) 'Reservoir Monitoring of the Draugen Field Through Time-Lapse Seismic and It's Business Impact', International Petroelum Exhibition and Conference, Abu Dhabi,United Arab Emirates.

Kragh, E. and Christie, P. (2002) 'Seismic repeatability, normalized rms, and predictability', *The Leading Edge*, vol. 21, no. 7, Jul, pp. 640-647.

Kristiansen, T.G., Barkved, O. and pattillo, P.D. (2000) 'Use of passive seismic monitoring in well and casing design in the compacting and subsidising Valhall field, North Sea', *In Society of Petroleum Engineers, Reprint No.65134*, Oct.

Lancaster, S. and Conolly, P. (2007) 'Fractal layering as a model for colour inversion and blueing', In EAGE Conference and Technical Exhibition , Rome, Italy.

Lancaster, S. and Whitcombe, D.N. (2000) 'Fast-track 'coloured' inversion', In SEG International Exposition and Technical Exhibition, St. Julians, Malta.

Landrø, M. (1999) 'Discrimination between pressure and fluid saturation changes', SEG International Exposition and Annual Meeting, Houston,USA.

Landrø, M. (2001) 'Descrimination between pressure and fluid saturation changes from time from time-lapse seismic data', *Geophysics*, pp. 836-844.

Landrø, M. (2002) 'Uncertainties in quantitative time-lapseseismic analysis', *GeophysicalProspecting*, vol. 50, no. 5, pp. 527-538.

Landrø, M., Veire, H., Duffaut, K. and Najjar, N. (2003) 'Discrimination between pressure and fluid saturation changes from marine multicomponent time-lapse seismic data', *Geophysics*, vol. 15921599, no. 68(5).

Laws, R. and Kragh, E. (2002) 'Rough seas and time-lapse seismic', *Geophysical Prospecting*, vol. 50, no. 2, pp. 195-208.

Leach, H.M., Herbert, N., LOS, A. and Smith, R.L. (1999) 'The Schiehallion development', *Petroleum Geology Conference series* , vol. 5, pp. 683-692.

Lynch, D. (2011) 'The Role of Seismic in Life-of-Field', EAGE Workshop on Permanent Reservoir Monitoring (PRM) - Using Seismic Data , Trondheim,Norway.

MacBeth, C. (2007) 'An introduction to quantitative 4D seismic interpretation for dynamic reservoir description', EAGE Education Days.

MacBeth, C., Floricich, M. and Soldo, J. (2006) 'Going quantitative with 4D seismic analysis', *Geophysical Prospecting*, vol. 54, p. 303–317.

Malme, T.N., Landrø, M. and Mittet, R. (2005) 'Overburden distortions—implications for seismic AVO analysis and time-lapse seismic ', *Journal of Geophysics and Engineering*, vol. 2, no. 2, pp. 1742-2132.

Manzocchi, T., Walsh, J.J., Nell, P. and Yielding, G. (1999) 'Fault transmissibility multipliers for flow simulation models', *Petroleum Geoscience*, May, pp. 53-63.

Marsh, M. (2004) '4D in reservoir managment - Success and Challenges', IOR Views e-Newsletter, 8.

Martin, K. and MacDonald, C. (2010) 'The Schiehallion field: Applying a Geobody Modelling Approach to Piece Together a Complex Turbidite Reservoir', DEVEX, Aberdeen.

Meadows, M., Adams, D., Wright, R., Tura, A., Cole, S. and Lumley, D. (2005) 'Rock physics analysis for time-lapse seismic at Schiehallion Field,', *Geophysical Prospecting*, vol. 53, p. 205–213.

Meunier, J. and Herculin, S. (2003) 'Evaluation and handling of positioning differences in 4D seismic', In SEG International Exposition and Annual meeting, Expanded Abstract, Dallas, USA.

Meunier, J. and Huguet, F. (1998) 'Cere-la-Ronde: A laboratory for time-lapse seismic monitoring in the Paris Basin', *The Leading Edge*, pp. 1388,1390,1392-1394.

Mikkelsen, P.L. and Guderian, K. (2008) 'Improved Reservoir Management Through Integration of 4D-Seismic Interpretation, Draugen Field, Norway', *SPE Reservoir Evaluation & Engineering*, vol. 1, no. 1, Feb, pp. 9-17.

Morice, S., Svendsen, M., Larsen, L. and Kristiansen, P. (2000) '4D-ready towed-streamer data and the Foinaven benchmark', In SPE International Exposition and Annual Meeting, Dallas, USA.

Morton, A., Anderson, M. and Thompson, M. (2009) 'Field Trial of Focused Seismic Monitoring on the Snorre Field', In EAGE Conference and Technical Exhibition, Amsterdam, Netherland.

Musser, J.A., Burnham, M., Guillot, C. and Bouligny, L. (2006) 'Optimising 4D Repeatability - Use of Enhanced Acquisition Technologies', *Hydro International*, Dec.

Naess, O.E. (2006) 'Repeatability and 4D seismic acquisition', In SEG International Exposition and Annual Meeting, New Orleans, USA, 3300-3303.

Nederveen, N. and Damm, M. (1993) 'Basal Waterflooding of a Tight Chalk Field With Long Horizontal Fractured Injectors', Offshore Europe, Aberdeen.

NPD website (2010) *Norne field facts*, [Online], Available: http://www.npd.no/en/publications/facts/facts-2010/chapter-11/norne/ [19 Jun 2011].

NTNU (2010) 'Introduction to Norne Field', http://www.ipt.ntnu.no/~norne/wiki/data/media/english/gfi/introduction-to-the-norne-field.pdf.

Nykjaer, O. (1994) 'Development of a Thin Oil Rim With Horizontal Wells in a Low Relief Chalk Gas Field, Tyra Field, Danish North Sea', European Petroleum Conference, London.

O'Donovan, A.R., Smith, S.G. and Kristiansen, P. (2000) 'Foinaven 4D Seismic - Dynamic Reservoir Parameters and Reservoir Management', SPE Annual Technical Conference and Exhibition, Dallas,Texas.

Osdal, B. and Alsos, T. (2002) 'Seismic modeling of eclipse simulation and comparison with real 4D data at the Norne field', 64th Mtg.:Eur.Assn.Geosci.Eng., A029.

Osdal, B., Husby, O., Aronsen, H.A., Chen, N. and Alsos, T. (2006) 'Mapping the fluid front and pressure buildup using 4D data on Norne Field', *The Leading Edge*, vol. 9, Sep, pp. 1134-1141.

Ovens, J.E.V., Larsen, F.P. and Cowie, D.R. (1997) 'Making Sense of Water Injection Fractures in the Dan Field ', San Antonio, Texas, SPE Annual Technical Conference and Exhibition.

Parr, R.S. and Marsh, M. (2000) *Development of 4D management West of Shetland*, September, [Online], Available: http://www.worldoil.com/September-2000-Development-of-4D-management-West-of-Shetland.html [10 Jan 2011].

Peaceman, D.W. (1977) *Fundamentals of numerical reservoir simulation*, 6th edition, Amsterdam: Elsevier scientific publishing company.

Ribeiro, C. and MacBeth, C. (2004) 'A petroelastic-based approach to pressure and saturation estimation using 4D seismic', SEG International Exposition and Annual meetings, Denver, Colorado.

Ribeiro, C. and MacBeth, C. (2005) 'Inversion for reservoir pressure and saturation changes in Foinaven field', SEG International Exposition and Annual meeting, Houston, USA.

Ricketts, T.A. and Barkved, O. (2011) 'Clair Permanent Reservoir Monitoring - A pilot that shows potential', EAGE Workshop on Permanent Reservoir Monitoring (PRM) - Using Seismic Data , Trondheim,Norway.

Rogers, S., Enachescu, C. and Golder, A. (2007) *Model helps Valhall water flooding*, Jan, [Online], Available: http://www.epmag.com/archives/features/251.htm [27 Feb 2011].

Ross, C.P. and Altan, M.S. (1997) 'Time-lapse seismic monitoring: Some shortcomings in nonuniform processing', *The Leading Edge*, vol. 16, no. 6, pp. 931-937.

Ruddy, I., Andersen, M.A., Pattillo, P.D., Bishlawi, M. and Foged, N. (1989) 'Rock compressibility, compaction and subsidence in a high porosity chalk reservoir: a case study of Valhall Field', *Journal Petroleum Technology*, vol. 41, no. 7, pp. 741-746.

Sandø, I.A., Munkvold, O.P. and Elde, R. (2009) '4D Geophysical Data', *Geoexpo Magazine*, Available: http://www.geoexpro.com/reservoir/4dgeophysicaldata/ [3 Jun 2011].

Saunders, M., Howe, D. and Kommedal, J. (2004) 'Source signature repeatability and source array directivity - Measurments from the Valhall 4D survey', In SEG International Exposition and Annual Meeting, Denver, USA.

Sheriff, R.E. (1991) 'Encyclopedic Dictionary of Exploration Geophysics, Third Edition', *Society of Exploration Geophysicists*, p. 384.

Smit, F., Ligtendag, M., Wills, P. and Calvert, R. (2006) 'Toward affordable permanent seismic reservoir monitoring using the sparse OBC concept', *The leading edge*, vol. 4, Apr, pp. 454-459.

Soroka, W.L., Melville, P., Kleiss, E., Al-Jenaibi, M.\., Al-Jeelani, A.B., Hafez, H.H. and Modavi, A. (2005) 'Successful pilot onshore Abu Dhabi shows that 4D can monitor fluid changes in a giant Middle East carbonate field', In SEG International Exposition and Annual Meeting, Houston, USA, 2430-2433.

Stammeijer, J. and Staples, R. (2003) 'Putting 4D pressures in perspective', In SEG International Exposition and Annual Meeting, Dallas, USA.

Statoil (2001) 'PL128-Norne Field Reservoir Management Plan', Internal Presentation, Harstad, Norway.

Statoil (2008) 'G-segment – update 2008 4D', Internal Presentation, Harstad, Norway.

Steffensen, I. and Karstadt, P. (1996) 'Norne Field Development - Fast Track From Discovery to Production', *Journal of Petroleum Technology*, Apr.

Stephen, K. and MacBeth, C. (2006) 'Seismic history matching in the UKCS Schiehallion field', *First Break*, vol. 24, pp. 43-49.

Stephen, K.D., Soldo, J., MacBeth, C. and Christie, M. (2006) 'Multiple-model seismic and production history matching: A case study', *SPE Journal*, no. 94173, Dec, pp. 418-430.

Stewart, G. and Whaballa, A.E. (1988) 'Pressure behaviour of compartmentalised reservoir', *Society of Petroleum Engineers. Reprint No. 19779*.

Thedy, E.A., Ramos Filho, W.L., Johann, P.R.S. and Seth, S. (2011) 'Jubarte - PRM In Ultradeep Water and with an Innovative Optics System', EAGE Workshop on Permanent Reservoir Monitoring (PRM) - Using Seismic Data, Trondheim, Norway.

Thompson, M. (2011) 'Snorre FSM - Monitoring Focused on the Ambitious Reservoir Recovery Plan', EAGE Workshop on Permanent Reservoir Monitoring (PRM) - Using Seismic Data , Trondheim, Norway.

Tura, A., Etuk, U. and Udo, S. (2006) 'Using time-lapse seismic for field development at Nembe Creek, Nigeria', *The Leading Edge*, vol. 25, no. 9, pp. 1142-1149.

Tura, A. and Lumley, E.D. (1999) 'Estimating pressure and saturation changes from time-lapse AVO data', In SEG International Exposition and Annual Meeting, Houston, USA, 1655-1658.

Van Everdingen, A.F. and Hurst, W. (1949) 'The application of the Laplace transformation to flow problems in reservoirs', *Trans.Amer.Inst.Min.Met.Eng.*, vol. 186, pp. 305-24.

Van Gestel., J., Tjetland, G., Parikh, M.J., Kommedal, J.H. and Barkved, O.I. (2010) 'Business impact of frequent time-lapse observations around valhall water injection well', In EAGE Conference and Technical Exhibition, Barcelona, Spain, L1009.

Vasco, D.W., Datta-Gupta, A., Behrens, R., Condon, P. and Rickett, J. (2004) 'Seismic imaging of reservoir flow properties: Time-lapse amplitude', *Geophysics*, 69, pp. 1425-1442.

Villegas, R., Dorn, O., Moscoso, M., Kindelan, M. and Mustieles, F. (2006) 'Simultaneous Characterization of Geological Shapes and Permeability', Proceeding of SPE Europec/EAGE Annual Conference, Vienna,Austria, SPE 1002911.

Villegas, R., MacBeth, C. and Paydayesh, M. (2009) 'Permeability updating of the simulation model using 4D seismic data', SPE/EAGE Reservoir Characterization and Simulation Conference , Abu Dhabi,UAE, SPE 125632.

Watts, K. (2005) 'The development of 4D seismic', *E&P*, 1 Mar.

Watts, G.F.T., Jizba, D., Gawith, D.E. and Putteridge, P. (1996) 'Reservoir monitoring of the Magnus Field through 4D time-lapse seismic analysis', *Petroleum Geoscience*, 1 Nov, pp. 361-372.

York, S.D., Pong, C.P. and Joslin, T.H. (1992) 'Reservoir Management of Valhall Field, Norway ', *Journal of Petroleum Technology*, vol. 44, no. 8, pp. 918-923.

Yun, L., Xuri, H., Jun, G., Deshen, S. and Jixiang, L. (2007) 'Land time-lapse seismic processing techniques with nonrepeatability factors', In SEG International Exposition and Annual Meeting, San Antonio,USA, 2999-3003.